

**FACTS-BASED STABILIZERS FOR POWER
SYSTEM STABILITY ENHANCEMENT**

BY

SALEH MOHAMMAD BAMASAK

A Thesis presented to the

DEANSHIP OF GRADUATE STUDIES

**KING FAHD UNIVERSITY OF PETROLEUM &
MINERALS**

DHAHRAN, SAUDI ARABIA

In Partial Fulfillment of the

Requirement for the Degree of

MASTER OF SCIENCE

In

ELECTRICAL ENGINEERING

May 2005

KING FAHD UNIVERSITY OF PETROLEUM & MINERALS

DHAHRAN 31261, SAUDI ARABIA

DEANSHIP OF GRADUATE STUDIES

This thesis, written by

SALEH MOHAMMAD BAMASAK

under the direction of his Thesis Advisors and approved by his Thesis Committee, has been presented to and accepted by the Dean of Graduate Studies, in partial fulfillment of the requirements for the degree of

MASTER OF SCIENCE IN ELECTRICAL ENGINEERING

Thesis Committee



Dr. Jamil M. Bakhshwain
(Department Chairman)

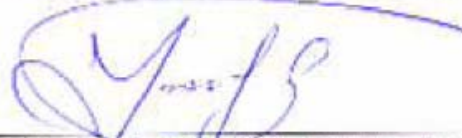


Dr. Mohammad A. Al-Ohuli
(Dean of Graduate Studies)

24/7/11
Date
24-7-2005



Dr. Mohammad A. Abido (Chairman)



Dr. Youssef L. Abdel-Magid (Member)



Dr. A. H. Abdur-Rahim (Member)

Dedicated to

My Parents

My Sincere Wife

My Son . . . Mohannad; and

My Daughter . . . Bayan

ACKNOWLEDGMENT

All praise, glory and gratitude be to Allah who said in the Holy Qura'n that "He who taught (the use of) the pen. Taught the man that which he knew not". Peace be upon the Prophet Mohammad, his family, his comanions, and all those who followed him until the Day of Judgment.

Allah said (9-105):

And say: "Work (righteousness): Soon will Allah observe your work, and his messenger, and the believers."

First of all I wish to express my deepest gratitude to my thesis advisor Dr. Mohammad Abido for his invaluable advice, personal attention, and continuous encouragement throughout my master program at KFUPM. It was a great experience working and learning with him. I am also deeply grateful to my thesis committee members, Dr. Youssef L. Abdel-Magid, and Dr. A. H. Abdur-Rahim for their involvement and the time they spared to review this thesis.

I would like to thanks my company, Saudi Electricity Company-Eastern Region Branch (SEC-ERB), for giving me the support during the course of doing my MS Program and continue encouragement to peruse the research.

Special thanks to Mr. Fahad Al-Saho, Manager of Substation Maintenance Department-East (SMED) for giving me the opportunities and chances to publish, present, and contribute in international conferences some results of this work.

My appreciation is extended to the Protection Engineering Division (SMED/PED) staff and their Div. Manager Mr. Ma'amoun Al-Owaid for their strong support and encouragement to complete the study.

Special and deep thanks to my wonderful parents, wife, kids, brothers and sister for their moral support and motivation. Last but not least, I extend my thanks and appreciation to my friends, colleagues and everyone who helped to get this work done.

“Excellence is not a destination; it is a continuous journey that never ends”

2.1.2	Power Flow Modulation	18
2.1.3	Damping Controller Model	19
2.2	Static VAR Compensator (SVC)	20
2.2.1	Introduction and Basic Operating Principles	20
2.2.2	Power Flow Modulation	22
2.2.3	Damping Controller Model	23
2.3	Thyristor-Controlled Phase Shifter (TCPS)	24
2.3.1	Introduction and Basic Operating Principles	24
2.3.2	Power Flow Modulation	25
2.3.3	Damping Controller Model	26
2.4	Static Synchronous Compensator (STATCOM)	26
2.4.1	Introduction and Basic Operating Principles	26
2.4.2	Power Flow Modulation	28
2.4.3	Damping Controller Model	29
3	POWER SYSTEM MODEL	31
3.1	Generator and Excitation Model	31
3.2	Single Machine Infinite Bus (SMIB) System	33
3.2.1	Phillips-Heffron Model Of SMIB System Installed With PSS, and G1 FACTS	33
3.2.2	Phillips-Heffron Model of SMIB System Installed With STATCOM	38
3.3	Multimachine Power System	41
3.3.1	Phillips-Heffron Model of Multi-Machine Power System	42

3.3.2	Phillips-Heffron Model of Multi-Machine System Installed With SVC & TCSC	46
4	PROPOSED APPROACH	49
4.1	Modal Analysis	49
4.2	Participation Factor	51
4.3	Controllability Measure	52
4.4	Implementation	53
4.4.1	Objective Function	53
4.4.2	Optimization Problem Formulation	53
4.5	Particle Swarm Optimization (PSO) Algorithm	54
4.5.1	Overview	54
4.5.2	PSO Algorithm	55
5	ANALYSIS AND DESIGN OF A PSS, AND G1 FACTS-BASED STABILIZERS IN A SMIB SYSTEM	57
5.1	Controllability Measure	57
5.2	Stabilizers Tuning and Simulation Results	60
5.2.1	Single Point Tuning	61
5.2.1.1	Individual Design	61
5.2.1.2	Coordinated Design [PSS & SVC]	67
5.2.1.3	Coordinated Design [PSS & TCSC]	72
5.2.2	Multiple Point Tuning	77
5.2.2.1	Individual Design	78
5.2.2.2	Coordinated Design [PSS & TCSC]	82

6	ANALYSIS AND DESIGN OF A STATCOM-BASED STABILIZER IN A SMIB SYSTEM	88
6.1	Controllability Measure	88
6.2	Stabilizer Tuning and Simulation Results	91
6.2.1	Single Point Tuning	91
6.2.1.1	Individual and Coordinated Design [C & ψ]	91
6.2.1.2	Coordinated Design [C & PSS]	98
6.2.2	Multiple Point Tuning	106
6.2.2.1	Individual Design	107
6.2.2.2	Coordinated Design [C & PSS]	114
7	ANALYSIS AND DESIGN OF PSS, TCSC, AND SVC-BASED STABILIZERS IN MULTIMACHINE POWER SYSTEMS	121
7.1	EXAMPLE 1 (3-MACHINES SYSTEM)	121
7.1.1	System Analysis	122
7.1.2	Individual Design	124
7.1.2.1	Stabilizer Design	124
7.1.2.2	Eigenvalue Analysis	125
7.1.2.3	Nonlinear Time Domain Simulation	126
7.1.3	Coordinated Design [TCSC & PSS]	133
7.1.3.1	Stabilizer Design	133
7.1.3.2	Eigenvalue Analysis	134
7.1.3.3	Nonlinear Time Domain Simulation	135

7.1.4	Coordinated Design [SVC & PSS]	139
7.1.4.1	Stabilizer Design	139
7.1.4.2	Eigenvalue Analysis	141
7.1.4.3	Nonlinear Time Domain Simulation	141
7.2	EXAMPLE 2 (TWO-AREA , 4-MACHINES SYSTEM)	146
7.2.1	System Analysis	147
7.2.2	Individual Design	149
7.2.2.1	Stabilizer Design	149
7.2.2.2	Eigenvalue Analysis	150
7.2.2.3	Nonlinear Time Domain Simulation	151
7.2.3	Coordinated Design [TCSC & PSS]	162
7.2.3.1	Stabilizer Design	162
7.2.3.2	Eigenvalue Analysis	164
7.2.3.3	Nonlinear Time Domain Simulation	165
7.2.4	Coordinated Design [SVC & PSS]	171
7.2.4.1	Stabilizer Design	171
7.2.4.2	Eigenvalue Analysis	172
7.2.4.3	Nonlinear Time Domain Simulation	173
8	CONCLUSION AND FUTURE WORK	177
8.1	Conclusion	177
8.2	Contribution	178
8.3	Future Work	179
	APPENDICES	181

NOMENCLATURE	185
BIBLIOGRAPHY	188
Vita	199
LIST OF PUBLICATIONS	200

LIST OF TABLES

Table	Table Title	Page
5.1	Optimal parameter settings, single point tuning, individual design	61
5.2	System eigenvalues of nominal loading condition, single point tuning, individual design	63
5.3	System eigenvalues of light loading condition, single point tuning, individual design	63
5.4	System eigenvalues of Heavy loading condition, single point tuning, individual design	63
5.5	Optimal parameter settings, single point tuning, coordinated design	68
5.6	System eigenvalues of nominal loading condition, single point tuning, coordinated design	69
5.7	System eigenvalues of light loading condition, single point tuning, coordinated design	69
5.8	System eigenvalues of heavy loading condition, single point tuning, coordinated design	69
5.9	Optimal parameter settings, single point tuning, coordinated design	73
5.10	System eigenvalues of nominal loading condition, single point tuning, coordinated design	74
5.11	System eigenvalues of light loading condition, single point tuning, coordinated design	74
5.12	System eigenvalues of Heavy loading condition, single point tuning, coordinated design	74
5.13	Loading conditions and parameter uincertainties	77
5.14	Open-loop eigenvalues associated with the electromechanical modes of all points considered in robust design process	77
5.15	Damping ratio of open-loop eignvalues associated with the electromechanical modes for all point considered in the robust design	78
5.16	Optimal Parameter Settings, multiple point tuning, individual design	78
5.17	System eigenvalues of nominal loading condition, multiple point tuning, individual design	79
5.18	System eigenvalues of light loading condition, multiple point tuning, individual design	80
5.19	System eigenvalues of heavy loading condition, multiple point tuning, individual design	80
5.20	Optimal Parameters Setting, multiple point tuning, coordinated design	83
5.21	System eigenvalues of nominal loading condition, multiple point tuning, coordinated design	85
5.22	System eigenvalues of light loading condition, multiple point tuning, coordinated design	85

5.23	System eigenvalues of heavy loading condition, multiple point tuning, coordinated design	85
6.1	Optimal parameter settings of C & ψ , single point tuning, individual and coordinated design	92
6.2	System eigenvalues of nominal loading condition, for C and ψ -based stabilizers, individual and coordinated design	94
6.3	System eigenvalues of light loading condition, for C and ψ -based stabilizers, individual and coordinated design	94
6.4	System eigenvalues of heavy loading condition, for C and ψ -based stabilizers, individual and coordinated design	94
6.5	Optimal Parameter Settings of C & PSS for individual and coordinate design	99
6.6	System eigenvalues of nominal loading condition, for PSS and C - based stabilizers, individual and coordinated design	101
6.7	System eigenvalues of light loading condition, for PSS and C -based stabilizers, individual and coordinated design	101
6.8	System eigenvalues of Heavy loading condition, for PSS and C - based stabilizers, individual and coordinated design	101
6.9	Loading condition and parameter uncertainties	106
6.10	Open-loop eigenvalues associated with the electromechanical modes of all points considered in robust design process	106
6.11	Damping ratio of open-loop eigenvalues associated with the electromechanical modes for all point considered in the robust design process	107
6.12	Optimal parameter settings for C & ψ , multiple point tuning, individual design	107
6.13	System eigenvalues of nominal loading condition, for C & ψ , multiple point tuning, individual design	109
6.14	System eigenvalues of light loading condition, for C & ψ , multiple point tuning, individual design	109
6.15	System eigenvalues of heavy loading condition, for C & ψ , multiple point tuning, individual design	109
6.16	Optimal parameters Setting of C & PSS, multiple point tuning, individual and coordinated design	115
6.17	System eigenvalues of nominal loading condition for C & PSS, multiple point tuning, individual and coordinated design	116
6.18	System eigenvalues of light loading condition for C & PSS, multiple point tuning, individual and coordinated design	116
6.19	System eigenvalues of Heavy loading condition for C & PSS, multiple point tuning, individual and coordinated design	117
7.1	3-machine system eigenvalues analysis	123
7.2	Modal analysis result for 3-machine system	123
7.3	Optimal parameter settings of PSS, SVC & TCSC single point tuning and individual design for 3-machine system	124
7.4	System eigenvalues in case of individual design of PSS, SVC & TCSC in 3-machine system	126

7.5	Optimal parameter settings of PSS and TCSC, coordinated design for 3-machine system	133
7.6	System eigenvalues with coordinated design of PSS2 & TCSC in 3-machine system	135
7.7	Optimal parameter settings of PSS and SVC, coordinated design for 3-machine system	140
7.8	System eigenvalues with coordinated design of PSS2 & SVC in 3-machine system	141
7.9	Two-area system eigenvalues analysis	147
7.10	Modal analysis result for two-area system	148
7.11	Optimal parameter settings for PSSs, SVC, & TCSC in two-area system	149
7.12	System eigenvalues in case of PSS, SVC & TCSC, two-area system	151
7.13	Optimal parameters setting of coordinated PSS's & TCSC design	163
7.14	System eigenvalues with coordinated design of PSS & TCSC in two-area system	164
7.15	Optimal parameters setting of coordinated PSS's & SVC design	171
7.16	System eigenvalues with coordinated design of PSS & SVC in two-area system	173
8.1	3-machine System bus data in per unit value.	181
8.2	3-machine System line data in per unit value.	182
8.3	Machines Data, for 3-machine system	182
8.4	Load flow result of the 3-machine system	182
8.5	Two-area System bus data in per unit value.	183
8.6	Two-area System line data in per unit value.	183
8.7	Machines Data, for two-area system	184
8.8	Load flow result of the two-area system	184

LIST OF FIGURES

Figure	Figure Title	Page
2.1	TCSC Configuration	18
2.2	Transmission line with a TCSC	19
2.3	TCSC with lead-lag controller	20
2.4	SVC Configuration	21
2.5	SVC V-I Characteristic	22
2.6	Transmission line with a SVC	23
2.7	SVC with lead-lag controller	23
2.8	TCPS Configuration	25
2.9	Transmission line with a TCPS	25
2.10	TCPS with lead-lag controller	26
2.11	STATCOM Configuration	27
2.12	STATCOM V-I characteristic	28
2.13	STATCOM dynamic model of AC Voltage Regulator and Stabilizer (with PWM)	30
2.14	STATCOM dynamic model of DC Voltage Regulator and Stabilizer (with PWM)	30
3.1	IEEE type-ST1 excitation system with PSS	32
3.2	SMIB with TCSC, SVC and TCPS	33
3.3	Block diagram of the linearized SMIB model	38
3.4	Single machine with STATCOM	39
3.5	Linearized model of the i^{th} machine in multimachine power system	45
3.6	Linearized model of the i^{th} machine in multimachine power system with SVC & TCSC	48
5.1	Minimum singular value with all stabilizers at $Q = -0.4$ pu	59
5.2	Minimum singular value with all stabilizers at $Q = 0$ pu	59
5.3	Minimum singular value with all stabilizers at $Q = +0.4$ pu	60
5.4	Variation of the objective function of all stabilizers	62
5.5	Rotor angle response for 6-cycle fault with nominal loading single point tuning, individual design	64
5.6	Rotor speed response for 6-cycle fault with nominal loading, single point tuning, individual design	65
5.7	Terminal voltage response for 6-cycle fault with nominal loading, single point tuning, individual design	65
5.8	PSS stabilizing signal response for 6-cycle fault with nominal loading, single point tuning, individual design	66
5.9	X_{tcsc} stabilizing signal response for 6-cycle fault with nominal loading, single point tuning, individual design	66
5.10	Variation of the objective function of PSS & SVC-based stabilizer	68
5.11	Rotor angle response for 6-cycle fault with nominal loading, single point tuning, coordinated design	70

5.12	Rotor speed response for 6-cycle fault with nominal loading, single point tuning, coordinated design	71
5.13	Terminal voltage response for 6-cycle fault with nominal loading, single point tuning, coordinated design	71
5.14	Variation of the objective function of PSS & TCSC-based stabilizer	73
5.15	Rotor angle response for 6-cycle fault with light loading, single point tuning, coordinated design	75
5.16	Rotor speed response for 6-cycle fault with nominal loading, single point tuning, coordinated design	76
5.17	Terminal voltage speed response for 6-cycle fault with nominal loading, single point tuning, coordinated design	76
5.18	Variation of the objective function of PSS & FACTS-based stabilizers, multiple-point tuning, individual design	79
5.19	Rotor angle response for 6-cycle fault with nominal loading, multiple point tuning, individual design	81
5.20	Rotor speed response for 6-cycle fault with nominal loading, multiple point tuning, individual design	81
5.21	Terminal voltage response for 6-cycle fault with nominal loading, multiple point tuning, individual design	82
5.22	Variation of the objective function of PSS & TCSC-based stabilizers, multiple-point tuning, coordinated design	84
5.23	Rotor angle response for 6-cycle fault with nominal loading, multiple point tuning, coordinated design	86
5.24	Rotor speed response for 6-cycle fault with nominal loading, multiple point tuning, coordinated design	87
5.25	Terminal voltage response for 6-cycle fault with nominal loading, multiple point tuning, coordinated design	87
6.1	Minimum singular value with STATCOM stabilizer at $Q = -0.4$ pu	89
6.2	Minimum singular value with STATCOM stabilizer at $Q = 0.4$ pu	90
6.3	Minimum singular value with STATCOM stabilizer at $Q = 0.0$ pu	90
6.4	Variation of the objective function of C and ψ -based stabilizers, individual and coordinated design	93
6.5	Rotor speed response for 6-cycle fault with nominal loading C & ψ , individual and coordinated design	96
6.6	Electrical power response for 6-cycle fault with nominal loading C & ψ , individual and coordinated design	96
6.7	STATCOM DC voltage response for 6-cycle fault with nominal loading, C & ψ , individual and coordinated design	97
6.8	Rotor angle response for 6-cycle fault with light loading C & ψ , individual and coordinated design	97
6.9	Electrical power response for 6-cycle fault with light loading, C & ψ , individual and coordinated design	98
6.10	Variation of the objective function of PSS and C -based stabilizers, individual and coordinated design	100
6.11	Rotor angle response for 6-cycle fault with nominal loading C & PSS, individual and coordinated design	103

6.12	Rotor speed response for 6-cycle fault with nominal loading, C & PSS, individual and coordinated design	103
6.13	STATCOM "C" controller response for 6-cycle fault with nominal loading, C & PSS, individual and coordinated design	104
6.14	PSS response for 6-cycle fault with nominal loading, C & ψ , individual and coordinated design	104
6.15	Rotor angle response for 6-cycle fault with light loading, C & PSS, individual and coordinated design	105
6.16	Rotor speed response for 6-cycle fault with light loading, C & PSS, individual and coordinated design	105
6.17	Variation of the objective function of ψ and C -based stabilizers, multiple point tuning, individual design	108
6.18	Rotor angle response for 6-cycle fault with nominal loading, multiple point tuning, individual design for C & ψ	110
6.19	STATCOM DC voltage response for 6-cycle fault with nominal loading, multiple point tuning, individual design for C & ψ	111
6.20	STATCOM C controller response for 6-cycle fault with nominal loading, multiple point tuning, individual design for C & ψ	111
6.21	STATCOM ψ controller response for 6-cycle fault with nominal loading, multiple point tuning, individual design for C & ψ	112
6.22	Rotor angle response for 6-cycle fault with light loading, multiple point tuning, individual design for C & ψ	112
6.23	STATCOM bus voltage response for 6-cycle fault with light loading, multiple point tuning, individual design for C & ψ	113
6.24	STATCOM DC voltage response for 6-cycle fault with light loading, multiple point tuning, individual design for C & ψ	113
6.25	Variation of the objective function of PSS & C-based stabilizers, multiple-point tuning, coordinated design	115
6.26	Rotor angle response for 6-cycle fault with nominal loading, multiple point tuning, coordinated design for C & PSS	118
6.27	Rotor speed response for 6-cycle fault with nominal loading, multiple point tuning, coordinated design for C & PSS	118
6.28	Rotor angle response for 6-cycle fault with light loading, multiple point tuning, coordinated design for C & PSS	119
6.29	Rotor speed response for 6-cycle fault with light loading, multiple point tuning, coordinated design for C & PSS	119
6.30	Rotor angle response for 6-cycle fault with heavy loading, multiple point tuning, coordinated design for C & PSS	120
6.31	Rotor speed response for 6-cycle fault with heavy loading, multiple point tuning, coordinated design for C & PSS	120
7.1	Single line diagram of WSCC 3 generator 9 bus system	122
7.2	Variation of the objective function of PSS, TCSC, & SVC stabilizers in 3-machine power system	125
7.3	Speed response for 6-cycle fault with PSS2, individual design	127
7.4	Rotor angle response for 6-cycle fault with PSS2, individual design	127
7.5	PSS-2 response for 6-cycle fault, individual design	128

7.6	Speed response for 6-cycle fault with TCSC, individual design	128
7.7	Rotor angle response for 6-cycle fault with TCSC, individual design	129
7.8	TCSC response for 6-cycle fault, individual design	129
7.9	Speed response for 6-cycle fault with SVC5, individual design	130
7.10	Rotor angle response for 6-cycle fault with SVC5, individual design	130
7.11	SVC5 response for 6-cycle fault, individual design	131
7.12	Speed response of machine-2 for 6-cycle fault with PSS, SVC and TCSC individual design	131
7.13	Speed response of machine-3 for 6-cycle fault with PSS, SVC and TCSC individual design	132
7.14	Rotor angle response of machine-3 for 6-cycle fault with PSS, SVC and TCSC individual design	132
7.15	Variation of the objective function of PSS & TCSC-based stabilizer, Individual & Coordinated design	134
7.16	Speed response for 6-cycle fault with PSS2 & TCSC, coordinated design	136
7.17	Rotor angle response for 6-cycle fault with PSS2 & TCSC, coordinated design	136
7.18	TCSC response for 6-cycle fault, PSS2 & TCSC, coordinated design	137
7.19	PSS response for 6-cycle fault, with PSS2 & TCSC, coordinated design	137
7.20	Speed response for 6-cycle fault with PSS2 & TCSC, coordinated and individual design	138
7.21	Rotor angle response for 6-cycle fault with PSS2 & TCSC, individual and coordinated design	138
7.22	TCSC response for 6-cycle fault, PSS2 & TCSC, coordinated design	139
7.23	Variation of the objective function of PSS & SVC5-based stabilizer, Individual & Coordinated design	140
7.24	Speed response for 6-cycle fault with PSS2 & SVC5, coordinated design	142
7.25	Rotor angle response for 6-cycle fault with PSS2 & SVC5, coordinated design	143
7.26	SVC5 response for 6-cycle fault, PSS2 & SVC5, coordinated design	143
7.27	PSS response for 6-cycle fault, with PSS2 & SVC5, coordinated design	144
7.28	Speed response for 6-cycle fault with PSS2 & SVC5, individual and coordinated design	144
7.29	Rotor angle response for 6-cycle fault with PSS2 & SVC5, individual and coordinated design	145
7.30	SVC5 response for 6-cycle fault, PSS2 & SVC5, individual and coordinated design	145

7.31	Single line diagram of the two-area system	146
7.32	Variation of the objective function of PSS, TCSC, & SVC stabilizers in multimachine two-area power system	150
7.33	Speed response for 6-cycle fault with PSS's, individual design	152
7.34	Rotor angle response for 6-cycle fault with PSSs, individual design	152
7.35	Electrical power response for 6-cycle fault with PSSs, individual design	153
7.36	Terminal voltage response for 6-cycle fault with PSSs, individual design	153
7.37	PSSs response for 6-cycle fault, individual design	154
7.38	Comparison speed response machine # 1, Kundur & proposed settings	154
7.39	Comparison speed response machine # 2, Kundur & proposed settings	155
7.40	Comparison speed response machine 3, Kundur & proposed setting	155
7.41	Comparison speed response machine # 4, Kundur & proposed setting	156
7.42	Comparison rotors' angle response, Kundur & proposed settings	156
7.43	Speed response for 6-cycle fault with TCSC-based stabilizer	157
7.44	Rotor angle response for 6-cycle fault with TCSC-based stabilizer	157
7.45	Terminal voltage response for 6-cycle fault with TCSC-based stabilizer	158
7.46	TCSC response for 6-cycle fault with TCSC-based stabilizer	158
7.47	Speed response for 6-cycle fault with SVC-based stabilizer	159
7.48	Rotor angle response for 6-cycle fault with SVC-based stabilizer	159
7.49	SVC response for 6-cycle fault with SVC-based stabilizer	160
7.50	Speed response of machine-4 for 6-cycle fault with PSS, SVC, and TCSC stabilizer	160
7.51	Speed response of machine-3 for 6-cycle fault with PSS, SVC, and TCSC stabilizer	161
7.52	Rotor angle response for 6-cycle fault with PSS, SVC, and TCSC stabilizer	161
7.53	Rotor angle response for 6-cycle fault with PSS, SVC, and TCSC stabilizer	162
7.54	Variation of the objective function of PSS's & TCSC stabilizers in multimachine two-area power system	163
7.55	Speed response for 6-cycle fault with PSS's & TCSC, coordinated design in the two-area system	165
7.56	Rotor angle response for 6-cycle fault with PSS's & TCSC, coordinated design in the two-area system	166
7.57	Electrical power response for 6-cycle fault PSS's & TCSC, coordinated design in the two-area system	166
7.58	Terminal voltage response for 6-cycle fault with PSS's & TCSC, coordinated design in the two-area system	167
7.59	TCSC response for 6-cycle fault, coordinated design with PSS's in the two-area system	167

7.60	PSS's response for 6-cycle fault, coordinated design with TCSC in the two-area system	168
7.61	Speed response for 6-cycle fault with PSS's & TCSC, individual and coordinated design in the two-area system	168
7.62	Speed response for 6-cycle fault with PSS's & TCSC, individual and coordinated design in the two-area system	169
7.63	Rotor angle response for 6-cycle fault with PSS's & TCSC, individual and coordinated design in the two-area system	169
7.64	Rotor angle response for 6-cycle fault with PSS's & TCSC, individual and coordinated design in the two-area system	170
7.65	TCSC response for 6-cycle fault, individual and coordinated design in the two-area system	170
7.66	Variation of the objective function of PSS's & SVC-based stabilizers in multimachine two-area power system	172
7.67	Speed response for 6-cycle fault with PSS's & SVC, coordinated design in the two-area system	174
7.68	Rotor angle response for 6-cycle fault with PSS's & SVC, coordinated design in the two-area system	174
7.69	Electrical power response for 6-cycle fault PSS's & SVC, coordinated design in the two-area system	175
7.70	SVC response for 6-cycle fault, coordinated design with PSS's in the two-area system	175
7.71	PSS's response for 6-cycle fault, coordinated design with TCSC in the two-area system	176

THESIS ABSTRACT

Name SALEH MOHAMMAD OMAR BAMASAK
Title FACTS-BASED STABILIZERS FOR POWER SYSTEM STABILITY ENHANCEMENT
Degree MASTER OF SCIENCE
Major Field ELECTRICAL ENGINEERING
Date of Degree June 2005

The objective of this thesis is to investigate the power system stability enhancement via power system stabilizers (PSSs) and Flexible AC Transmission System (FACTS) based controllers. This study includes possible coordination between PSSs and FACTS-based controllers. The different proposed FACTS-Based stabilizers recently reported in the literature are discussed. The design problem of PSS and FACTS controller is formulated as an optimization problem. The particle swarm optimization (PSO) algorithm is employed to search for optimal controller's parameters. In addition, this study is presented a singular value decomposition (SVD) based approach to assess and measure the controllability of the poorly damped electromechanical modes by different inputs. The nonlinear time-domain simulation is carried out throughout the thesis to validate the effectiveness of the proposed controllers. The controllers are simulated and tested under different operating conditions.

Keywords: *Power system stabilizer, PSS, FACTS, SVC, TCSC, TCPS, STATCOM, singular value, particle swarm optimization.*

MASTER OF SCIENCE DEGREE

KING FAHD UNIVERSITY OF PETROLEUM & MINERALS, DHAHRAN

MAY 2005

خلاصة الرسالة

الاسم	صالح محمد عمر بامسق
عنوان الرسالة	تصميم قوي الثبات لمضبطات شبكة الطاقة والمضبطات المستندة على الأنظمة المرنة لنقل التيار المتردد بهدف تحسين ثبات شبكة الطاقة الكهربائية
الدرجة	الماجستير في العلوم
التخصص	الهندسة الكهربائية
تاريخ التخرج	مايو 2005 م

الهدف من البحث هو دراسة كفاءة التصميم المتزامن لمضبط شبكة الطاقة الكهربائية مع المضبطات المستندة على الأنظمة المرنة لنقل التيار المتردد لغرض تحسين مضايلة نظام الطاقة. يدرس البحث ثلاثة أنظمة للطاقة: نظام طاقة ماكينة واحدة ذو ناقل لامتناهي مجهز بأجهزة الجيل الأول من الأنظمة المرنة لنقل التيار المتردد، و نظام طاقة ماكينة واحدة ذو ناقل لا متناهي مجهز بجهاز STATCOM، ونظام طاقة متعدد المكائن. لتقدير مدى قدرة هذه المضبطات المختلفة على مضايلة الشكل الكهروميكانيكي، يتم تطبيق طريقة تحليل القيمة الشاذة. تصاغ مسألة تصميم المضبطات بشكل مسألة الحل الأمثل بحيث تستخدم طريقة سرب الجسيمات للبحث عن أفضل قيم لمكونات كل مضبط على حدة لتحقيق أمثل قيمة لمقياس الأداء باعتبار نقطة تشغيل واحدة. يتم بعد ذلك تصميم أكثر من مضبط بشكل متزامن بنفس الطريقة. من أجل التأكد من أن المضبطات المقترحة ذات ثبات قوي، يعاد تصميمها باعتبار نقاط تشغيل عديدة. للتحقق من كفاءة التصاميم المقترحة، يجرى اختبارها عن طريق تحليل مضايلة الشكل الكهروميكانيكي، والمحاكاة الزمنية غير الخطية لإشارات الشبكة.

درجة الماجستير في العلوم

جامعة الملك فهد للبترول والمعادن، الظهران

مايو 2005

CHAPTER 1

INTRODUCTION

Today's Power system is a complex network, sometimes made of thousands of buses and hundreds of generators. Available power generation usually does not situated near a growing of load center. In order to meet the growing power demand, utilities have an interest in better utilization of available power system capacities, existing generation and existing power transmission network, instead of building new transmission lines and expanding substations. On the other hand, power flows in some of the transmission lines are overloaded, which has as an overall effect of deteriorating voltage profiles and decreasing system stability and security. In addition, existing traditional transmission facilities, in most cases, are not designed to handle the control requirements of complex and highly interconnected power systems. This overall situation requires the review of traditional transmission methods and practices, and the creation of new concepts, which would allow the use of existing generation and transmission lines up to their full capabilities without reduction in system stability and security.

The line impedance, the receiving and sending ends voltages, and phase angle between the voltages determine the transmitted electrical power over a line. Therefore, by controlling, one or more of the transmitted power factors; it is possible to control the active as well as the reactive power flow over a line.

In the past, power systems could not be controlled fast enough to handle dynamic system condition. This problem was solved by over-design; transmission systems were designed with generous stability margins to recover from anticipated operating contingencies caused by faults, line and generator outages, and equipment failures.

Series capacitor, shunt capacitor, and phase shifter are different approaches to increase the power system transmission lines loadability. In past days, all these devices were controlled and switched mechanically and were, therefore, relatively slow. They are very useful in a steady state operation of power systems but from a dynamical point of view, their time response is too slow to effectively damp transient oscillations. If mechanically controlled systems were made to respond faster, power system security would be significantly improved, allowing the full utilization of system capability while maintaining adequate levels of stability. This concept and advances in the field of power electronics led to a new approach introduced by the Electric Power Research Institute (EPRI) in the late 1980. Called Flexible AC Transmission Systems or simply FACTS, it was an answer to a call for a more efficient use of already existing resources in present power systems while maintaining and even improving power system security.

In order to clearly determine the goals of this thesis, the concept of “stability” must be defined. A definition given in [1] is as follows:

“Power system stability may be broadly defined as that property of a power system that enables it to remain in a state of operating equilibrium under normal operating conditions and to regain an acceptable state of equilibrium after being subjected to a disturbance.”

From this general definition, two categories of stability are derived: small-signal and transient stability. Small-signal stability is the ability of the system to return to a normal operating state following a small disturbance. Investigations involving this stability concept usually involve the analysis of the linearized state space equations that define the power system dynamics. Transient stability is the ability of the system to return to a normal operating state following a severe disturbance, such as a single or multi-phase short-circuit or a generator loss. Under these conditions, the linearized power system model does not usually apply and the nonlinear equations must be used directly for the analysis, and must be solved by direct methods or by iterative step-by-step procedures.

Since the development of interconnection of large electric power systems, there have been spontaneous system oscillations at very low frequencies in order of 0.2-3.0Hz. Once started, the oscillation would continue for a while and then disappear, or continue to grow, causing system separation [3]. There are two electromechanical modes of oscillations have reported [4];

- *local mode*, with a frequency 0.8-3 Hz, which is related to oscillation in a single generator or a group of generators in the same area oscillate against each other; and
- *Inter-area mode*, with frequency 0.2-0.8 Hz, in which the units in one area oscillate against those in other area.

In order to damp these power system oscillations and increase system oscillations stability, the installation of Power System Stabilizer (PSS) is both economical and effective. PSSs have been used for many years to add damping to electromechanical oscillations. To date, most major electric power system plants in many countries are equipped with PSS [5]. However, PSSs suffer a drawback of being liable to cause great variations in the voltage profile and they may even result in leading power factor operation and losing system stability under severe disturbances. In addition, in a deregulated environment, placement may be problematical due to generator ownership.

Recently appeared FACTS (Flexible AC Transmission System)-based stabilizer offer an alternative way in damping power system oscillation. Although, the damping duty of FACTS controllers often is not their primary function, the capability of FACTS-based stabilizers to increase power system oscillation damping characteristics has been recognized [6].

However, uncoordinated local control FACTS devices and PSSs always causes destabilizing interaction. To improve overall system performance, many studies were made on the coordinated design between FACTS and PSSs controllers.

1.1 Literature Review

1.1.1 Power System Stabilizers

The power system stabilizer is a supplementary control system, which is often applied as part of excitation control system. The basic function of the PSS is to apply a signal to the

excitation system, creating electrical torques to the rotor, in phase with speed variation, that damp out power oscillations.

In the past decades, the utilization of supplementary excitation control signals for improving the dynamic stability of power systems has received much attention. Extensive research has been conducted in such fields as effect of PSS on power system stability, PSS input signals, PSS optimum locations, and PSS tuning techniques.

DeMello and Concordia in 1969 [7] presented the concepts of synchronous machine stability as affected by excitation control. They established an understanding of the stabilizing requirements for static excitation systems. Their work developed insights into effects of excitation systems and requirement of supplementary stabilizing action for such systems based on the concept of damping and synchronizing torques.

Klein et al. [8, 9] presented the simulation studies into the effects of stabilizers on inter-area and local modes of oscillations in interconnected power systems. It was shown that the PSS location and the voltage characteristics of the system loads are significant factor in the ability of a PSS to increase the damping of inter-area oscillations.

Nowadays, the conventional lead-lag power system stabilizer is widely used by the power system utility [10]. Other types of PSS such as proportional-integral power system stabilizer (PI-PSS) and proportional-integral-derivative power system stabilizer (PID-PSS) have also been proposed [11-12].

Several approaches have been applied to PSS design problem. These include pole placement, H_∞ , optimal control, adaptive control, variable structure control, and different optimization and artificial intelligence techniques [13-28].

Since the primary function of the PSS is to add damping to the power oscillations, basic control theory would indicate that any signal in which the power oscillation is observable is a good candidate for input signal. Some readily available signals are generator rotor speed, calculated bus frequency, and electrical power. Most PSS controls today are based on an accelerating power input design, providing robust damping over a wide range of operating conditions, with minimum interaction [29].

The problem of the most appropriate locations for PSSs in multi-machines power system has been addressed in many papers. Sequentially select the optimum location of PSS using eigenvalue analysis techniques has been introduced in [30]. Hsu and Chen [31] have proposed a novel technique to identify the optimum PSS locations by participation factor (PF).

1.1.2 FACTS Devices

Series capacitor, shunt capacitor, and phase shifter are different approaches to increase the power system loadability. In past decades, all these devices were controlled mechanically and were, therefore, relatively slow. They are very useful in a steady state operation of power systems but from a dynamical point of view, their time response is too slow to effectively damp transient oscillations. If mechanically controlled systems were made to respond faster, power system security would be significantly improved, allowing the full utilization of system capability while maintaining adequate levels of stability. This concept and advances in the field of power electronics led to a new approach introduced by the Electric Power Research Institute (EPRI) in the late 1980. Called Flexible AC

Transmission Systems or simply FACTS, it was an answer to a call for a more efficient use of already existing resources in present power systems while maintaining and even improving power system security. In [33], the author introduced this new concept, initiating a new direction in power system research. Developments in the field of high voltage power electronics have made possible the practical realization of FACTS controllers.

1.1.2.1 First Generation FACTS Devices (G1)

Developments in the field of high voltage power electronics have made possible the practical realization of FACTS controllers. By the 1970s, the voltage and current rating of Thyristor had been increased significantly making them suitable for applications in high voltage power systems [34-35]. This made construction of modern Static Var Compensators (SVCs), Thyristor Controlled/Switched Series Capacitors (TCSCs/TSSCs), and Thyristor Controlled Phase Shifter Regulators (TCPSs). A fundamental feature of the thyristor based switching controllers is that the speed of response of passive power system components such as a capacitor or a reactor is enhanced, but their compensation capacity is still solely determined by the size of the reactive component.

A lot of different technique has been reported in the literature pertaining to investigating the effect of G1 FACTS devices "SVC, TCSC, and TCPS" on power system stability [38-64].

Wang and Swift [38] developed a novel unified Phillips-Heffron model for a power system equipped with a SVC, a TCSC and a TCPS. Damping torque coefficient

analysis has been performed, based on the proposed model, to study the effect of FACTS controllers damping for different loading conditions.

Abido & Abdel-Magid [39, 40] investigated the effectiveness of PSS and FACTS-based controllers on power stability enhancements. For the proposed stabilizer design problem, an eigenvalue-based objective function to increase the system damping was developed. Then the GA used to search for the optimal stabilizer parameters.

Many approaches have been adopted to design the FACTS controller. Several approaches based on modern control theory have been applied to TCSC controller design [41-49]. Chen et al. [41] presented a state feedback controller for TCSC by using a pole placement technique. Cang and Chow [42] developed a time optimal control strategy for the TCSC where a performance index of time was minimized. A fuzzy logic controller for a TCSC was proposed in [43]. Heuristic optimization techniques have been implemented to search for the optimum TCSC based stabilizer parameters for the purpose of enhancing SMIB system stability [45-46]. In addition, different control schemes for a TCSC were proposed such as variable structure controller [48], bilinear generalized predictive controller [49], and H_∞ -based controller [50].

A considerable attention has been directed to realization of various TCPS schemes. Baker et al [51] developed a control algorithm for SPS using stochastic optimal control theory. Edris [52] proposed a simple control algorithm based on equal area criterion. Jiang et al [53] proposed an SPS control technique based on nonlinear variable structure control theory.

In the literature, SVCs have been applied successfully to improve the transient stability of a synchronous machine [56]. Hammad [57] presented a fundamental analysis of the application of SVC for enhancing the stability performance of power systems. Then, the power damping enhancement by application of SVC has been analyzed [58-68]. It is shown that the SVC enhances the system damping of local as well as inter-area oscillation modes. Wang and Swift [58] used damping torque coefficients approach to investigate the SVC damping control of a SMIB system on the basis of Phillips-Heffron model. It was shown that the SVC damping control provides the power system with negative damping when it operates at a lower load condition than the dead point, the point at which SVC control produces zero damping effect. Robust SVC controllers based on H_∞ , structured singular value μ , and quantitative feedback theory QFT also have been presented to enhance system damping [63-65].

M. Noroozian [73-76] examined the enhancement of multimachine power system stability by use TCSCs and SVCs. SVC was found to be more effective for controlling power swings at higher levels of power transfer; when it design to damp the inter-area modes, it might excite the local modes, and its damping effect dependent on load characteristics. While TCSC is not sensitive to the load characteristic and when it is designed to damp the inter-area modes, it does not excite the local modes.

1.1.2.2 Second Generation FACTS Devices

A normal thyristor, having no current interruption capability, changes from on-state to off-state when the current drops below the holding current and, therefore, has a serious

deficiency that prevents its use in switched mode applications. With the development of the high voltage, high current Gate Turn-Off thyristors (GTOs, IGBTs ... etc), it became possible to overcome this deficiency. Like the normal thyristor, a gate current pulse can turn on the GTO thyristor, while to turn it off, a negative gate-cathode voltage can be applied at any time. This feature and the improved ratings of GTOs made possible the use of Voltage-Sourced Converters (VSC) in power system applications [78].

Voltage-sourced converters employ converters with GTOs/IGBTs or other turn-off devices, diodes and a dc capacitor to generate a synchronous voltage of fundamental frequency and controllable magnitude and phase angle. If a VSC is connected to the transmission system via a shunt transformer, it can generate or absorb reactive power from the bus to which it is connected. Such devices are Static Compensator or STATCOM, Static Synchronous Series Compensator (SSSC), and a Unified Power Flow Controller (UPFC). STATCOM form the 2nd generation FACTS device is considered.

STATCOM previously referred to as STATCON, ASVC or ASVG, resembles in many respects a rotating machine used for reactive power compensation. The principles of a STATCOM can be found in [36].

Application of STATCOM for stability improvement has been discussed in the literature [79-107]. A comparative study between the conventional SVC and STATCOM in damping power system oscillation is given in [79]. The results show the superiority of STATCOM-based controller over SVC-based controller in increasing the damping of low frequency oscillations.

Wang in [80], established the linearized Phillips-Hefferon model of power system installed with a STATCOM and demonstrated the application of the model in analyzing the damping effect of the STATCOM. Both cases of SMIB and multimachine power system were studied. Then the work was extended in [81, 82] to study the negative interactions between STATCOM AC and DC control. To overcome the reported negative interaction a technique to design a decoupled multivariable sampled regulator for multi-input multi output systems was applied for the coordinated control of STATCOM AC and DC voltage.

A robust controller for providing damping to power system through STATCOM is presented in [83-86]. The loop-shaping technique has been employed to design the controllers. It was observed that a robust controller in the speed loop, with nominal voltage feedback, effectively damps the electromechanical oscillations for a wide range of operating conditions.

In [87], an adaptive fuzzy controller is incorporated into the supplementary control of STATCOM to enhance the damping of inter-area oscillation exhibited by a two-area four-machine interconnected power system.

Two new variable structure fuzzy control algorithms for controlling the reactive component of the STATCOM current are presented in [88]. The signal input to the proposed controller obtained from a combination of generator speed deviation and STATCOM bus voltage deviation.

Lee and Sun in [89], used the Linear Quadratic Regulator (LQR) method to design the state feedback gain of STATCOM controller to increase the damping of a SMIB power system.

Nonlinear control theory has been applied to design STATCOM damping controller in [90]. Comparison of PSS, SVC, and STATCOM controllers for damping power system oscillations using Hopf bifurcation theory is presented in [97].

STATCOM active power injection/absorption control function has better performance for the power swing damping and can improve the transient stability. But STATCOM itself cannot control the active power injection/absorption to power system. A STATCOM with energy storage system can control both the reactive and the active power, thus providing more flexible power system operation [98].

With more advanced energy storage systems, such as Battery Energy Storage System (BESS) and Superconducting Magnetic Energy Storage (SMES) [99], are commercially available for power system transmission and distribution level application. In [100], the steady-state characteristics of STATCOM with energy storage were discussed in detail. Power system stability improvement by energy storage type STATCOM has been studied in [101-104].

1.1.2.3 Coordination Design Between FACTS-Based Controllers and PSS

Uncoordinated FACTS-based stabilizers and PSSs always cause destabilizing interactions. To improve overall system performance, many researches were made on the

coordination between PSSs and FACTS Power Oscillation Damping (POD) controllers [105-117].

Gibbard et al. [106] investigated the interactions between and the effectiveness of PSSs and FACTS- based controllers in multimachine systems based on the analysis of both the perturbations in induced torque coefficients and the shifts in rotor modes resulting from increments in stabilizer gains.

A little work has been devoted in the literature to study the coordination control of excitation and FACTS stabilizers. A coordinated optimal controller for the excitation system and a SVC located on the generator bus of a SMIB system was presented in [107]. Rahim and Nassimi [108] presented optimum control strategies for both the SVC and exciter. Hiyama et al [109] presented a coordinated fuzzy logic-based scheme for PSS and switched series capacitor modules to enhance overall power system stability. Abdel-Magid and Abido [110] presented Robust coordinated design of excitation and TCSC-based stabilizers using genetic algorithm. Pourbeik and Gibbard [111] presented a two-stage method for the simultaneous coordination of PSSs and FACTS-based lead-lag controllers in multimachine power systems by using the concept of induced damping and synchronizing torque coefficients.

Coordination between PSS and STATCOM-based stabilizer has also been studied [113-115]. Stabilization of generator oscillations using PID STATCOM damping controllers and PID PSSs is presented in [113]. The parameters of the proposed damping controllers were solved by left shifting both modes to the desired locations on the complex plane using a unified approach based on modal control theory.

1.2 Thesis Objectives

The objective of this thesis is to investigate the power system stability enhancement via power system stabilizers (PSSs) and Flexible AC Transmission System (FACTS) based controllers. This study includes coordination design between PSSs and FACTS-based controllers. The procedure to achieve the thesis objective is as follows:

1. For a SMIB system equipped with PSS and FACTS devices namely (TCSC, SVC, TCPS, and STATCOM), the linearized models were developed.
2. Singular Value Decomposition (SVD) analysis is employed as a controllability measure of the different control signals on the system electromechanical mode that will be identified using Participation Factor (PF) technique.
3. The design problem of PSS and different FACTS controllers are formulated as an optimization problem. The Particle Swarm Optimization (PSO) algorithm is employed to search for optimal controller's parameters by maximizes the minimum damping ratio of all complex eigenvalues.
4. Eigenvalue analysis is carried out to assess the effectiveness of the proposed stabilizers on enhancing the EM mode stability.
5. Coordination design of PSS and FACTS controllers is carried out by considering more than one stabilizer in the design process.
6. The design process is extended to make the controller robust. This done by considering a wide range of the operation conditions during the design.

7. For more practical power system the TCSC and SVC are modeled in two different multimachine power systems and the linearized model are developed accordingly.
8. Steps 3-5 are repeated for the multimachine power system.
9. The eigenvalue analysis and the nonlinear time-domain simulation used throughout the thesis to validate the effectiveness of the proposed controllers. The controllers are simulated and tested under different operating conditions.

1.3 Thesis Organization

This thesis is organized as follows: in Chapter 2, introduction and basic operating principles of FACTS devices namely (TCSC, SVC, TCPS, and STATCOM) are introduced in addition to their power oscillation damping (POD) controller structure used in this thesis.

Chapter 3 concentrates on the power system linear and non-linear models. These models include: a SMIB system model equipped with PSS, and G1 FACTS devices (TCSC, SVC and TCPS), a SMIB system model equipped with a STATCOM, and a multimachine power system equipped with PSS, TCSC and SVC.

Chapter 4 presents some tools and techniques used in the controllers design process. These tools are Particle Swarm Optimization (PSO), controllability measurement, participation factor, and modal analysis. In addition, the problem formulation is outlined in this chapter.

The stabilizers design, eigenvalue analysis, and nonlinear simulation of a SMIB equipped with PSS, and G1 FACTS-based stabilizers are presented in chapter 5, while chapter 6 is devoted to SMIB with a PSS and a STATCOM-based stabilizer.

Chapter 7 concentrates on the multimachine system equipped with PSS, TCSC, and SVC. Eigenvalue analysis and nonlinear simulation results for two different multimachine systems are presented. Conclusions and future work are discussed in chapter 8.

CHAPTER 2

FLEXIBLE AC TRANSMISSION SYSTEM (FACTS)

2.1 Controlled Series Capacitor (CSC)

2.1.1 Introduction and Basic Operating Principles

Series capacitors are connected in series with transmission lines to compensate for the inductive reactance of the line, increasing the maximum transmittable power and reducing the effective reactive power loss. Power transfer control can be done continuously and rather fast using, for example, the Thyristor Controlled Series Capacitors (TCSC) or Thyristor Switch Series Capacitors (TSSC), making it very useful to dynamically control power oscillations in power systems [24-28]. However, the problem with these devices is that that it can form a series resonant circuit in series with the reactance of the transmission line, thus limiting the rating of the TCSC to a range of 20 to 70 % the line reactance. Fig. 2.1 shows the basic configuration of a TCSC. Same figure could be used for TSSC but without a series reactance with the thyristor.

TCSC controllers use thyristor controlled reactors (TCR) in parallel with capacitor segments (C) of a series capacitor bank. This combination allows the capacitive reactance

to be smoothly controlled over a wide range and switched upon command to a condition where the bi-directional thyristor pairs conduct continuously (full cycle) and insert an inductive reactance into the line.

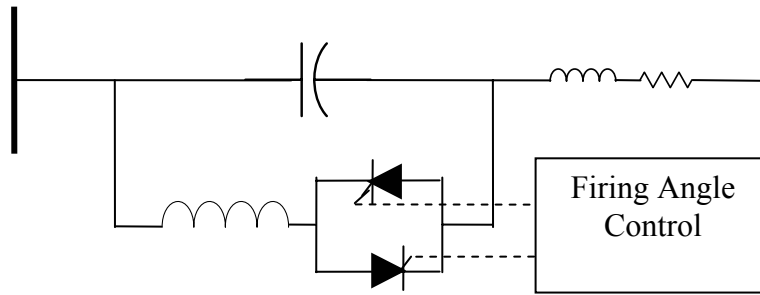


Fig.2.1: TCSC Configuration

2.1.2 Power Flow Modulation

The real power flow through a transmission line, between bus i & j, equipped with a TCSC or TSSC, Fig. 2.2, is obtained by:

$$P = \frac{V_i V_j}{X_{ij}(1-k)} \sin(\delta_{ij}) \quad (2.1)$$

Where k represents the TCSC compensation level and is given by

$$k = \frac{X_{CSC}}{X_{ij}} \quad (2.2)$$

The equivalent reactance of the TCSC, X_{CSC} , is given by

$$X_{CSC} = \frac{X_C X_L(\alpha)}{X_C - X_L(\alpha)} \quad (2.3)$$

and

$$P = \frac{\pi}{2\pi - 2\alpha + \sin(2\alpha)} X_L; \quad \pi/2 \leq \alpha \leq \pi \quad (2.4)$$

where α is the thyristor firing angle.

Hence, the real power flow through the transmission line can be adjusted by controlling the compensation level k .

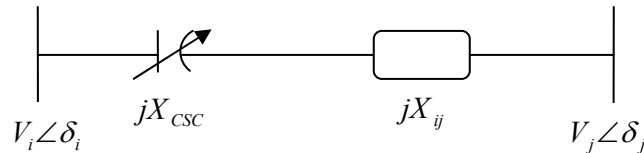


Fig. 2.2: Transmission line with a TCSC

2.1.3 Damping Controller Model

To utilize the Controlled Series Compensation devices for improving the system damping, a supplementary damping controller is installed. The conventional Lead-Lag controller is used throughout this thesis as a damping controller.

The damping controllers are design to produce an electrical torque in phase with the speed deviation. The speed deviation $\Delta\omega$ is considered as the input to the damping controllers. The lead-lag block contains the stabilizer Gain block determines the amount of damping. Next, the washout sub-block, used to reduce the over-response of the damping during severe event and serves as a high-pass filter, with a time constant that allows the signal associated with oscillations in rotor speed to pass unchanged; without this block, the steady state changes would modify the terminal voltages. Finally, the time constants of the Phase compensator block are chosen so that the phase lag/lead of the system is fully compensated.

The complete TCSC controller structure is shown in Fig. 2.3. The output signal of the TCSC is the desired capacitive/inductive compensation signal, noted as X_{TCSC} .

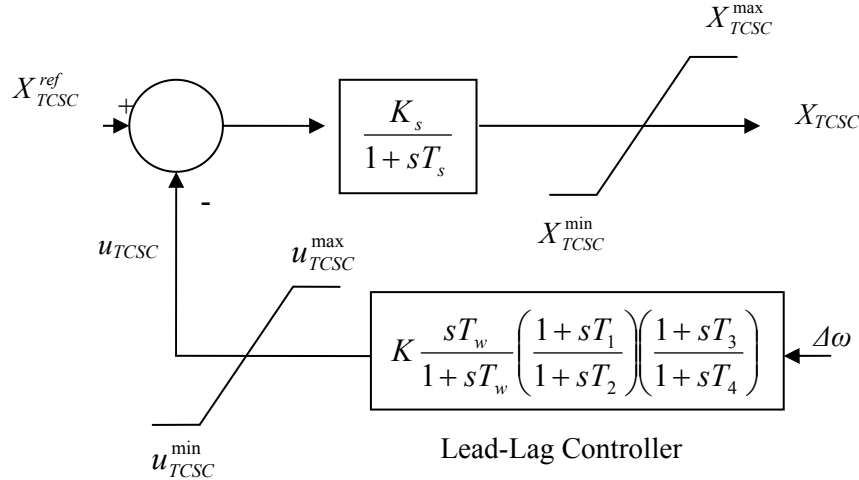


Fig. 2.3: TCSC with lead-lag controller

The structure shown in Fig. 2.3 is expressed as

$$\dot{X}_{TCSC} = (K_s (X_{TCSC}^{ref} - u_{TCSC}) - X_{TCSC}) / T_s \quad (2.5)$$

2.2 Static VAR Compensator (SVC)

2.2.1 Introduction and Basic Operating Principles

The SVC is the most important FACTS device that has been used for a number of years to improve transmission line economics by resolving dynamic voltage problems. The accuracy, availability and fast response enable SVC's to provide high performance steady state and transient voltage control compared with classical shunt compensation. SVCs can perform the duty of providing rapidly controlled Vars more appropriately and thus, by maintaining the voltage, inherently improve transient stability.

In addition to maintaining the reference voltage, SVC can improve the system damping by modulate the reference voltage signal. Such controller use auxiliary control signals to modulate the voltage level to suit the rate of change of phase angle or power follow.

Fig. 2.4 and Fig. 2.5 show typical configuration of a SVC with voltage control and its V-I characteristic respectively. The Fixed Capacitor FC that provides a permanently reactive power and also it designed to act as a harmonic filter. Other two thyristors, Thyristor Controlled Reactor (TCR) and Thyristor Switched Capacitor (TSC) are controlled to provide the required reactive power by the system. Not every SVC needs all above elements.

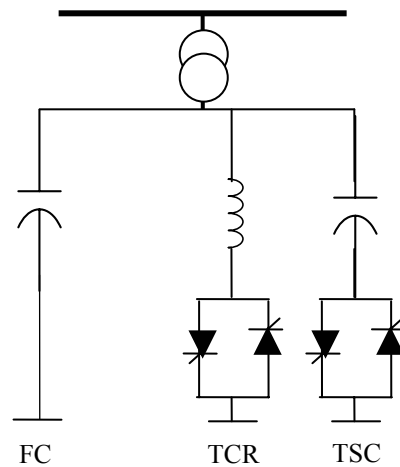


Fig.2.4: SVC Configuration

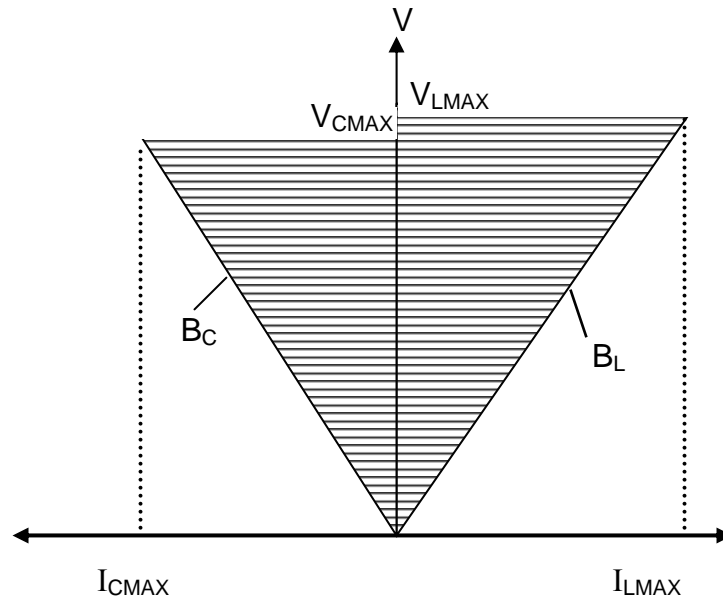


Fig. 2.5: SVC V-I Characteristic

2.2.2 Power Flow Modulation

The real power flow through a transmission line with a SVC located at the middle of the line, Fig. 2.6 is described by:

$$P = 2 \frac{V_i V_m}{X_{ij}} \sin(\delta_{im}) \quad (2.6)$$

where $\delta_{im} = \delta_i - \delta_m$. Since the SVC is located at the electrical midpoint of the line, $\delta_{im} \approx \delta_{ij}/2$ and $V_m \approx V_j$. therefore, the real power can be obtained by:

$$P = 2 \frac{V_i V_j}{X_{ij}} \sin(\delta_{ij}/2) \quad (2.7)$$

The equivalent susceptance of the SVC, B_{SVC} , is given by

$$B_{SVC} = \frac{1}{X_C} - B_L(\alpha) \quad (2.8)$$

and

$$B_L(\alpha) = \frac{2\pi - 2\alpha + \sin(2\alpha)}{\pi X_L}; \quad \pi/2 \leq \alpha \leq \pi \quad (2.9)$$

where α is the thyristor firing angle.

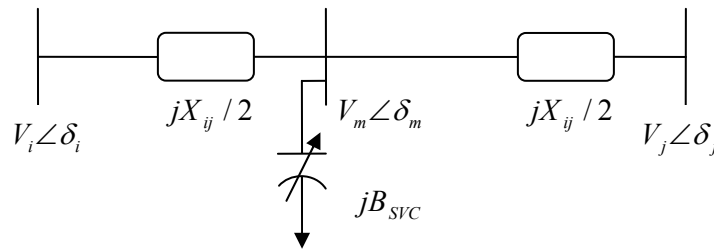


Fig. 2.6: Transmission line with a SVC

2.2.3 Damping Controller Model

The SVC damping controller structure is shown in Fig. 2.7. The susceptance of the SVC, B_{SVC} , could be expressed as:

$$\dot{B}_{SVC} = (K_s (B_{SVC}^{ref} - u_{SVC}) - B_{SVC}) / T_s \quad (2.10)$$

where B_{SVC}^{ref} is the SVC reference susceptance.

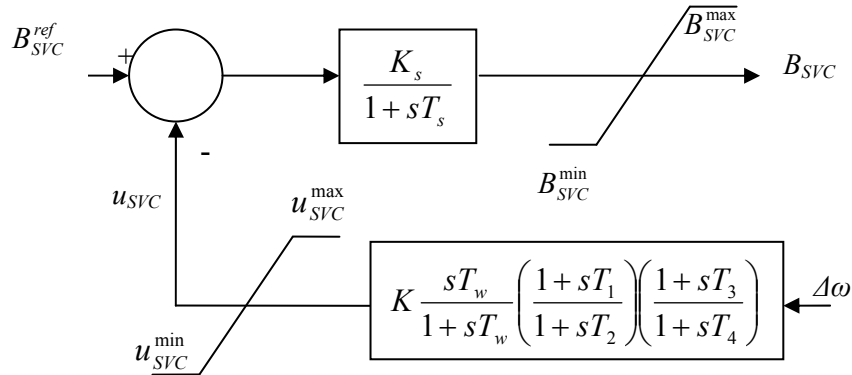


Fig. 2.7: SVC with lead-lag controller

2.3 Thyristor-Controlled Phase Shifter (TCPS)

2.3.1 Introduction and Basic Operating Principles

The basic function of a phase shifter is to provide a means to control power flow in a transmission line. This is accomplished by modifying the voltage phase angle by inserting a variable quadrature voltage in series with the transmission line. The phase of the output voltage can be varied relative to that of the input voltage by simply varying the magnitude of the series quadrature voltage.

Historically, this has been accomplished by specially connected mechanical regulating transformers; because the power flow on the transmission line is proportional to the sine of the angle across the line, the steady state power flow can be controlled by utilizing a phase-shifter to vary the angle across the line. The effectiveness of traditional phase shifters in performing this function is well demonstrated in practice.

Just as traditional phase shifters can be employed to alter steady-state power flow, they can be used to alter transient power flow during system disturbances or outages, if the phase shifter angle can be changed rapidly. Rapid phase angle control could be accomplished by replacing the mechanical tap changer of by a thyristor-switching network.

Transmission angle control can also be applied to damp power oscillations. This could be achieved by varying the active power flow in the line so as to counteract the accelerating and decelerating swings of the disturbed machine(s).

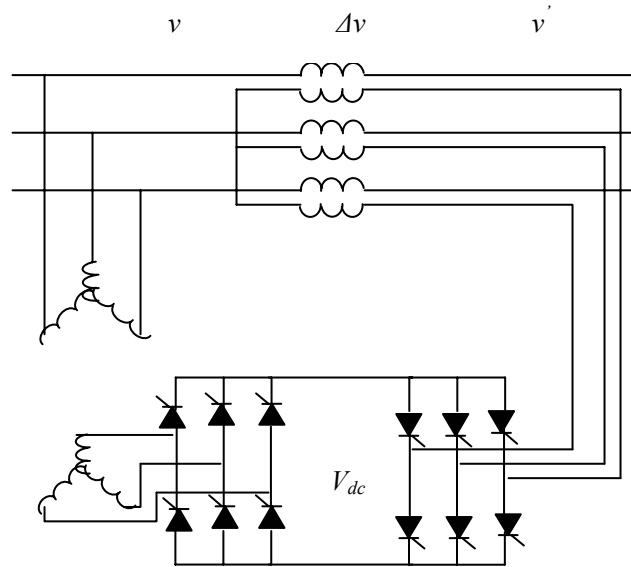


Fig.2.8: TCPS Configuration

2.3.2 Power Flow Modulation

The real power flow through a transmission line equipped with a TCPS is obtained by:

$$P = \frac{V_i V_j}{X_{ij}} \sin(\delta_{ij} - \Phi) \tag{2.11}$$

where Φ is the phase shift in the voltage phase angle resulting from the TCPS.

Hence, the real power flow through the transmission line can be modulated by controlling the angle Φ .

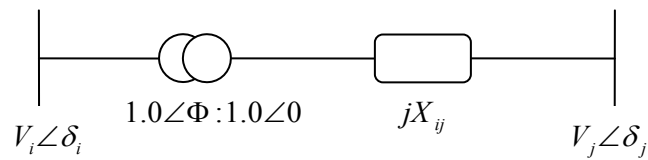


Fig. 2.9: Transmission line with a TCPS

2.3.3 Damping Controller Model

Similarly, Fig. 2.10 shows a TCPS equipped with a lead-lag stabilizer. The TCPS phase angle is expressed as

$$\dot{\Phi}_{TCPS} = (K_s (\Phi_{TCPS}^{ref} - u_{TCPS}) - \Phi_{TCPS}) / T_s \quad (2.12)$$

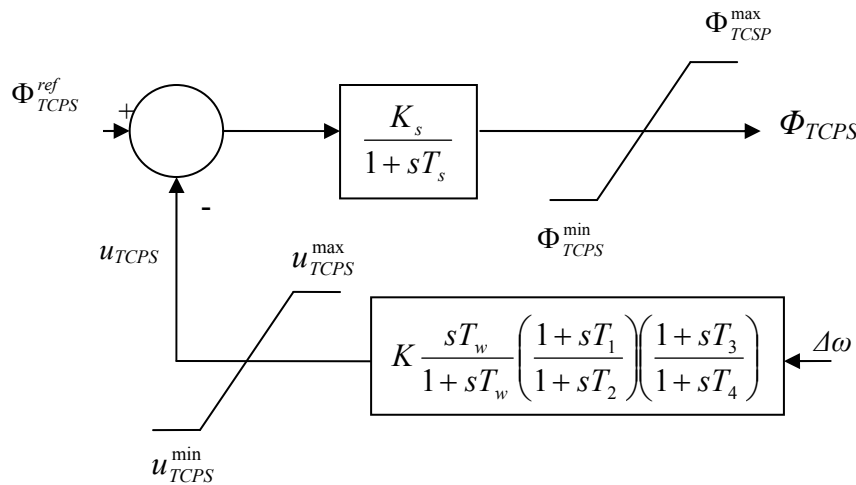


Fig. 2.10: TCPS with lead-lag controller

2.4 Static Synchronous Compensator (STATCOM)

2.4.1 Introduction and Basic Operating Principles

The STATCOM is given this name because in a steady state operating regime it replicates the operating characteristics of a rotating synchronous compensator. The basic electronic block of a STATCOM is a voltage-sourced converter that converts a dc voltage at its input terminals into a three-phase set of ac voltages at fundamental frequency with controllable magnitude and phase angle.

A STATCOM can be used for voltage regulation in a power system, having as an ultimate goal the increase in transmittable power, and improvements of steady-state transmission characteristics and of the overall stability of the system. Under light load conditions, the controller is used to minimize or completely diminish line over voltage; on the other hand, it can be also used to maintain certain voltage levels under heavy loading conditions.

In its simplest form, the STATCOM is made up of a coupling transformer, a VSC, and a dc energy storage device. The energy storage device is a relatively small dc capacitor, and hence the STATCOM is capable of only reactive power exchange with the transmission system. If a dc storage battery or other dc voltage source were used to replace the dc capacitor, the controller can exchange real and reactive power with the transmission system, extending its region of operation from two to four quadrants. Figs. 2.11 and 2.12 show a functional model and the V-I characteristic of a STATCOM respectively.

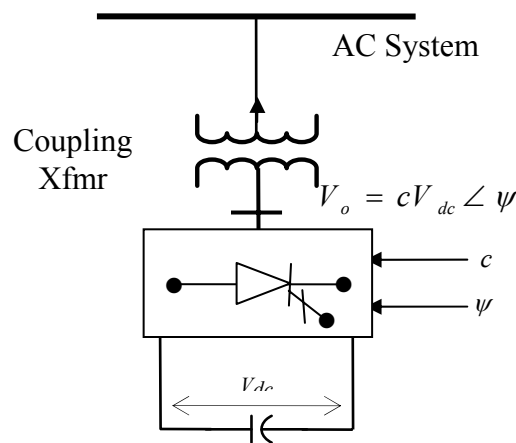


Fig.2.11: STATCOM Configuration

The STATCOM's output voltage magnitude and phase angle can be varied. By changing the phase angle ψ of the operation of the converter switches relative to the phase of the ac system bus voltage, the voltage across the dc capacitor can be controlled, thus controlling the magnitude of the fundamental component of the converter ac output voltage, as $V_o = cV_{dc}$.

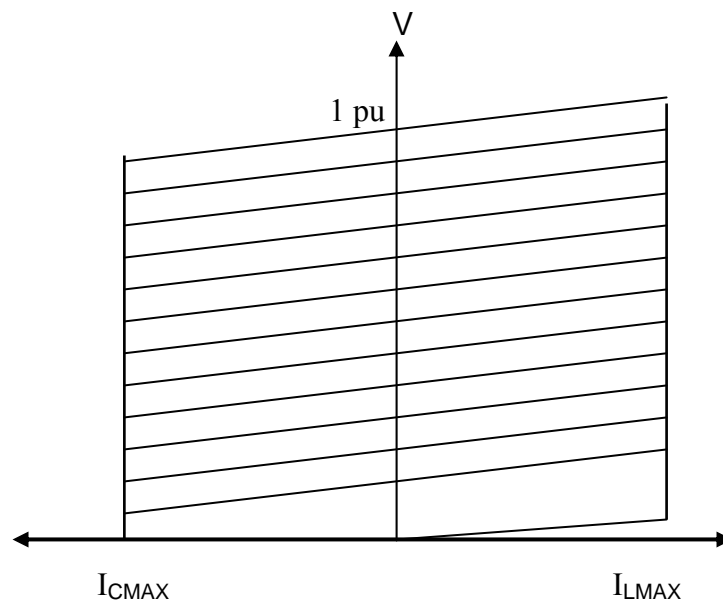


Fig. 2.12: STATCOM V-I characteristic

2.4.2 Power Flow Modulation

The STATCOM is modeled as a voltage-sourced converter behind a step down transformer as shown in Fig. 2.11. The STATCOM generates a controllable AC-voltage source $V_{out}(t) = V_o \sin(\omega t - \psi)$ behind the leakage reactance. The voltage difference between the STATCOM bus AC voltage and $V_{out}(t)$ produces active and reactive power exchange between the STATCOM and the power system.

$$V_o = cV_{DC}(\cos\psi + i\sin\psi) = cV_{DC}\angle\psi \quad (2.13)$$

$$\frac{dV_{DC}}{dt} = \frac{c}{C_{DC}}(I_{LD}\cos\psi + I_{LQ}\sin\psi) \quad (2.14)$$

Where, for the PWM inverter, $c = mk$ and k is the ratio between AC and DC voltage; m is the modulation ratio defined by PWM, and ψ is defined by the PWM.

2.4.3 Damping Controller Model

There are two basic controllers implemented in STATCOM, an AC voltage regulation and a DC voltage regulation shown in Fig. 2.13 and Fig. 2.14 respectively. The AC voltage controller regulates the reactive power exchange while the DC controller regulates the active power exchange with the power system. The DC voltage across the DC capacitor of the STATCOM is controlled to be constant for normal operation of the PWM inverter.

Installing both PI DC and PI AC voltage regulators lead to system instability [81,82], if they are designed independently, because of the interaction of the two controllers. Coordination design of the two controllers is necessary to avoid negative damping to the power system.

Because both of AC and DC STATCOM voltage regulators controllers are not designed for power oscillation damping (POD) duty, an auxiliary conventional lead-lag structure damping controller on the AC/DC voltage control loops of the STATCOM as shown are proposed in the design.

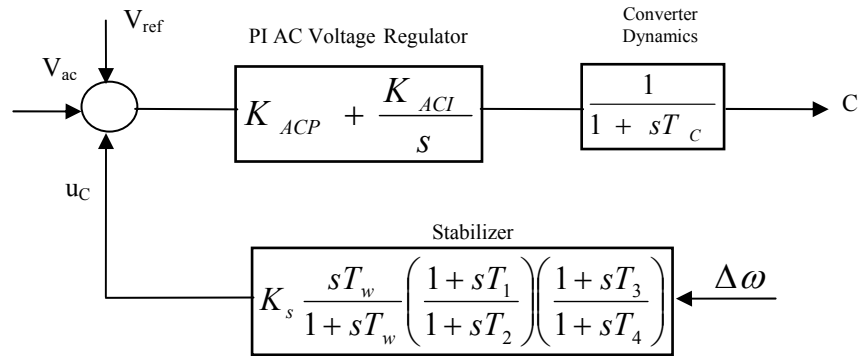


Fig. 2.13: STATCOM dynamic model of AC Voltage Regulator and Stabilizer (with PWM)

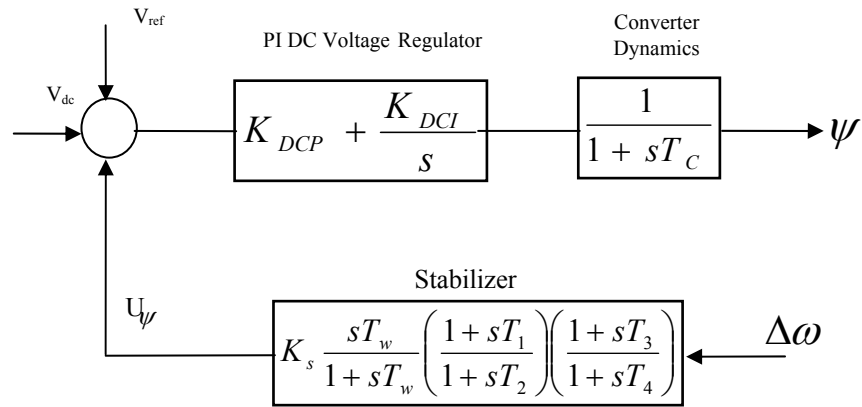


Fig. 2.14: STATCOM dynamic model of DC Voltage Regulator and Stabilizer (with PWM)

CHAPTER 3

POWER SYSTEM MODEL

3.1 Generator and Excitation model

The generator is represented by the 3rd order model consisting of the swing equation and the generator internal voltage equation. The swing equation can be written as

$$\dot{\delta} = \omega_b(\omega - 1) \quad (3.1)$$

$$\dot{\omega} = (P_m - P_e - D(\omega - 1)) / M \quad (3.2)$$

The internal voltage, E_q' , is given by

$$\dot{E}_q' = (E_{fd} - (x_d - x_d')i_d - E_q') / T_{do}' \quad (3.3)$$

The real power output of the generator is described as

$$P_e = v_d i_d + v_q i_q \quad (3.4)$$

The excitation system can be represented by the IEEE type-ST1 system shown in Fig. 3.1, and is described by

$$\dot{E}_{fd} = (K_A (V_{ref} - v + u_{PSS}) - E_{fd}) / T_A \quad (3.5)$$

$$v = (v_d^2 + v_q^2)^{1/2} \quad (3.6)$$

$$v_d = x_q i_q \quad (3.7)$$

$$v_q = E_q' - x_d' i_d \quad (3.8)$$

A conventional lead-lag PSS is installed in the feedback loop to generate a supplementary stabilizing signal u_{pss} , see Fig. 3.1. The PSS input is the change in the machine speed.

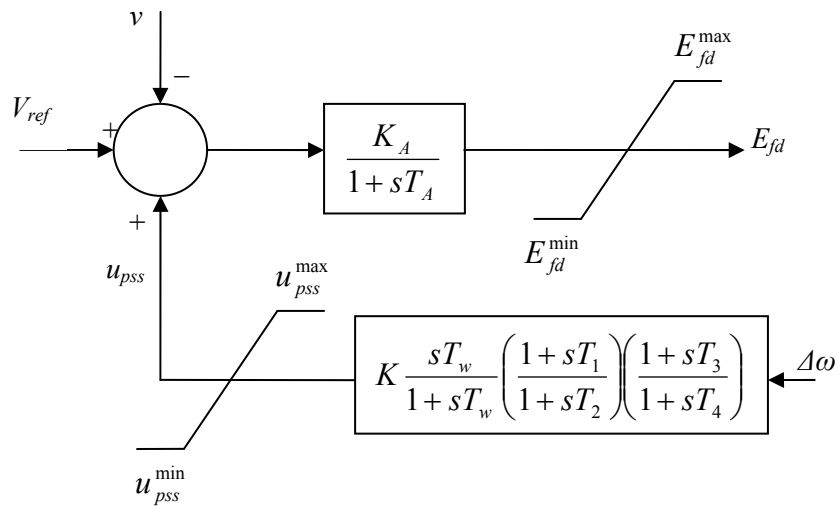


Fig. 3.1: IEEE type-ST1 excitation system with PSS

3.2 Single Machine Infinite Bus (SMIB) Power System

3.2.1 Phillips-Heffron model of SMIB system installed with G1 FACTS Devices

In the design of electromechanical mode damping controllers, the linearized incremental model around a nominal operating point is usually employed. The SMIB system shown in Fig. 3.2 is considered, where the detailed system data is shown the Appendix A.

Referring to Fig. 3.2, the d and q components of the machine current i and terminal voltage v can be written as

$$i = i_d + ji_q \quad (3.9)$$

$$v = v_d + jv_q \quad (3.10)$$

The voltage v_s can be written as

$$v_s = v - jX_{TCSC}i, \quad (3.11)$$

where i is the generator armature current.

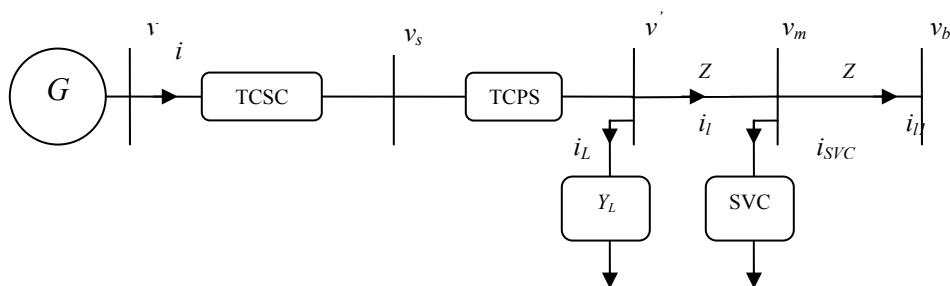


Fig. 3.2: SMIB with G1 FACTS Devices

The d and q components of v_s can be written as

$$v_{sd} = x_{qs} i_q \quad (3.12)$$

$$v_{sq} = E'_q - x'_{ds} i_d \quad (3.13)$$

where

$$x_{qs} = x_q + X_{TCSC} \quad (3.14)$$

$$x'_{ds} = x'_d + X_{TCSC} \quad (3.15)$$

The voltage v' can be written as

$$v' = \frac{v_s}{k} = \frac{v_s}{k \angle \Phi_{TCPS}} \quad (3.16)$$

The d and q components of v' can be written as

$$v'_d = \frac{1}{k} [v_{sd} \cos \Phi + v_{sq} \sin \Phi] \quad (3.17)$$

$$v'_q = \frac{1}{k} [v_{sq} \cos \Phi - v_{sd} \sin \Phi] \quad (3.18)$$

The load current

$$i_L = v' Y_L, \quad (3.19)$$

where the load admittance Y_L is given as

$$Y_L = g + jb \quad (3.20)$$

The d and q components of i_L can be written as

$$i_{Ld} = g v'_d - b v'_q \quad (3.21)$$

$$i_{Lq} = g v'_q + b v'_d \quad (3.22)$$

Then, the line current

$$i_l = i - i_L \quad (3.23)$$

The d and q components of i_l can be written as

$$i_{ld} = i_d - i_{Ld} \quad (3.24)$$

$$i_{lq} = i_q - i_{Lq} \quad (3.25)$$

The midpoint voltage

$$v_m = v' - i_l Z \quad (3.26)$$

Hence, the d and q components of v_m can be written as

$$v_{md} = c_1 v'_d - c_2 v'_q - R i_d + X i_q \quad (3.27)$$

$$v_{mq} = c_2 v'_d + c_1 v'_q - X i_d - R i_q \quad (3.28)$$

where

$$c_1 = 1 + Rg - Xb \quad (3.29)$$

$$c_2 = Rb + Xg \quad (3.30)$$

The SVC current can be given as

$$i_{SVC} = v_m Y_{SVC} \quad (3.31)$$

Then the line current in this section i_{ll} is given as

$$i_{ll} = i_l - i_{SVC} \quad (3.32)$$

The infinite bus voltage

$$v_b = v_m - i_{ll} Z \quad (3.33)$$

The components of v_b can be written as

$$v_{bd} = v_b \sin \delta = v_{md} - R i_{d1} + X i_{q1} \quad (3.34)$$

$$v_{bq} = v_b \cos \delta = v_{mq} - Xi_{d1} - Ri_{q1} \quad (3.35)$$

Substituting (3.12)-(3.33) into (3.34) and (3.35), the following two equations can be obtained

$$c_3 i_d + c_4 i_q = v_b \sin \delta + c_7 E'_q \quad (3.36)$$

$$c_5 i_d + c_6 i_q = v_b \cos \delta - c_8 E'_q \quad (3.37)$$

Solving (3.36) and (3.37) simultaneously, i_d and i_q expressions can be obtained.

Linearizing (3.36) and (3.37) at the nominal loading condition, Δi_d and Δi_q can be expressed in terms of $\Delta \delta$, $\Delta E'_q$, ΔB_{SVC} , ΔX_{TCSC} , and $\Delta \Phi_{TCPS}$ as follows.

$$c_3 \Delta i_d + c_4 \Delta i_q = v_b \cos \delta \Delta \delta + c_7 \Delta E'_q + c_9 \Delta B_{SVC} + c_{11} \Delta X_{TCSC} + c_{13} \Delta \Phi_{TCPS} \quad (3.38)$$

$$c_5 \Delta i_d + c_6 \Delta i_q = -v_b \sin \delta \Delta \delta - c_8 \Delta E'_q + c_{10} \Delta B_{SVC} + c_{12} \Delta X_{TCSC} + c_{14} \Delta \Phi_{TCPS} \quad (3.39)$$

Solving (3.38) and (3.39) simultaneously, Δi_d and Δi_q can be expressed as

$$\Delta i_d = c_{15} \Delta \delta + c_{17} \Delta E'_q + c_{19} \Delta B_{SVC} + c_{21} \Delta X_{TCSC} + c_{23} \Delta \Phi_{TCPS} \quad (3.40)$$

$$\Delta i_q = c_{16} \Delta \delta + c_{18} \Delta E'_q + c_{20} \Delta B_{SVC} + c_{22} \Delta X_{TCSC} + c_{24} \Delta \Phi_{TCPS} \quad (3.41)$$

The constants c_1 - c_{24} are expressions of :

$$Z, Y_L, x'_d, x'_q, i_{d0}, i_{q0}, E'_{q0}, B_{SVC}, X_{TCSC0}, \text{ and } \Phi_{TCPS0}$$

The linearized form of v_d and v_q can be written as

$$\Delta v_d = x'_q \Delta i_q \quad (3.42)$$

$$\Delta v_q = \Delta E'_q - x'_d \Delta i_d \quad (3.43)$$

Using Equations (3.40) to (3.41), the following expressions can be easily obtained

$$\Delta P_e = K_1 \Delta \delta + K_2 \Delta E'_q + K_{pB} \Delta B_{SVC} + K_{pX} \Delta X_{TCSC} + K_{p\Phi} \Delta \Phi_{TCPS} \quad (3.44)$$

$$(K_3 + sT'_{do}) \Delta E'_q = \Delta E_{fd} - K_4 \Delta \delta - K_{qB} \Delta B_{SVC} - K_{qX} \Delta X_{TCSC} - K_{q\Phi} \Delta \Phi_{TCPS} \quad (3.45)$$

$$\Delta v = K_5 \Delta \delta + K_6 \Delta E'_q + K_{vB} \Delta B_{SVC} + K_{vX} \Delta X_{TCSC} + K_{v\Phi} \Delta \Phi_{TCPS} \quad (3.46)$$

where the constants K_1 - K_6 , K_{pB} , K_{pX} , $K_{p\Phi}$, K_{qB} , K_{qX} , $K_{q\Phi}$, K_{vB} , K_{vX} , and $K_{v\Phi}$ are expressions of c_1 - c_{24} .

The above linearizing procedure yields the following linearized power system model

$$\begin{bmatrix} \dot{\Delta \delta} \\ \dot{\Delta \omega} \\ \dot{\Delta E'_q} \\ \dot{\Delta E_{fd}} \end{bmatrix} = \begin{bmatrix} 0 & 377 & 0 & 0 \\ -\frac{K_1}{M} & -\frac{D}{M} & -\frac{K_2}{M} & 0 \\ -\frac{K_4}{T'_{do}} & 0 & -\frac{K_3}{T'_{do}} & \frac{1}{T'_{do}} \\ -\frac{K_A K_5}{T_A} & 0 & -\frac{K_A K_6}{T_A} & -\frac{1}{T_A} \end{bmatrix} \begin{bmatrix} \Delta \delta \\ \Delta \omega \\ \Delta E'_q \\ \Delta E_{fd} \end{bmatrix} + \begin{bmatrix} 0 & 0 & 0 & 0 \\ 0 & -\frac{K_{pB}}{M} & -\frac{K_{pX}}{M} & -\frac{K_{p\Phi}}{M} \\ 0 & -\frac{K_{qB}}{T'_{do}} & -\frac{K_{qX}}{T'_{do}} & -\frac{K_{q\Phi}}{T'_{do}} \\ \frac{K_A}{T_A} & -\frac{K_A K_{vB}}{T_A} & -\frac{K_A K_{vX}}{T_A} & -\frac{K_A K_{v\Phi}}{T_A} \end{bmatrix} \begin{bmatrix} u_{PSS} \\ \Delta B_{SVC} \\ \Delta X_{TCSC} \\ \Delta \Phi_{TCPS} \end{bmatrix} \quad (3.47)$$

$$\frac{dV_{DC}}{dt} = \frac{c}{C_{DC}} (I_{LD} \cos\psi + I_{LQ} \sin\psi) \quad (3.50)$$

Where, for the PWM inverter, $c = mk$ and k is the ratio between AC and DC voltage; m is the modulation ratio defined by PWM, and ψ is defined by the PWM.

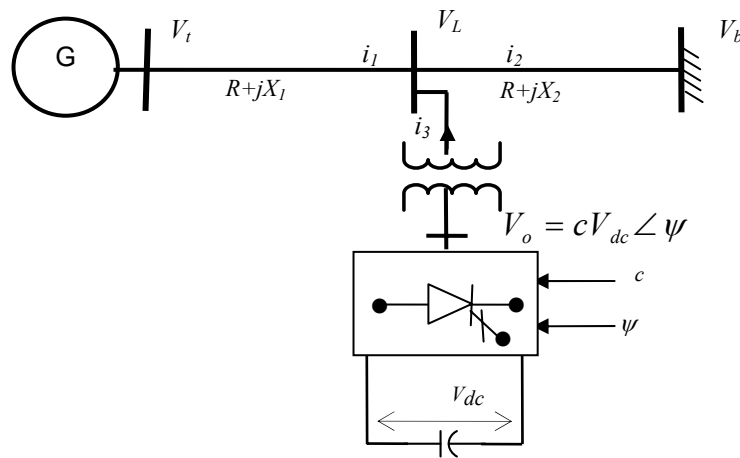


Fig. 3.4: Single machine with STATCOM

The terminal voltage V_t can be written as

$$V_t = \left[i_1(jX_1) + i_1(jX_2) - \frac{X_2}{X_t} V_t + j \frac{X_2 X_1}{X_t} i_1 + \frac{X_2}{X_t} V_o + V_b \right] \quad (3.51)$$

Rearranging the above equation to be

$$C_1 V_t - C_2 V_o - V_b = j C_3 i_1$$

where

$$V_b = V_b \sin \delta + j V_b \cos \delta$$

$$i_1 = i_{1d} + j i_{1q}$$

$$V_t = V_d + j V_q = X_q i_{1q} + j(e_{q'} - X_d i_{1d})$$

C_1 , C_2 , and C_3 are constant.

From the above it is possible to obtain

$$i_{1q} = \frac{C_2 c V_{dc} \cos \psi + V_b \sin \delta}{C_1 X_q + C_3} \quad (3.52)$$

$$i_{1d} = \frac{C_1 e_{q'} - C_2 c V_{dc} \sin \psi + V_b \cos \delta}{C_1 X_{d'} + C_3} \quad (3.53)$$

Linearizing equation 3.52 & 3.53 yield to

$$\Delta i_{1d} = C_7 \Delta E_{q'} + C_{13} \Delta \delta + C_{14} \Delta \psi + C_{15} \Delta c + C_{16} \Delta V_{dc} \quad (3.54)$$

$$\Delta i_{1q} = C_9 \Delta \delta + C_{10} \Delta \psi + C_{11} \Delta c + C_{12} \Delta V_{dc} \quad (3.55)$$

The linearized form of v_d and v_q can be written as

$$\Delta v_d = x_q \Delta i_q \quad (3.56)$$

$$\Delta v_q = \Delta E_q' - x_d' \Delta i_d \quad (3.57)$$

Using Equations (5.54) to (5.57), the following expressions can be easily obtained

$$\Delta P_e = K_1 \Delta \delta + K_2 \Delta E_q' + K_{pdc} \Delta V_{dc} + K_{pc} \Delta c + K_{p\psi} \Delta \psi \quad (3.58)$$

$$(K_3 + s T_{do}') \Delta E_q' = \Delta E_{fd} - K_4 \Delta \delta - K_{qdc} \Delta V_{dc} + K_{qc} \Delta c + K_{q\psi} \Delta \psi \quad (3.59)$$

$$\Delta v = K_5 \Delta \delta + K_6 \Delta E'_q + K_{vdc} \Delta V_{dc} + K_{vc} \Delta c + K_{v\psi} \Delta \psi \quad (3.60)$$

where the constants K_1 - K_6 , K_{pdc} , K_{pc} , $K_{p\psi}$, K_{qdc} , K_{qc} , $K_{q\psi}$, K_{vdc} , K_{vc} , and $K_{v\psi}$ are expressions of c_1 - c_{12} .

The above linearizing procedure yields the following linearized power system model:

$$\begin{bmatrix} \dot{\Delta \delta} \\ \dot{\Delta \omega} \\ \dot{\Delta E}'_q \\ \dot{\Delta E}'_{fd} \\ \dot{\Delta V}_{DC} \end{bmatrix} = \begin{bmatrix} 0 & 377 & 0 & 0 & 0 \\ -\frac{K_1}{M} & -\frac{D}{M} & -\frac{K_2}{M} & 0 & -\frac{K_{PDC}}{M} \\ \frac{K_4}{T'_{do}} & 0 & -\frac{K_3}{T'_{do}} & \frac{1}{T'_{do}} & \frac{K_{qDC}}{T'_{do}} \\ -\frac{K_A K_5}{T_A} & 0 & -\frac{K_A K_6}{T_A} & -\frac{1}{T_A} & -\frac{K_A K_{vDC}}{T_A} \\ K_7 & 0 & K_8 & 0 & K_9 \end{bmatrix} \quad (3.61)$$

$$\times \begin{bmatrix} \Delta \delta \\ \Delta \omega \\ \Delta E'_q \\ \Delta E'_{fd} \\ \Delta V_{dc} \end{bmatrix} + \begin{bmatrix} 0 & 0 & 0 \\ 0 & -\frac{K_{PC}}{M} & -\frac{K_{P\psi}}{M} \\ 0 & \frac{K_{qC}}{T'_{do}} & \frac{K_{q\psi}}{T'_{do}} \\ \frac{K_A}{T_A} & -\frac{K_A K_{vC}}{T_A} & -\frac{K_A K_{v\psi}}{T_A} \\ 0 & K_{dc} & K_{d\psi} \end{bmatrix} \times \begin{bmatrix} \Delta u_{PSS} \\ \Delta C \\ \Delta \psi \end{bmatrix}$$

3.3 Multimachine Power System

In this section the SMIB model is extended to describe a multi-machine electric power system. Because of the interaction among machines, the K_1 - K_6 become matrices. Same machine model describe in section 3.1 is used but for n-machine.

3.3.1 Phillips-Heffron model of multi-machine system

To find K1-K6 matrices, the initial conditions must be found first and the admittance matrix reduced to be in order of machines number.

Let the generator current matrix equation be

$$[I] = [Y_t][V] \quad (3.62)$$

For the i^{th} machine of an n-machine system in the machine coordinates d-q, the current has n terms [1].

$$i_i = i_{di} + ji_{qi} = \sum_{j=1}^n Y_{ij} [E_{qj} e^{j(90^\circ + \delta_{ik} + \beta_{ij})} + (X_{qj} - X'_{dj}) I_{qj} e^{j(\beta_{ij} + \delta_{ik})}] \quad (3.63)$$

$$i_{di} = \sum_{j=1}^n Y_{ij} [-S_{ij} E'_{qj} + (X_{qj} - X'_{dj}) C_{ij} I_{qj}] \quad (3.63.a)$$

$$i_{qi} = \sum_{j=1}^n Y_{ij} [C_{ij} E'_{qj} + (X_{qj} - X'_{dj}) S_{ij} I_{qj}] \quad (3.64)$$

where

$$C_{ij} = \cos(\beta_{ij} - \delta_{ij}) ,$$

$$S_{ij} = \sin(\beta_{ij} - \delta_{ij})$$

Linearizing (3.63) & (3.64) yields

$$[\Delta I_d] = [P_d][\Delta \delta] + [Q_d][\Delta E'_q] + [M_d][\Delta I_q] \quad (3.65)$$

$$[L_q][\Delta I_q] = [P_q][\Delta \delta] + [Q_q][\Delta E'_q] \quad (3.66)$$

Where

$$P_{dij} = -Y_{ij} [C_{ij} E'_{qj} + (X_{qj} - X'_{dj}) S_{ij} I_{qj}] \quad j \neq i$$

$$P_{qij} = -Y_{ij} [S_{ij} E'_{qj} - (X_{qj} - X'_{dj}) C_{ij} I_{qj}] \quad j \neq i$$

$$P_{dii} = -\sum_{j \neq i} P_{dij} \quad , \quad P_{qii} = -\sum_{j \neq i} P_{qij}$$

$$Q_{dij} = -Y_{ij} S_{ij} \quad , \quad Q_{qij} = -Y_{ij} C_{ij} \quad j = 1, \dots, n$$

$$L_{qij} = -Y_{ij} (X_{qi} - X'_{di}) S_{ij}$$

$$L_{qii} = 1 - Y_{ii} (X_{qi} - X'_{di}) S_{ii} \quad , \quad M_{dij} = Y_{ij} (X_{qj} - X'_{dj}) C_{ij} \quad , j = 1, \dots, n$$

Initial values of $E'_q, I_{qj},$ and δ_{ij} (for C_{ij} and S_{ij}), $j = 1, \dots, n$, must be used.

The solutions of $[\Delta I_d]$ and $[\Delta I_q]$ 3.65 & 3.66 become

$$[\Delta I_d] = [Y_d][\Delta E'_q] + [F_d][\Delta \delta] \quad (3.67)$$

$$[\Delta I_q] = [Y_q][\Delta E'_q] + [F_q][\Delta \delta] \quad (3.68)$$

Solving (3.04)-(3.08), linearizing, and substituting for Δi_{di} and Δi_{qi} from (3.67) and (3.68)

results in

$$\Delta P_e = K_1 \Delta \delta + K_2 \Delta E'_q \quad (3.69)$$

where

$$K_1 = D_t [F_d] + Q_t [F_q] \quad ,$$

$$K_2 = D_t [Y_d] + Q_t [Y_q] + [I_{qii}]$$

$$\text{and} \quad D_t = (X_{qi} - X'_{di}) I_{qio} \quad ,$$

$$Q_t = (X_{qi} - X'_{di}) I_{dio} + E'_{qio}$$

The internal voltage equation for n-machines may be written

$$[1 + sT'_{doi} K_{3ii}] \Delta E'_{qi} = K_{3ii} [\Delta E_{FDi} - \sum_{j \neq i}^n \frac{1}{K_{3ij}} \Delta E'_{qj} - \sum_{j=1}^n K_{4ij} \Delta \delta_j] \quad (3.70)$$

Where

$$K_3 = [[1] + [X_{di} - X'_{di}][Y_{dii}]]^{-1},$$

$$K_4 = [X_{di} - X'_{di}][F_{dii}]$$

Moreover, linearizing the terminal voltage to be:

$$\Delta v = K_5 \Delta \delta + K_6 \Delta E'_q \quad (3.71)$$

Where

$$K_5 = D_v x_q F_q - Q_v x'_d F'_d \quad (3.72)$$

$$K_6 = D_v x_q Y_q - Q_v x'_d Y'_d + Q_v \quad (3.73)$$

$$D_v = v_0^{-1} v_{d0} \quad (3.74)$$

$$Q_v = v_0^{-1} v_{q0} \quad (3.75)$$

It should be noticed that v_0 and v_{d0} are diagonal matrices of the respective initial conditions.

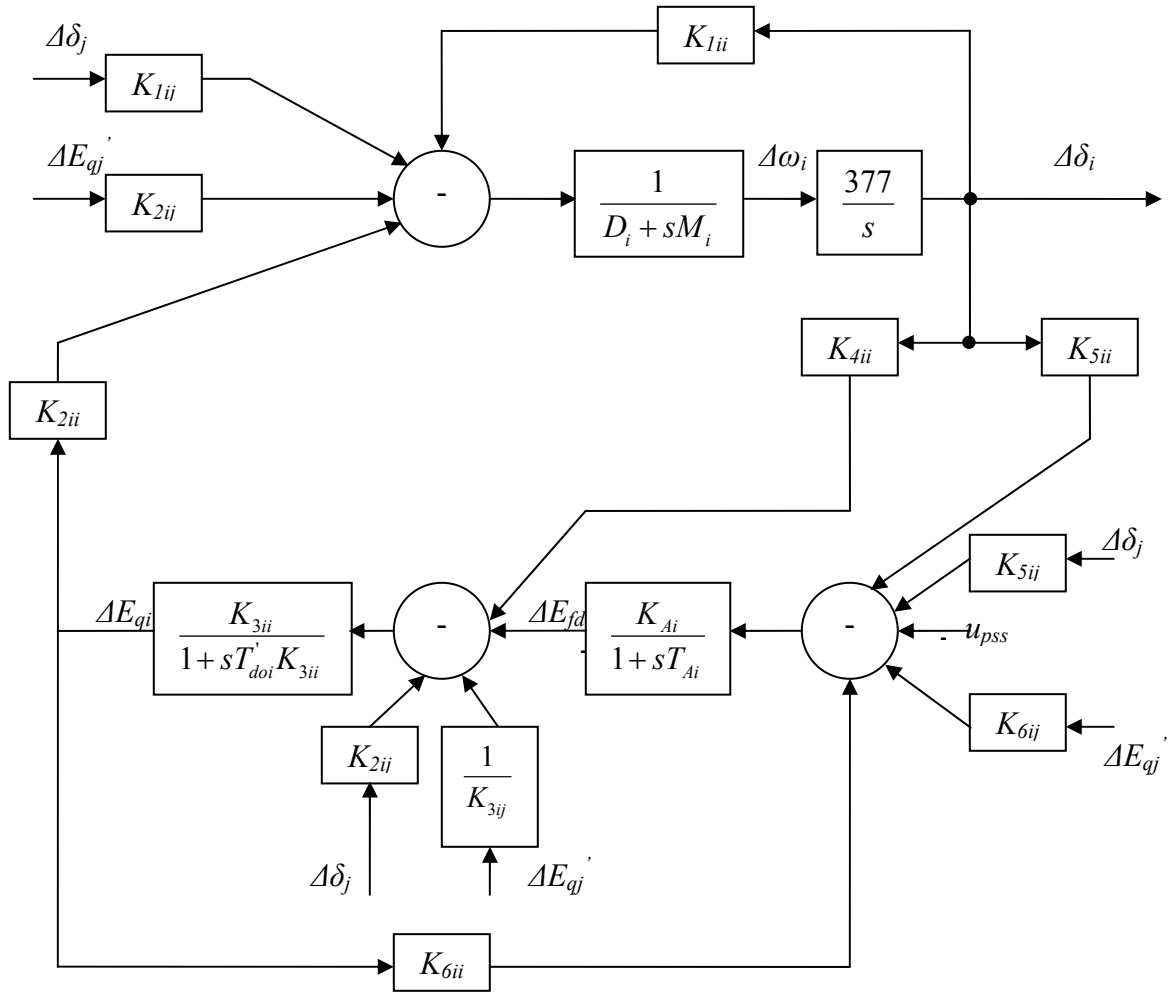


Fig. 3.5: Linearized model of the i^{th} machine in multimachine power system

3.3.2 Phillips-Heffron model of multi-machine Installed With SVC & TCSC

In the previous multimachine model, the Y -matrix is assumed to be constant. If a FACTS-device is to be added to the system, this assumption is no longer valid. The Y -matrix will be a function of the FACTS device control signal. We assume, for n -machines power system, a FACTS device will be installed at node K for SVC and between nodes R and K for TCSC. In order to obtain a systematic expression for Y_{ij} which includes the influence of the FACTS-based stabilizers, the following procedure is carried out:

1. From the load flow, convert the loads as a constant admittance in the admittance matrix.
2. Form Y_{aug} by modifying the admittance matrix to include the transient reactance X'_d of the machines.
3. Reduce the Y_{aug} by deleting all buses except the internal generator and FACTS device nodes to form Y_{FACTS} .

If n is the number of machines, the Y_{FACTS} size will be:

- $(n+1) \times (n+1)$ in case of SVC is installed; and
 - $(n+2) \times (n+2)$ in case of TCSC is installed.
4. Y_{RR} sub matrix shown below contains nodes associated with FACTS-stabilizer,

$$Y_{FACTS} = \begin{bmatrix} Y_{NN} & Y_{NR} \\ Y_{RN} & Y_{RR} \end{bmatrix} \quad (3.76)$$

- For SVC-based stabilizer Y_{RR} is 1×1 matrix and the output signal B_{SVC} is modeled as:

$Y_{RR} = y_{kk} - jB_{SVC}$, where y_{kk} is the self admittance at node K

- For TCSC-based stabilizer Y_{RR} is 2×2 matrix and the output signal X_{CSC} is modeled as:

$$Y_{RR} = \begin{bmatrix} y_{kk} + \frac{jX_{CSC}}{z_{KR}(z_{KR} - jX_{CSC})} & y_{kr} - \frac{jX_{CSC}}{z_{KR}(z_{KR} - jX_{CSC})} \\ y_{rk} - \frac{jX_{CSC}}{z_{KR}(z_{KR} - jX_{CSC})} & y_{rr} + \frac{jX_{CSC}}{z_{KR}(z_{KR} - jX_{CSC})} \end{bmatrix} \quad (3.77)$$

5. Y_{FACTS} is further reduced to

$$Y = Y_{NN} - Y_{NR}Y_{RR}^{-1}Y_{RN} \quad (3.78)$$

Now, linearizing equation (3.63) taking into account the FACTS-based stabilizer output ΔF , which can be ΔB_{SVC} or ΔX_{CSC} .

$$\Delta I_i = \Delta I_{di} + j\Delta I_{qi} = \sum_{k=1}^n \left\{ \begin{array}{l} Y_{ik0} \Delta [E_{qi} e^{j(90^\circ + \delta_{ik})} + (X_{qk} - X'_{dk}) I_{qk} e^{j\delta_{ik}}] - \\ [E_{qi} e^{j(90^\circ + \delta_{ik})} + (X_{qk} - X'_{dk}) I_{qk} e^{j\delta_{ik}}]_0 \frac{\partial Y_{ik}(\Delta F)}{\partial \Delta F} \Delta F \end{array} \right\} \quad (3.79)$$

$$[\Delta I_d] = [P_d][\Delta \delta] + [Q_d][\Delta E'_q] + [M_d][\Delta I_q] + [A_d I_n][\Delta F] \quad (3.80)$$

$$[L_q][\Delta I_q] = [P_q][\Delta \delta] + [Q_q][\Delta E'_q] + [A_q I_n][\Delta F] \quad (3.81)$$

Thus we can obtain

$$[\Delta I_d] = [Y_d][\Delta E'_q] + [F_d][\Delta \delta] + [B_d I_n][\Delta F] \quad (3.82)$$

$$[\Delta I_q] = [Y_q][\Delta E'_q] + [F_q][\Delta \delta] + [B_q I_n][\Delta F] \quad (3.83)$$

Linearizing (3.1)-(3.8) for n-machine system the following model is obtained,

$$s\Delta \delta = \omega_0 \Delta \omega \quad (3.84)$$

$$s\Delta\omega = M^{-1}(-K_1\Delta\delta - D\Delta\omega - K_2\Delta E'_q - K_p I_n \Delta F) \quad (3.85)$$

$$[K_3 + sT'_{doi}]\Delta E'_{qi} = \Delta E_{FDi} - K_4\Delta\delta_j - K_q I_n \Delta F \quad (3.86)$$

$$(1 + sT_A)\Delta E_{FD} = -K_A[K_5\Delta\delta + K_6\Delta E'_q + \Delta U_{PSS} + K_V I_n \Delta F] \quad (3.87)$$

Fig. 3.6 shows a block diagram of the i th machine in a multimachine power system equipped with a G1 FACTS device.

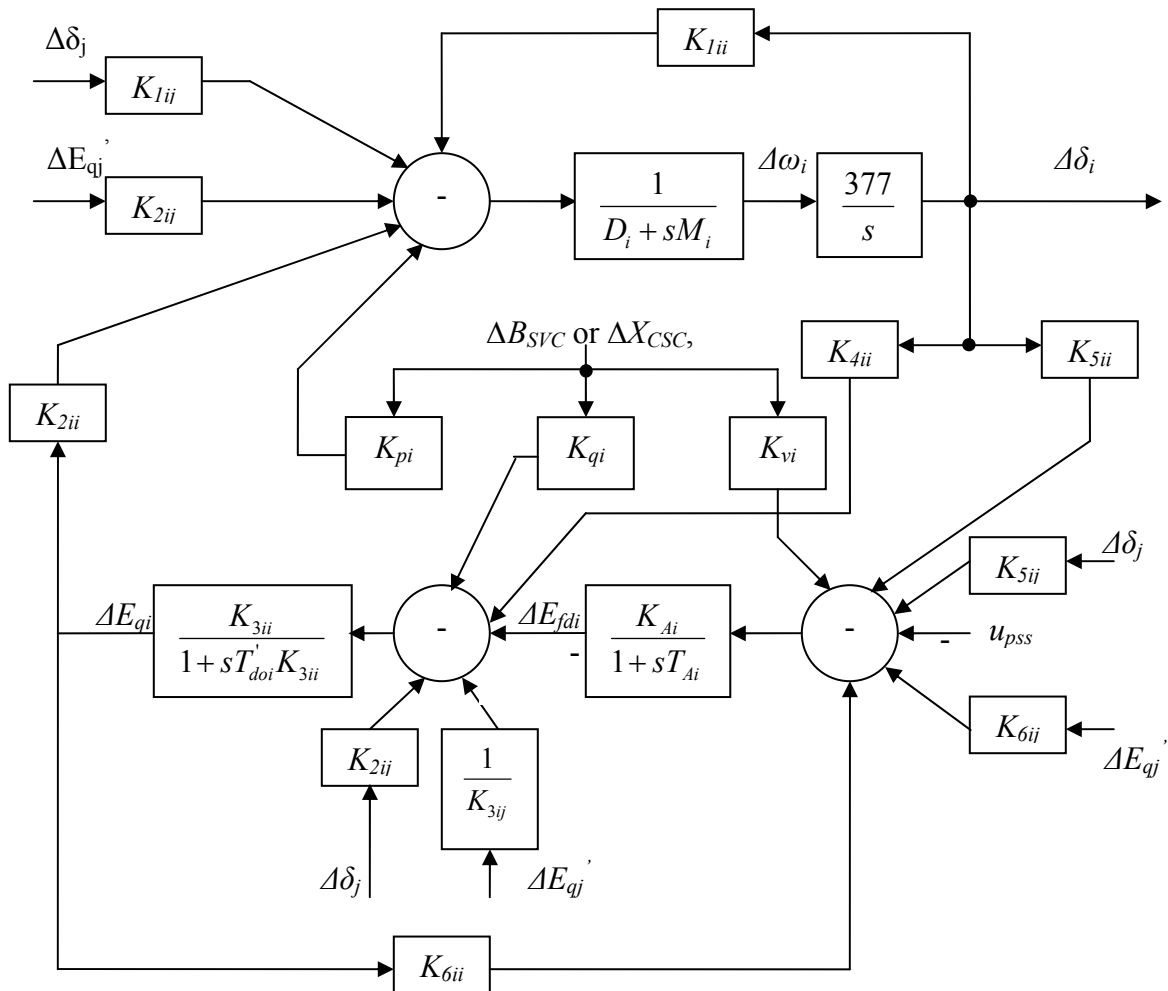


Fig. 3.6: Linearized model of the i^{th} machine in multimachine power system with SVC & TCSC

CHAPTER 4

PROPOSED APPROACH

In this chapter the proposed approach is illustrated as follows. The location of the reactive power compensation devices and PSSs are identified in multimachine power system by using modal analysis method and participation factor technique respectively. Then, the controllability measurement is employed by different controllers' inputs. Finally, the PSO is proposed in this thesis to search for optimal parameters setting.

4.1 Modal Analysis Method

The modal analysis method is based on the linear steady-state power flow equations of the system, which usually expressed in the following form

$$\begin{bmatrix} \Delta P \\ \Delta Q \end{bmatrix} = \begin{bmatrix} J_{P\theta} & J_{PV} \\ J_{Q\theta} & J_{QV} \end{bmatrix} \begin{bmatrix} \Delta\theta \\ \Delta V \end{bmatrix} \quad (4.1)$$

Where

ΔP = Vector of increment changes in bus active power

ΔQ = Vector of increment changes in bus reactive power

$\Delta\phi$ = Vector of increment changes in bus voltage angle

ΔV = Vector of increment changes in bus voltage magnitude

and the matrix relating the variables is the Jacobian matrix. The voltage stability is affected by variations in both P and Q, but the method of modal analysis examines only variation of Q with respect to V. therefore, if we set $\Delta P = 0$, we have the following result for ΔQ .

$$\begin{aligned}\Delta Q &= \left[J_{QV} - J_{Q\theta} J_{P\theta}^{-1} J_{PV} \right] \Delta V \\ &= J_R^{-1} \Delta Q\end{aligned}\tag{4.2}$$

where J_R is called the reduced Jacobian matrix of the system. This matrix determines the change in voltage that occurs from injection of reactive power into the system at any bus.

We can also write the equation in another way that is more helpful, by using the eigenvalues and eigenvectors of the reduced Jacobian, with the following result.

$$\Delta V = \sum_i \frac{\xi_i \eta_i}{\lambda_i} \Delta Q\tag{4.3}$$

where

ξ_i = Right eigenvector matrix of \mathbf{J}_R

η_i = Left eigenvector matrix of \mathbf{J}_R

λ_i = The *ith* eigenvalue of \mathbf{J}_R

This technique permits the use of eigen analysis to determine the voltage sensitivity of reactive power injections. The technique is referred to as "modal analysis." The system is voltage stable if the eigenvalues of the Jacobian are all positive, which means that the V-Q sensitivity is positive.

4.2 Participation Factor (PF) Technique

The state equations of the linearized model can be used to determine the eigenvalues of the system matrix A . Out of these eigenvalues; there is a mode of oscillations related to machine inertia. For the stabilizers to be effective, it is extremely important to identify the eigenvalue associated with the electromechanical mode. In this study, the participation factors (PF) method [37] is used.

PF analysis aids in the identification of how each dynamic variable affects a given mode or eigenvalue. Specifically, given a linear system:

$$\dot{x} = Ax \quad (4.4)$$

a participation factor is a sensitivity measure of an eigenvalue to a diagonal entry of the system A matrix. This is defined as

$$p_{ki} = \frac{\partial \lambda_i}{\partial a_{kk}} \quad (4.5)$$

where λ_i is the i^{th} system eigenvalue, a_{kk} is a diagonal entry in the system A matrix, and p_{ki} is the participation factor relating the k^{th} state variable to the i^{th} eigenvalue. The participation factor may also be defined by

$$p_{ki} = \frac{w_{ki} v_{ik}}{w_i^t v_i} \quad (4.6)$$

where w_{ki} and v_{ki} are the k^{th} entries in the left and right eigenvector associated with the i^{th} eigenvalue.

4.3 Controllability Measurement

To measure the controllability of the electromechanical mode by a given input, the singular value decomposition (SVD) is employed in this study. Mathematically, if G is an $m \times n$ complex matrix then there exist unitary matrices W and V with dimensions of $m \times m$ and $n \times n$ respectively such that G can be written as

$$G = W \Sigma V^H \quad (4.7)$$

$$\text{Where } \Sigma = \begin{bmatrix} \Sigma_1 & 0 \\ 0 & 0 \end{bmatrix}, \quad \Sigma_1 = \text{diag}(\sigma_1, \dots, \sigma_r) \quad (4.8)$$

with $\sigma_1 \geq \dots \geq \sigma_r \geq 0$

where $r = \min\{m, n\}$ and $\sigma_1, \dots, \sigma_r$ are the singular values of G .

The minimum singular value σ_r represents the distance of the matrix G from the all matrices with a rank of $r-1$. This property can be utilized to quantify modal controllability. In this study, the matrix H in (4.7) can be written as $H = [h_1, h_2, h_3, h_4]$ where h_i is the column of matrix H corresponding to the i -th input. The minimum singular value, σ_{\min} , of the matrix $[\lambda I - A \quad h_i]$ indicates the capability of the i -th input to control the mode associated with the eigenvalue λ . As a matter of fact, the higher the σ_{\min} , the higher the controllability of this mode by the input considered. Having been identified, the controllability of the electromechanical mode can be examined with all inputs in order to identify the most effective one to control that mode.

4.4 Implementation

4.4.1 Objective Function

To optimize the stabilizers parameters, an eigenvalue based objective function is considered. The objective function is formulated to increase the damping factor or the damping ratio of the electromechanical mode eigenvalues. Therefore, the system response to disturbances will be improved. The function can be defined as

$$J = \min\{\zeta_i : \zeta_i \text{ is the minimum electromechanical mode damping ratio of} \\ \text{of the } i\text{th loading condition}\} \quad (4.9)$$

where ζ_i is the damping ratio of the electromechanical mode eigenvalue. It is clear that the objective function will identify the minimum value of the damping ratio among electromechanical modes of all loading conditions considered in the design process. Hence, it is aimed to *Maximize* J in order to increase the damping ratios of electromechanical modes. This will reduce the system response overshoots and enhance the system damping characteristics.

4.4.2 Optimization Problem Formulation

In this study, the proposed objective function is optimized individually. The problem constraints are the stabilizer optimized parameter bounds. Therefore, the design problem can be formulated as the following optimization problem.

Maximize J

Subject to

$$K_i^{\min} \leq K_i \leq K_i^{\max}$$

$$T_{1i}^{\min} \leq T_{1i} \leq T_{1i}^{\max}$$

$$T_{3i}^{\min} \leq T_{3i} \leq T_{3i}^{\max}$$

The proposed approach employs PSO algorithm to solve this optimization problem and search for optimal set of the stabilizer parameters, $\{K_i, T_{1i}, T_{3i}, i = \text{Number of stabilizers considered}\}$.

4.5 Particle Swarm Optimization Algorithm

4.5.1 Overview

Like evolutionary algorithms, PSO technique conducts search using a population of particles. Each particle represents a candidate solution to the problem. In PSO System, particles change their positions by flying around in a multi dimensional search space until a relatively unchanging position has been encountered, or until computational limitations are exceeded. In social science context, a PSO system combines a social-only model and a cognition-only model [49]. The social-only component suggests that individuals ignore their own experience and adjust their behavior according to the successful beliefs of individuals in the neighborhood. On the other hand, the cognition-only component treats individuals as isolated beings. The advantages of PSO over other traditional optimization techniques can be summarized as follows: -

- PSO is a population-based search algorithm i.e., PSO has implicit parallelism. This property ensures PSO to be less susceptible to getting trapped on local minima.
- PSO uses objective function information to guide the search in the problem space. Therefore, PSO can easily deal with non-differentiable objective functions.
- PSO uses probabilistic transition rules, not deterministic rules. Hence, PSO is a kind of stochastic optimization algorithm that can search a complicated and uncertain area. This makes PSO more flexible and robust than conventional methods.
- Unlike GA and other heuristic algorithms, PSO has the flexibility to control the balance between the global and local exploration of the search space.

4.5.2 PSO Algorithm

The basic elements of PSO technique are briefly stated and defined as follows: -

- **Particle**, $X(t)$, It is a candidate solution represented by an m -dimensional real-valued vector, where m is the number of optimized parameters. At time t , the j^{th} particle $X_j(t)$ can be described as $X_j(t)=[x_{j,1}(t), \dots, x_{j,m}(t)]$, where x_s are the optimized parameters and $x_{j,k}(t)$ is the position of the j^{th} particle with respect to the k^{th} dimension, i.e., the value of the k^{th} optimized parameter in the j^{th} candidate solution.
- **Population**, $pop(t)$,: It is a set of n particles at time t , i.e., $pop(t)=[X_1(t), \dots, X_n(t)]^T$.
- **Swarm**: it is an apparently disorganized population of moving particles that tend to cluster together while each particle seems to be moving in a random direction.
- **Particle velocity**, $V(t)$,: It is the velocity of the moving particles represented by an m -dimensional real-valued vector. At time t , the j^{th} particle velocity $V_j(t)$ can be

described as $V_j(t) = v_{j,1}(t), \dots, v_{j,m}(t)$, where $v_{j,k}(t)$ is the velocity component of the j^{th} particle w.r.t. k^{th} dimension.

- **Inertia weight**, $w(t)$,: It is a control parameter that is used to control the impact of the previous velocities on the current velocity. Hence, it influences the trade-off between the global and local exploration abilities of the particles [12] For initial stages of the search process, large inertia weight to enhance the global exploration is recommended while, for last stages, the inertia weight is reduced for better local exploration.
- **Individual best**, $X^*(t)$,: As a particle moves through the search space, it compares its fitness value at the current position to the best fitness value it has ever attained at any time up to the current time. The best position that is associated with the best fitness encountered so far is called the individual best, $X^*(t)$. For each particle in the swarm, $X^*(t)$ can be determined and updated during the search. In a minimization problem with objective function J , the individual best of the j^{th} particle $X_j^*(t)$ is determined.
- **Global best**, $X^{**}(t)$, : It is the best position among all individual best positions achieved so far. Hence, the global best can be determined as $J(X^{**}(t)) < J(X_j^*(t))$, $j = 1, \dots, n$. For simplicity, assume that $J^{**} = J(X^{**}(t))$.
- **Stopping criteria**: These are the conditions under which the search will terminate. In this study, the search will stop if one of the following criteria is satisfied: (a) the number of iterations since the last change of the best solution is greater than a pre specified number; or (b) the number of iterations reaches the maximum allowable number.

CHAPTER 5

ANALYSIS AND DESIGN OF A PSS, AND G1 FACTS-BASED STABILIZERS IN A SMIB SYSTEM

This chapter shows the analysis and design of a PSS and G1 FACTS-Based stabilizers in a single machine infinite bus system. Some work has been reported in [39] using Genetic Algorithm (GA) as controller parameters tuning tool. While in this thesis PSO has been applied to the optimization problem to search for optimal settings of the proposed stabilizers. This will test and validate the developed work in this thesis in terms of modeling, PSO technique and the developed computer codes.

5.1 Controllability Measure

With each input signal of PSS, SVC-based stabilizer, TCSC-based stabilizer, and TCPS-based stabilizer in the linearized model given in (3.47), the minimum singular value σ_{\min} has been estimated to measure the controllability of the electromechanical mode from that input. For comprehensive understanding of the coordination problem requirements, the minimum singular value has been estimated for each stabilizer over a wide range of

operating conditions. Specifically, for a range of 84 loading conditions specified by $P = [0.05 - 1.4]$ pu with a step of 0.05 pu and $Q = [-0.4 - 0.4]$ pu with a step of 0.4 pu, σ_{\min} has been estimated. At each loading condition in the specified range, the system model is linearized, the electromechanical mode is identified, and the SVD-based controllability measure is implemented.

For comparison purposes, the minimum singular values for all inputs at $Q_e = -0.4, 0.0$ and 0.4 pu are shown in Figs. 5.1-5.3, respectively. From these Figs., the following can be noticed:

- (a) At light loading conditions, the capabilities of PSS, SVC, and TCSC to control the electromechanical mode are considerably lower compared to that of TCPS.
- (b) The electromechanical mode controllability via PSS and SVC is almost the same over the entire range of loading conditions.
- (c) The electromechanical mode is more controllable with TCSC and TCPS compared to PSS and SVC.
- (d) The electromechanical mode controllability by TCSC changes almost linearly with the practical system loading.
- (e) The electromechanical mode is most controllable by TCSC at heavy loading.
- (f) As Q increases, the electromechanical mode controllability via TCSC becomes dominant at lower loading levels.

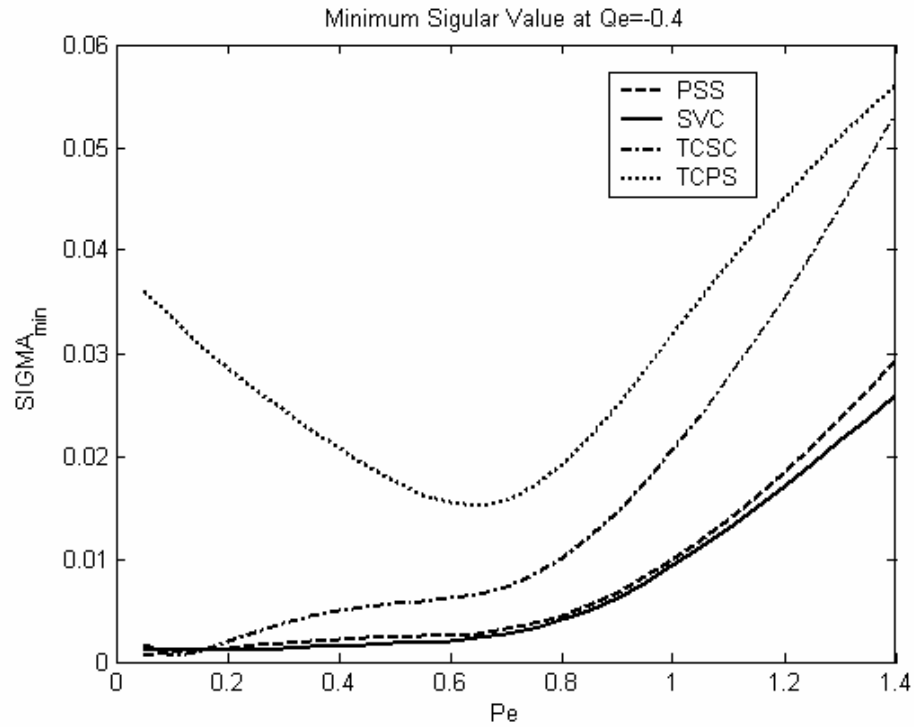


Fig. 5.1: Minimum singular value with all stabilizers at $Q = -0.4$ pu

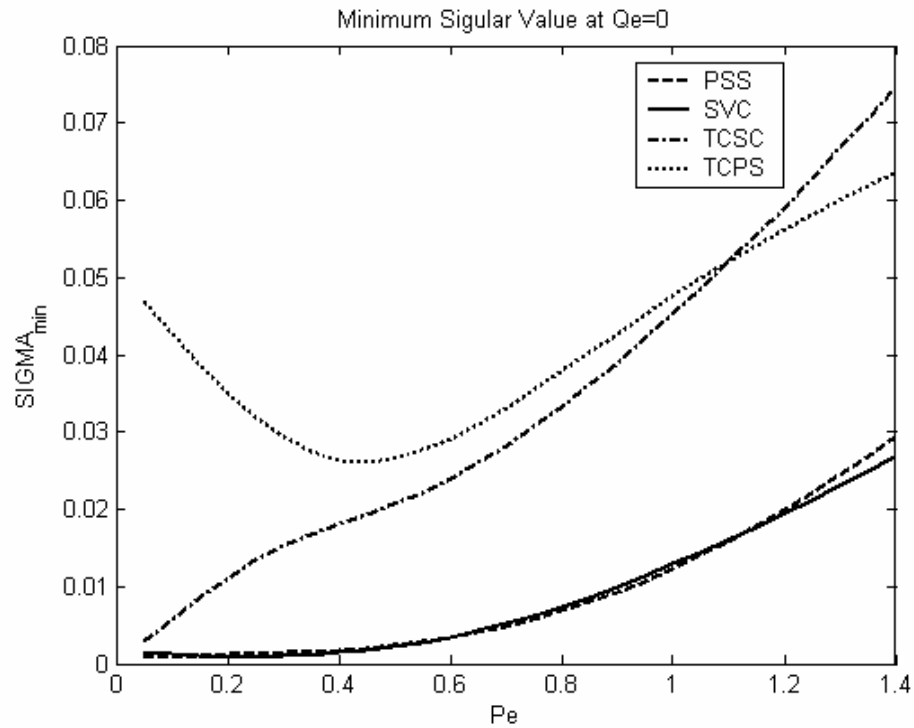


Fig. 5.2: Minimum singular value with all stabilizers at $Q = 0$ pu

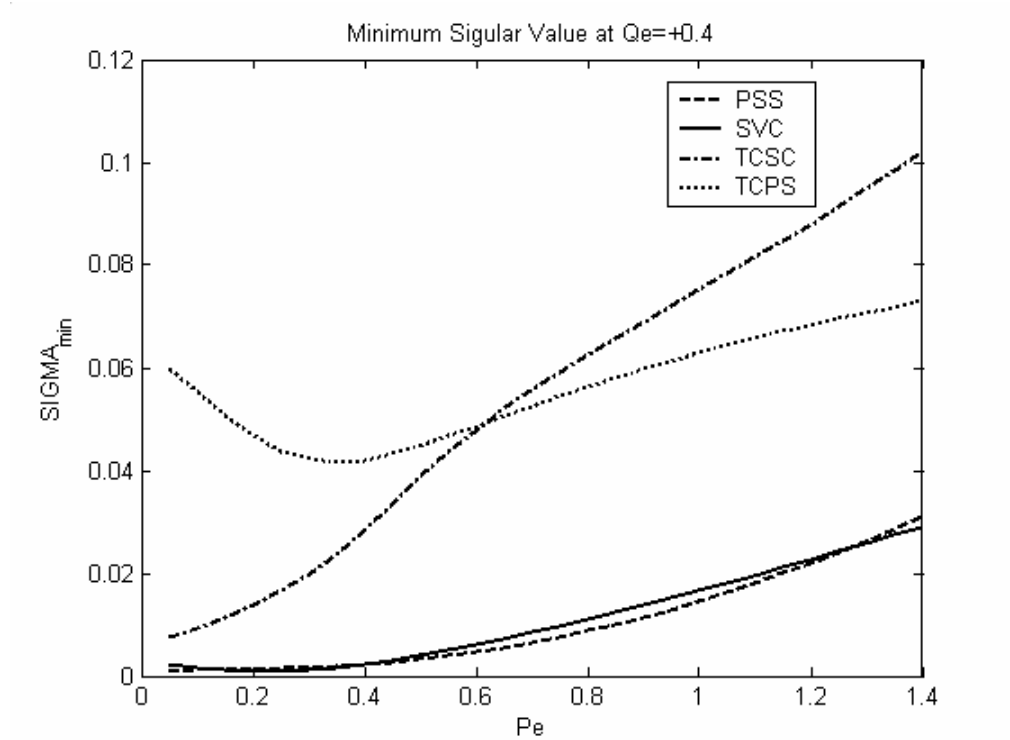


Fig. 5.3: Minimum singular value with all stabilizers at $Q = +0.4$ pu

5.2 Stabilizer Tuning and Simulation Results

To increase the system damping to the electromechanical model, the objective function J defined below is proposed.

$$J = \min \{ \zeta \}$$

Where ζ is the electromechanical mode damping ratio.

This objective function will identify the minimum value of damping ratio among electromechanical modes of all loading condition considered in the design process

To assess the effectiveness of the proposed controllers, four different loading conditions are considered for eigenvalue analysis. These conditions and disturbances are:

1. Nominal loading $(P_e, Q_e) = (1.0, 0.015)$ pu.

2. Light loading (P_e, Q_e)=(0.3,0.015) pu.
3. Heavy loading (P_e, Q_e)=(1.1,0.40) pu.

5.2.1 Single Point Tuning

In this section, the stabilizers are tuned with only the nominal loading condition, (P_e, Q_e)=(1.0,0.015) pu, taken into account.

5.2.1.1 Individual Design

a) Stabilizer design

Based on the linearized power system model in equation (3.47), PSO has been applied to the optimization problem to search for optimal settings of the proposed stabilizers. The final settings of the optimized parameters for the proposed stabilizers are given in Table 5.1. The convergence rate of the objective function is shown in Fig. 5.4.

Table 5.1: Optimal parameter settings, single point tuning, individual design

	<i>PSS</i>	<i>SVC</i>	<i>TCSC</i>	<i>TCPS</i>
<i>K</i>	22.7119	94.4022	100	100
<i>T₁</i>	0.1538	1	0.0759	0.0846
<i>T₂</i>	0.1	0.3	0.1	0.1
<i>T₃</i>	0.1714	0.01	0.0787	0.0844
<i>T₄</i>	0.1	0.3	0.1	0.1

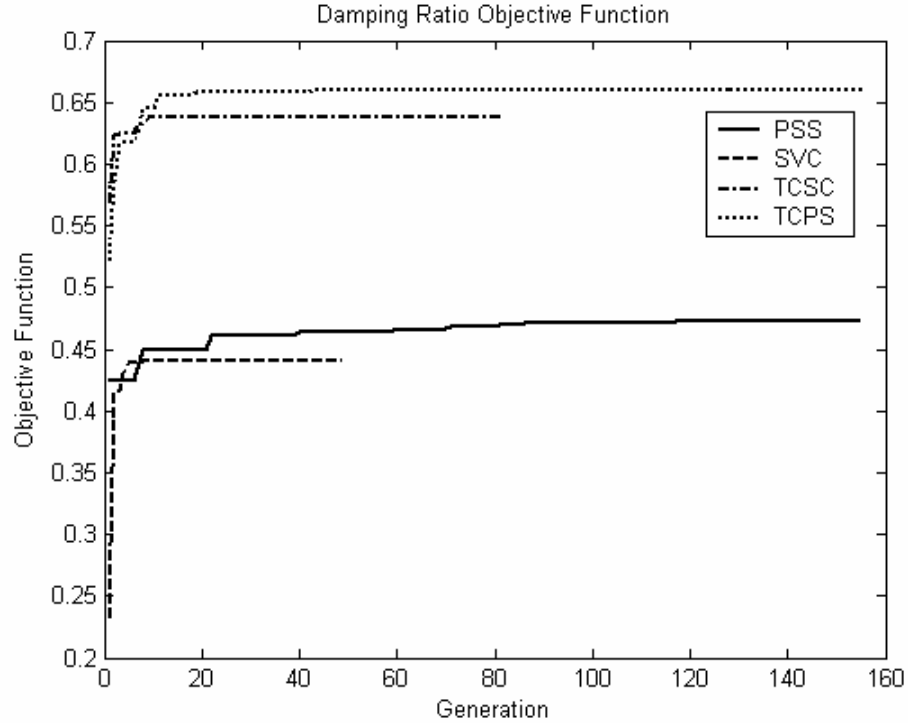


Fig. 5.4: Variation of the objective function of all stabilizers

b) Eigenvalue Analysis

The system eigenvalues with the proposed stabilizers for nominal, light and heavy loading conditions are given in Tables 5.2-5.4, respectively, where the first row represents the electromechanical mode eigenvalues and their damping ratios.

The first bolded rows of these tables represent the EM mode eigenvalue and its damping ratio. It is clear that the proposed stabilizers greatly improve the system stability. It is also clear that the PSS, SVC and TCSC have relatively poor capabilities to enhance the EM mode damping when the system operates at light loading.

Table 5.2: System eigenvalues of nominal loading condition, single point tuning, individual design

Base Case	PSS	SVC	TCSC	TCPS
0.2954±i4.9569	-3.24±i5.6425	-2.267±i4.615	-3.502±i4.062	-3.134±i3.574
-0.0595	0.4716	0.4443	0.6384	0.6510
10.393± i3.287	-3.399±i5.919	-2.491±i5.072	-5.784±i6.710	-7.012±i7.995
	-19.497	-20.4518	-11.4678±i1.2	-11.04±i0.835
	-7.414	-14.2613	-18.679	-17.8032
	-0.2055	-2.6307	-0.209	-0.2099
		-0.2010		

Table 5.3: System eigenvalues of light loading condition, single point tuning, individual design

Base Case	PSS	SVC	TCSC	TCPS
-0.009±i4.8503	-0.874±i5.0613	-0.1818±i4.72	-0.829±i5.1324	-4.513±i6.612
0.0019	0.1548	0.0387	0.1631	0.5826
-11.08± i3.834	-6.986±i5.539	-7.048±i2.084	-9.9196±i3.821	-9.343±i3.493
	-16.77	-19.9164	-19.534	-17.3745
	-7.7027	-9.9346	-10.7282	-10.763
	-0.2023	-2.5516	-8.4324	-4.3337
		-0.1998	-0.2031	-0.2121

Table 5.4: System eigenvalues of Heavy loading condition, single point tuning, individual design

Base Case	PSS	SVC	TCSC	TCPS
0.4852±i3.6903	-1.4861±i3.587	-2.8346±i5.266	-5.838±i7.6134	-7.657±i8.583
-0.1304	0.3141	0.4948	0.6014	0.8495
-11.583± i3.696	-5.111±i7.088	-1.4863±i2.67	-10.356±i0.763	-2.9227±i1.72
	-19.628	-20.9455	-18.0527	-10.85±i0.856
	-7.363	-13.1445	-7.4194	-17.2997
	-0.2092	-4.1267	-2.3077	-0.2230
		-0.2039	-0.227	

c) Non linear time domain simulation

The single machine infinite bus system shown in Fig. 3.2 is considered for nonlinear simulation studies. 6-cycle 3- ϕ fault, on the infinite bus was created, at all loading conditions, to study the performance of the proposed controllers. Simulation results at nominal condition are only shown.

The rotor angle, speed deviation, and electrical power responses at nominal operating condition, are shown in Figs. 5.5-5.7 respectively. It can be readily seen that the TCSC and TCPS performs better than PSS in terms of reduction of overshoot and settling time. This is consistent with the eigenvalues analysis results. Figs. 5.8 and 5.9 show the control effort provided by the stabilizing signal of PSS, U_{PSS} and the reactance of TCSC, X_{TCSC} respectively.

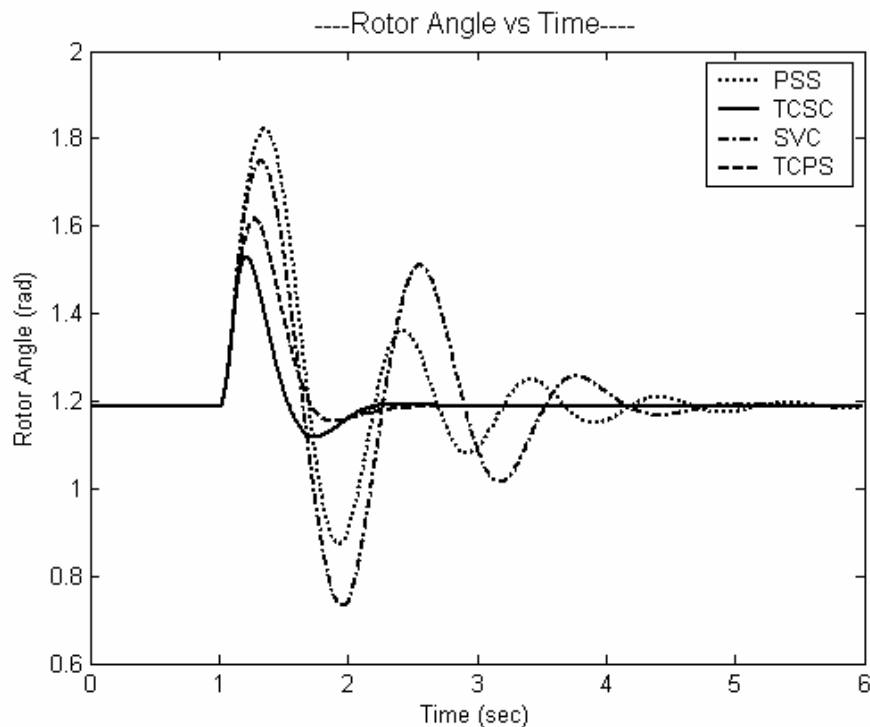


Fig. 5.5: Rotor angle response for 6-cycle fault with nominal loading single point tuning, individual design

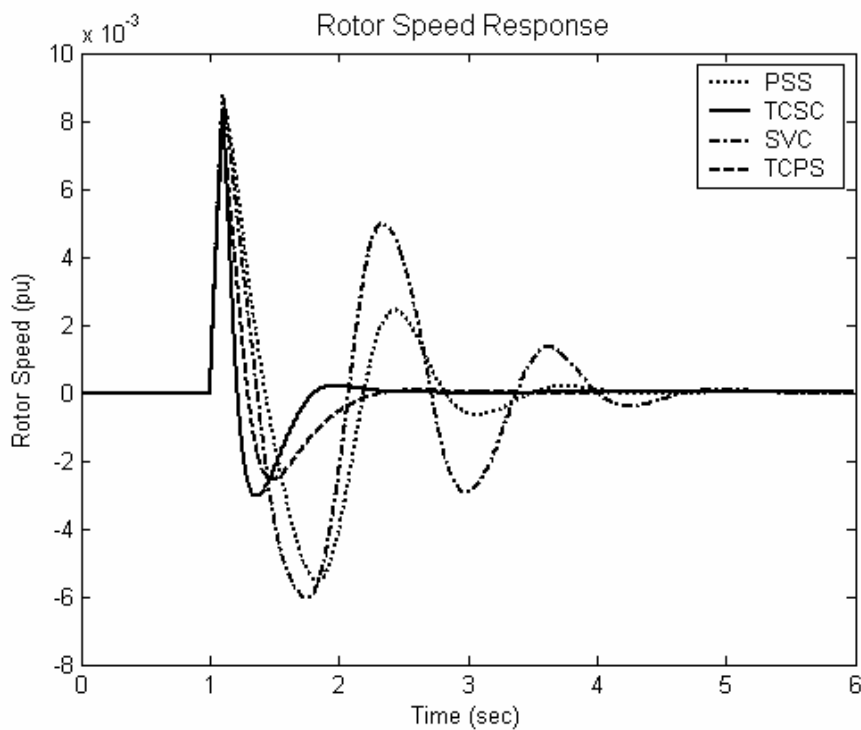


Fig. 5.6: Rotor speed response for 6-cycle fault with nominal loading, single point tuning, individual design

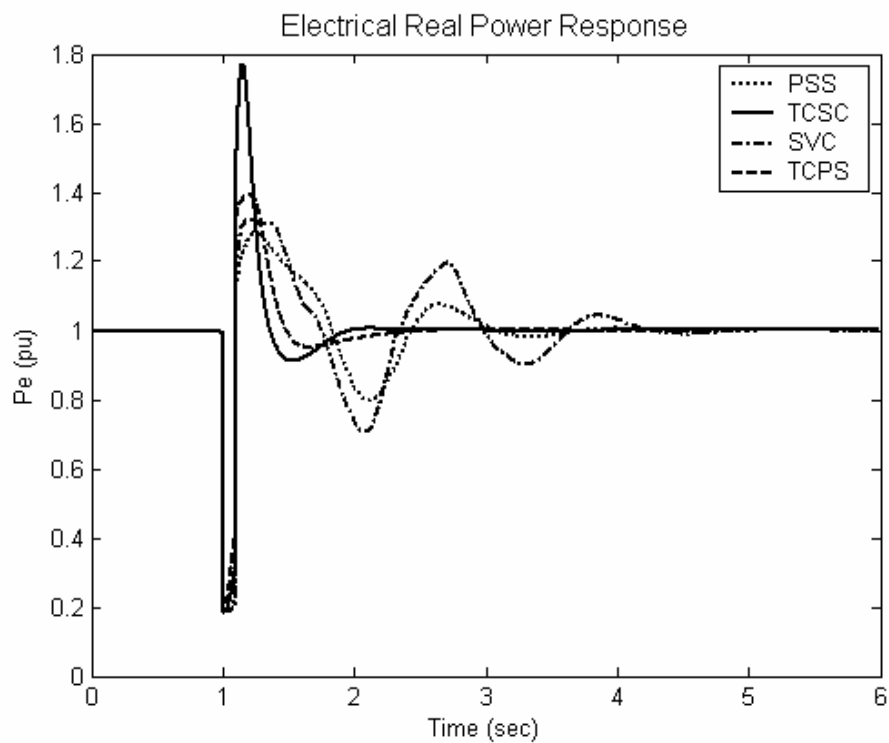


Fig. 5.7: Electrical power response for 6-cycle fault with nominal loading, single point tuning, individual design

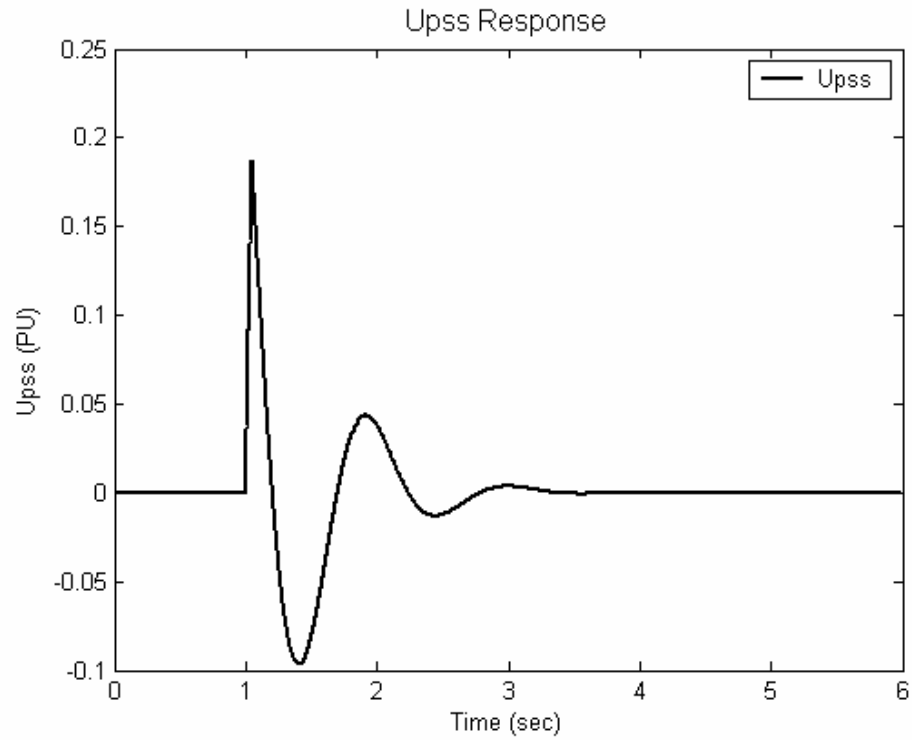


Fig. 5.8: PSS stabilizing signal response for 6-cycle fault with nominal loading, single point tuning, individual design

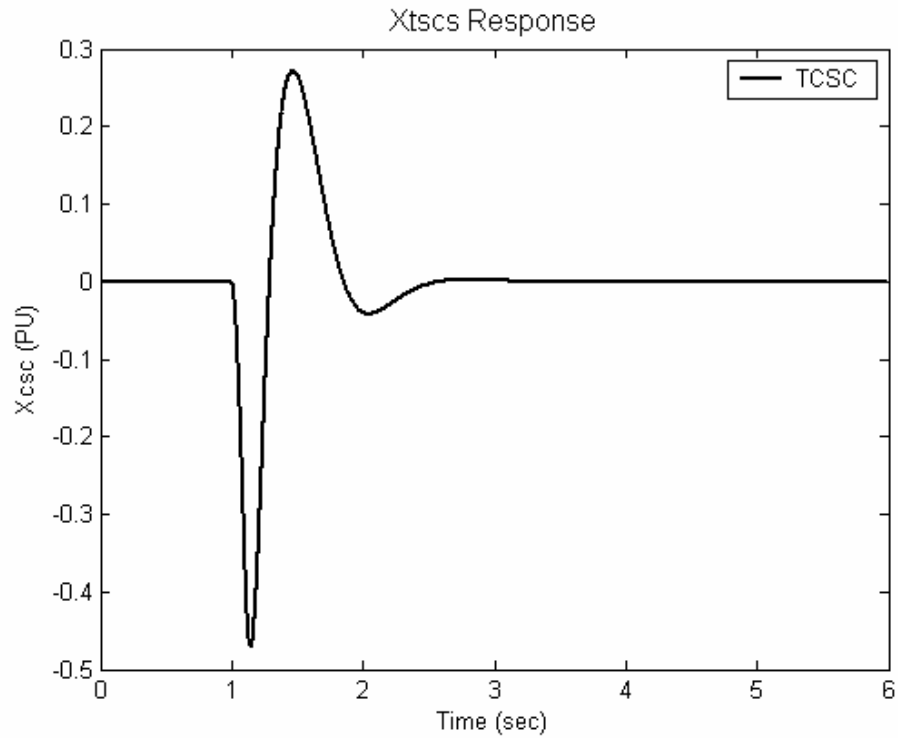


Fig. 5.9: X_{tscs} stabilizing signal response for 6-cycle fault with nominal loading, single point tuning, individual design

5.2.1.2 Coordinated Design [PSS & SVC]

The singular value decomposition-based controllability measure analysis shows that the PSS and SVC-based stabilizer need to be coordinated for better performance of the system. In this section the coordinated design of PSS and SVC-based stabilizer is addressed at the nominal operating point.

a) Stabilizer design

Both stabilizers PSS & SVC are simultaneously tuned by PSO search for the optimum controllers parameter settings that maximize the minimum damping ratio of all the system complex eigenvalues at nominal loading condition. The final settings of the optimized parameters for the proposed stabilizers are given in Table 5.5.

It can be noticed when both proposed stabilizers are available, SVC and PSS, the parameters' settings of the stabilizers are retuned in coordinated approach in order to avoid the negative interaction between stabilizers and to get better system performance compared with individual stabilizer.

The convergence rate of the objective function when PSS and SVC-based controller are designed individually and in a coordinated manner is shown in Fig. 5.10. It is clear that the coordinated design of PSS and SVC-based stabilizer improves greatly the system damping compared to their individual application.

Table 5.5: Optimal parameter settings, single point tuning, coordinated design

	<i>Individual</i>		<i>Coordinated</i>	
	<i>PSS</i>	<i>SVC</i>	<i>PSS</i>	<i>SVC</i>
K	22.7119	94.4022	47.6518	100
T_1	0.2751	1	0.0922	0.6782
T_2	0.1	0.3	0.1	0.3
T_3	-----	0.01	-----	-----
T_4	-----	0.3	-----	-----

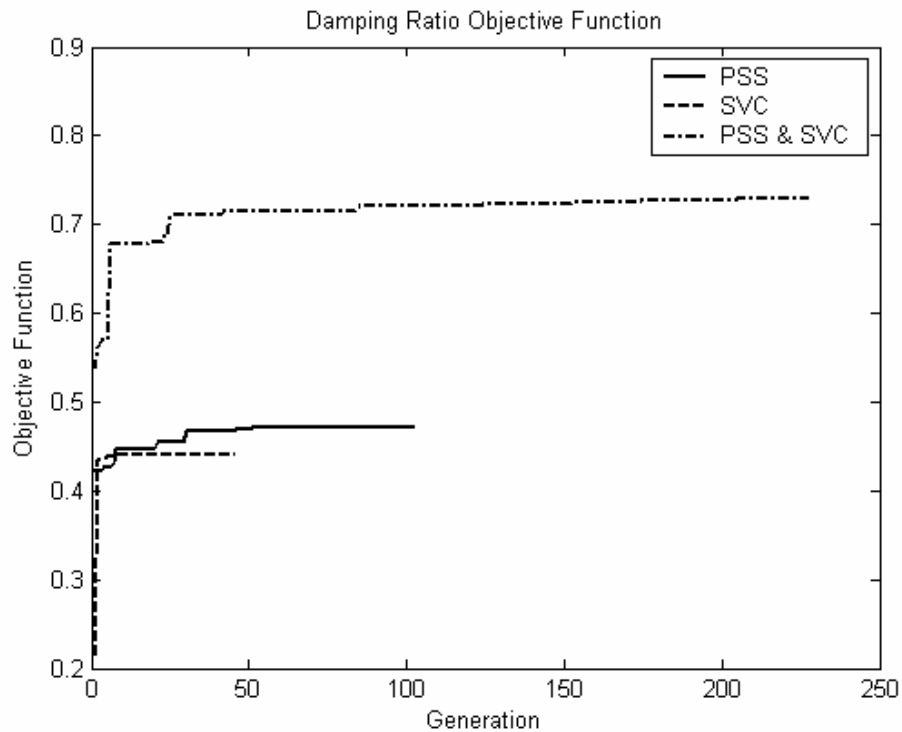


Fig. 5.10: Variation of the objective function of PSS & SVC-based stabilizer

b) Eigenvalue Analysis

The system eigenvalues along with damping ratios with and without the proposed PSS and SVC when applied individually and through coordinated design are given in Tables 5.6, 5.7, and 5.8 for nominal, light, and heavy loading conditions respectively. It is quite

evident that the system stability is greatly enhanced with the coordinated design approach as damping ratio of the electromechanical mode eigenvalue has been greatly improved. The first bolded rows of these tables represent the EM mode eigenvalue and its damping ratio.

Table 5.6: System eigenvalues of nominal loading condition, single point tuning, coordinated design

Base Case	PSS	SVC	PSS & SVC
0.2954±i4.9569	-2.742±i5.1325 (0.4713)*	-2.4914±i5.0715 (0.4409)*	-6.4334±i6.0455 (0.7287)*
10.393± i3.287	-3.2078±i6.0025 -18.2917 -0.2043	-2.2673±i4.6153 -20.4518 -2.6307 -0.2010	-6.0325±i5.6683 -18.8178 -17.268 -2.4971 -0.2142 , -0.2

Table 5.7: System eigenvalues of light loading condition, single point tuning, coordinated design

Base Case	PSS	SVC	PSS & SVC
0.2954±i4.9569	-0.7834±i5.0205 (0.1542)*	-0.1819±i4.7239 (0.0385)*	-0.9533±i5.5766 (0.1685)*
10.393± i3.287	-6.584±i4.969 -15.4592 -0.2018	-7.0478±i2.084 -19.9164 -9.9351 -2.5516 -0.1998	-10.1032±i3.3448 -20.3168 -8.11 -2.9841 -0.205, -0.2

Table 5.8: System eigenvalues of heavy loading condition, single point tuning, coordinated design

Base Case	PSS	SVC	PSS & SVC
0.2954±i4.9569	-2.742±i5.1325 (0.4713)*	-2.4914±i5.0715 (0.4409)*	-7.2294±i7.7547 (0.682)*
10.393± i3.287	-3.2078±i6.0025 -18.2917 -0.2043	-2.2673±i4.6153 -20.4518 -2.6307 -0.2010	-8.6767±i3.652 -2.4001±i0.5035 -16.8875 -0.229 -0.2

c) Non linear time domain simulation

A 6-cycle 3- ϕ fault has been simulated on the infinite bus of SMIB system shown Fig. 3.2 at all loading conditions, in order to study the performance of the proposed controllers. Simulation results at nominal condition only are shown.

Figs. 5.11-5.13 show the system responses at the nominal loading condition where the coordinated design of PSS and SVC is compared to individual design. It can be seen that the coordinated design of PSS and SVC provide the best damping characteristics.

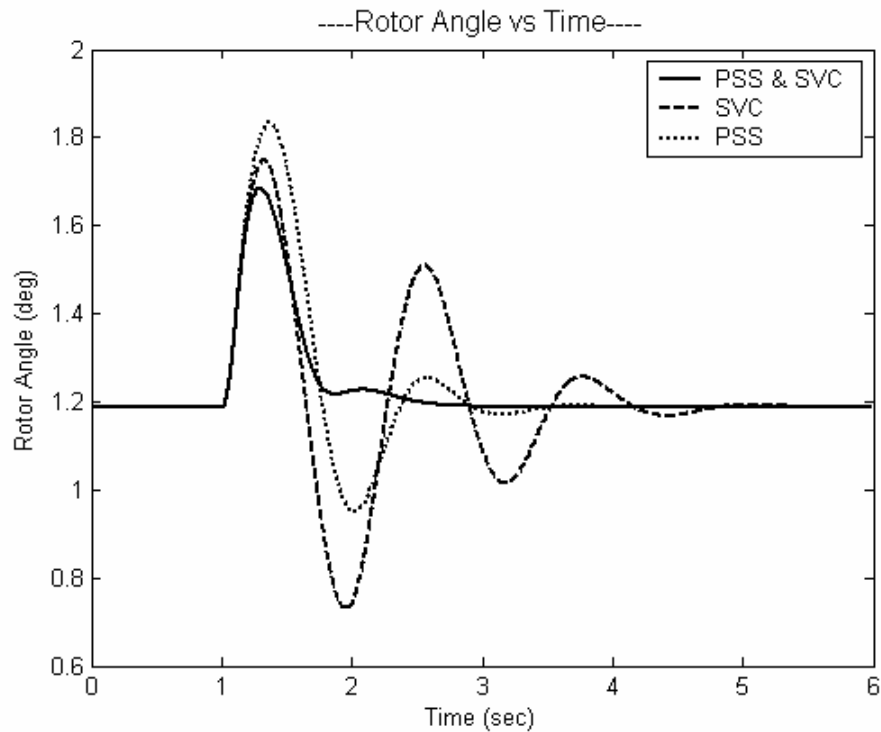


Fig. 5.11: Rotor angle response for 6-cycle fault with nominal loading, single point tuning, coordinated design

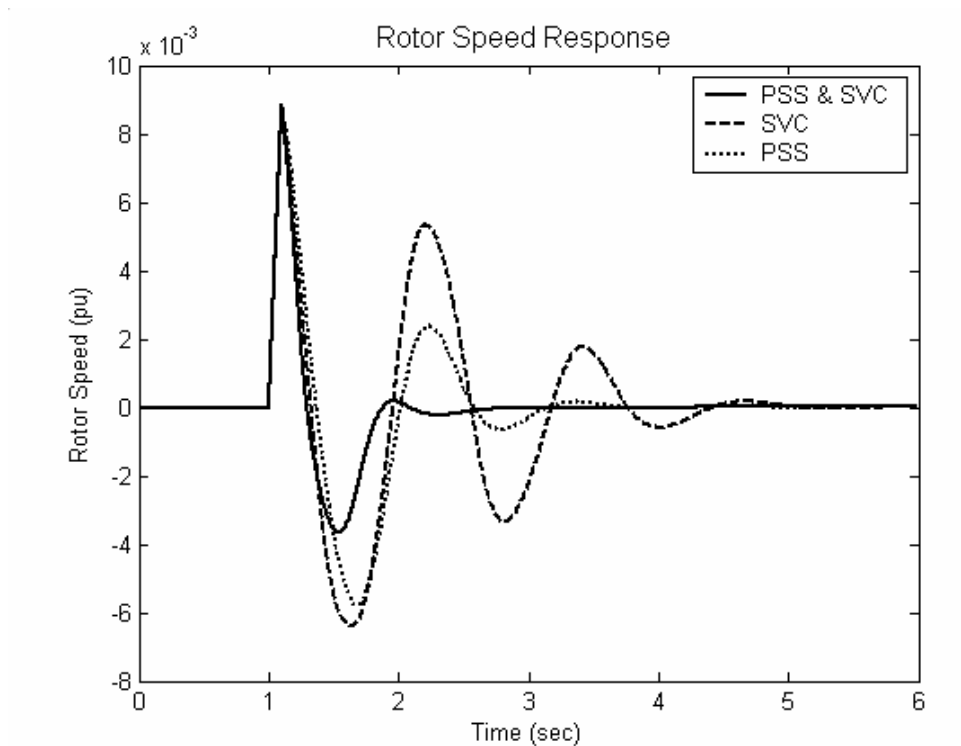


Fig. 5.12: Rotor speed response for 6-cycle fault with nominal loading, single point tuning, coordinated design

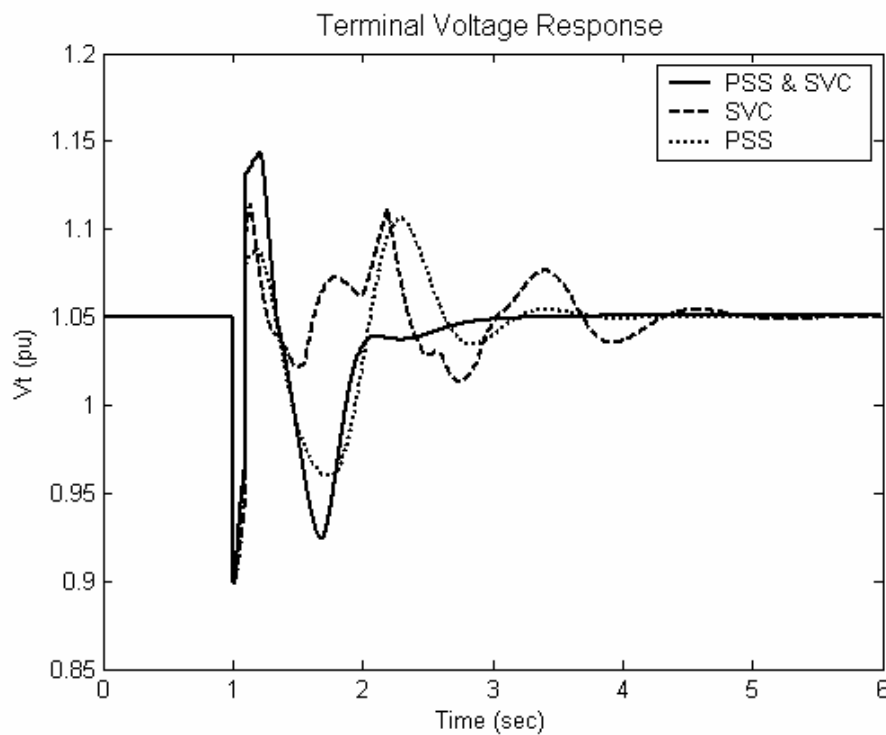


Fig. 5.13: Terminal voltage response for 6-cycle fault with nominal loading, single point tuning, coordinated design

5.2.1.3 Coordinated Design [PSS & TCSC]

The controllability measure analysis based on the singular value decomposition indicates that the PSS and TCSC-based stabilizers do not perform well individually at light loading condition. In this section, a coordinated design of PSS and TCSC-based stabilizer is considered at the nominal loading condition.

a) Stabilizer design

Both stabilizers PSS & TCSC are simultaneously tuned by PSO searching for the optimum controllers parameter settings that maximize the minimum damping ratio of all the system complex eigenvalues at nominal loading condition. The final settings of the optimized parameters for the proposed stabilizers are given in Table 5.9.

It can be noticed when both proposed stabilizers, PSS and TCSC, are available, the parameters' settings of the stabilizers are retuned in coordinated approach in order to avoid the negative interaction between stabilizers and to get better system performance compared with individual stabilizer.

The convergence rate of the objective function when PSS and TCSC-based controllers are designed individually and in a coordinated manner is shown in Fig. 5.14. It is clear that the coordinated design of PSS and TCSC-based stabilizer improves greatly the system damping compared to their individual application.

Table 5.9: Optimal parameter settings, single point tuning, coordinated design

	<i>Individual</i>		<i>Coordinated</i>	
	<i>PSS</i>	<i>TCSC</i>	<i>PSS</i>	<i>TCSC</i>
K	18.0815	100	30.6035	55.1371
T_1	0.2751	0.0598	0.1305	0.2052
T_2	0.1	0.1	0.1	0.1

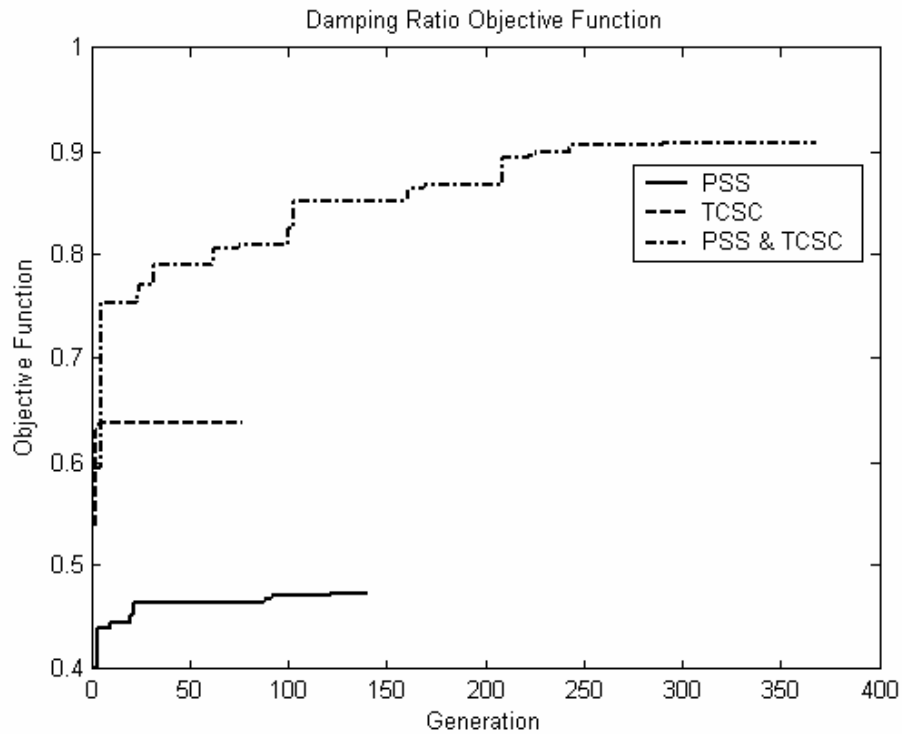


Fig. 5.14: Variation of the objective function of PSS & TCSC-based stabilizer

b) Eigenvalue Analysis

The system eigenvalues without and with the proposed stabilizers at nominal, light, and heavy loading conditions are given in Tables 5.10, 5.11, and 5.12 respectively, where the first row represents the electromechanical mode eigenvalues and their damping ratios.

Table 5.10: System eigenvalues of nominal loading condition, single point tuning, coordinated design

Base Case	PSS	TCSC	PSS & TCSC
0.2954±i4.9569	-2.742±i5.1325 (0.4713)*	-6.0555±i7.2993 (0.6385)*	-5.9399±3.199i (0.8804)*
10.393± i3.287	-3.2078±i6.0025 -18.2917 -0.2043	-3.2762±i3.949 -19.1764 -12.3468 -0.209	-6.9852±3.7456i -12.166±6.6527i -10 -0.2132 -0.2

Table 5.11: System eigenvalues of light loading condition, single point tuning, coordinated design

Base Case	PSS	TCSC	PSS & TCSC
0.2954±i4.9569	-0.7834±i5.0205 (0.1542)*	-0.8483±i5.1189 (0.1635)*	-1.5346±5.268i (0.2797)*
10.393± i3.287	-6.584±i4.969 -15.4592 -0.2018	-9.8646±i3.8603 -19.695 -9.0717 -2.5516 -0.2031	-7.3358±3.5404i -16.225±2.6325i -10 -0.205 -0.2

Table 5.12: System eigenvalues of heavy loading condition, single point tuning, coordinated design

Base Case	PSS	TCSC	PSS & TCSC
0.2954±i4.9569	-2.742±i5.1325 (0.4713)*	-6.0961±i8.086 (0.602)*	-12.611±9.676i (0.7943)*
10.393± i3.287	-3.2078±i6.0025 -18.2917 -0.2043	-18.8166 -10.3688 -6.3914 -2.3998 -0.2269	-9.1436±5.682 -10 -4.1877 -2.4685 -0.2375,-0.2

c) Non linear time domain simulation

A 6-cycle 3- ϕ fault has been simulated on the infinite bus of SMIB system shown Fig. 3.2 at all loading conditions, in order to study the performance of the proposed controllers. Simulation results at light condition only are shown.

Figs. 5.15-17 show the system responses at the nominal loading condition where the coordinated design is compared to individual design. It can be seen that the coordinated design of PSS & TCSC provide the best damping characteristics.

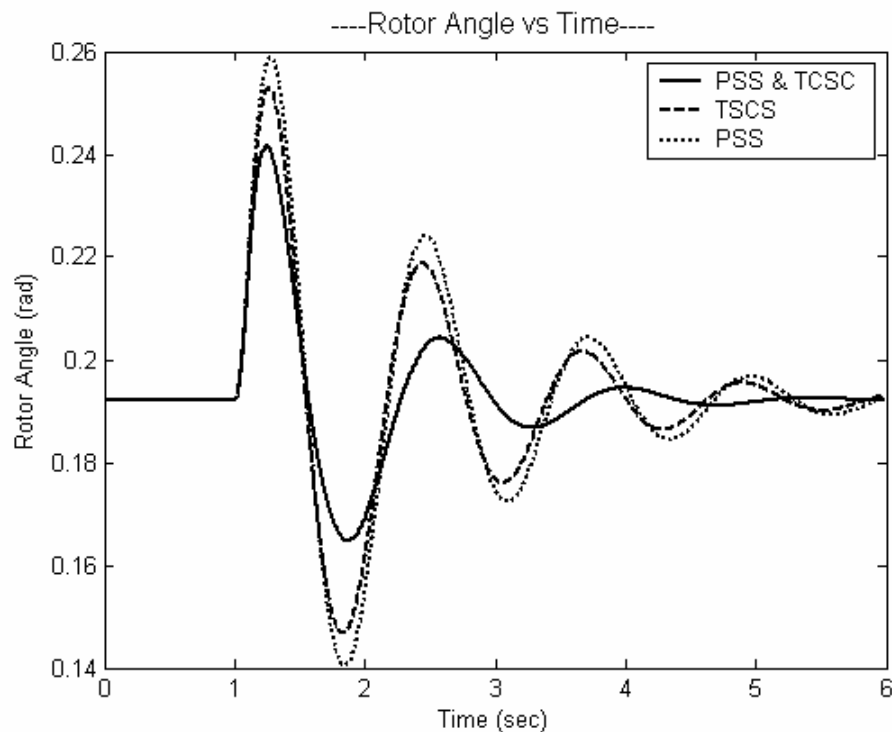


Fig. 5.15: Rotor angle response for 6-cycle fault with light loading, single point tuning, coordinated design

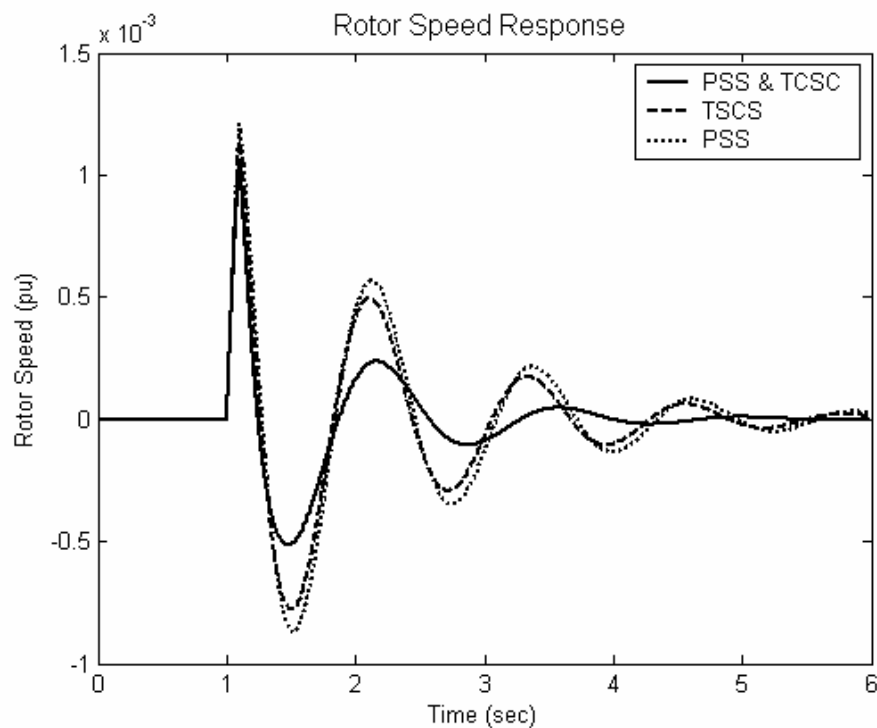


Fig. 5.16: Rotor speed response for 6-cycle fault with light loading, single point tuning, coordinated design

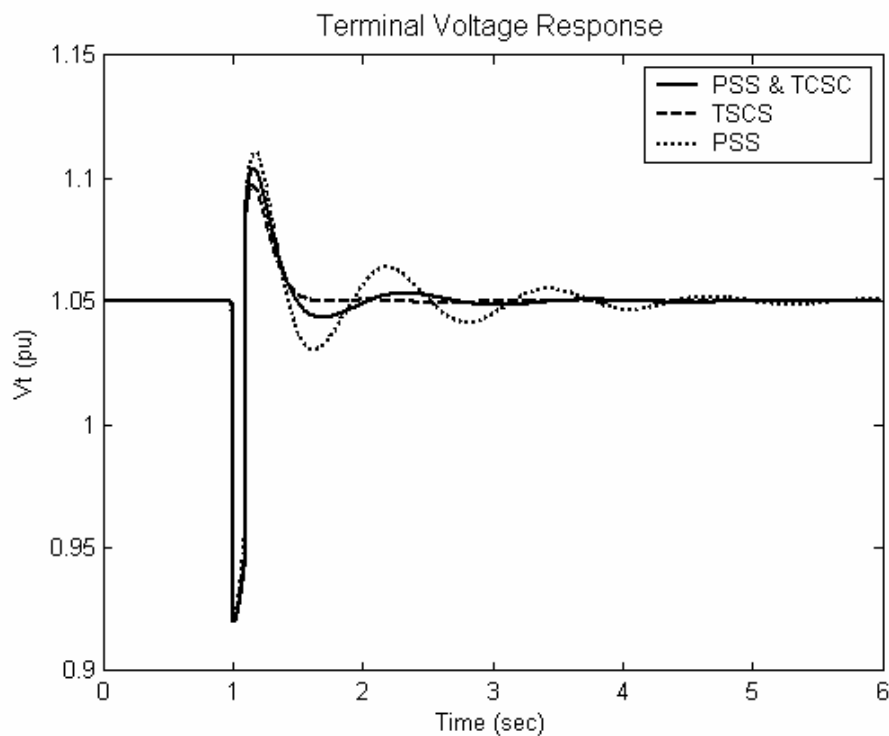


Fig. 5.17: Terminal voltage speed response for 6-cycle fault with light loading, single point tuning, coordinated design

5.2.2 Multiple Point Tuning

In this section, the FACTS-based controllers' parameters are optimized over a wide range of operating conditions and system parameter uncertainties in order to have robust stabilizers. Four loading conditions represent nominal, light, heavy, and leading power factor are considered. Each loading condition is considered without and with parameter uncertainties as given in Table 5.13. Hence, the total number of points considered for design process is 16.

Tables 5.14 and 5.15 list the open-loop eigenvalues and corresponding damping ratios associated with the EM modes of all the 16 points considered in the robust design process, respectively. It is evident that most of these modes are unstable.

Table 5.13: Loading conditions and parameter uncertainties

Loading Condition	(P, Q) in pu	Parameter uncertainties
Normal	(1.0 , 0.015)	No parameter uncertainties
Heavy	(1.1 , 0.1)	30% increase of line reactance X
Light	(0.3 , 0.015)	25% decrease of machine inertia M
Leading <i>pf</i>	(0.7, -0.3)	30% decrease of field time constant T_{do}

Table 5.14: Open-loop eignvalues associated with the electromechanical modes of all points considered in robust design process

	No parameter uncertainties	30% increase of line reactance X	25% decrease of machine inertia M	30% decrease of field time constant T_{do}
Normal	0.2954±4.957i	0.367±4.227i	0.3516±5.6718i	0.2742±5.0473i
Heavy	0.413±4.7252i	0.5042±3.8936i	0.4944±5.387i	0.3786±4.847i
Light	-.0053±4.675i	-0.0026±3.929i	-0.0066±5.400i	-0.0041±4.674i
Leading <i>pf</i>	0.0264±5.487i	0.0603±5.0166i	0.03±6.3302i	0.0283±5.4943i

Table 5.15: Damping ratio of open-loop eigenvalues associated with the electromechanical modes for all point considered in the robust design process

	No parameter uncertainties	30% increase of line reactance X	25% decrease of machine inertia M	30% decrease of field time constant T_{do}
Normal	-0.0595	-0.0874	-0.0619	-0.0541
Heavy	-0.0871	-0.1288	-0.0914	-0.0777
Light	0.0011	0.0006	0.0012	0.0009
Leading pf	-0.0048	-0.0121	-0.0047	-0.0052

5.2.2.1 Individual Design

The PSS, TCSC, SVC, and TCPS stabilizers will be designed in this section but taking in to account all operation conditions mentioned above during the design process.

a) Stabilizer design

PSO is applied to tune the stabilizers' parameters in order to maximize the minimum damping ratio of all the complex eigenvalues associated with the 16 operating points. The final settings of the optimized parameters for the proposed stabilizers are given in Table 5.16. The convergence rate of the objective function is shown in Fig. 5.18.

Table 5.16: Optimal Parameter Settings, multiple point tuning, individual design

	<i>PSS</i>	<i>SVC</i>	<i>TCSC</i>	<i>TCPS</i>
K	26.237	100	100	100
T_1	0.1918	0.01	0.018	0.1388
T_2	0.1	0.3	0.1	0.1
T_3	0.2016	1	0.2741	0.0489
T_4	0.1	0.3	0.1	0.1

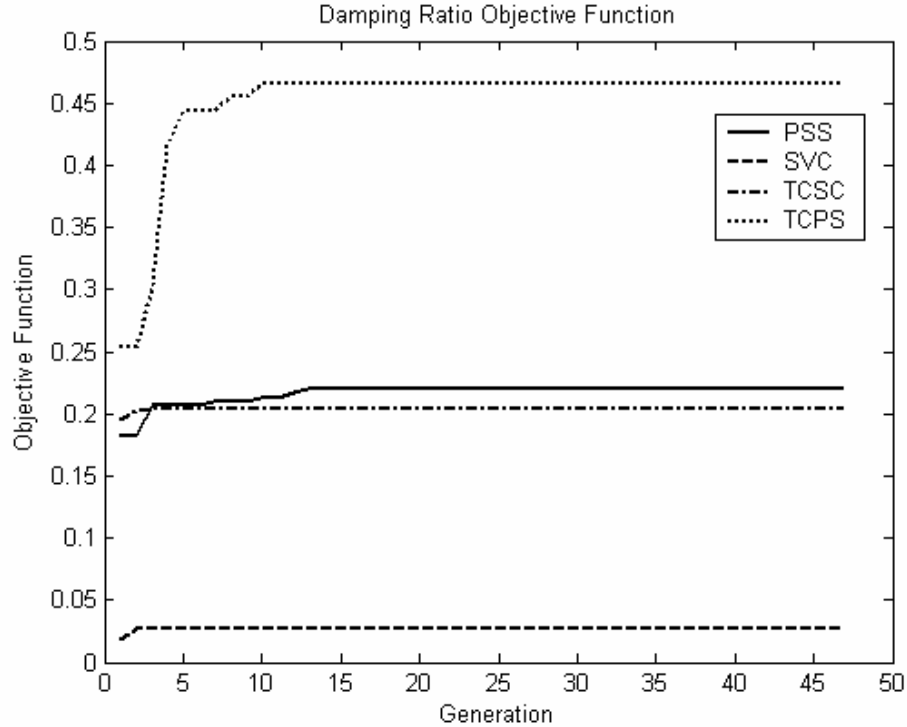


Fig. 5.18: Variation of the objective function of PSS & FACTS-based stabilizers, multiple-point tuning, individual design

b) Eigenvalue Analysis

The system eigenvalues without and with the proposed stabilizers at nominal, light, and heavy loading conditions are given in Tables 5.17, 5.18, and 5.19 respectively, where the first row represents the electromechanical mode eigenvalues and their damping ratios.

Table 5.17: System eigenvalues of nominal loading condition, multiple point tuning, individual design

Base Case	PSS	SVC	TCSC	TCPS
0.2954±i4.9569	-2.187±3.703i (0.5086)*	-2.106±4.129i (0.4543)*	-1.7396±2.933i (0.5101)*	-2.6992±3.354i (0.627)*
10.393± i3.287	-3.679±9.698i -21.9581 -6.4977 -0.2063	-2.581±5.689i -20.4815 -14.3843 -2.6205 -0.2011	-5.052±13.226i -26.0657 -13.8848 -6.653 -0.2087	-6.673±9.84i -20.1497 -13.3961 -7.8953 -0.2099

Table 5.18: System eigenvalues of light loading condition, multiple point tuning, individual design

Base Case	PSS	SVC	TCSC	TCPS
-0.009±i4.8503	-1.2186±4.758i	-0.192±4.715i	-1.312±4.608i	-5.719±8.0537i
-11.08± i3.834	(0.2481)*	(0.0407)*	(0.2738)*	(0.579)*
	-6.1162±7.042i	-6.866±2.34i	-7.3889±6.334i	-4.411±2.327i
	-18.5957	-19.9112	-9.995±3.004i	-9.8844±2.821i
	-6.9276	-10.2981	-22.7998	-20.1527
	-0.2027	-2.5365	-0.203	-0.2121
		-0.1998	-----	-----

Table 5.19: System eigenvalues of heavy loading condition, multiple point tuning, individual design

Base Case	PSS	SVC	TCSC	TCPS
0.4852±i3.6903	-1.4308±2.926i	-1.4374±2.536i	-1.615±1.561i	-2.471±1.836i
-11.583± i3.696	(0.4393)*	(0.493)*	(0.7191)*	(0.8027)
	-4.453±9.557i	-2.8078±5.576i	-4.799±14.163i	-7.072±10.36i
	-21.89	-21.0007	-27.1984	-20.1725
	-6.5262	-13.257	-11.0208	-12.7972
	-0.2106	-4.1101	-9.1219	-8.1166
		-0.2041	-0.2258	-0.2229

c) Non linear time domain simulation

The nonlinear time domain simulations have been carried out at different loading conditions. System responses at nominal loading are only shown.

Figs. 5.19-5.21 show the system response for 6-cycle fault disturbance at the nominal loading condition. It can be seen that both TCSC & TCPS-based stabilizers provide the best damping characteristics and enhance the first swing stability at this loading condition.

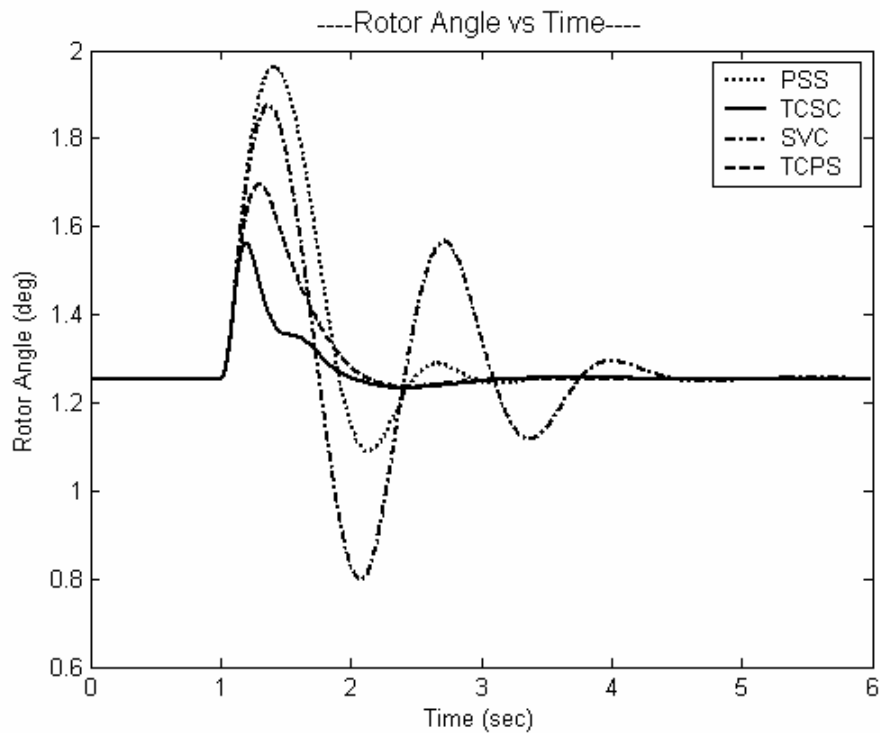


Fig. 5.19: Rotor angle response for 6-cycle fault with nominal loading, multiple point tuning, individual design

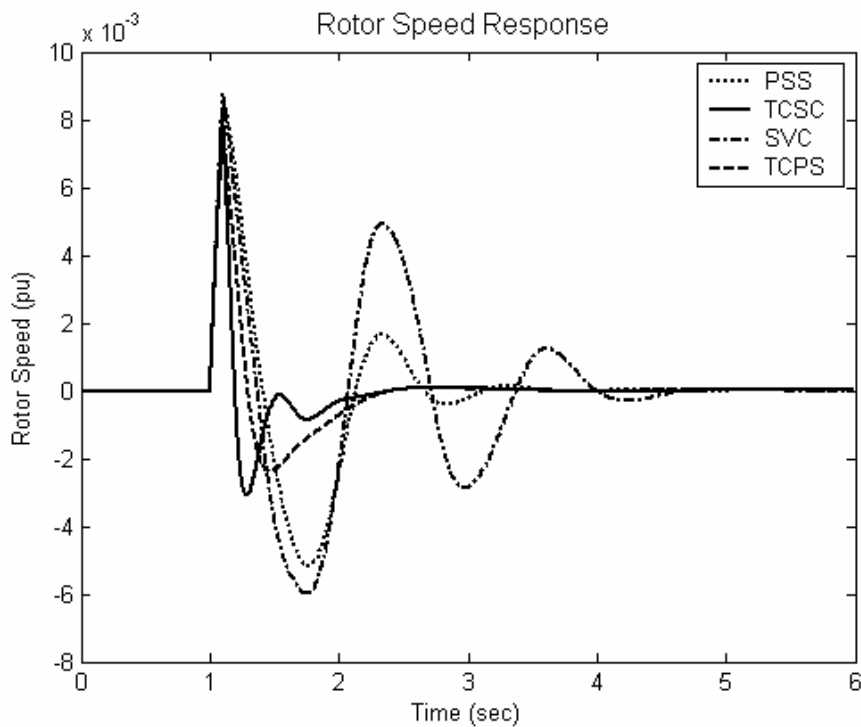


Fig. 5.20: Rotor speed response for 6-cycle fault with nominal loading, multiple point tuning, individual design

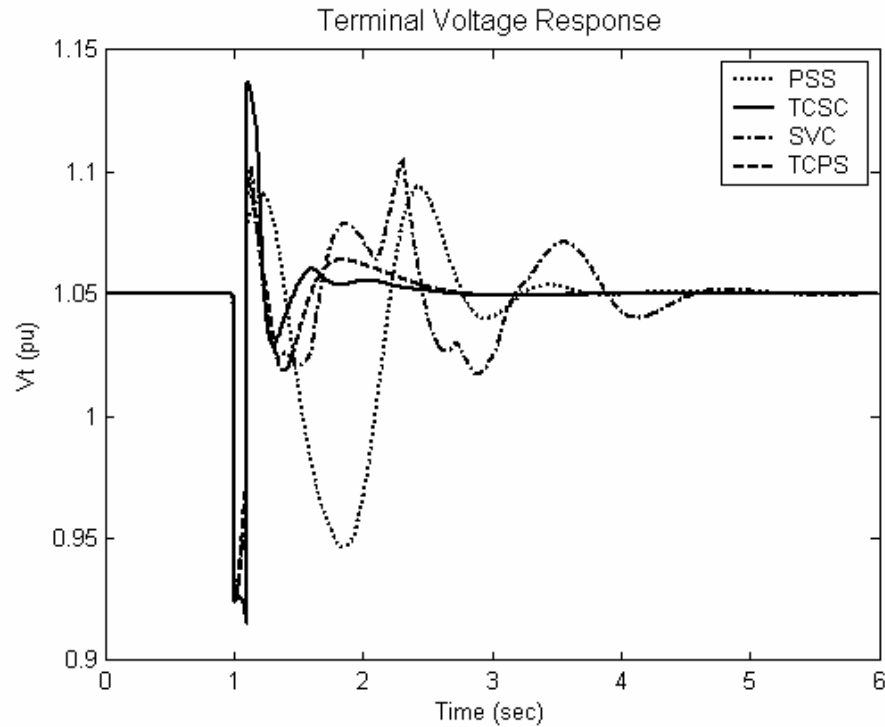


Fig. 5.21: Terminal voltage response for 6-cycle fault with nominal loading, multiple point tuning, individual design

5.2.2.2 Coordinated Design [PSS & TCSC]

In this section the coordinated design of PSS and TCSC-based stabilizer is carried out considering all the 16 operating points mentioned earlier in Table 5.13.

a) Stabilizer design

Both stabilizers PSS and TCSC-based stabilizer are simultaneously tuned by PSO search for the optimum controllers' parameter settings that maximize the minimum damping ratio of all the system complex eigenvalues at the all operating points considered in Table 5.13. The final settings of the optimized parameters for the proposed stabilizers are given in Table 5.20.

It can be noticed when both proposed stabilizers are available, PSS and TCSC, the parameters' settings of the stabilizers are retuned in coordinated approach in order to avoid the negative interaction between stabilizers and to get better system performance compared with individual stabilizer.

The convergence rate of the objective function when PSS and TCSC-based controller are designed individually and in a coordinated manner is shown in Fig. 5.22. It is clear that the coordinated design of PSS and TCSC-based stabilizer improves greatly the system damping compared to their individual application.

Table 5.20: Optimal Parameters Setting, multiple point tuning, coordinated design

	<i>Individual</i>		<i>Coordinated</i>	
	<i>PSS</i>	<i>TCSC</i>	<i>PSS</i>	<i>TCSC</i>
K	17.6843	100	36.627	100
T_1	0.4399	0.1101	0.1356	0.1869
T_2	0.1	0.1	0.1	0.1

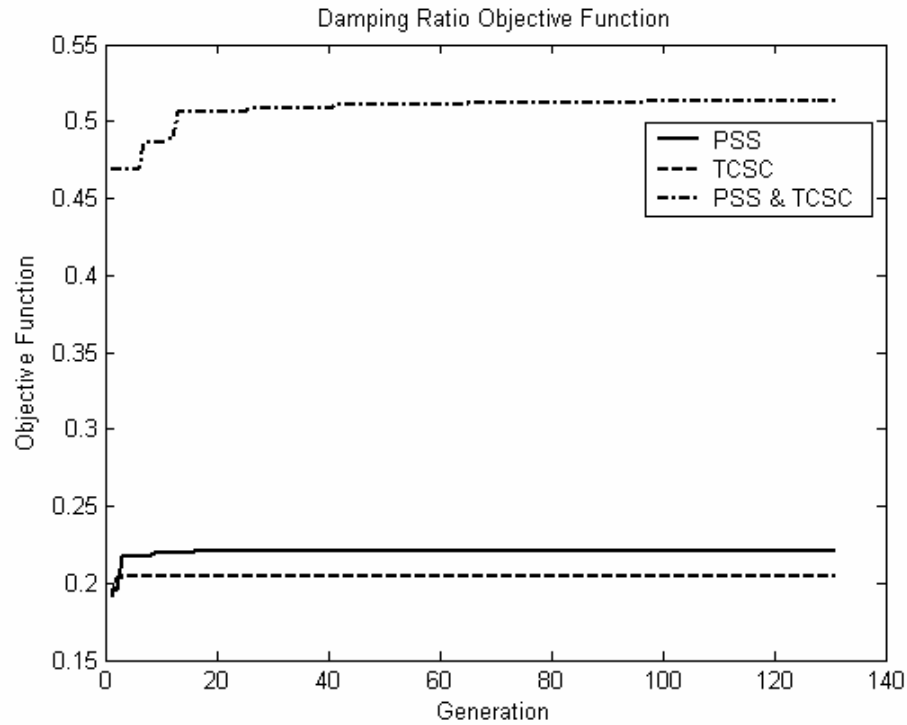


Fig. 5.22: Variation of the objective function of PSS & TCSC-based stabilizers, multiple-point tuning, coordinated design

b) Eigenvalue Analysis

The system eigenvalues along with damping ratios without and with the proposed PSS and TCSC-based stabilizer when applied individually and through coordinated design are given in Tables 5.21, 5.22, and 5.23 for nominal, light, and heavy loading conditions respectively. It is quite evident that the system stability is greatly enhanced with the coordinated design approach as damping ratio of the electromechanical mode eigenvalue has been greatly improved.

Table 5.21: System eigenvalues of nominal loading condition, multiple point tuning, coordinated design

Base Case	PSS	TCSC	PSS & TCSC
0.2954±i4.9569	-1.7797±3.5104i	-2.2811±3.6808i	-10.2418±2.2651i
10.393± i3.287	(0.4522)*	(0.5268)*	(0.9764)*
	-3.2445±9.0286i	-10.2153±9.8381i	-10.6052±13.086i
	-20.1432	-15.7506	-10
	-0.204	-9.4434	-5.2044
		-0.2089	-3.2772
			-0.2201 , -0.2

Table 5.22: System eigenvalues of light loading condition, multiple point tuning, coordinated design

Base Case	PSS	TCSC	PSS & TCSC
0.2954±i4.9569	-1.159±4.6623i	-0.9376±4.8891i	-2.5849±5.194i
10.393± i3.287	(0.2412)*	(0.1884)*	(0.4455)*
	-5.4599±6.294i	-10.1213±4.0989i	-6.469±3.9289i
	-16.9561	-17.88	-16.060±4.1408i
	-0.2017	-10.2668	-10
		-0.203	-0.2071
			-0.2

Table 5.23: System eigenvalues of heavy loading condition, multiple point tuning, coordinated design

Base Case	PSS	TCSC	PSS & TCSC
0.2954±i4.9569	-1.01±2.8409i	-2.8201±1.4207i	-10.28±4.467
10.393± i3.287	(0.335)*	(0.8931)*	(0.9172)*
	-4.045±8.7143i	-10.8002±11.06i	-11.5737±15.507
	-20.0789	-13.0194	-10
	-0.2067	-9.9091	-5.3502
		-0.2265	-1.0825
			-0.2556,-0.2

c) Non linear time domain simulation

The nonlinear time domain simulations have been carried out at different loading conditions. System responses at light loading condition are only shown.

Figs. 5.23-5.25 show the system response for 6-cycle fault disturbance at the light loading condition. It can be seen that the coordinated design provides the best damping characteristics and enhance the system stability at this loading condition.

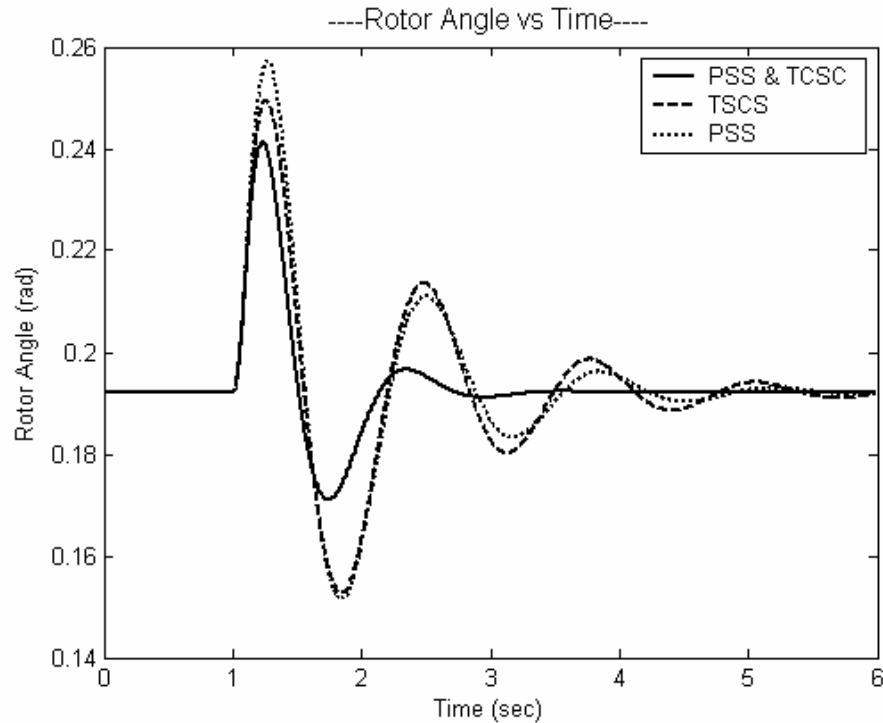


Fig. 5.23: Rotor angle response for 6-cycle fault with light loading, multiple point tuning, coordinated design

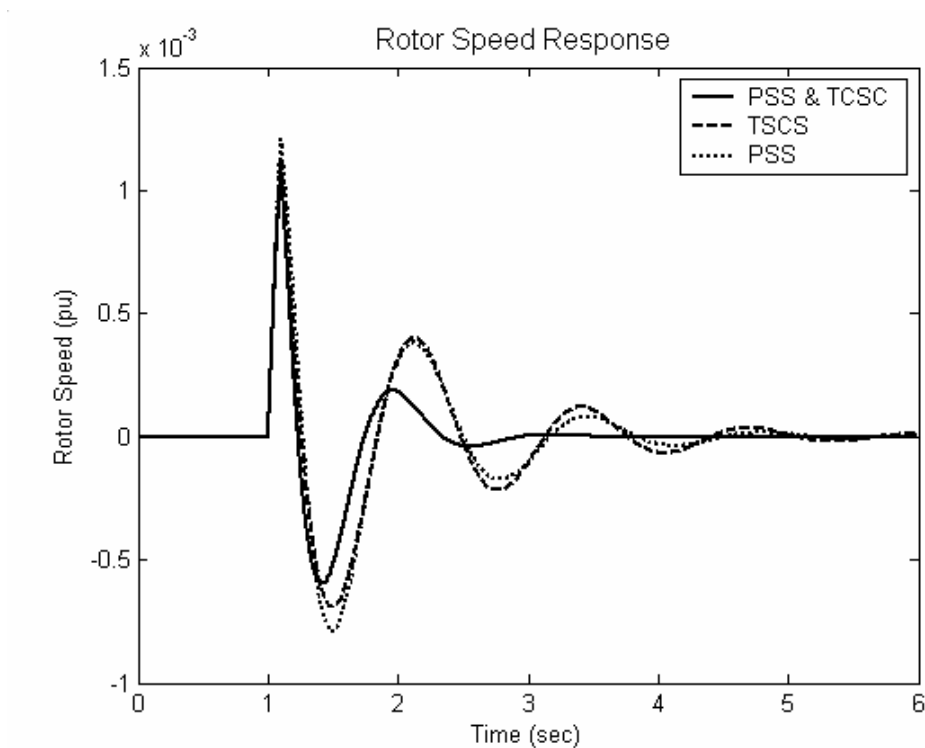


Fig. 5.24: Rotor speed response for 6-cycle fault with light loading, multiple point tuning, coordinated design

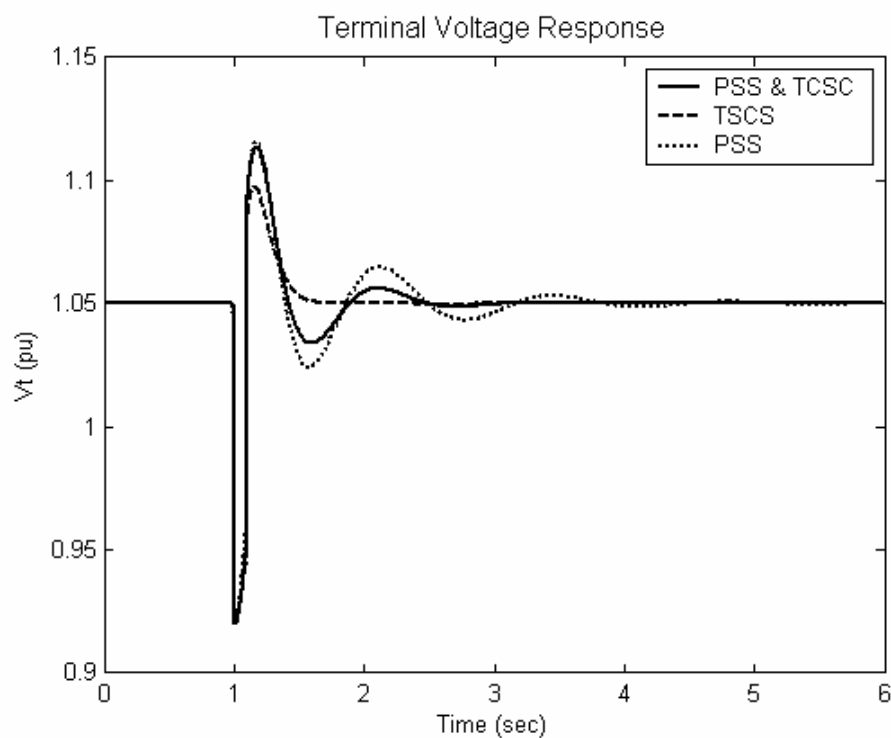


Fig. 5.25: Terminal voltage response for 6-cycle fault with light loading, multiple point tuning, coordinated design

CHAPTER 6

ANALYSIS AND DESIGN OF A STATCOM-BASED STABILIZER IN A SMIB SYSTEM

6.1 Controllability Measure

With each input signals of STATCOM-based stabilizer (ψ & C) in the linearized model, the minimum singular value σ_{\min} has been estimated to measure the controllability of the electromechanical mode from that input. The minimum singular value has been estimated for each STATCOM signal over a wide range of operating conditions. Specifically, for a range of 84 loading conditions specified by $P = [0.05 - 1.0] pu$ with a step of $0.05 pu$ and $Q = [-0.4 - 0.4] pu$ with a step of $0.4 pu$, σ_{\min} has been estimated. At each loading condition in the specified range, the system model is linearized, the electromechanical mode is identified, and the SVD-based controllability measure is implemented.

The capabilities of ψ & C STATCOM signals to control the electromechanical modes over the specified range of operating conditions are given in Figs 6.1-6.3.

It can be seen that the controllability of the electromechanical mode with the ψ and C increases with loading at lagging and leading power factor and slightly increasing

at unity power factor. However, the controllability of the electromechanical mode with the ψ is higher in all cases.

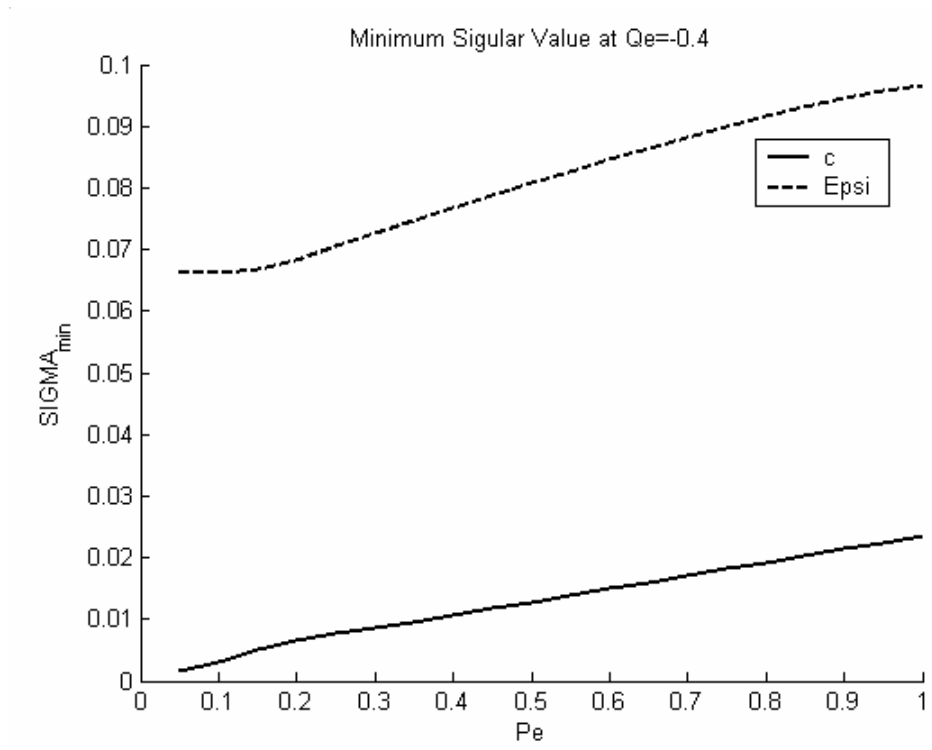


Fig. 6.1: Minimum singular value with STATCOM stabilizer at $Q = -0.4$ pu

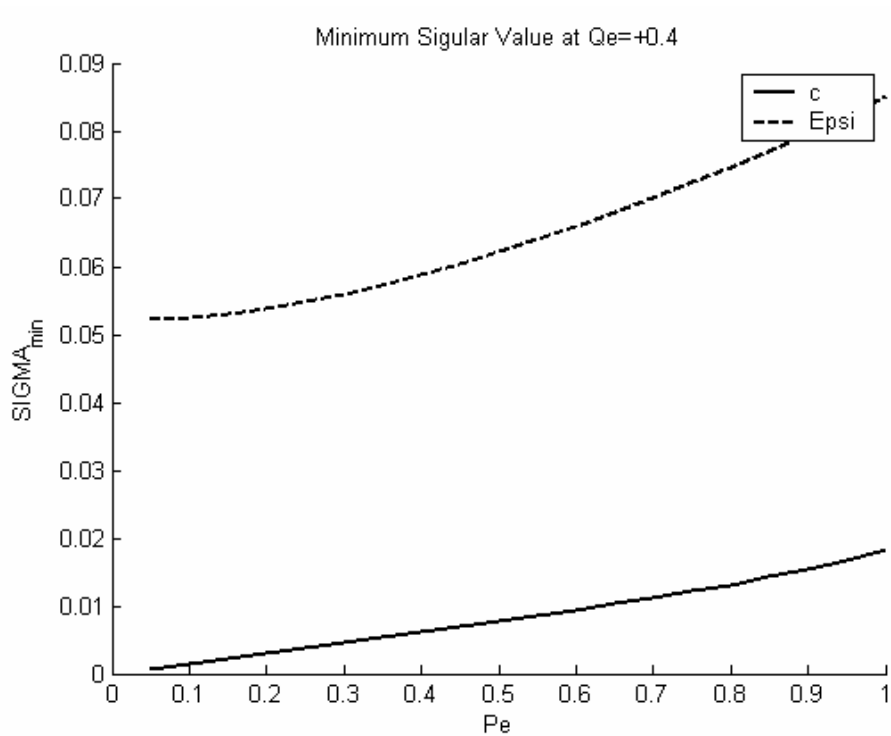


Fig. 6.2: Minimum singular value with STATCOM stabilizer at $Q = 0.4$ pu

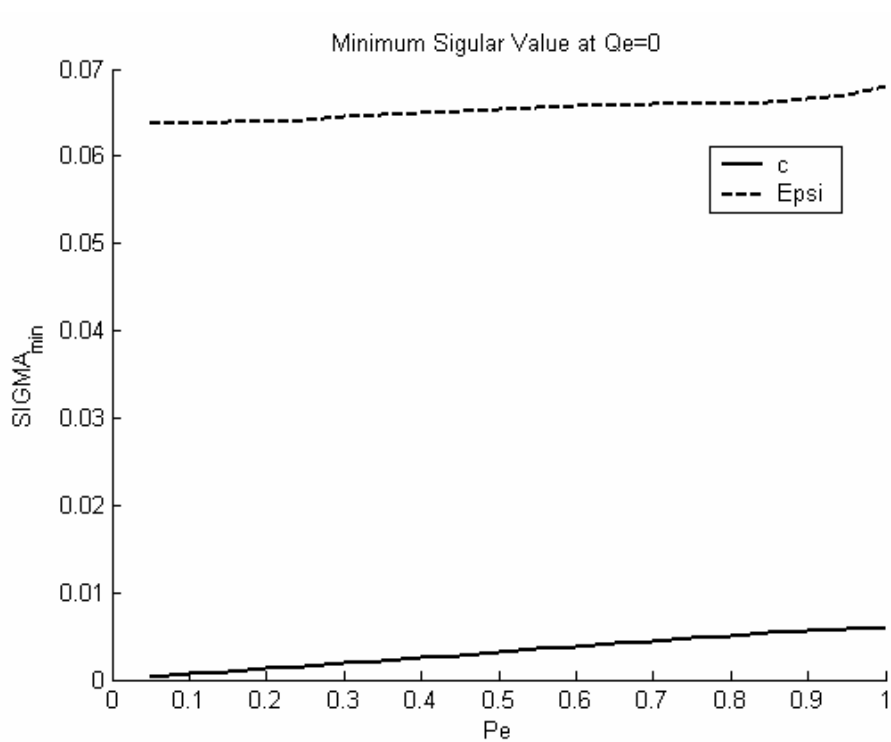


Fig. 6.3: Minimum singular value with STATCOM stabilizer at $Q = 0.0$ pu

6.2 Stabilizer Tuning and Simulation Results

To increase the system damping to the electromechanical model, the objective function J defined below is proposed.

$$J = \max\{\zeta\}$$

Where ζ is the minimum electromechanical mode damping ratio.

This objective function will identify the minimum value of damping ratio among electromechanical modes of all loading condition considered in the design process

To assess the effectiveness of the proposed controllers, four different loading conditions are considered for eigenvalue analysis. These conditions and disturbances are:

4. Nominal loading (P_e, Q_e)=(1.0,0.015) pu.
5. Light loading (P_e, Q_e)=(0.3,0.015) pu.
6. Heavy loading (P_e, Q_e)=(1.1,0.40) pu.

6.2.1 Single Point Tuning

6.2.1.1 Individual and Coordinated Design [C & ψ]

In this section, the stabilizers are tuned with only the nominal loading condition, (P_e, Q_e)=(1.0,0.015) pu, taken into account.

a. Stabilizer Design

Based on the linearized power system model in Equation (3.61), PSO has been applied to the optimization problem to search for optimal settings of the proposed stabilizers for

individual and coordinate design. The final settings of the optimized parameters for the proposed stabilizers are given in Table 6.1.

It can be noticed when both proposed stabilizers are available the parameters' setting of the stabilizers are retuned in coordinated approach in order to avoid the negative interaction between them and to get better system performance compared with individual stabilizer.

The convergence rate of the objective function when (C and ψ)-based controllers are designed individually and in a coordinated manner is shown in Fig. 6.4. It is clear that the coordinated design of (C and ψ)-based controllers improves greatly the system damping compared to their individual application.

Table 6.1: Optimal parameter settings of C & ψ , single point tuning

	<i>Individual</i>		<i>Coordinated</i>	
	<i>C-based Controller</i>	<i>ψ-based Controller</i>	<i>C-based Controller</i>	<i>ψ-based Controller</i>
<i>Controller gain- K</i>	64.9796	100	100	73.0863
<i>T₁</i>	0.2360	1	1	0.01
<i>T₂</i>	0.3	0.3	0.3	0.03
<i>T₃</i>	0.01	0.1194	0.1928	0.0227
<i>T₄</i>	0.3	0.3	0.3	0.3
<i>K_{DCP}</i>	4.1105	6.0994		6.526
<i>K_{DCI}</i>	0.1	30		8.7255

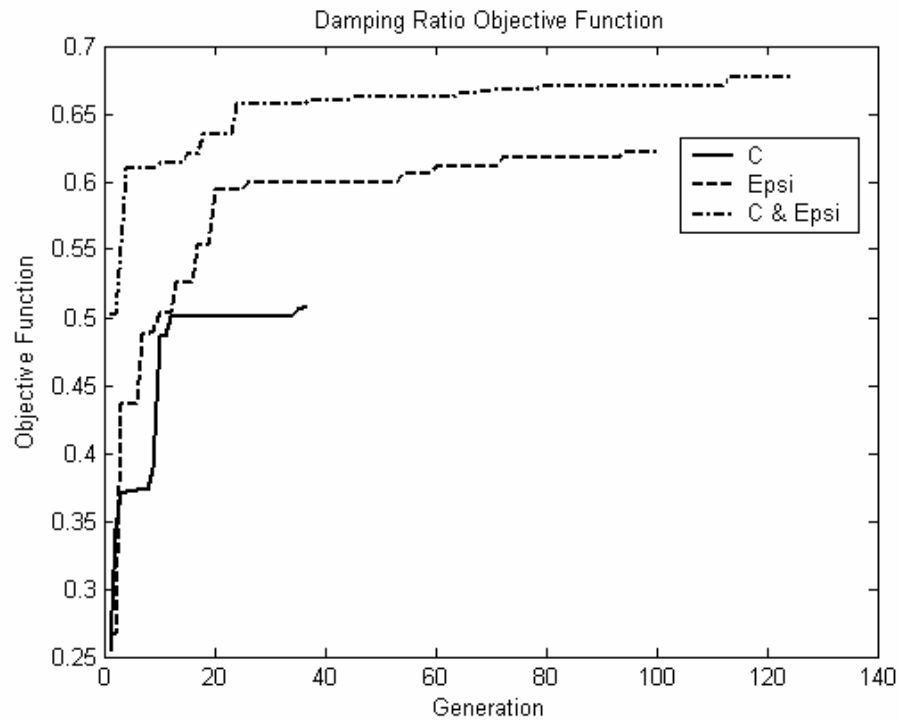


Fig. 6.4: Variation of the objective function of C and ψ -based stabilizers, individual and coordinated design

b. Eigenvalue Analysis

The system eigenvalues along with damping ratios with the proposed STATCOM stabilizer inputs when applied individually and through coordinated design are given in Tables 6.2, 6.3, and 6.4 for nominal, light, and heavy loading conditions respectively. The first bolded rows of these tables represent the EM mode eigenvalue and its damping ratio. It is quite evident that the system stability is greatly enhanced with the coordinated design approach as damping ratio of the electromechanical mode eigenvalue has been improved.

Table 6.2: System eigenvalues of nominal loading condition, for C and ψ -based stabilizers, individual and coordinated design

C-based controller	ψ-based controller	Coordinated [C & ψ]-based Controllers
-3.3450±i5.5037 (0.5194)*	-3.6099±i4.5054 (0.6253)*	-1.7522±2.0658i (0.6468)*
-8.266±i13.5474	-3.38±i4.2187	-4.7995±5.6680i
-2.9323±i4.8003	-7.052±i8.7904	-7.0383±8.2187i
-30.609	-33.5399	-12.0577±14.1712i
-10.0791	-13.926	-28.0022
-8.3729	-5.04	-3.3333, -3.3333
-2.4998, -0.2010	-0.2005, -0.073	-1.35, -0.2014, -0.2

Table 6.3: System eigenvalues of light loading condition, for C and ψ -based stabilizers, individual and coordinated design

C-based controller	ψ-based controller	Coordinated [C & ψ]-based Controllers
-0.0016±5.9385i (0.0003)*	-1.6141±3.3763i (0.4313)*	-1.5465±1.9132i (0.6286)*
-7.7107±11.2521i	-4.1675±8.1737i	-11.3038±12.6054i
-4.7197±1.5434i	-9.1086±1.8221i	-10.8543±7.5714i
-32.3761	-33.1148	-9.8525±1.8315i
-11.2558	-12.3299	-31.7381
-8.8406	-4.9544	-3.3333, -3.3333
-2.8775, -0.2004	-0.1997, -0.0349	-1.3619, -0.2001, -0.2

Table 6.4: System eigenvalues of heavy loading condition, for C and ψ -based stabilizers, individual and coordinated design

C-based controller	ψ-based controller	Coordinated [C & ψ]-based Controllers
-3.0825±7.6321i (0.3745)*	-3.0424±7.6094i (0.3712)*	-4.9094±8.7769i (0.4882)*
-2.1097±2.6633i	-1.8564±2.9938i	-1.2227±1.7363i
-9.2434±10.7717i	-9.0752±4.2969i	-6.8634±5.0554i
-9.7802±1.4011i	-33.6218	-14.3675±12.8397i
-29.0001	-14.2651	-24.5599
-3.233	-4.7629	-3.3333, -3.3333
-0.2029	-0.2022, -0.0677	-1.377, -0.2049, -0.2

c. Non linear time domain simulation

The single machine infinite bus system shown in Fig. 3.4 is considered for nonlinear simulation studies.

A 6-cycle 3- ϕ fault on the infinite bus was created, at all loading conditions, to study the performance of the proposed controllers.

Figs. 6.5- 6.7 show the speed deviation, electrical power, and STATCOM DC voltage responses at nominal operating condition where the coordinated design of STATCOM C & ψ controllers is compared to individual design. It can be seen that, at this loading condition, both individually design STATCOM controllers are performed well in stabilizing the system which confirm the eigenvalue analysis. While there is a good improvement in the system response when coordinated design is considered.

Similarly, the simulation results with 6-cycle fault at light loading condition are shown in Figs. 6.8-6.9. The simulation results obtained clearly indicate that the proposed coordinated design outperforms both the individual designs in terms of first swing stability, overshoot, and settling time. On the other hand, the damping effort provided by the C is not sufficient to keep the system stable at this loading condition. These results confirm the conclusion drawn for eigenvalues analysis. The coordinated design with ψ solves the problem of very low damping ratio at light loading when C controller is considered.

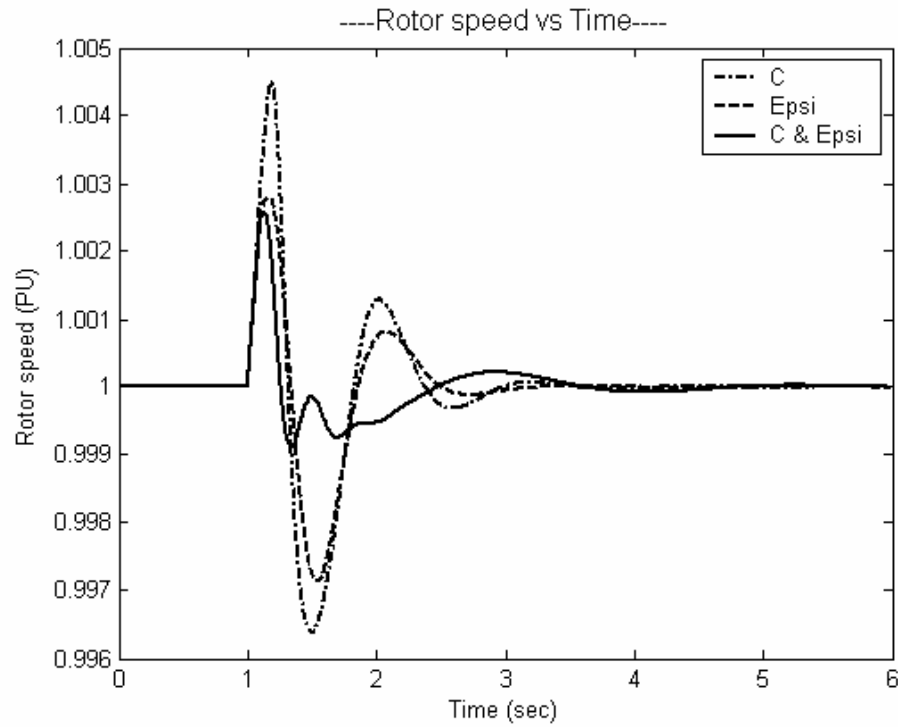


Fig. 6.5: Rotor speed response for 6-cycle fault with nominal loading C & ψ , individual and coordinated design

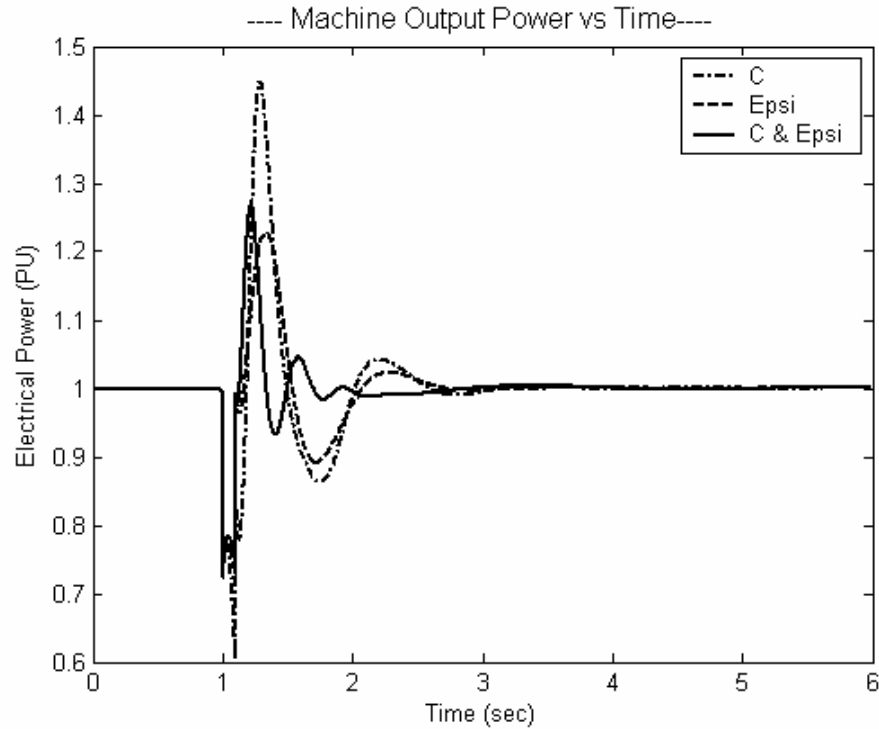


Fig. 6.6: Electrical power response for 6-cycle fault with nominal loading C & ψ , individual and coordinated design

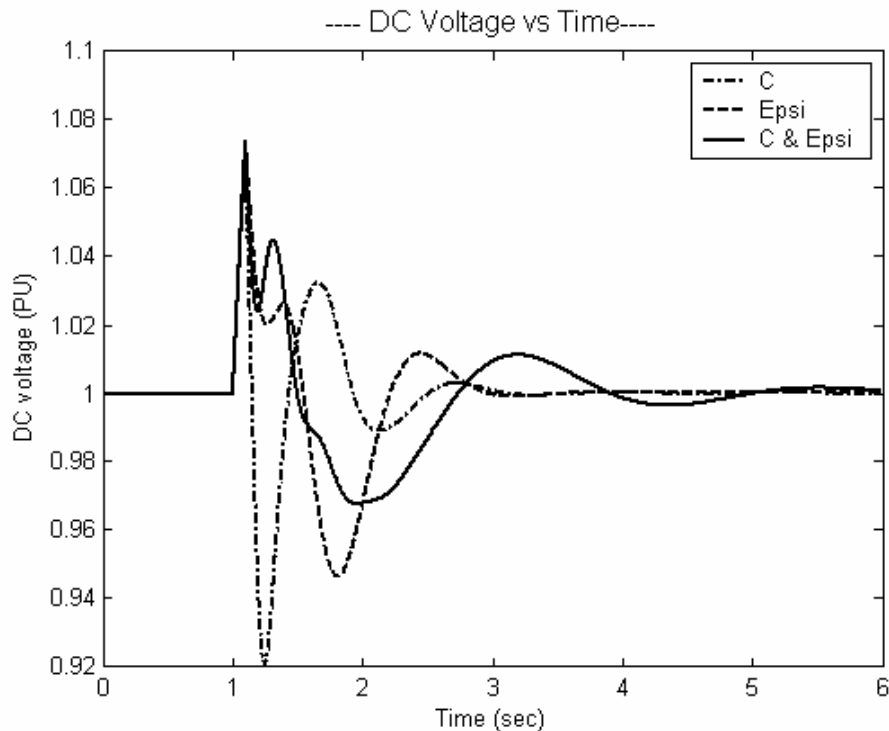


Fig. 6.7: STATCOM DC voltage response for 6-cycle fault with nominal loading, C & ψ , individual and coordinated design

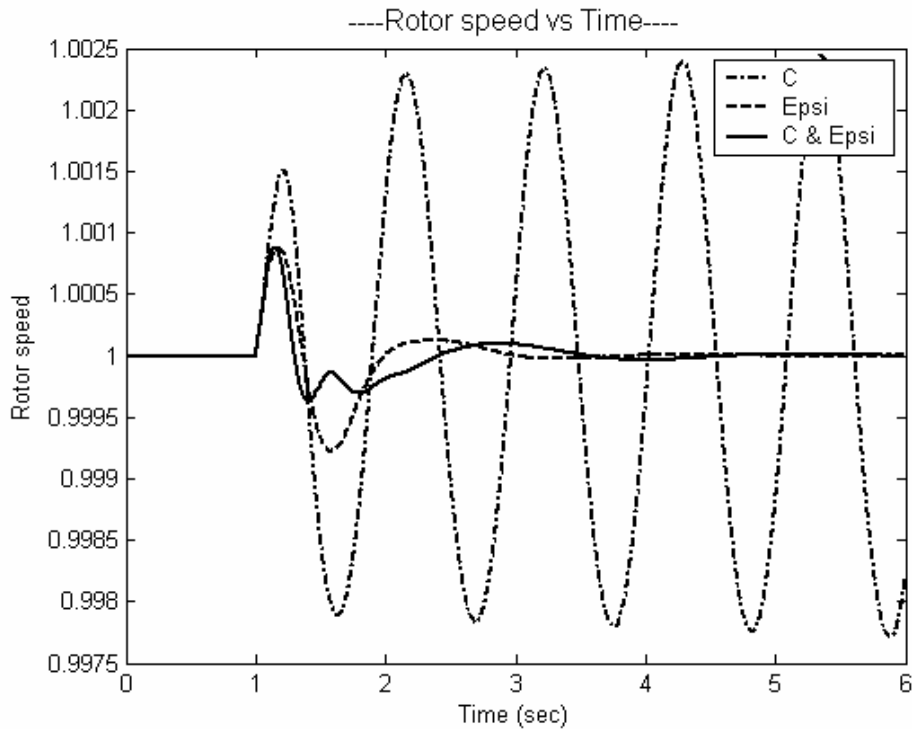


Fig. 6.8: Rotor speed response for 6-cycle fault with light loading, C & ψ individual and coordinated design

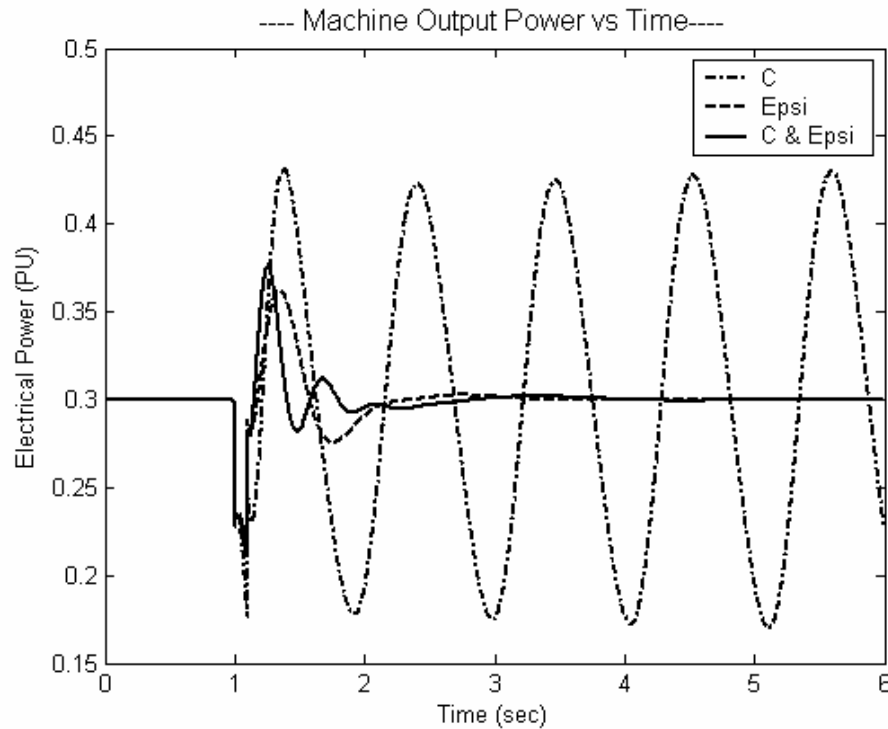


Fig. 6.9: Electrical power response for 6-cycle fault with light loading, C & ψ , individual and coordinated design

6.2.1.2 Coordinated Design [PSS & C]

Another way of solving the negative damping of STATCOM C controller at light loading condition is by coordinated design with PSS, since the STATCOM ψ controller not always could be utilized because it required a sufficient storage energy which is usually not available.

a. Stabilizer design

Both stabilizers PSS & C are simultaneously and individually tuned by PSO searching for the optimum controllers parameter settings that maximize the minimum damping ratio of all the system complex eigenvalues at nominal loading condition. The final settings of the optimized parameters for the proposed stabilizers are given in Table 6.5.

It can be noticed when both proposed stabilizers are available, C and PSS the parameters' settings of the stabilizers are retuned in coordinated approach in order to avoid the negative interaction between them and to achieve better system performance compared with individual stabilizer.

The convergence rate of the objective function when PSS and C-based controllers are designed individually and in a coordinated manner is shown in Fig. 6.10. It is clear that the coordinated design of PSS and C-based stabilizer improves greatly the system damping compared to their individual application.

Table 6.5: Optimal Parameter Settings of C & PSS for individual and coordinate design

	<i>Individual</i>		<i>Coordinated</i>	
	<i>PSS-based Controller</i>	<i>C-based Controller</i>	<i>PSS-based Controller</i>	<i>C-based Controller</i>
<i>Controller gain- K</i>	30.5918	100	100	100
T_1	0.1397	1	1	0.1539
T_2	0.1	0.3	0.1	0.3
T_3	0.3386	0.1198	0.435	0.0821
T_4	0.1	0.3	0.1	0.3
K_{DCP}	4.3113	6.0606		1.5638
K_{DCI}	11.0856	29.9173		0.1

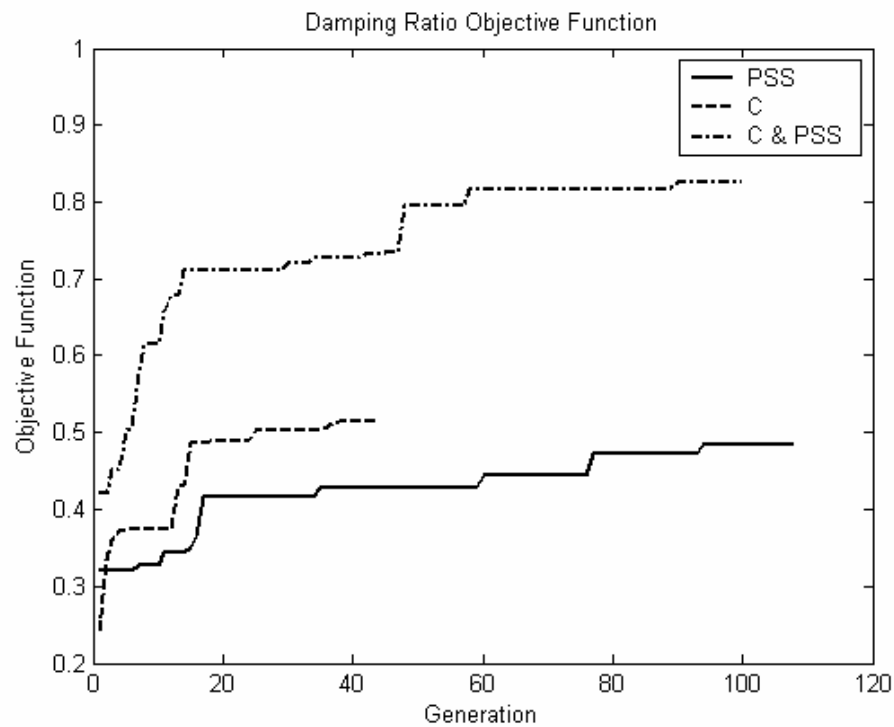


Fig. 6.10: Variation of the objective function of PSS and C -based stabilizers, individual and coordinated design

b. Eigenvalue Analysis

The system eigenvalues with the proposed stabilizers at nominal, light, and heavy loading conditions are given in Tables 6.6, 6.7, and 6.8 respectively, where the first bolded row represents the electromechanical mode eigenvalues and their damping ratios noted as a star. It is clear that the negative damping of PSS and C-based controller at light loading condition has been resolved the coordinated design.

Table 6.6: System eigenvalues of nominal loading condition, for PSS and C -based stabilizers, individual and coordinated design

PSS-based controller	C-based controller	Coordinated [C & PSS]-based Controllers
-4.5889±8.0127i (0.523)*	-2.9310±4.779i (0.5228)*	-3.507±2.4047i (0.8247)*
-5.9827±10.7845i	-3.3361±5.5459i	-11.8341±7.9225i
-3.1383±5.1145i	-8.2703±13.4600i	-3.0017±1.8594i
-33.661	-30.5981	-15.6458±10.2583i
-22.9822	-10.0375	-14.9053±2.0576i
-7.2552	-8.4381	-2.7756, -0.2223
-2.6544, -0.2051	-2.5001, -0.2010	-0.2, -0.064

Table 6.7: System eigenvalues of light loading condition, for PSS and C -based stabilizers, individual and coordinated design

PSS-based controller	C-based controller	Coordinated [C & PSS]-based Controllers
0.2482±5.6088i (-0.0442)*	0.0031±5.942i (-0.0005)*	-0.8527±4.1128i (0.203)*
-7.6015±9.7016i	-7.6977±11.1718i	-6.693±5.5251i
-8.262±2.7734i	-4.735±1.5462i	-14.1913±1.910i
-33.1629	-32.3736	-4.2378±1.6409i
-18.5597	-11.2622	-29.5845, -15.7221
-7.7277	-8.8411	-2.8875, -0.2065
-2.8651, -0.2017	-2.8779, -0.2004	-0.0642, -0.2

Table 6.8: System eigenvalues of heavy loading condition, for PSS and C -based stabilizers, individual and coordinated design

PSS-based controller	C-based controller	Coordinated [C & PSS]-based Controllers
-1.2221±4.9563i (0.2394)*	-2.1083±2.6648i (0.6205)*	-1.3217±1.5608i (0.6462)*
-4.3584±11.2561i	-3.0515±7.6399i	-16.9235±18.6221i
-8.0453±3.3585i	-9.2717±10.711i	-4.3267±2.5399i
-33.7839	-9.7933±1.3914i	-11.1952±5.044i
-22.4743	-28.9813	-15.2178±1.8584i
-7.6578	-3.2337	-2.5986, -0.2301
-2.8283, -0.2051	-0.2029	-0.2, -0.069

c. Non linear time domain simulation

The single machine infinite bus system shown in Fig. 3.4 is considered for nonlinear simulation studies. 6-cycle 3- ϕ fault on the infinite bus was created, at all loading conditions, to study the performance of the proposed controllers.

Figs. 6.11-6.14 show the system response at nominal operating condition where the coordinated design of STATCOM C and PSS controllers is compared to individual design. Similarly the system response at light loading condition is shown in Figs. 6.15-6.16. It can be seen that, at all loading conditions, the proposed coordinated design outperforms both the individual designs in terms of first swing stability, overshoot, and settling time. These results confirm the conclusion drawn for eigenvalues analysis. The coordinated design solves the problem of very low or negative damping ratio at light loading when C-based controller and PSS are considered.

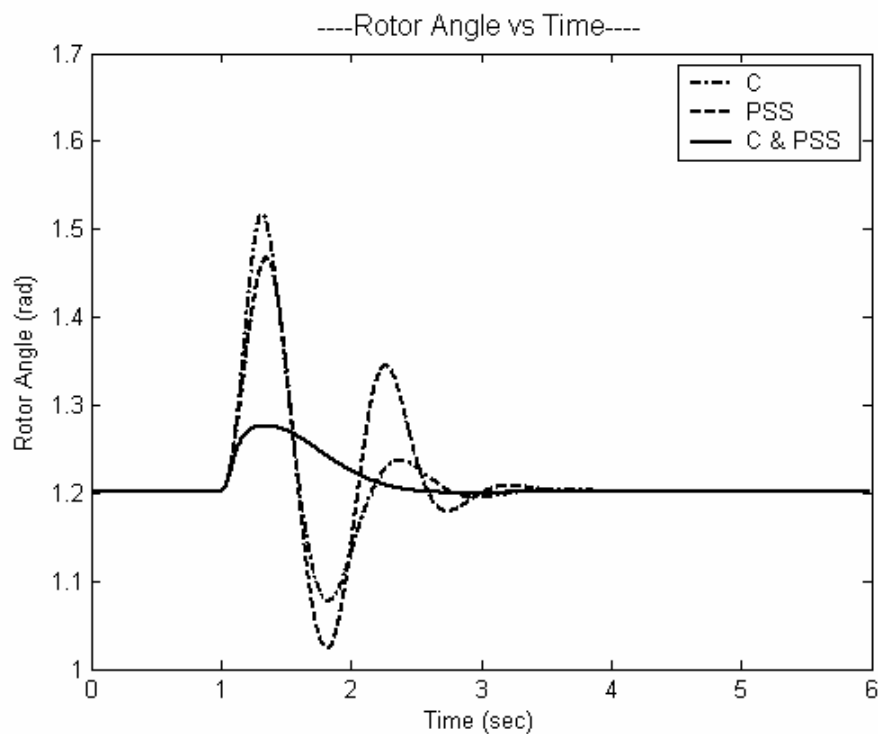


Fig. 6.11: Rotor angle response for 6-cycle fault with nominal loading C & PSS, individual and coordinated design

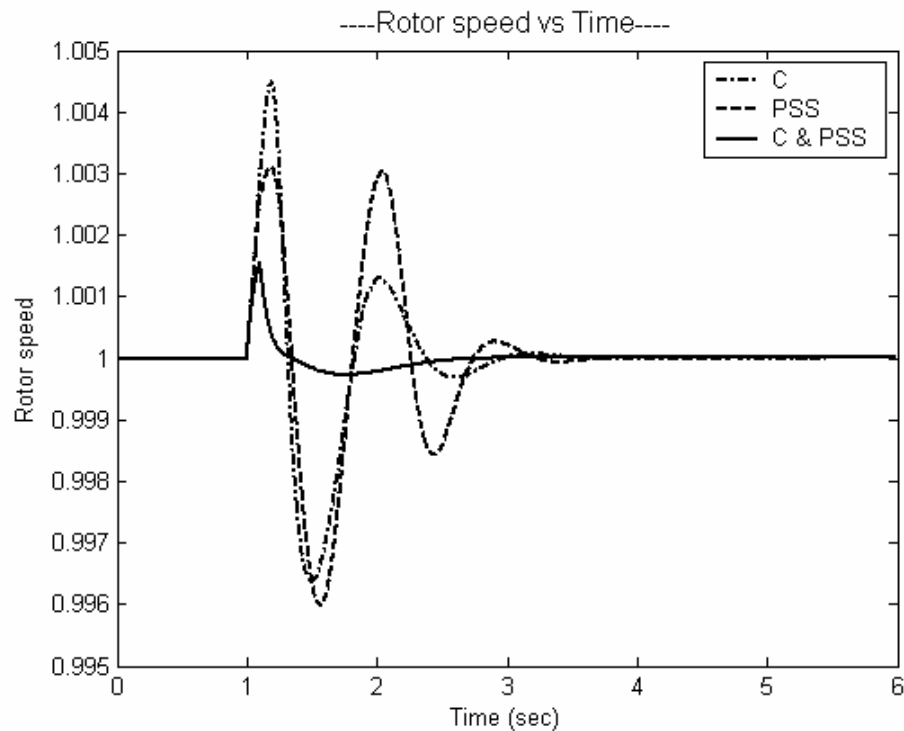


Fig. 6.12: Rotor speed response for 6-cycle fault with nominal loading, C & PSS, individual and coordinated design

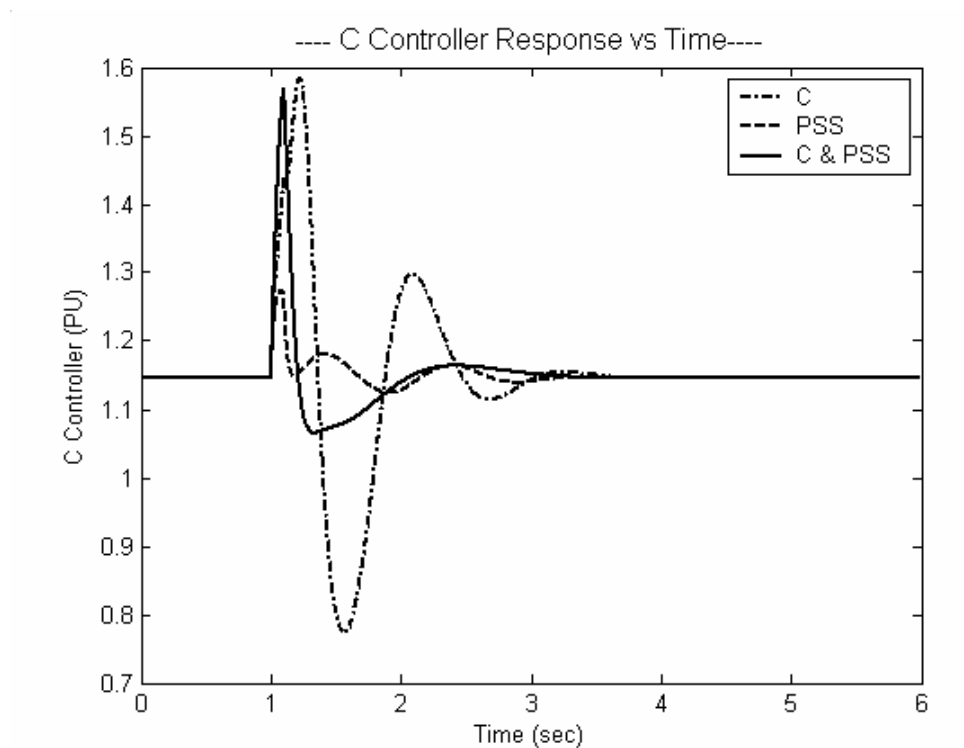


Fig. 6.13: STATCOM "C" controller response for 6-cycle fault with nominal loading, C & PSS, individual and coordinated design

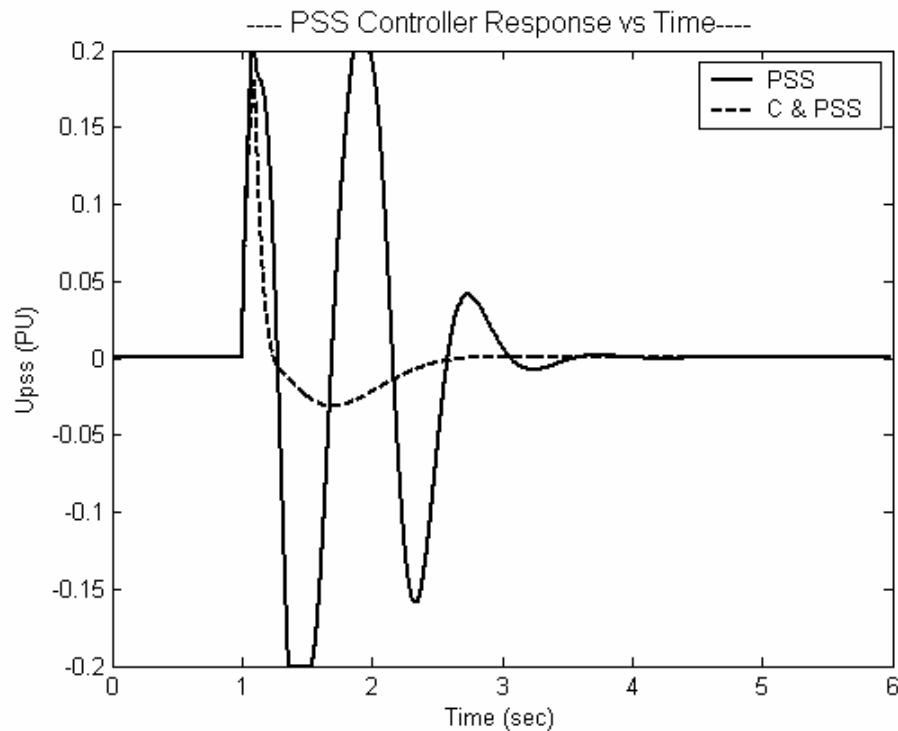


Fig. 6.14: PSS response for 6-cycle fault with nominal loading, C & ψ , individual and coordinated design

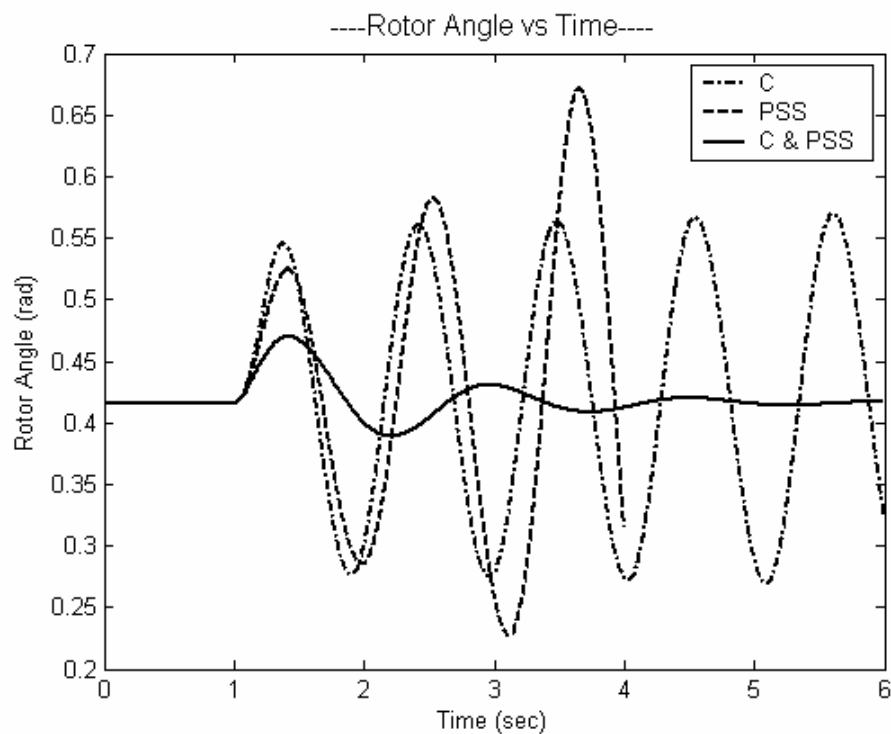


Fig. 6.15: Rotor angle response for 6-cycle fault with light loading, C & PSS, individual and coordinated design

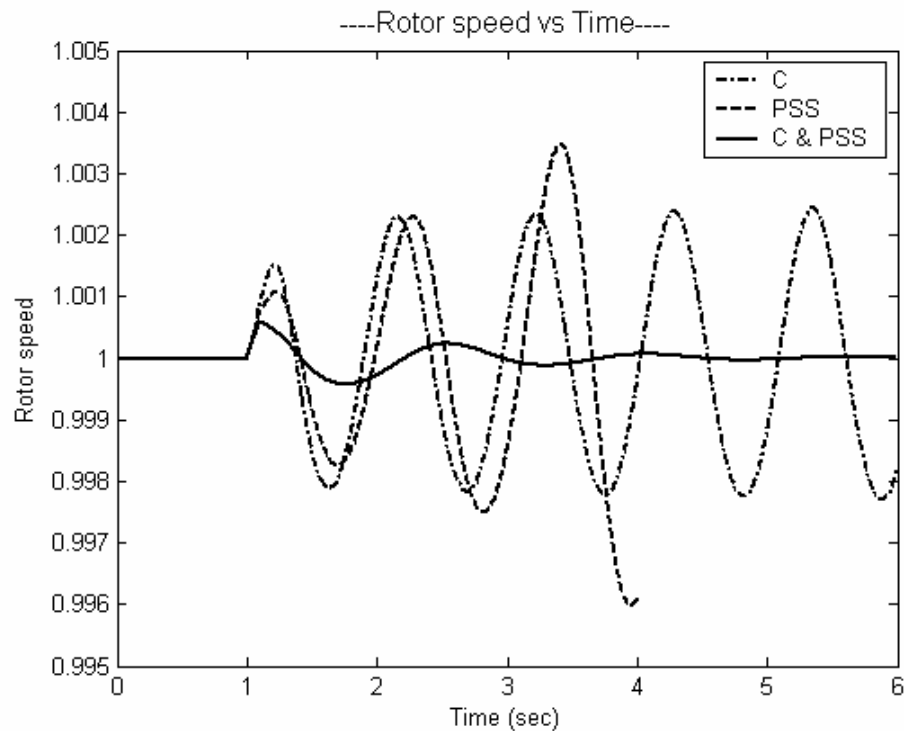


Fig. 6.16: Rotor speed response for 6-cycle fault with light loading, C & PSS, individual and coordinated design

6.2.2 Multiple Point Tuning

In this section, the STATCOM-based controllers' parameters with PSS are optimized over a wide range of operating conditions and system parameter uncertainties in order to have robust stabilizers. Four loading conditions represent nominal, light, heavy, and leading power factor are considered. Each loading condition is considered without and with parameter uncertainties as given in Table 6.9. Hence, the total number of points considered for design process is 16.

Tables 6.10 and 6.11 list the open-loop, STATCOM without POD controllers, eigenvalues and corresponding damping ratios associated with the EM modes of all the 16 points considered in the robust design process, respectively. It is evident that modes belong to leading power factor are unstable.

Table 6.9: Loading conditions and parameter uncertainties

Loading Condition	(P, Q) in pu	Parameter uncertainties
Normal	(1.0, 0.015)	No parameter uncertainties
Heavy	(1.1, 0.1)	30% increase of line reactance X
Light	(0.3, 0.015)	25% decrease of machine inertia M
Leading <i>pf</i>	(0.7, -0.3)	30% decrease of field time constant T_{do}

Table 6.10: Open-loop eigenvalues associated with the electromechanical modes of all points considered in robust design process

	No parameter uncertainties	30% increase of line reactance X	25% decrease of machine inertia M	30% decrease of field time constant T_{do}
Normal	-0.717±1.854i	-1.5057±2.38i	-0.9215±2.21i	-0.3153±2.4402i
Heavy	-1.1804±2.10i	-1.685±2.551i	-1.366±2.464i	-0.6484±2.48i
Light	-0.163±2.81i	-0.318±2.392i	-0.1786±3.249i	-0.1285±2.84i
Leading <i>pf</i>	0.5346±2.62i	0.1492±1.798i	0.4795±2.937i	0.5713±2.874i

Table 6.11: Damping ratio of open-loop eigenvalues associated with the electromechanical modes for all point considered in the robust design process

	No parameter uncertainties	30% increase of line reactance X	25% decrease of machine inertia M	30% decrease of field time constant T_{do}
Normal	0.3608	0.5346	0.3847	0.1281
Heavy	0.4885	0.5514	0.4849	0.253
Light	0.0579	0.1319	0.0549	0.0451
Leading pf	-0.2001	-0.0827	-0.1611	-0.195

6.2.2.1 Individual Design

The STATCOM-based (C & ψ) stabilizers are design on individual basis taking into consideration all of the operating points specified above. PSO algorithm is used to optimize the stabilizer parameters that maximize the minimum damping ratio of all complex eigenvalues.

a) Stabilizer design

The convergence rate of the objective function when C and ψ -based stabilizers are design individually is shown in Fig. 6.17. The final setting of the optimize parameters for the proposed stabilizers are given in Table 6.12.

Table 6.12: Optimal parameter settings for C & ψ , multiple point tuning, individual design

<i>Parameters</i>	<i>C-based Controller</i>	<i>ψ-based Controller</i>
Controller gain- K	100	64.9796
T_1	1	0.2360
T_2	0.3	0.3
T_3	0.1194	0.01
T_4	0.3	0.3
K_{DCP}	6.0994	4.1105
K_{DCI}	30	0.1

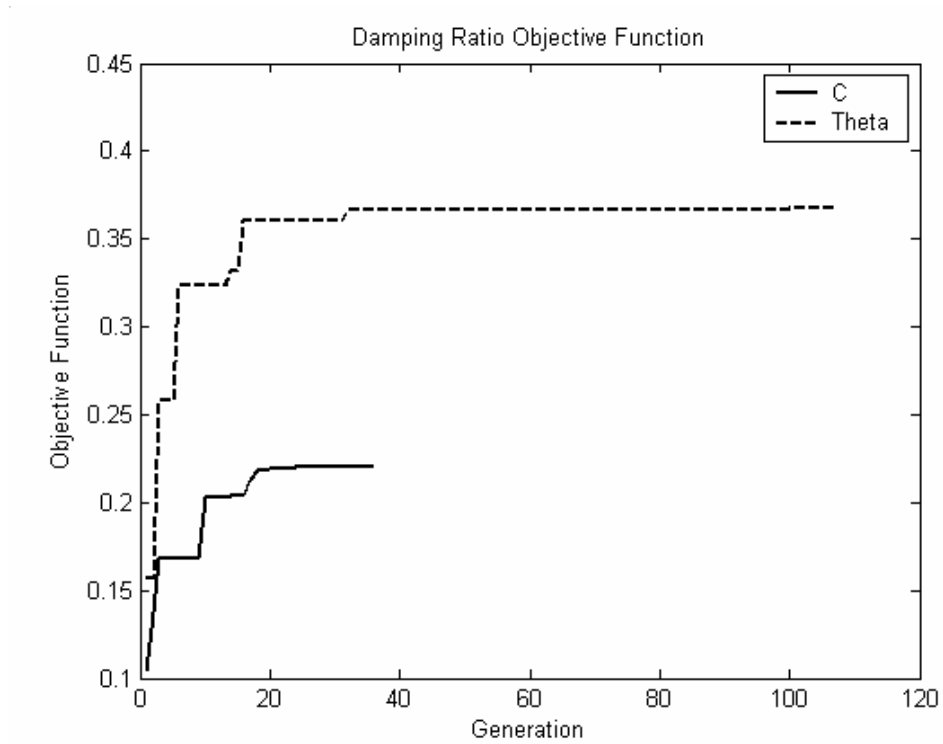


Fig. 6.17: Variation of the objective function of ψ and C -based stabilizers, multiple point tuning, individual design

b) Eigenvalue Analysis

The system eigenvalues without and with the proposed stabilizers at nominal, light, and heavy loading conditions are given in Tables 6.13, 6.14, and 6.15 respectively. The first row of these tables represents the electromechanical mode eigenvalues. It is clear that the proposed robust stabilizers are effective at all points considered.

Table 6.13: System eigenvalues of nominal loading condition, for C & ψ , multiple point tuning, individual design

system with STATCOM No POD controllers	C-based controller	ψ -based controller
-0.7174 ± 1.8546i (0.3608)*	-1.4176±2.765i (0.4562)*	-2.3108±2.2442i (0.7174)*
-13.5086	-4.157±10.2611i	-2.663±6.0705i
-5.3029	-5.738±23.4564i	-8.2258±17.7831i
-0.1542	-31.8664	-33.5313
	-14.1855	-13.5437
	-9.6084	-7.1361
	-2.3619, -0.2020	-0.2005, -0.0387

Table 6.14: System eigenvalues of light loading condition, for C & ψ , multiple point tuning, individual design

System with STATCOM No POD controllers	C-based controller	ψ -based controller
-0.1301 ± 2.8384i (0.0458)*	-1.4297±5.8473i (0.2375)*	-1.8372±2.5677i (0.5819)*
-11.1526	-4.1005±3.0398i	-3.9219±5.2608i
-8.8936	-5.4802±20.44i	-7.6081±14.937i
-0.0155	-32.67	-33.1106
	-12.5483	-11.9736
	-10.1345	-8.3866
	-2.8401, -0.2009	-0.1996, -0.0094

Table 6.15: System eigenvalues of heavy loading condition, for C & ψ , multiple point tuning, individual design

System with STATCOM No POD controllers	C-based controller	ψ -based controller
-1.0835±2.6517i (0.3783)*	-1.2747±1.8069i (0.5764)*	-1.8559±2.2192i (0.6415)*
-1.7071	-4.1875±11.5564i	-3.4708±6.1691i
-13.0972	-5.6067±19.7289i	-7.7395±14.3323i
-6.8040	-31.1149	-33.6159
	-13.4416	-13.2122
	-10.4998	-7.671
	-3.4676, -0.2062	-0.2023, -0.0337

* dampig ratio

c) Non linear time domain simulation

The nonlinear time domain simulations have been carried out at different loading conditions. Figs. 6.18-6.24 show the system response for 6-cycle fault disturbance at the nominal and light loading conditions. It can be seen that both C and ψ -based stabilizers provide an excellent damping characteristics and enhance the first swing stability at all loading conditions.

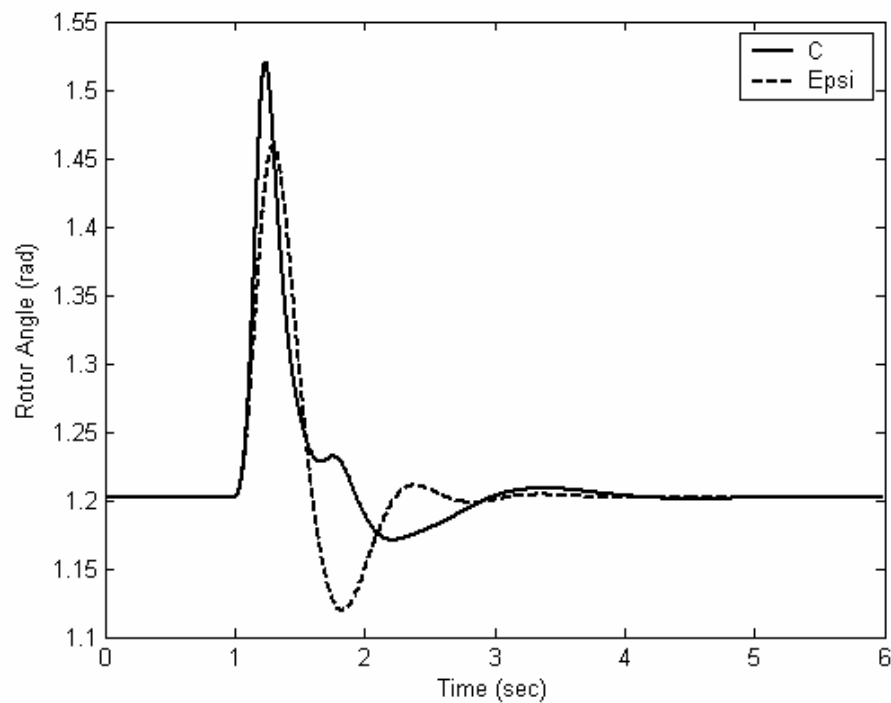


Fig. 6.18: Rotor angle response for 6-cycle fault with nominal loading, multiple point tuning, individual design for C & ψ

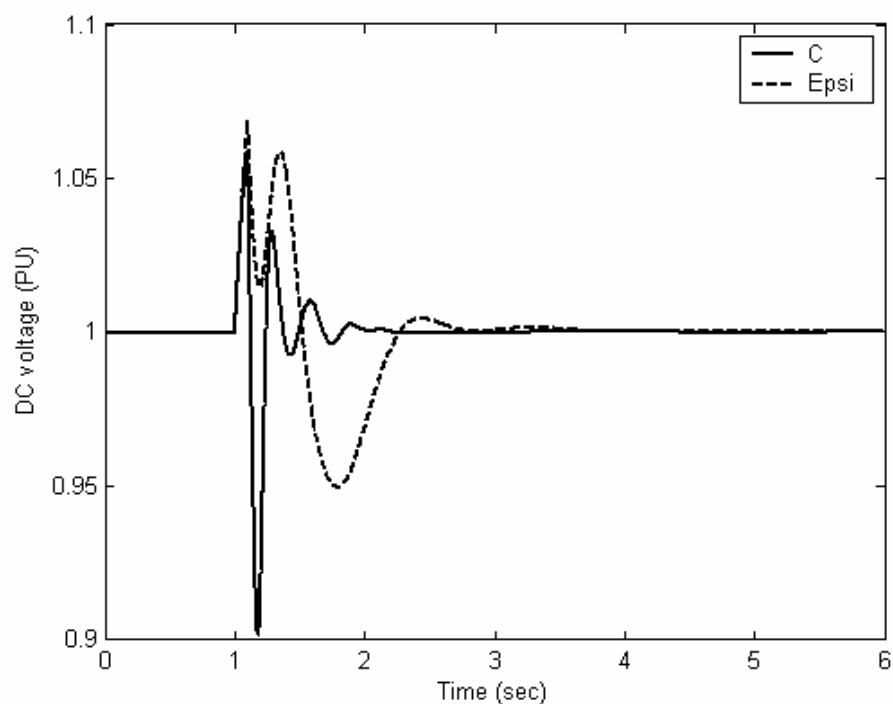


Fig. 6.19: STATCOM DC voltage response for 6-cycle fault with nominal loading, multiple point tuning, individual design for C & ψ

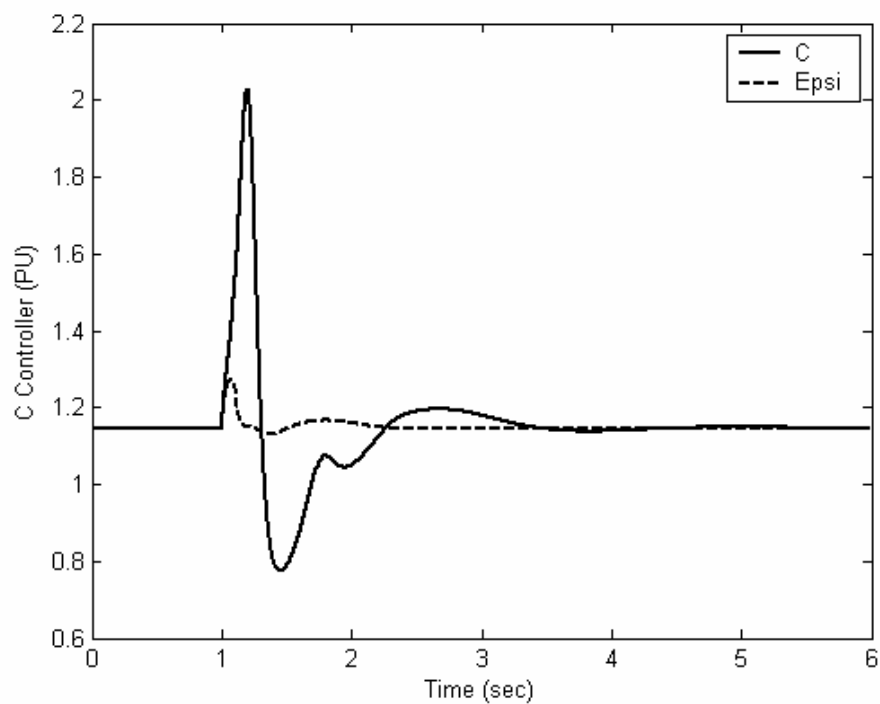


Fig. 6.20: STATCOM C controller response for 6-cycle fault with nominal loading, multiple point tuning, individual design for C & ψ

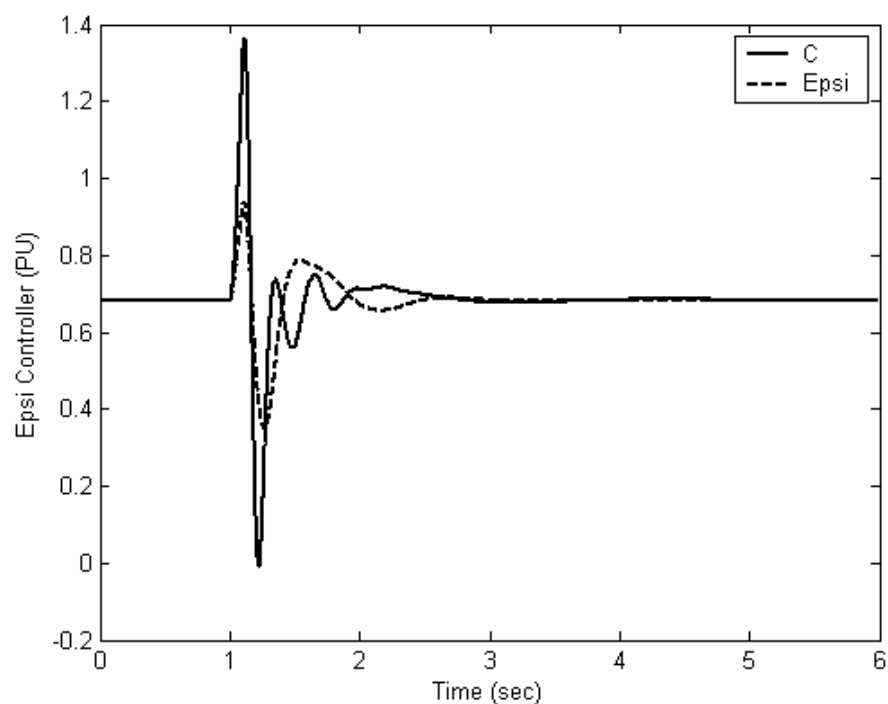


Fig. 6.21: STATCOM ψ controller response for 6-cycle fault with nominal loading, multiple point tuning, individual design for C & ψ

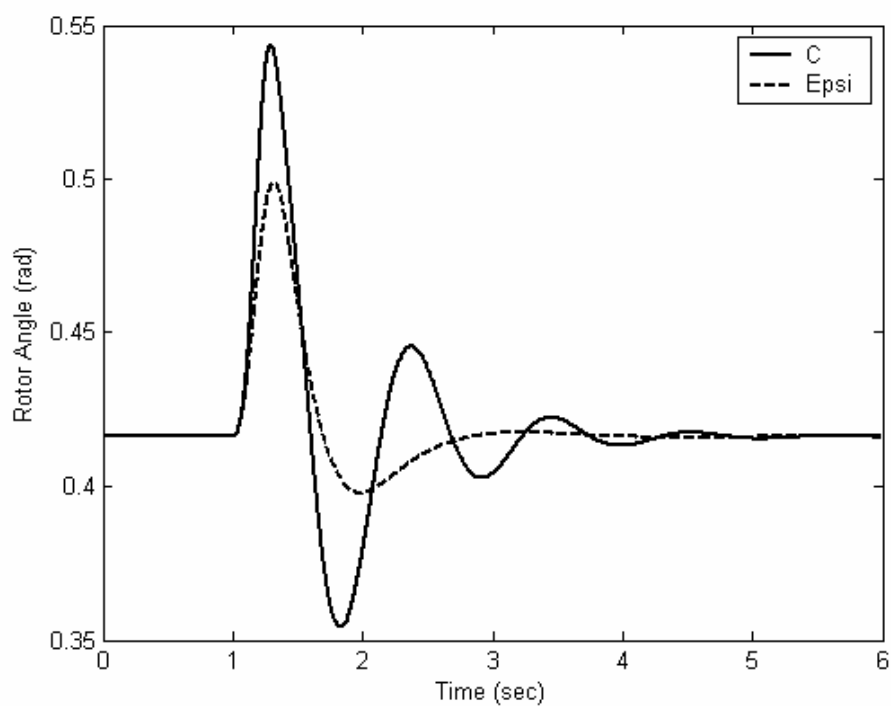


Fig. 6.22: Rotor angle response for 6-cycle fault with light loading, multiple point tuning, individual design for C & ψ

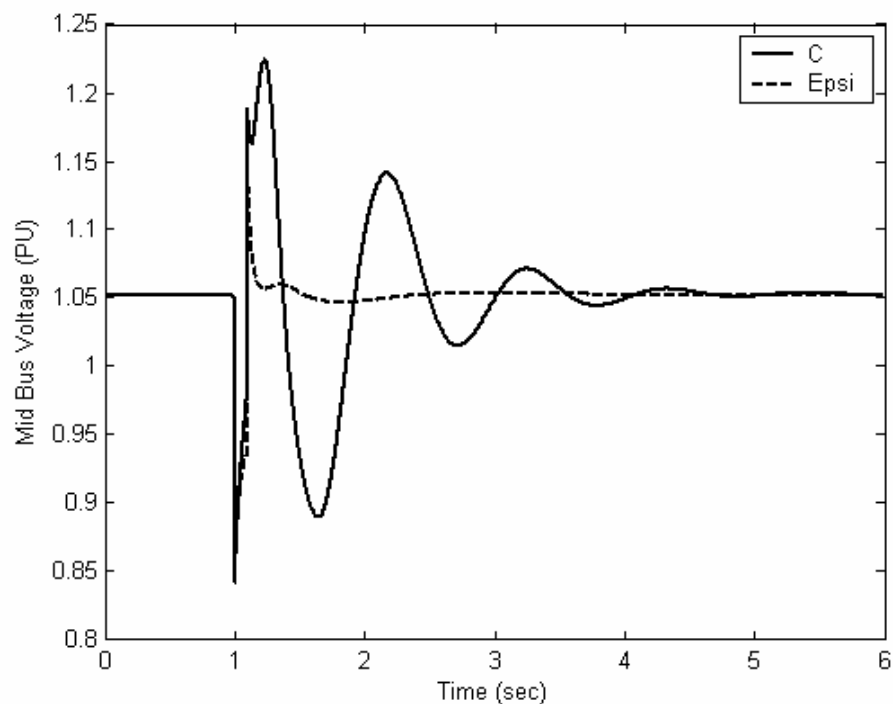


Fig. 6.23: STATCOM bus voltage response for 6-cycle fault with light loading, multiple point tuning, individual design for C & ψ

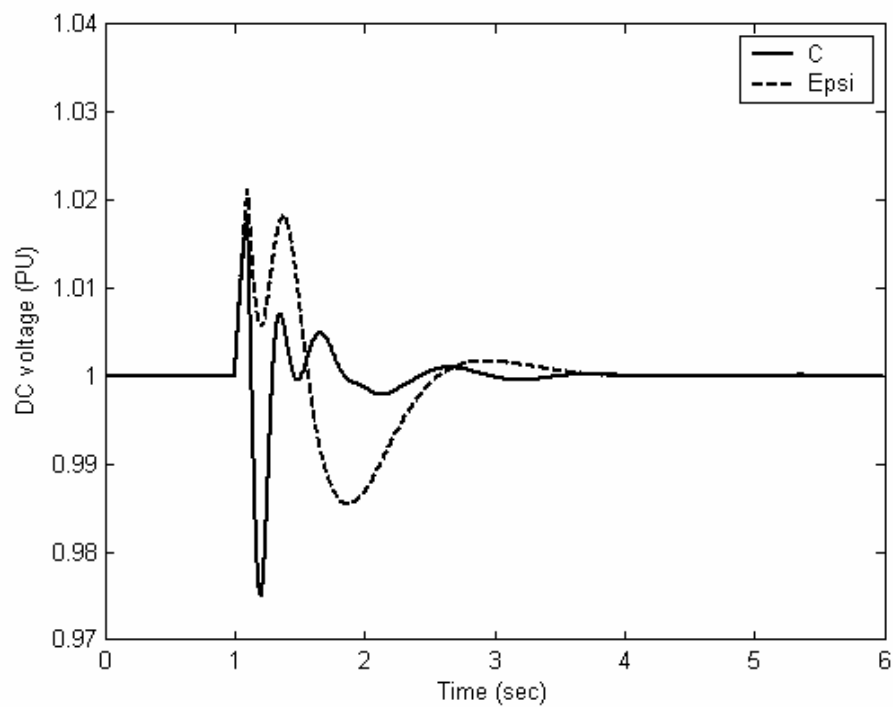


Fig. 6.24: STATCOM DC voltage response for 6-cycle fault with light loading, multiple point tuning, individual design for C & ψ

6.2.2.2 Coordinated Design [C and PSS]

In this section the coordinated design of STATCOM-based C stabilizer and PSS is address over a wide range of operating conditions. PSO algorithm is used to optimize simultaneously the stabilizers parameters that maximize the minimum damping ratio of all complex eigenvalues. It is worth mentioning that the 16 loading conditions specified above are taken into consideration during the design process.

a) Stabilizer design

The convergence rate of the objective function when PSS and C-based controller are designed individually and in a coordinated manner is shown in Fig. 6.25. It is clear that the coordinated design of PSS and C-based stabilizer improves greatly the system damping compared to their individual application. The final settings of the optimized parameters for the proposed stabilizers are given in Table 6.16.

It can be noticed when both proposed stabilizers, C and PSS, are available the parameters' settings of the stabilizers are retuned in coordinated approach in order to avoid the negative interaction between the controllers and to get better system performance compared with individual stabilizer.

Table 6.16: Optimal parameters Setting of C & PSS, multiple point tuning, individual and coordinated design

	<i>Individual</i>		<i>Coordinated</i>	
	<i>C-based Controller</i>	<i>PSS-based Controller</i>	<i>C-based Controller</i>	<i>PSS-based Controller</i>
<i>Controller gain- K</i>	100	14.7626	100	100
T_1	0.1	0.8355	0.7594	0.0303
T_2	0.3	0.1	0.3	0.1
T_3	1	0.1867	0.8527	0.2529
T_4	0.3	0.1	0.3	0.1
K_{DCP}	100	11.6042		7.5006
K_{DCI}	74	94.36		0.01

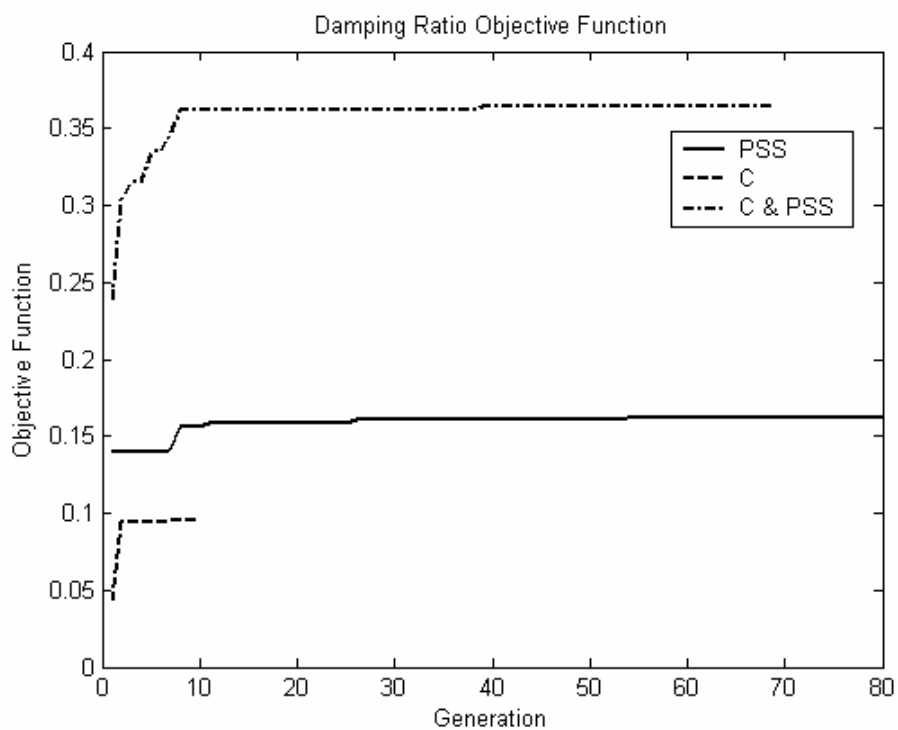


Fig. 6.25: Variation of the objective function of PSS & C-based stabilizers, multiple-point tuning, coordinated design

b) Eigenvalue Analysis

The system eigenvalues with the proposed stabilizers at nominal, light, and heavy loading conditions are given in Tables 6.17, 6.18, and 6.19 respectively, where the first bolded row represents the electromechanical mode eigenvalues and their damping ratios.

It is clear that the multiple point tuning approach greatly improve the damping of PSS and C-based controller when they designed individually and in coordinated base at all loading conditions compared to single point tuning approach.

Table 6.17: System eigenvalues of nominal loading condition for C & PSS, multiple point tuning, individual and coordinated design

PSS-based controller	C-based controller	Coordinated [C & PSS]-based Controllers
-1.3939±3.4064i (0.3787)*	-1.7807±4.1709i (0.3926)*	-2.18±0.3558i (0.9869)*
-4.6198±23.2043i	-5.6621±5.6945i	-2.4096±2.8059i
-3.1499±12.4421i	-9.7383±74.8348i	-3.0017±1.8594i
-33.7913	-31.1193	-7.3597±6.9137i
-25.7516	-11.8722	-8.0924±18.0377i
-10.5662	-2.5485	-19.4909±21.5831i
-5.5446, -0.2021	-0.7464, -0.2010	-21.56, -0.2212, -0.0013, -0.2

Table 6.18: System eigenvalues of light loading condition for C & PSS, multiple point tuning, individual and coordinated design

PSS-based controller	C-based controller	Coordinated [C & PSS]-based Controllers
-1.1856±4.9329i (0.2337)*	-0.5716±5.3103i (0.107)*	-2.2467±4.2434i (0.4679)*
-4.7757±19.9861i	-9.6973±66.6855i	-2.9996±0.3166i
-5.1595±7.9238i	-32.4474	-4.8401±6.2313i
-33.2020	-11.4559	-9.8591±14.0236i
-20.871	-7.2313	-16.5188±8.6456i
-11.3574	-4.8161, -2.9789	-27.2779, -0.2066
-5.8751, -0.2007	-0.7467, -0.2004	-0.2, -0.0013

Table 6.19: System eigenvalues of Heavy loading condition for C & PSS, multiple point tuning, individual and coordinated design

PSS-based controller	C-based controller	Coordinated [C & PSS]-based Controllers
-1.1873±3.4128i (0.3286)*	-1.9405±2.7727i (0.5734)*	-1.5317±1.9208i (0.6235)*
-3.6467±11.3826i	-5.8787±6.5827i	-8.3024±6.1164i
-4.1092±20.2565i	-9.7243±65.783i	-8.9218±15.6938i
-33.943	-29.9457	-19.0335±26.68211i
-25.1739	-11.2856	-15.2178±1.8584i
-11.3994	-3.599	-19.3247, -3.7895, -1.9486
-5.5964, -0.2021	-0.7474, -0.203	-0.2248, -0.2, -0.0014

c) Non linear time domain simulation

The single machine infinite bus system shown in Fig. 3.4 is considered for nonlinear simulation studies. A 6-cycle 3- ϕ fault near to the infinite bus was applied, at all loading conditions, to study the performance of the proposed controllers.

The machine rotor angle and speed deviation responses, at nominal, light and heavy operating conditions, are shown in Figs. 6.26-6.31. It can be readily seen that the coordinated design system performs better than the individually designed in terms of reduction of overshoot and settling time. This is consistent with the eigenvalues analysis results.

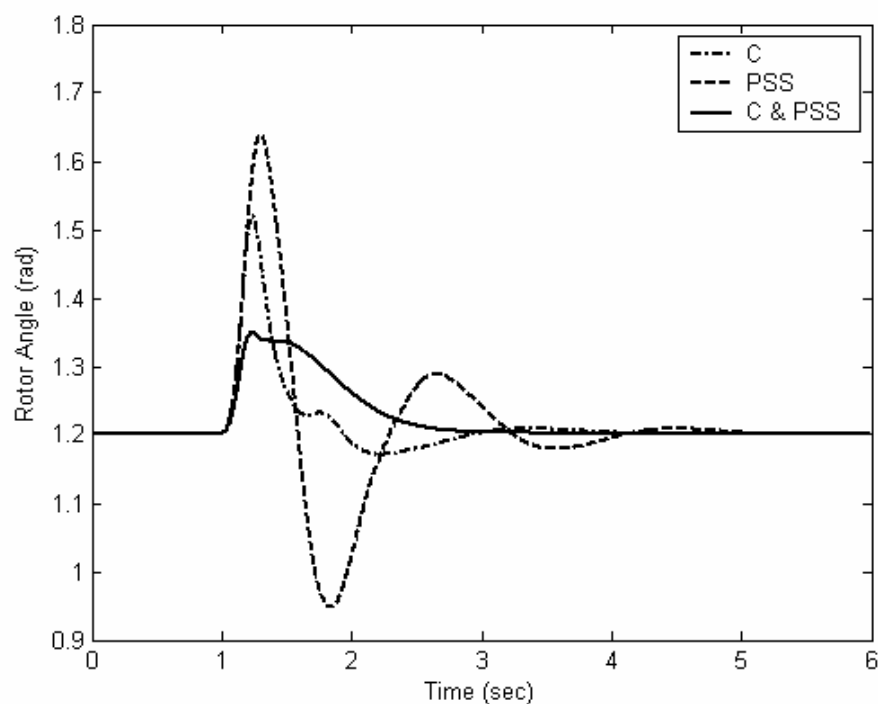


Fig. 6.26: Rotor angle response for 6-cycle fault with nominal loading, multiple point tuning, coordinated design for C & PSS

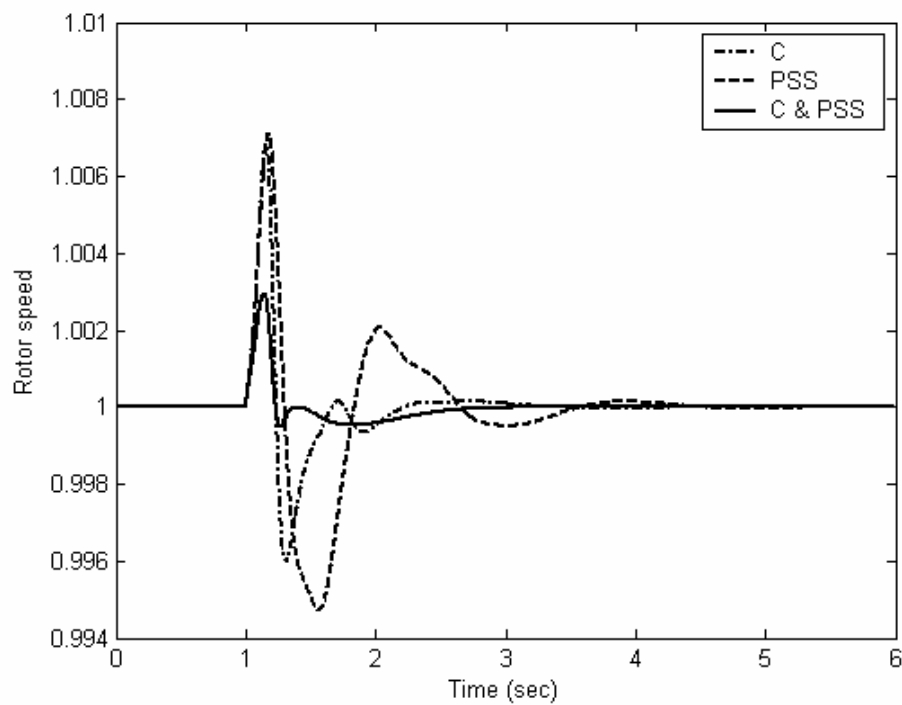


Fig. 6.27: Rotor speed response for 6-cycle fault with nominal loading, multiple point tuning, coordinated design for C & PSS

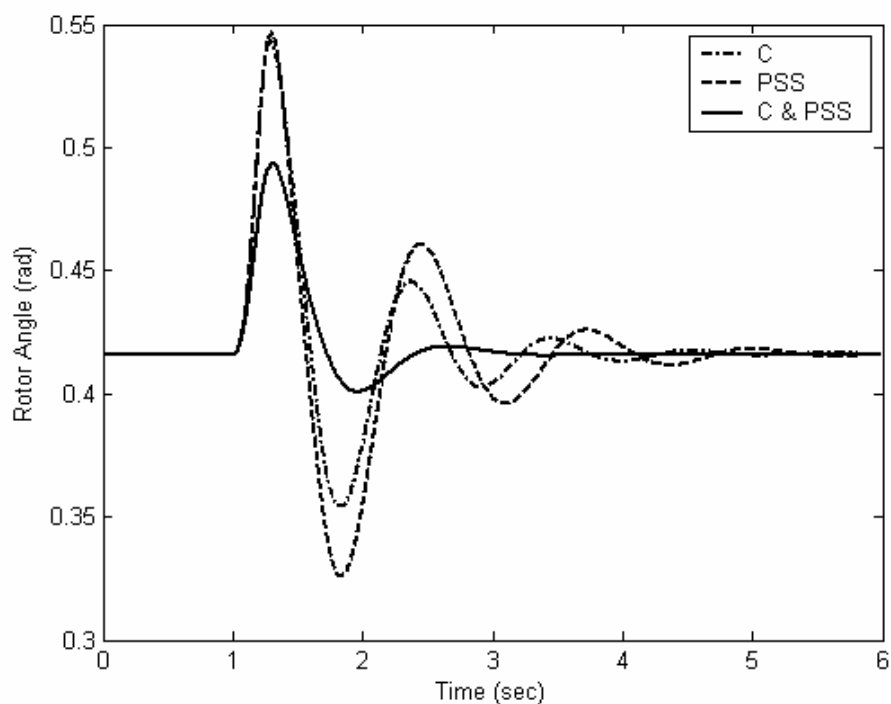


Fig. 6.28: Rotor angle response for 6-cycle fault with light loading, multiple point tuning, coordinated design for C & PSS

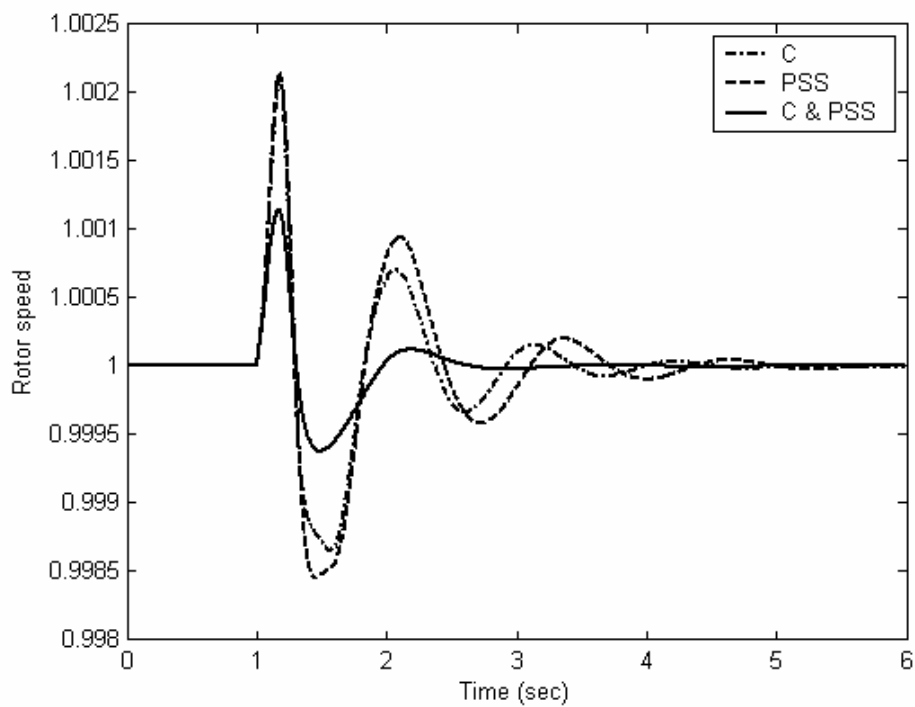


Fig. 6.29: Rotor speed response for 6-cycle fault with light loading, multiple point tuning, coordinated design for C & PSS

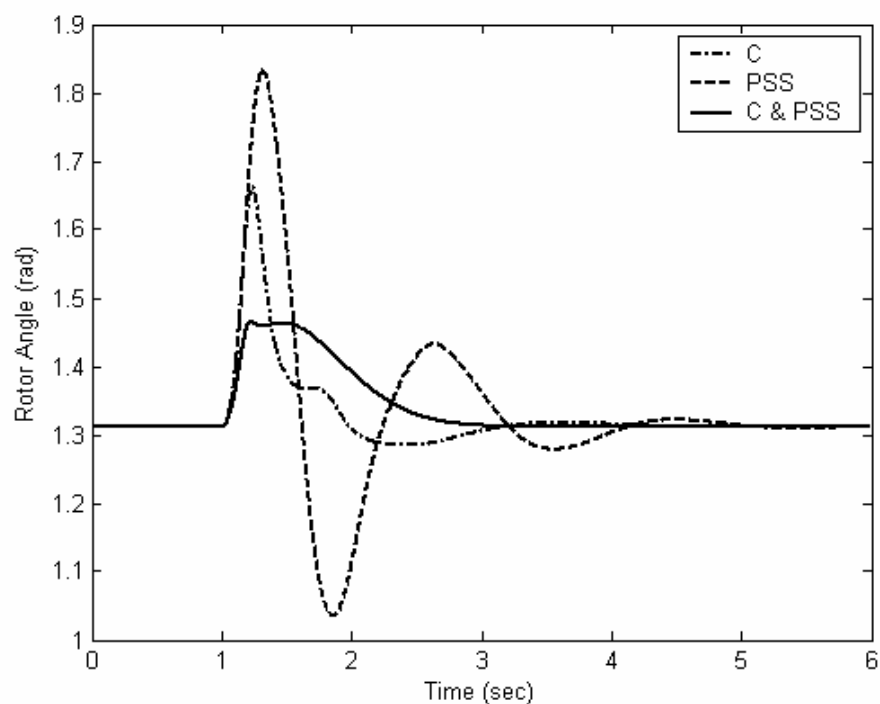


Fig. 6.30: Rotor angle response for 6-cycle fault with heavy loading, multiple point tuning, coordinated design for C & PSS

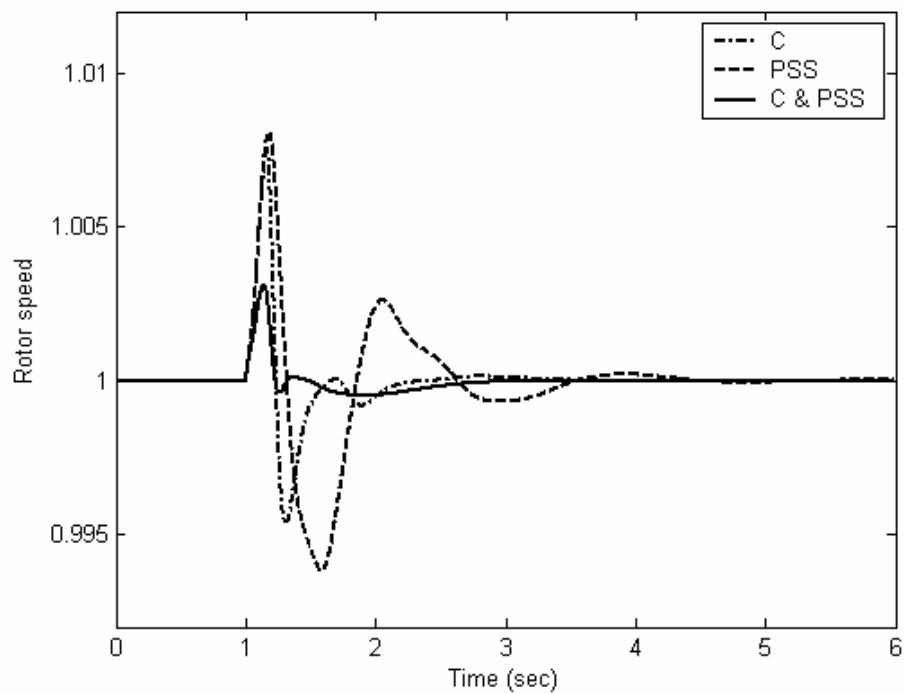


Fig. 6.31: Rotor speed response for 6-cycle fault with heavy loading, multiple point tuning, coordinated design for C & PSS

CHAPTER 7

ANALYSIS AND DESIGN OF PSS, TCSC, AND SVC-BASED STABILIZERS IN MULTIMACHINE POWER SYSTEMS

In this chapter the previous work is extended to multimachine power systems. Two multimachine power system examples are considered in this chapter. FACTS-based controllers namely TCSC and SVC are modeled one at a time in each power system.

7.1 Example 1 : (3-machine, 9-bus system)

The system considered in this section is the three-generator nine-bus system. The system one-line diagram is shown in Fig. 7.1. The details system data including the dynamic generators model and exciter data used along with load flow result are given in the Appendix B.

The system used consists of one area and it is called a loop system. Each load bus can be equipped with an SVC, while TCSC could be installed at any transmission line.

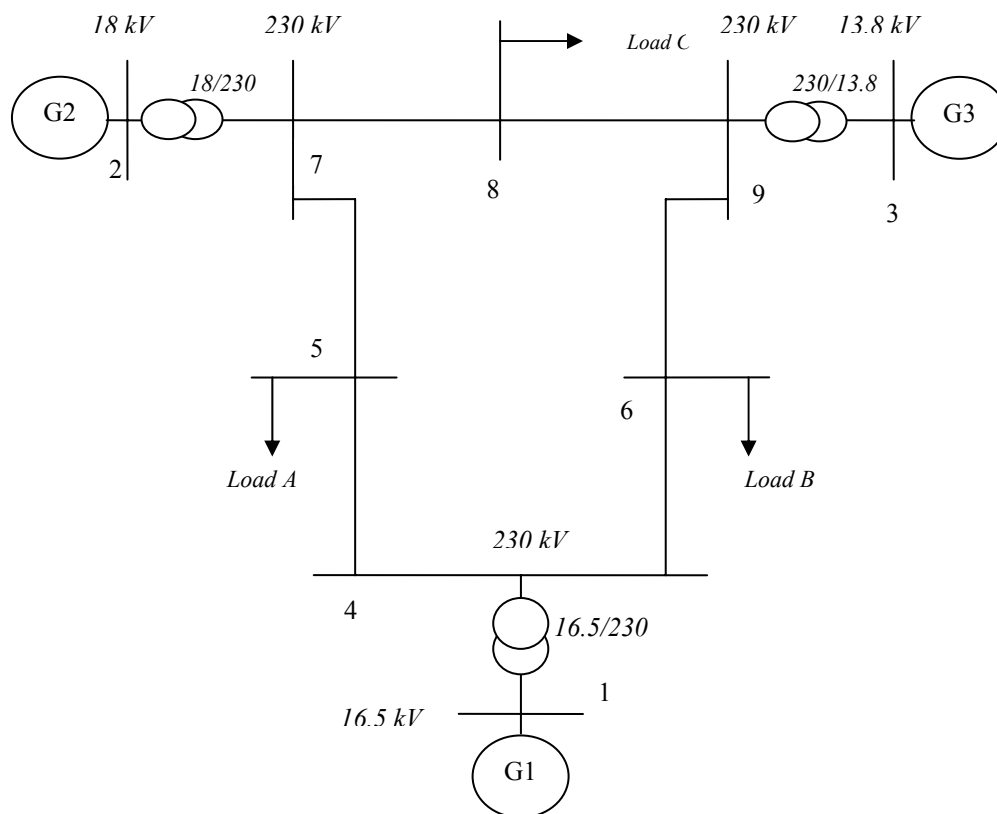


Fig. 7.1: Single line diagram of WSCC 3 generator 9 bus system

7.1.1 System Analysis

From the open loop system eigenvalue and participation factor analysis shown in Table 7.1, the system exhibits two electromechanical modes. Both of them are classified as local modes, since they are within frequency range of 0.7-3 Hz. The frequencies, damping ratios and participation factors for these two electromechanical modes are given in Table 7.1. The second electromechanical mode has a very low damping ratio equal to (0.0386) and Generator no. 2 has the significant participation factor of that mode. Therefore, PSS is located at machine number #2.

Table 7.1: 3-machine system eigenvalues analysis

<i>Eigenvalues</i>	<i>Freq.</i>	<i>Mode</i>	<i>Damping Ratio</i>	<i>Machines Participation Factor</i>		
				G1	G2	G3
-1.4716 ± 13.93i	2.2171	Local	0.1051	0.0106	0.227	1
-0.3567 ± 9.237i	1.4702	Local	0.0386	0.4195	1	0.1611
-9.8412 ± 11.556i	1.8393		0.6483			
-10.311 ± 6.827i	1.0866		0.8338			
-11.275 ± 3.119i	0.4964		0.9638			
-3.8355	0		1			
-2.2889	0		1			
-0.0901	0		1			
-2	0		1			

The location of SVC is selected based on the primary function of SVCs that is voltage and reactive power support. Then the SVC is utilized by installing POD controller to improve the system damping in addition to the main function. Modal Analysis Method is used to determine the voltage sensitivity of reactive power injections at each PQ buses.

From the Modal Analysis results shown in Table 7.2, the maximum contribution to the minimum eigenvalue of the reduced Jacobian is B-5. Therefore, bus number 5 is the most sensitive bus that required an SVC to improve the overall steady state voltage stability. While the location of TCSC is selected to be between bus # 5 and bus #7.

Table 7.2: Modal analysis result for 3-machine system

<i>PQ Buses</i>	<i>Eigenvalues of the reduced Jacobian</i>					
	<i>51.0829</i>	<i>46.6201</i>	<i>36.2943</i>	<i>5.9573</i>	<i>12.94</i>	<i>14.9075</i>
B-4	0.39413	0.40523	0.0019443	0.1258	0.066904	0.0059901
B-5	0.095235	0.020286	0.035946	0.29986	0.027198	0.52147
B-6	0.063316	0.032872	0.048438	0.27867	0.22398	0.35272
B-7	0.23229	0.28062	0.24878	0.084615	0.144	0.0097038
B-8	0.12824	0.19444	0.0082268	0.14538	0.49455	0.029159
B-9	0.086789	0.06655	0.65666	0.065678	0.043365	0.080952

7.1.2 Individual Design

Based on the linearized multimachine power system model shown in Fig. 3.6, PSO has been applied to the optimization problem to search for optimal settings of the proposed stabilizers for individual and coordinated design.

7.1.2.1 Stabilizer Design

The convergence rate of the objective function when PSS-2, SVC-based, and TCSC-based controllers are designed individually is shown in Fig. 7.2. The final settings of the optimized parameters for the proposed stabilizers are given in Table 7.3.

Table 7.3: Optimal parameter settings of PSS, SVC & TCSC single point tuning and individual design for 3-machine system

	<i>PSS</i>	<i>SVC</i>	<i>TCSC</i>
K	5.3502	296.9	235
T_1	0.1698	0.1138	0.25584
T_2	0.1	0.555	5.0
T_3	0.163	0.8567	4.04043
T_4	0.1	0.6579	1.0016

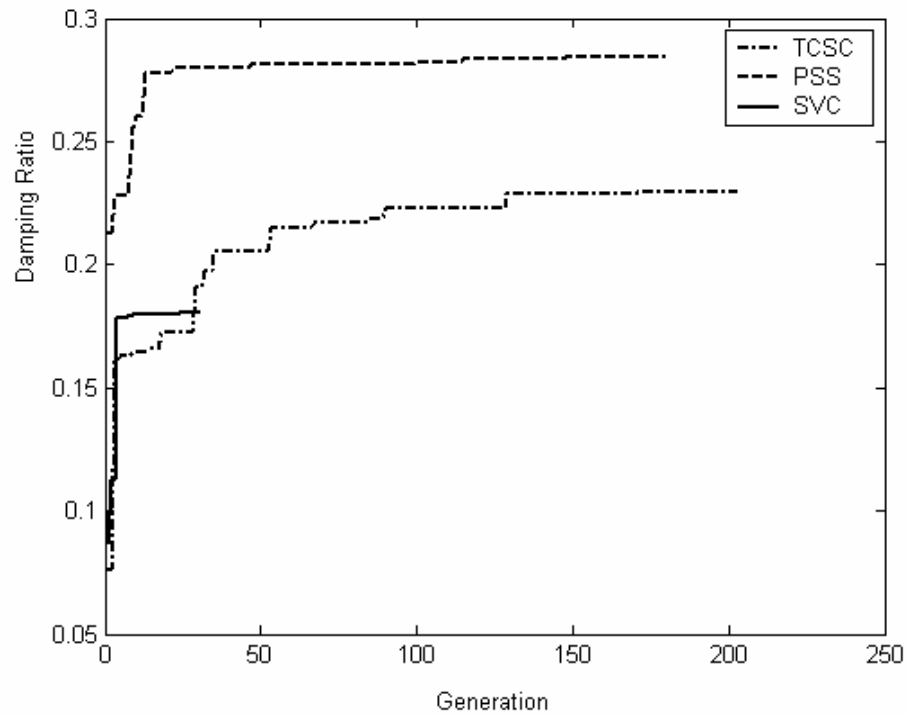


Fig. 7.2: Variation of the objective function of PSS, TCSC, & SVC stabilizers in 3-machine power system

7.1.2.2 Eigenvalue Analysis

The system eigenvalues along with damping ratios without and with the proposed PSS, SVC-based, and TCSC-based stabilizers when applied individually are given in Table 7.4. The first two bolded rows of the table represent the EM modes eigenvalue and their damping ratios.

It is quite evident that the system damping is slightly enhanced in case of SVC installed at bus number #5, while the system damping is greatly improved with the PSS and TCSC.

Table 7.4: System eigenvalues in case of individual design of PSS, SVC & TCSC in 3-machine system

<i>No Control</i>	<i>PSS2</i>	<i>SVC</i>	<i>TCSC</i>
-0.3567 ± 9.237i	-2.6197±8.8188i	-0.8749 ± 9.0971i	-3.0890 ±12.9722i
0.03*, 1.47**	0.2848*, 1.4036**	0.0957*, 1.4478**	0.2316*, 2.0716**
-1.4716 ±13.930i	-3.9378±13.3213i	-1.4034 ± 13.9371i	-3.1384 ±13.1498i
0.105*, 2.217**	0.2835*, 2.1202**	0.1002*, 2.218**	0.2321*, 2.14**
-9.8412 ±11.556i	-4.6439±15.7356i	-1.683 ± 0.7352i	-10.6325 ±11.5240i
-10.311 ± 6.827i	-9.3227±8.5425i	-2.7872 ± 0.4616i	-6.3092 ±5.0442i
-11.275 ± 3.119i	-10.9059±4.7682i	-9.6214 ± 11.6995i	-0.9104 ±2.9083i
-3.8355	-33.5124 , -10.0730	-10.027 ±6.8689i	-10.8508 ±3.5470i
-2.2889	-3.7845, -2.2644	-11.3463 ± 3.102i	-17.0440, -3.9188
-0.0901	-0.3867, -0.0460	-0.8842, -0.0193	-2.3042, -0.0005
	-2.00	-2.0	-0.20, -2.00

* damping ratio, ** frequency

7.1.2.3 Nonlinear Time domain Simulation

Figs. 7.3-7.5 show the speed deviations, rotor angles, and PSS2 controller responses respectively, for a 6-cycle three-phase fault at bus 7 at the end of line 5-7 at the base case while using the proposed PSS2.

Similarly, Figs. 7.6-7.8 show the simulation results with the proposed TCSC while Figs. 7.9-7.11 show results with SVC5.

Figs. 7.12-7.14 show the machines speed and angle response with the proposed PSS, SVC and TCSC all at one figure for better clarification.

It can be readily seen that PSS2 and TCSC are the most effective stabilizers in damping the EM modes oscillations. However, the system oscillations are relatively damped using SVC. This is in general consistency with eigenvalue analysis results.

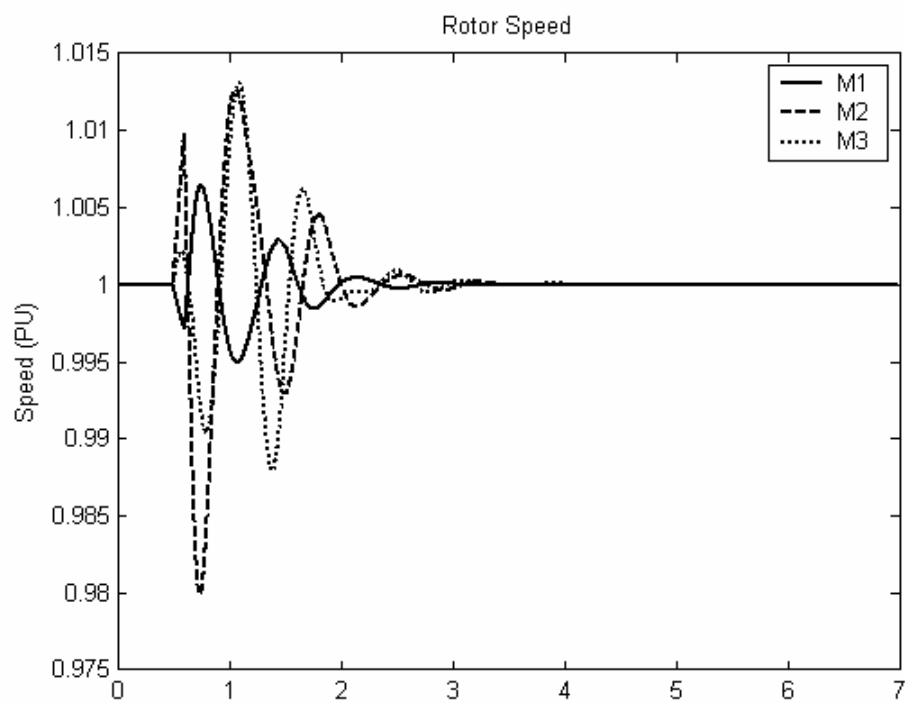


Fig. 7.3: Speed response for 6-cycle fault with PSS2, individual design

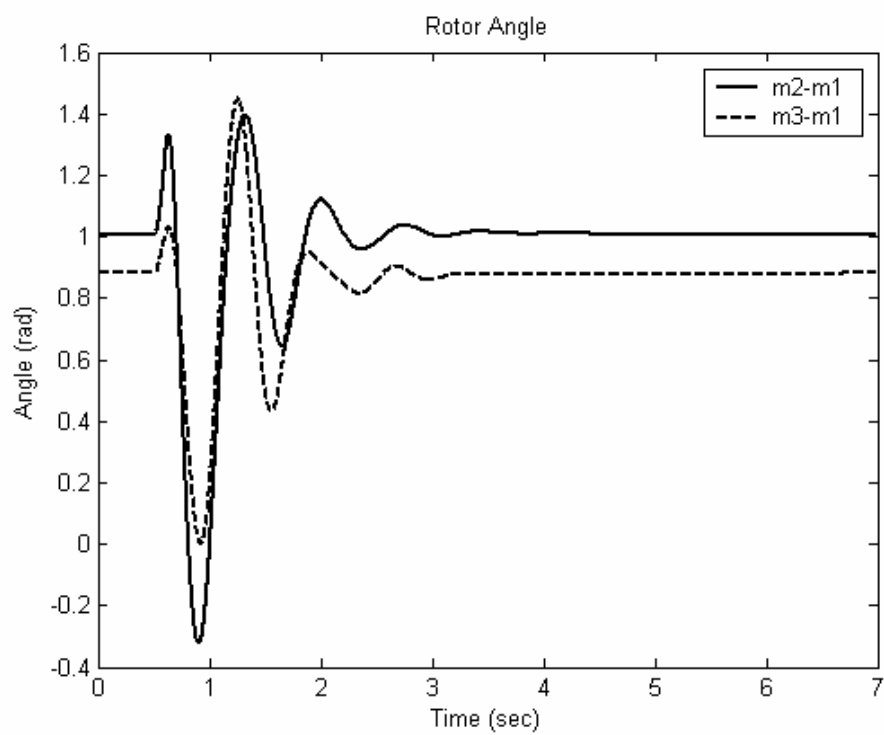


Fig. 7.4: Rotor angle response for 6-cycle fault with PSS2, individual design

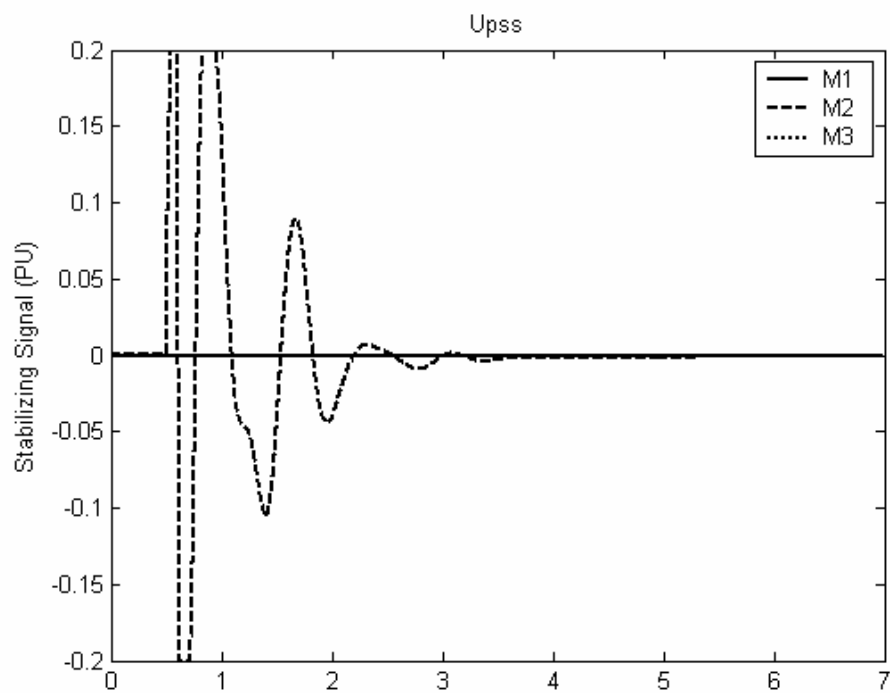


Fig. 7.5: PSS-2 response for 6-cycle fault, individual design

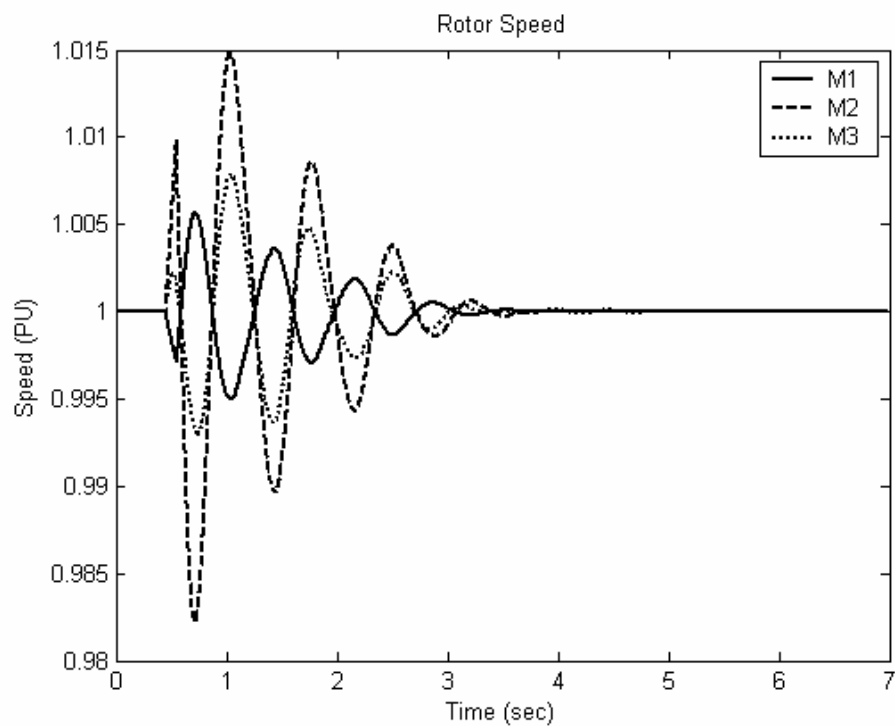


Fig. 7.6: Speed response for 6-cycle fault with TCSC, individual design

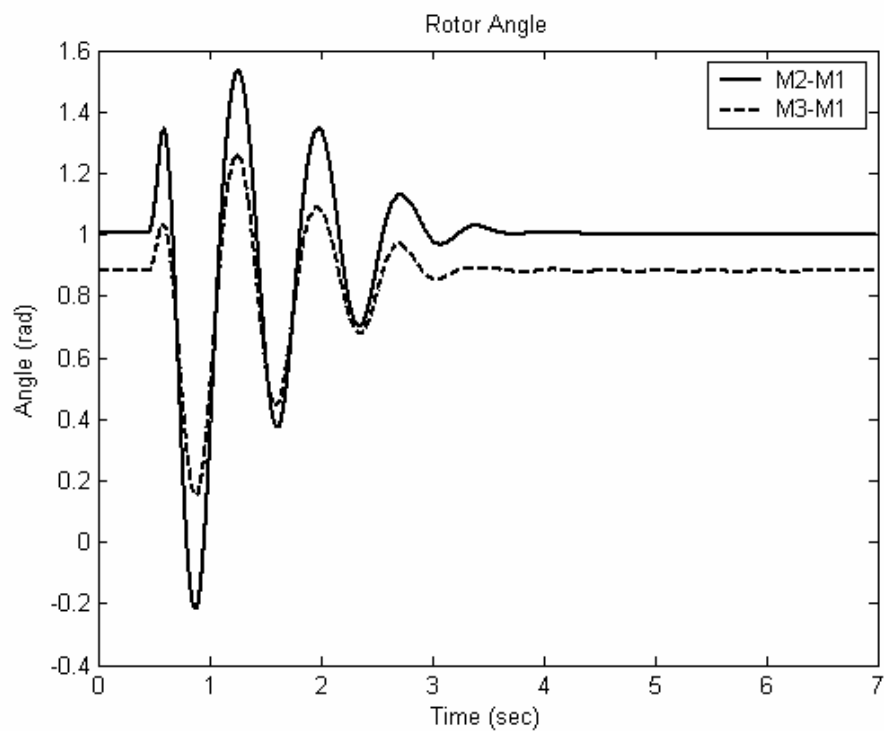


Fig. 7.7: Rotor angle response for 6-cycle fault with TCSC, individual design

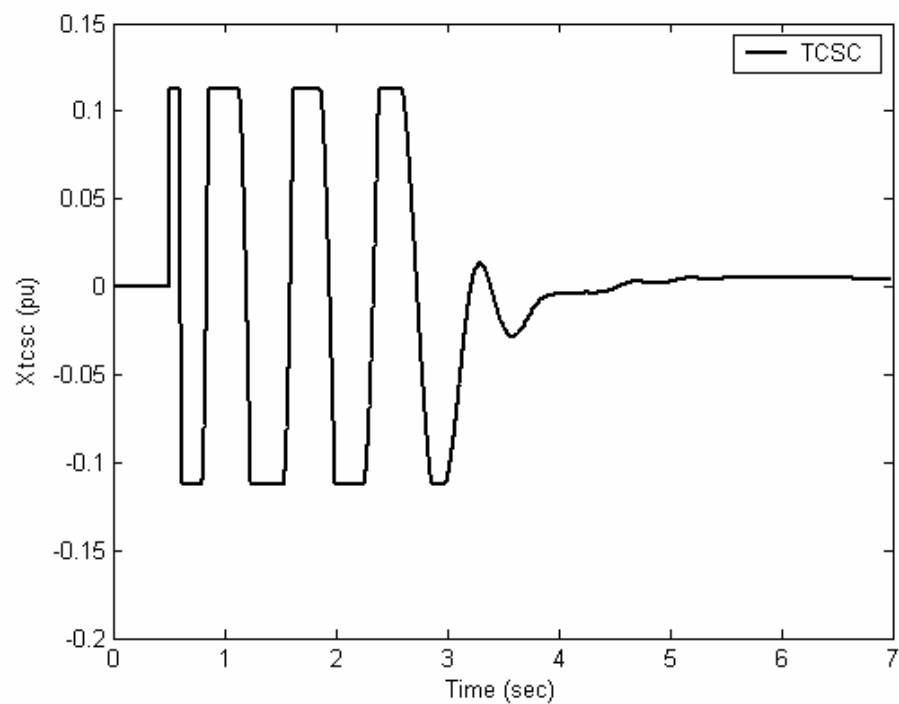


Fig. 7.8: TCSC response for 6-cycle fault, individual design

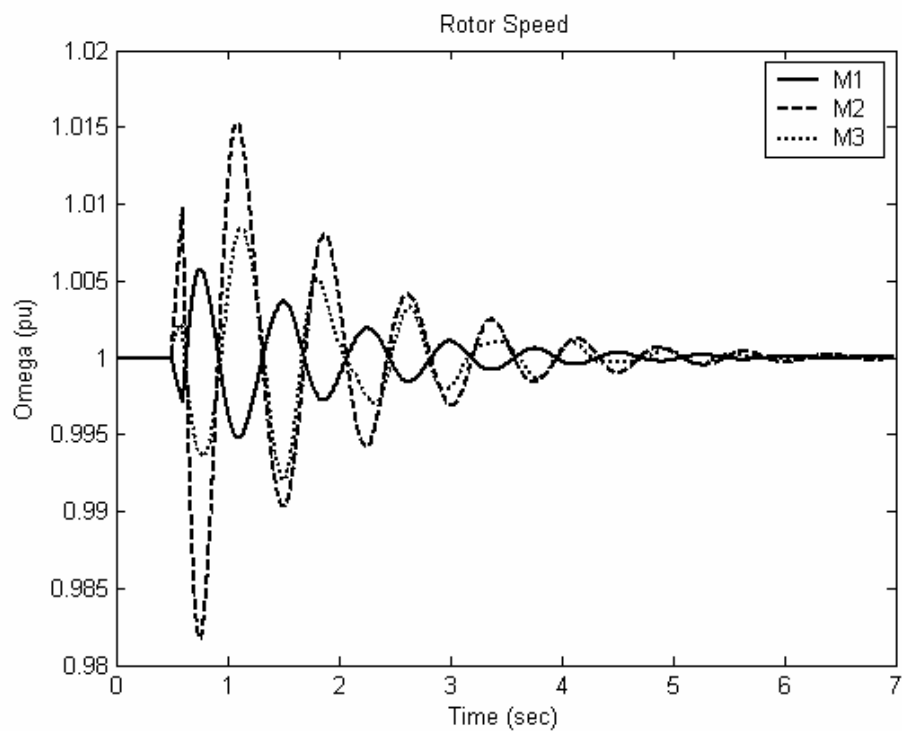


Fig. 7.9: Speed response for 6-cycle fault with SVC5, individual design

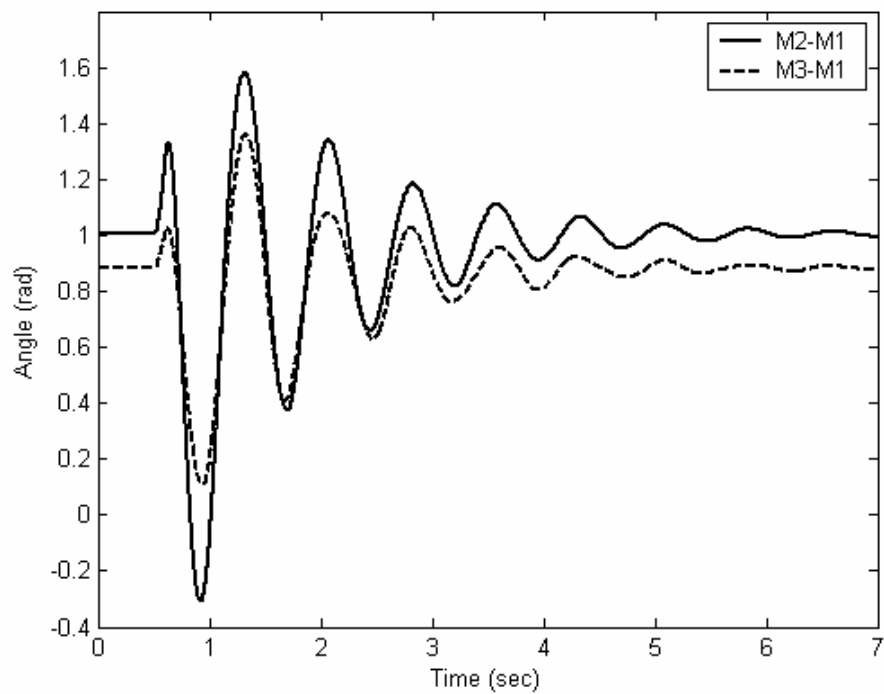


Fig. 7.10: Rotor angle response for 6-cycle fault with SVC5, individual design

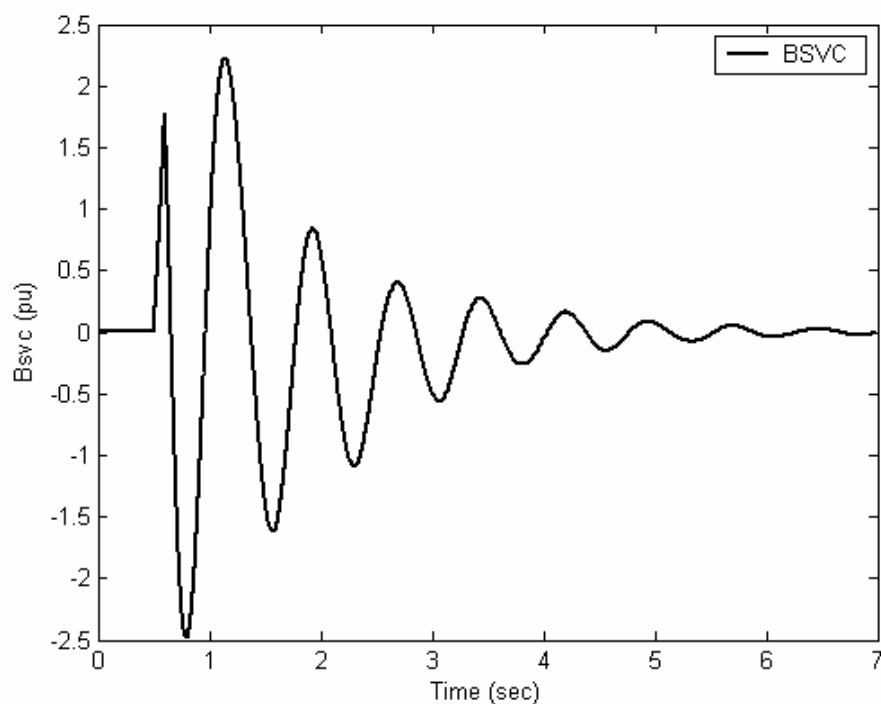


Fig. 7.11: SVC5 response for 6-cycle fault, individual design

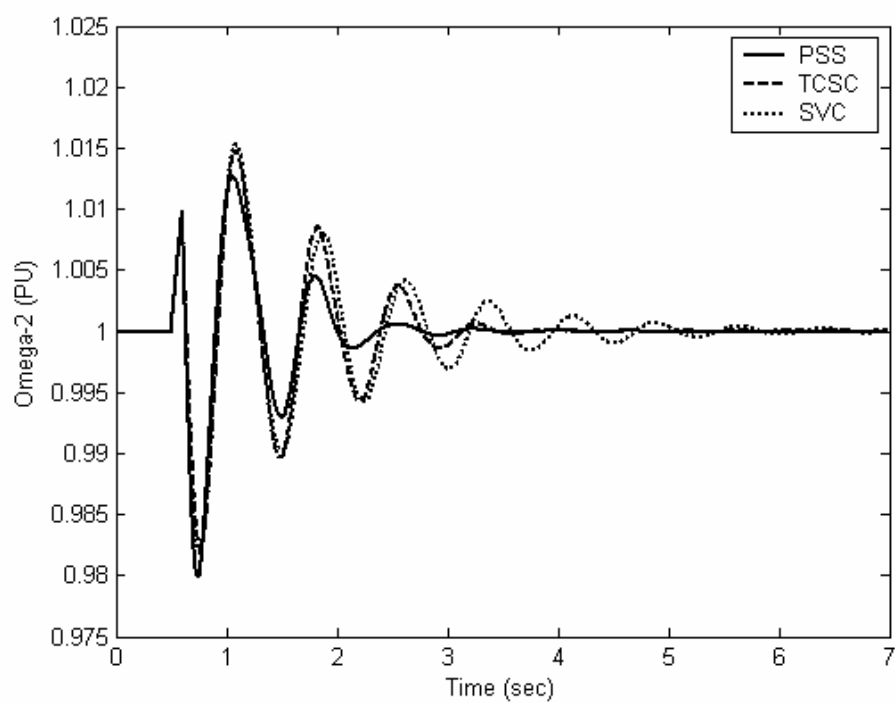


Fig. 7.12: Speed response of machine-2 for 6-cycle fault with PSS, SVC, and TCSC, individual design

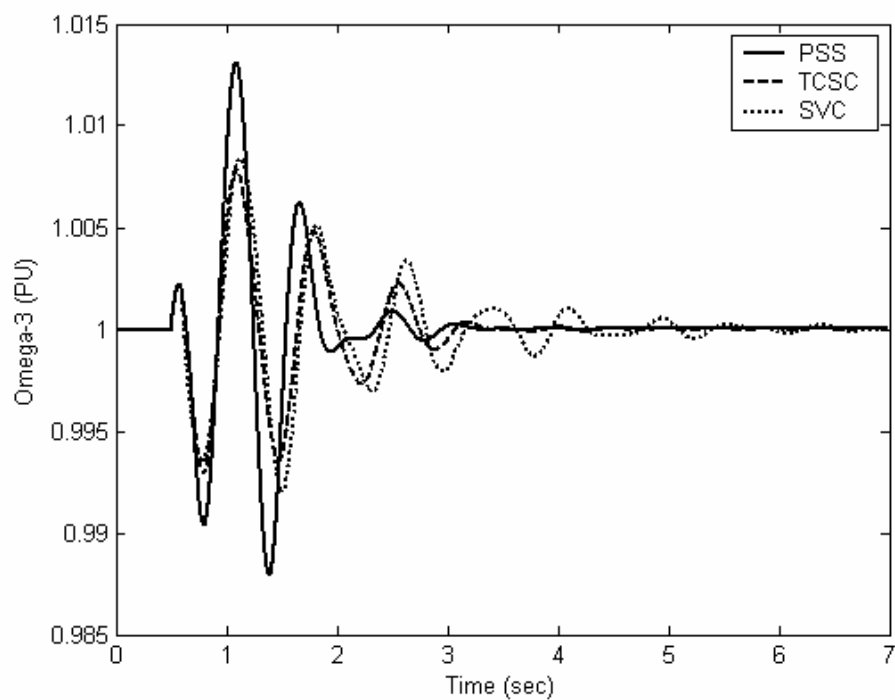


Fig. 7.13: Speed response of machine-3 for 6-cycle fault with PSS, SVC, and TCSC, individual design

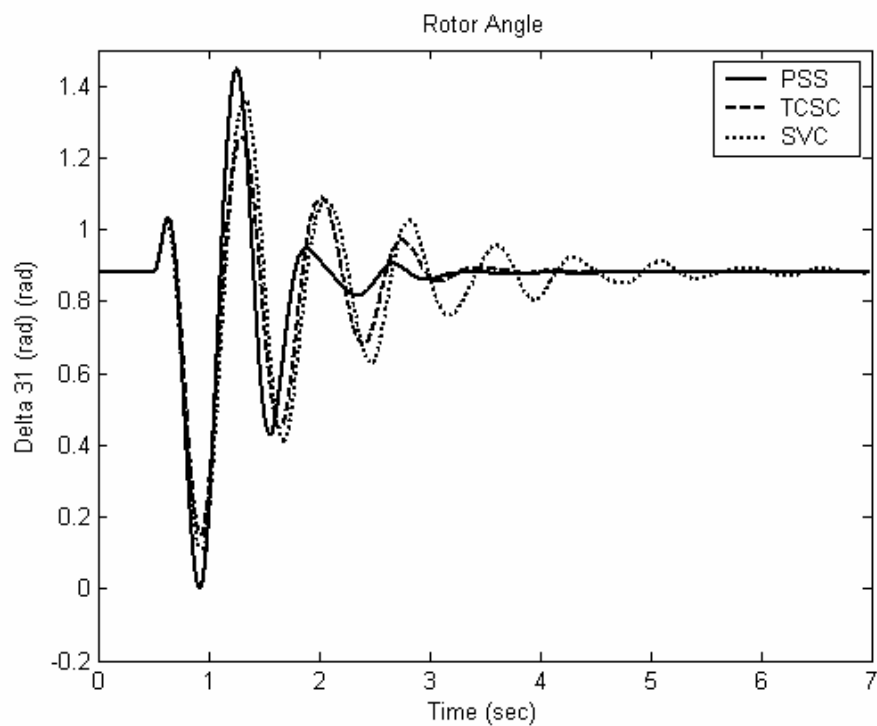


Fig. 7.14: Rotor angle response for 6-cycle fault with PSS, SVC, and TCSC, individual design

7.1.3 Coordinated Design [TCSC & PSS]

Both stabilizers PSS2 & TCSC are simultaneously tuned by PSO searching for the optimum controllers parameter settings that maximize the minimum damping ratio of all the system complex eigenvalues.

7.1.3.1 Stabilizer Design

The convergence rate of the objective function when PSS2 and TCSC-based controllers are designed individually and in a coordinated manner is shown in Fig. 7.15. It is clear that the coordinated design of PSS and TCSC-based stabilizer improves greatly the system damping compared to their individual application. The final settings of the optimized parameters for the proposed stabilizers are given in Table 7.5.

Table 7.5: Optimal parameter settings of PSS and TCSC, coordinated design for 3-machine system

<i>Parameters</i>	<i>Coordinated Design</i>	
	<i>PSS(2)</i>	<i>TCSC</i>
<i>K</i>	1.6086	6.9277
<i>T₁</i>	0.978	0.0101
<i>T₂</i>	0.010	0.3289
<i>T₃</i>	-----	0.0770
<i>T₄</i>	-----	0.050

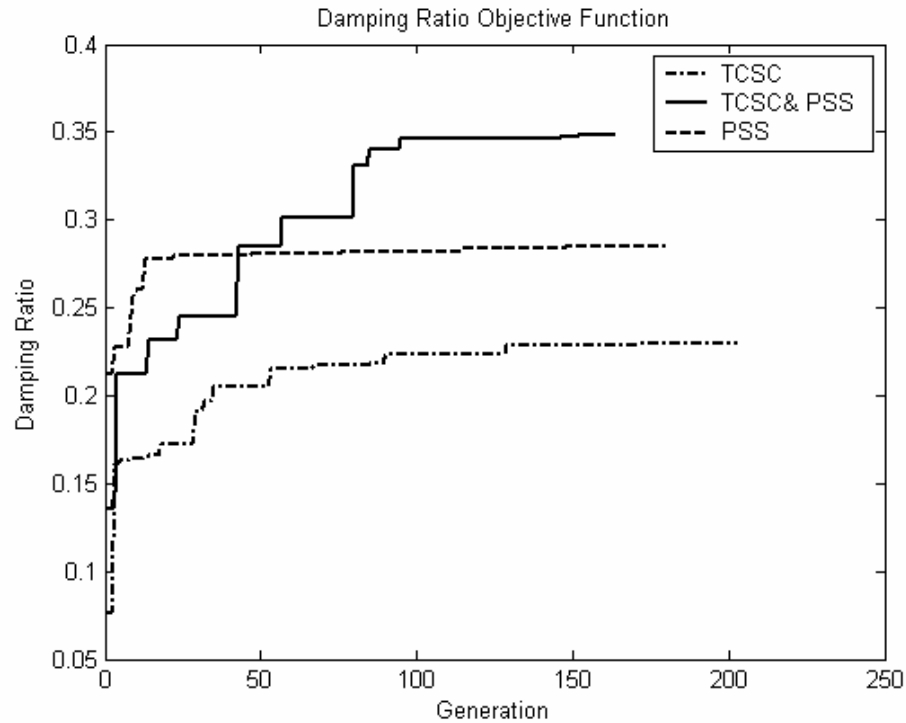


Fig. 7.15: Variation of the objective function of PSS & TCSC-based stabilizer, Individual & Coordinated design

7.1.3.2 Eigenvalue Analysis

The system eigenvalues with the proposed PSS2 and TCSC-based stabilizers when applied individually and by means of coordinated design is given in Table 7.6. The bold rows of this table represent the EM modes eigenvalues and their damping ratios. It is evident that, using the proposed coordinated stabilizers design, the damping ratio of the EM mode eigenvalue is greatly enhanced. Hence, it can be concluded that this improves the system stability.

Table 7.6: System eigenvalues with coordinated design of PSS2 & TCSC in 3-machine system

<i>PSS(2)</i>	<i>TCSC</i>	<i>PSS & TCSC</i>
-2.6197±8.8188i	-3.0890 ±12.9722i	-3.351±9.3204i
0.2848*, 1.4036**	0.2316*, 2.0716**	0.34*, 1.483**
-3.9378±13.3213i	-3.1384 ±13.1498i	-4.7746 ± 13.8311i
0.2835*, 2.1202**	0.2321*, 2.14**	0.326*, 2.2013**
-4.6439±15.7356i	-10.6325 ±11.5240i	-0.1759 ±0.17725i
-9.3227±8.5425i	-6.3092 ±5.0442i	-4.9191±14.21366i
-10.9059±4.7682i	-0.9104 ±2.9083i	-8.8257±7.73672i
-33.5124, -10.0730	-10.8508 ±3.5470i	-10.455±4.15703i
-3.7845, -2.2644	-17.0440, -3.9188	-100, -101.7
-0.3867, -0.0460	-2.3042, -0.0005	-19.99, -3.794
-2.00	-0.20, -2.00	-2.2538, -0.516
		-0.20, -2.00

* damping ratio, ** frequency

7.1.3.3 Nonlinear Time domain Simulation

Figs. 7.16-7.19 show the rotor angles and speed deviations responses, as well as PSS2 stabilizing signal and TCSC response, respectively, for a 6-cycle three-phase fault at bus 7 at the end of line 5-7 at the base case while using the proposed PSS2-TCSC coordinated design. These Figs. should be compared with Figs. 7.3-7.5, for individual PSS2 design, and 7.6-7.8, for individual TCSC design. For better result appearance Figs. 7.20-7.22 show the speed, angle, and TCSC responses with coordinated and individual design of PSS and TCSC.

The improvement on the system responses when using the coordinated design, especially for individual TCSC design, is quite evident. This is in agreement with eigenvalue analysis results.

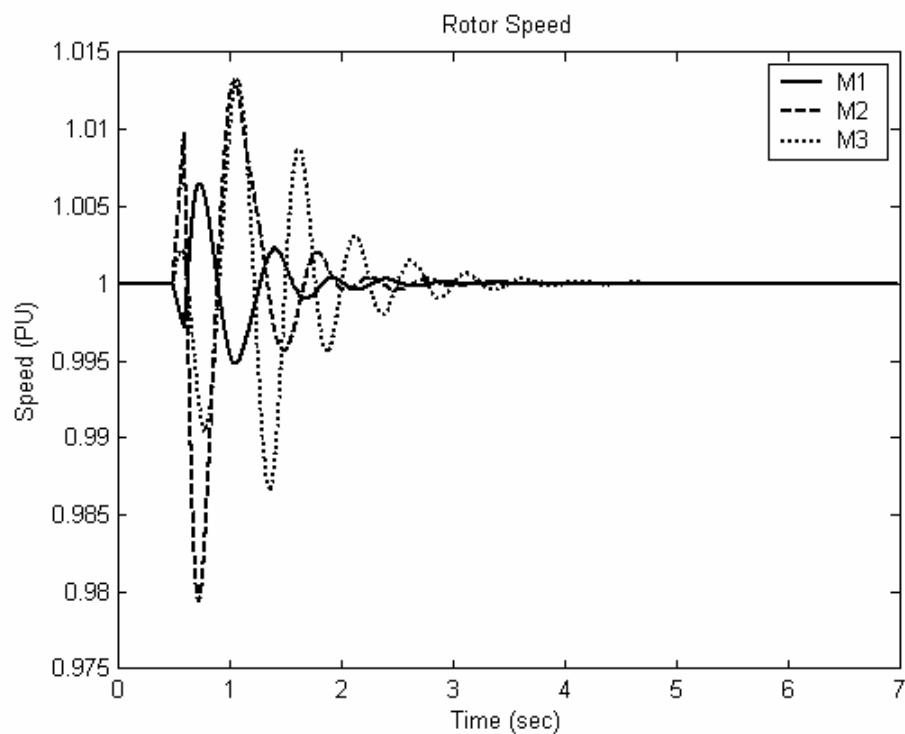


Fig. 7.16: Speed response for 6-cycle fault with PSS2 & TCSC, coordinated design

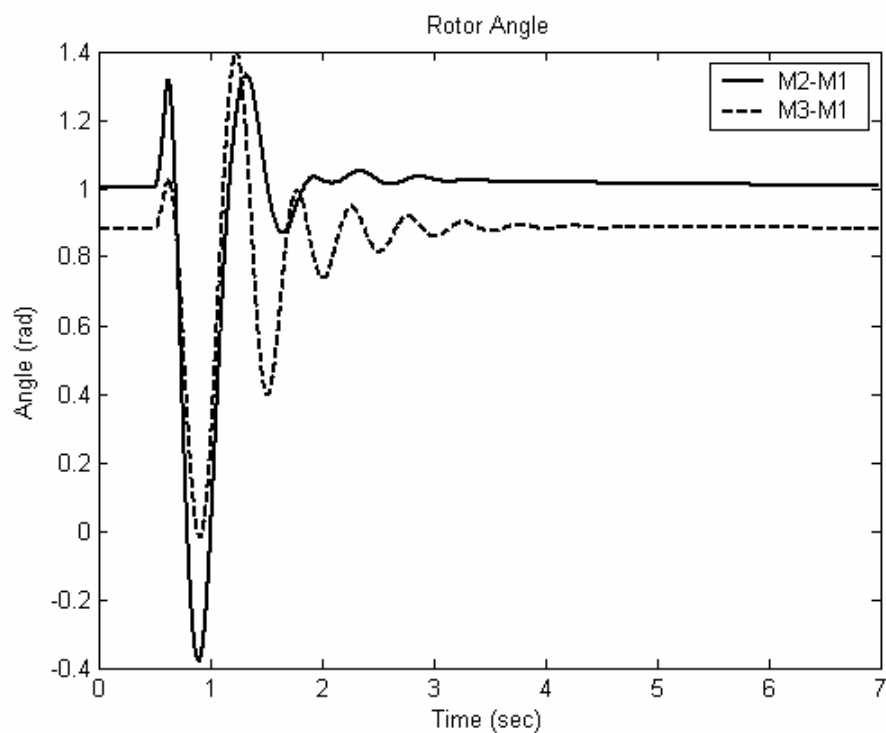


Fig. 7.17: Rotor angle response for 6-cycle fault with PSS2 & TCSC, coordinated design

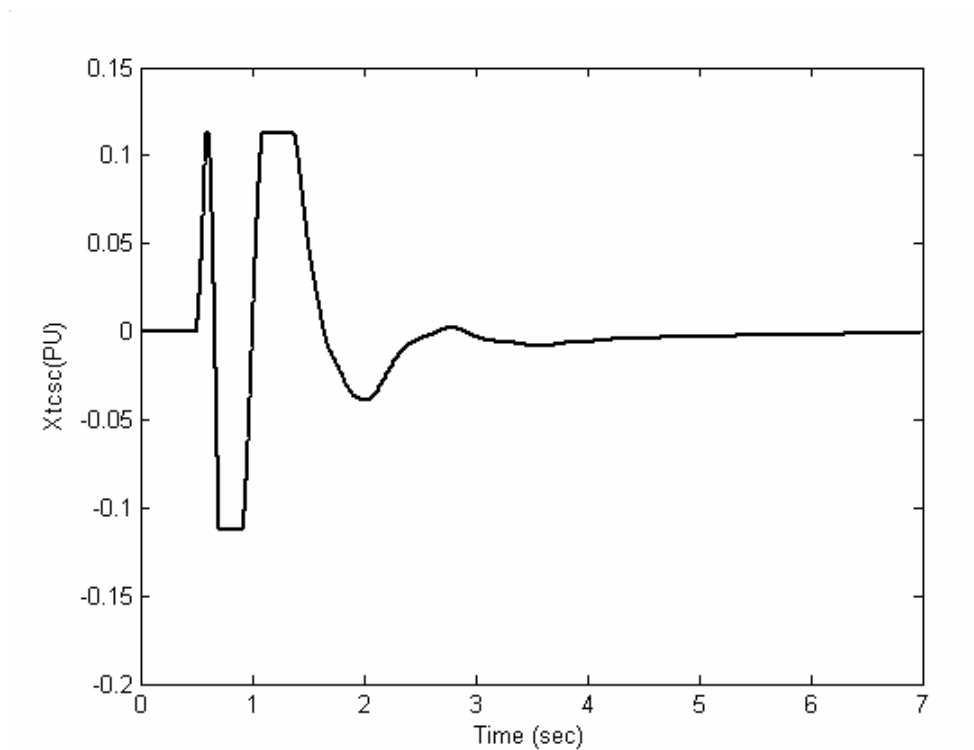


Fig. 7.18: TCSC response for 6-cycle fault, PSS2 & TCSC, coordinated design

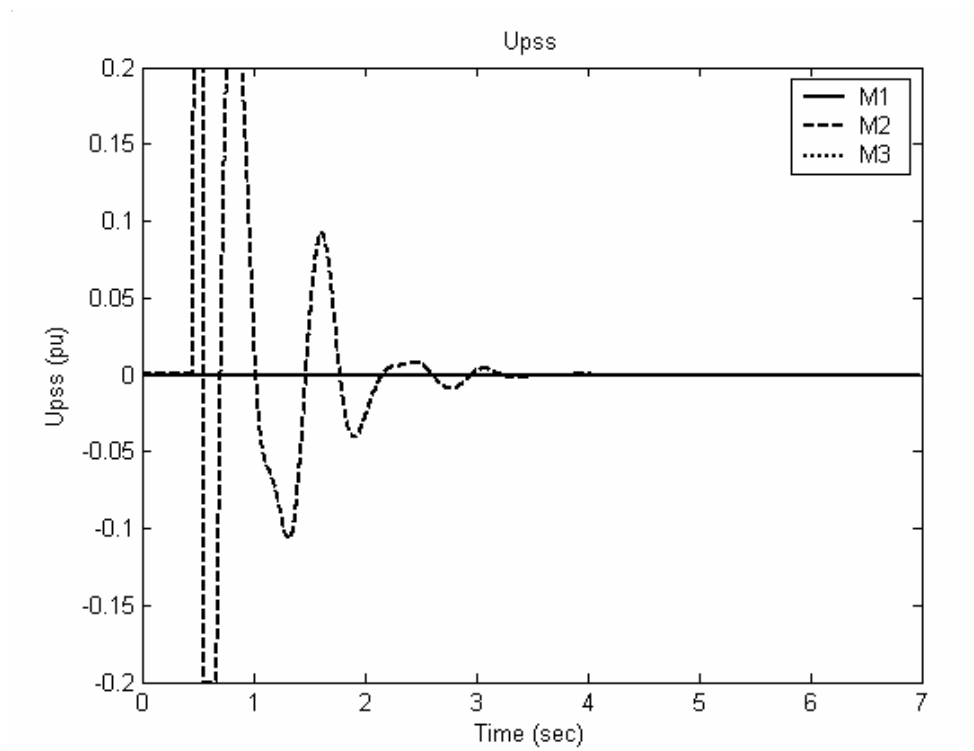


Fig. 7.19: PSS response for 6-cycle fault, with PSS2 & TCSC, coordinated design

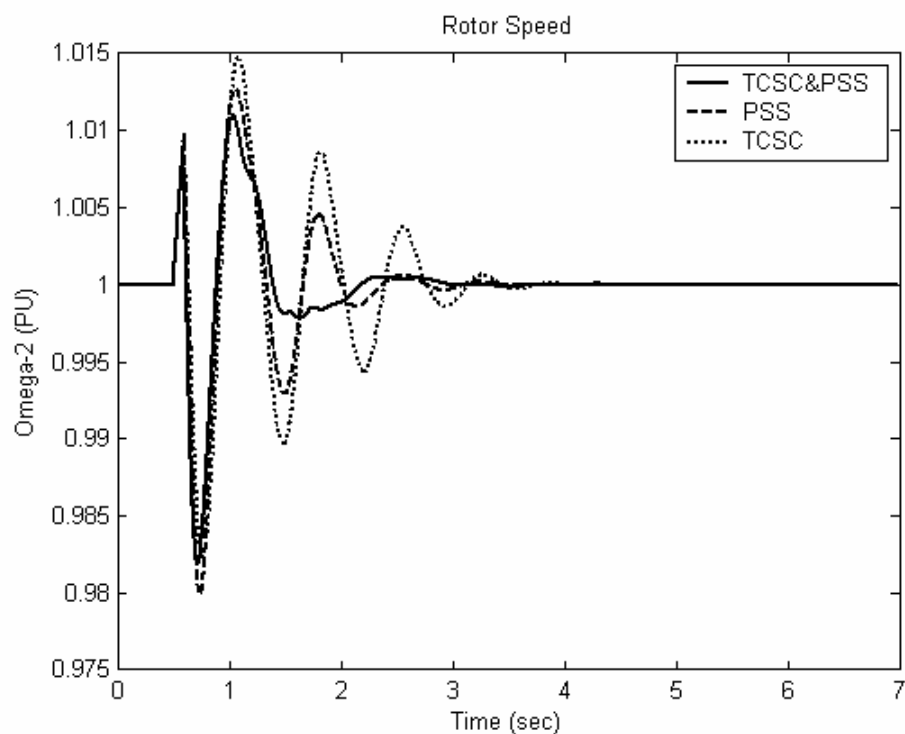


Fig. 7.20: Speed response for 6-cycle fault with PSS2 & TCSC, coordinated and individual design

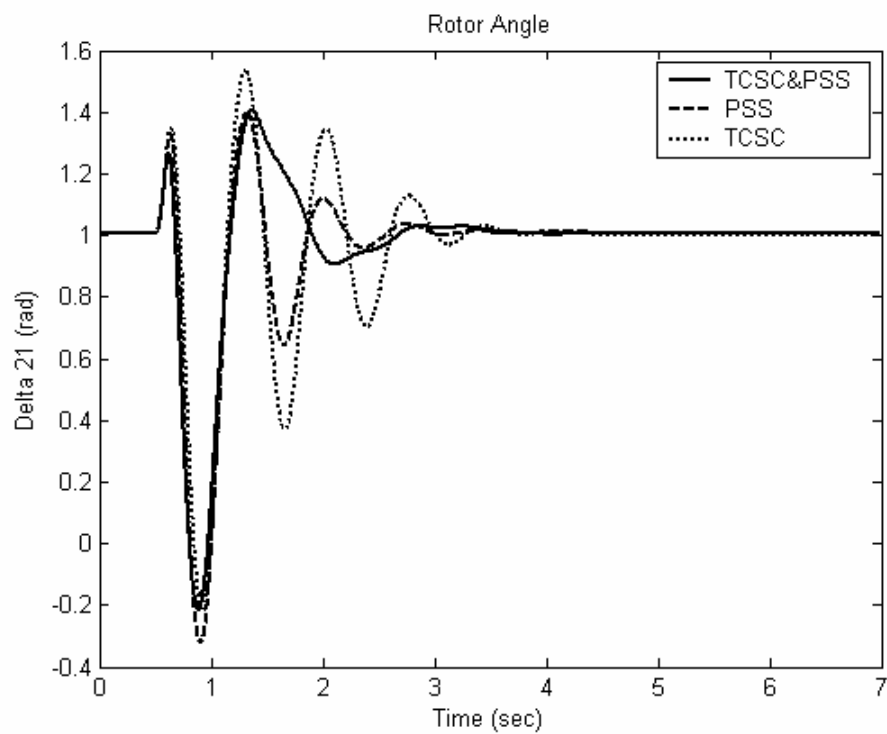


Fig. 7.21: Rotor angle response for 6-cycle fault with PSS2 & TCSC, coordinated and individual design

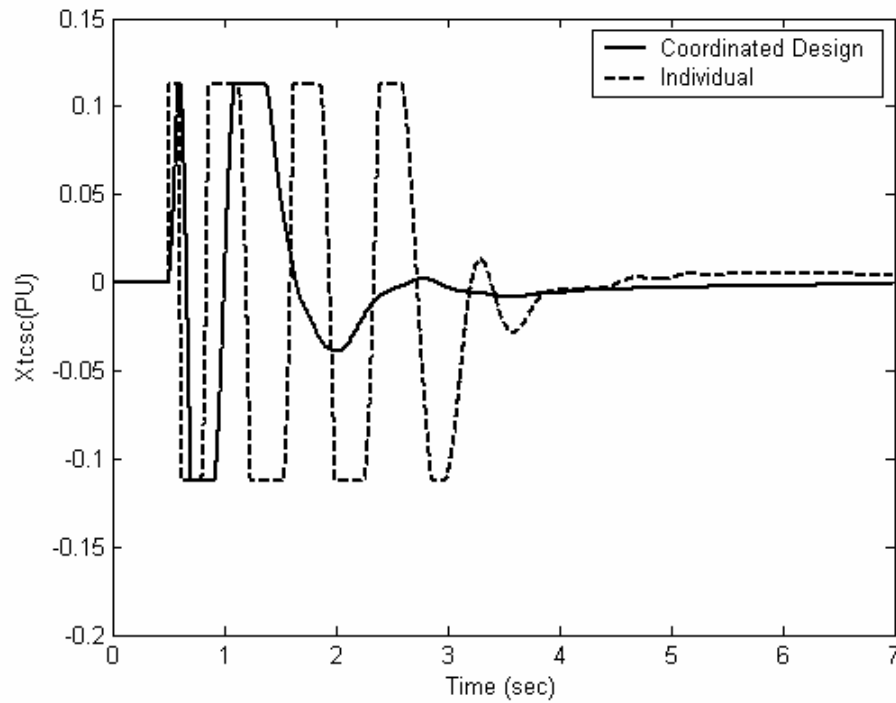


Fig. 7.22: TCSC response for 6-cycle fault with PSS & TCSC, coordinated and individual design

7.1.4 Coordinated Design [SVC & PSS]

Both stabilizers PSS2 & SVC5 are simultaneously tuned by PSO searching for the optimum controllers parameter settings that maximize the minimum damping ratio of all the system complex eigenvalues.

7.1.4.1 Stabilizer Design

The convergence rate of the objective function when PSS2 and SVC5-based controllers are designed individually and in a coordinated manner is shown in Fig. 7.23. It is clear that the coordinated design of PSS and SVC5-based stabilizer improves greatly the system damping compared to their individual application. The final settings of the optimized parameters for the proposed stabilizers are given in Table 7.7.

Table 7.7: Optimal parameter settings of PSS and SVC, coordinated design for 3-machine system

	<i>Coordinated Design</i>	
	<i>PSS(2)</i>	<i>SVC</i>
K	7.4649	1.025
T_1	0.2333	0.901
T_2	0.01	0.2276
T_3	-----	5.0
T_4	-----	4.9539

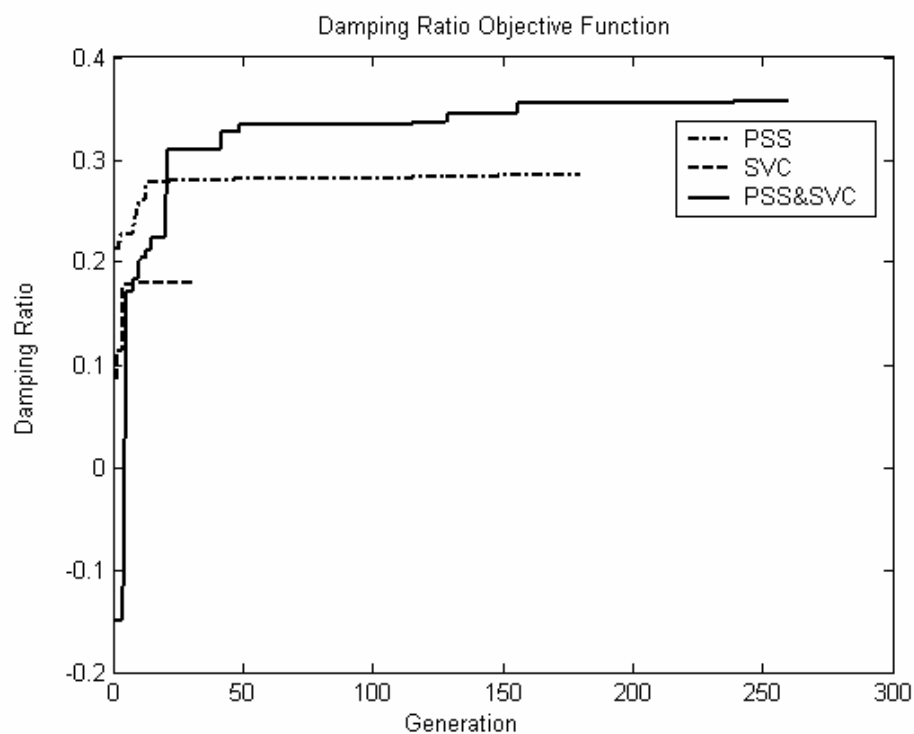


Fig. 7.23: Variation of the objective function of PSS & SVC5-based stabilizer, Individual & Coordinated design

7.1.4.2 Eigenvalue Analysis

The system eigenvalues with the proposed PSS2 and SVC5-based stabilizers when applied individually and by means of coordinated design is given in Table 7.8. The bold rows of this table represent the EM modes eigenvalues and their damping ratios. It is evident that, using the proposed coordinated stabilizers design, the damping ratio of the EM mode eigenvalue is greatly enhanced. Hence, it can be concluded that this improves the system stability.

Table 7.8: System eigenvalues with coordinated design of PSS2 & SVC in 3-machine system

<i>PSS(2)</i>	<i>SVC</i>	<i>PSS & SVC</i>
-2.6197±8.8188i	-0.8749 ± 9.0971i	-3.349 ± 9.2542i
0.2848*, 1.4036**	0.0957*, 1.4478**	0.3403*, 1.473**
-3.9378±13.3213i	-1.4034 ± 13.9371i	-4.5033 ± 13.7782i
0.2835*, 2.1202**	0.1002*, 2.218**	0.3106*, 2.1928**
-4.6439±15.7356i	-1.683 ± 0.7352i	-5.1682 ± 14.3245i
-9.3227±8.5425i	-2.7872 ± 0.4616i	-8.8307 ± 7.76811i
-10.9059±4.7682i	-9.6214 ± 11.6995i	-10.4648 ± 4.14817i
-33.5124, -10.0730	-10.027 ± 6.8689i	-101.73, -100, -199
-3.7845, -2.2644	-11.3463 ± 3.102i	-4.4736, -3.738
-0.3867, -0.0460	-0.8842, -0.0193	2.2545, -0.452
-2.00	-2.0	-0.04, -0.2018
		-0.2, -2

* damping ratio, ** frequency (Hz)

7.1.4.3 Nonlinear Time domain Simulation

Figs. 7.24-7.27 show the rotor angles, speed deviations, PSS2 stabilizing signal and SVC5 responses, respectively, for a 6-cycle three-phase fault at bus 7 at the end of line 5-7 at the base case while using the proposed PSS2- SVC5 coordinated design. These Figs. should

be compared with Figs. 7.3-7.5, for individual PSS2 design, and 7.9-7.11, for individual SVC5 design. Figs. 7.28-7.30 show the speed deviation, rotor angle, and SVC responses for PSS and SVC for individual and coordinated design.

The improvement on the system responses when using the coordinated design, especially for individual SVC5 design, is quite evident. This is in agreement with eigenvalue analysis results.

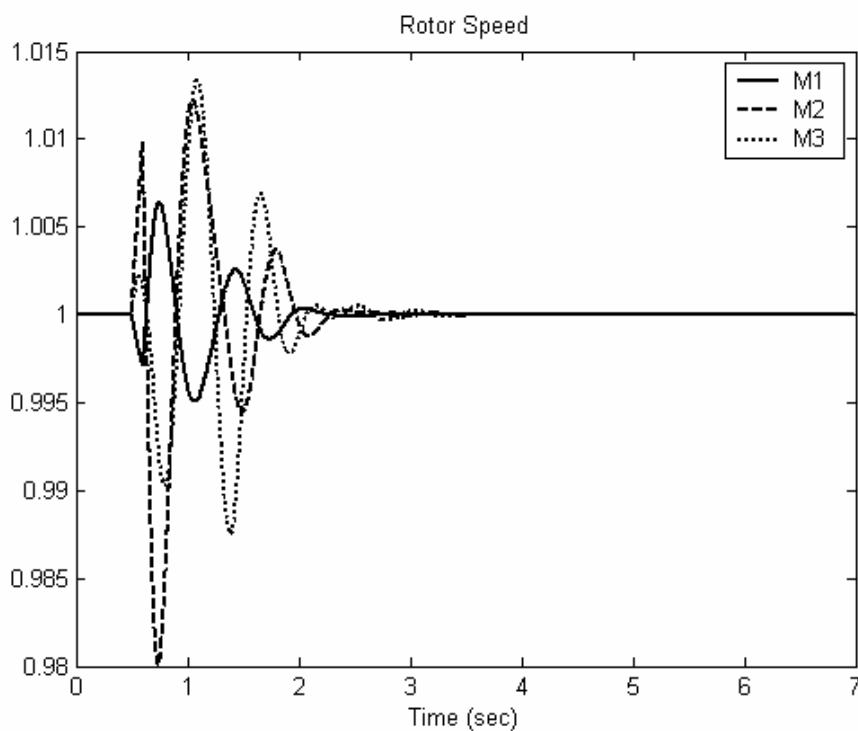


Fig. 7.24: Speed response for 6-cycle fault with PSS2 & SVC5, coordinated design

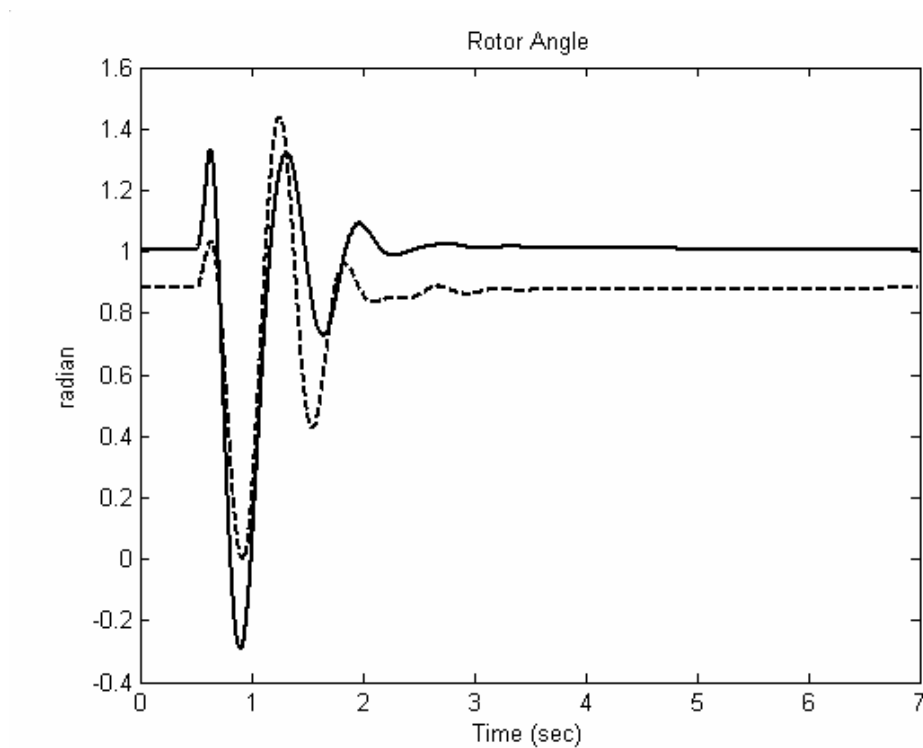


Fig. 7.25: Rotor angle response for 6-cycle fault with PSS2 & SVC5, coordinated design

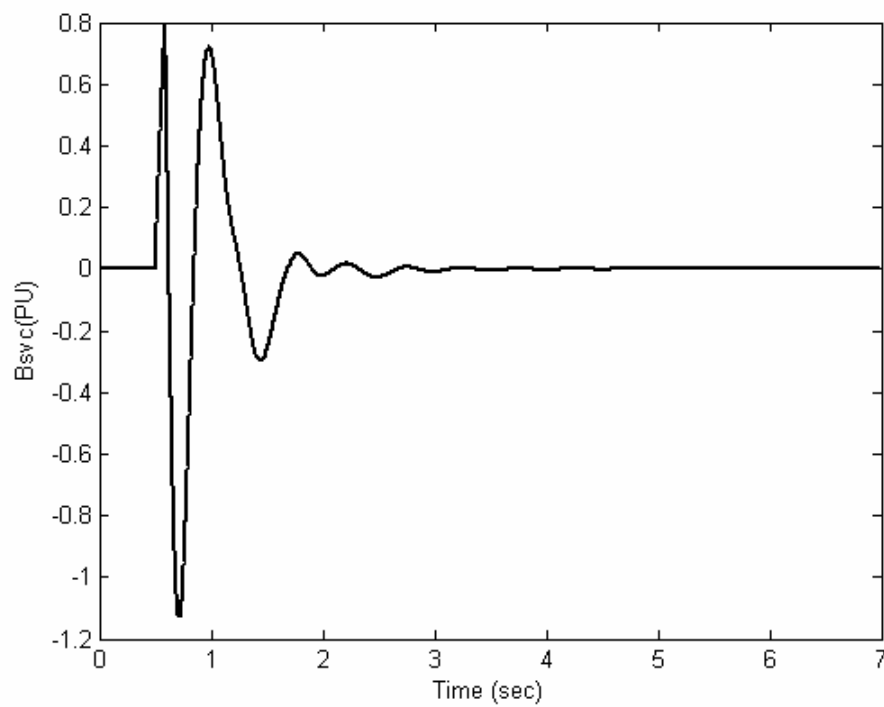


Fig. 7.26: SVC5 response for 6-cycle fault, PSS2 & SVC5, coordinated design

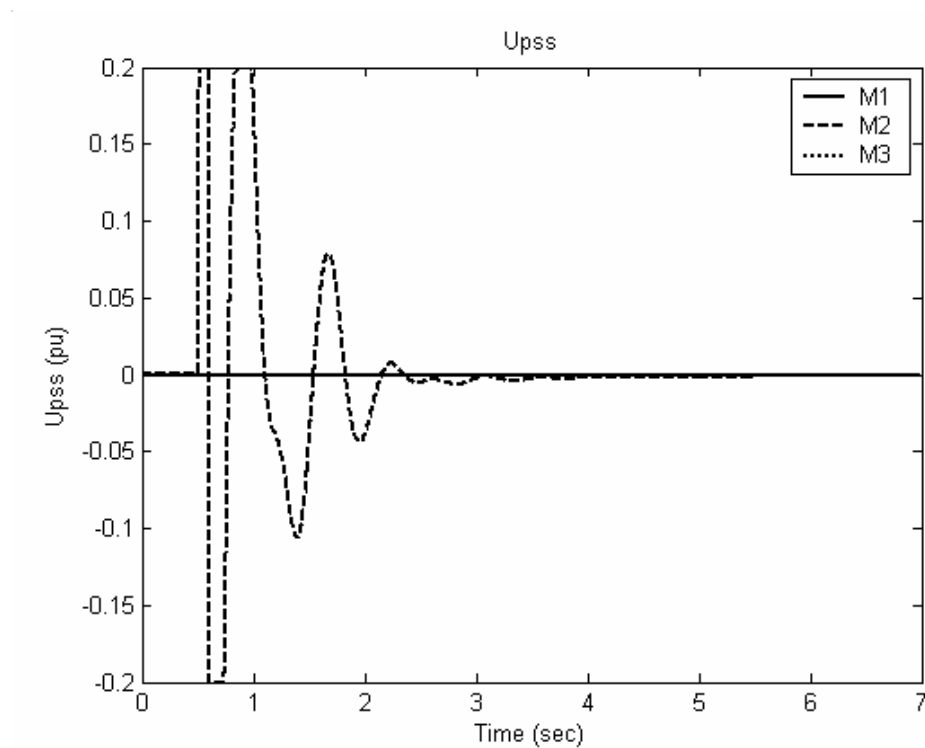


Fig. 7.27: PSS response for 6-cycle fault, with PSS2 & SVC5, coordinated design

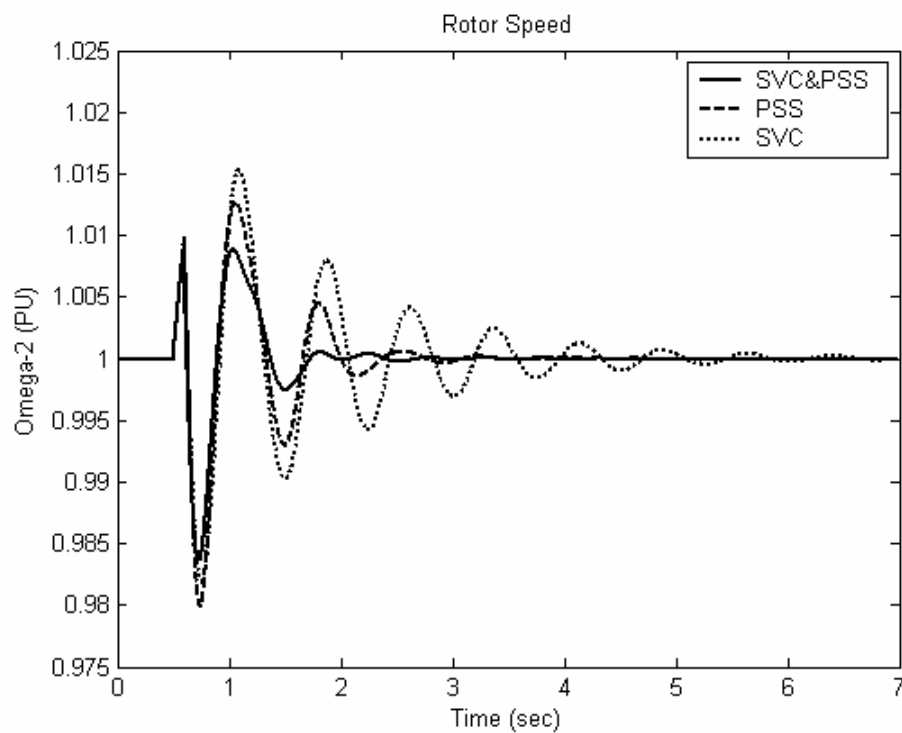


Fig. 7.28: Speed response for 6-cycle fault with PSS2 & SVC5, coordinated and individual design

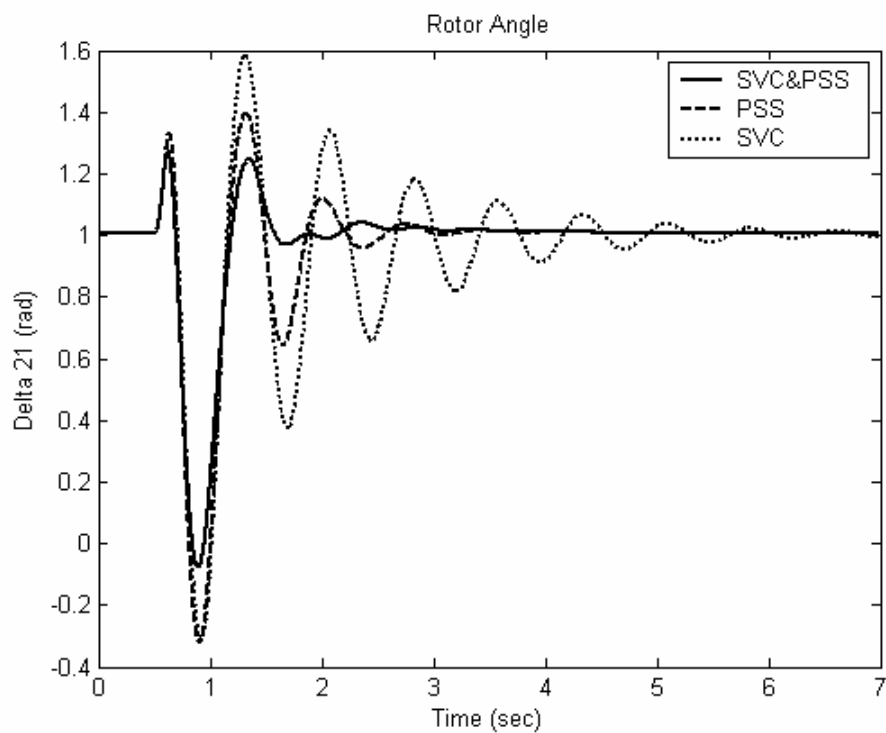


Fig. 7.29: Rotor angle response for 6-cycle fault with PSS2 & SVC5, coordinated and individual design

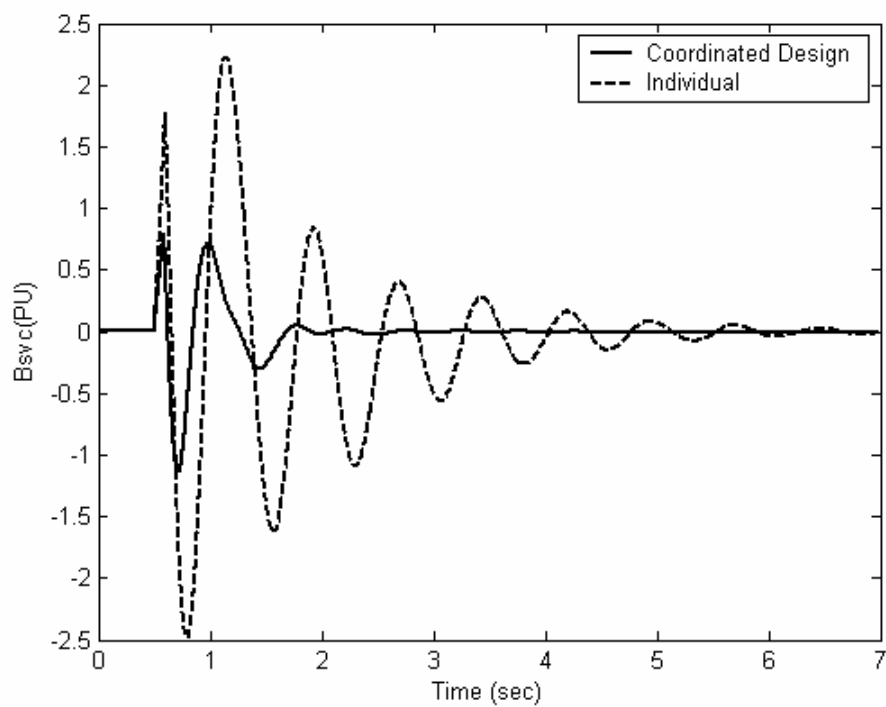


Fig. 7.30: SVC5 response for 6-cycle fault, PSS2 & SVC5, coordinated and individual design

7.2 Example 2 (4-machines, 10-bus system)

The system considered in this section is the two-area power system. The system one-line diagram is shown in Fig. 7.31. The details system data including the dynamic generators model and exciter data used along with load flow result are given in the Appendix C.

The system consists of two identical areas. Each includes two 900 MVA generating units equipped with fast static exciters. All four generating units are represented by the same dynamic model. The power transfer from Area 2 to Area 1 over a single tie line is considered.

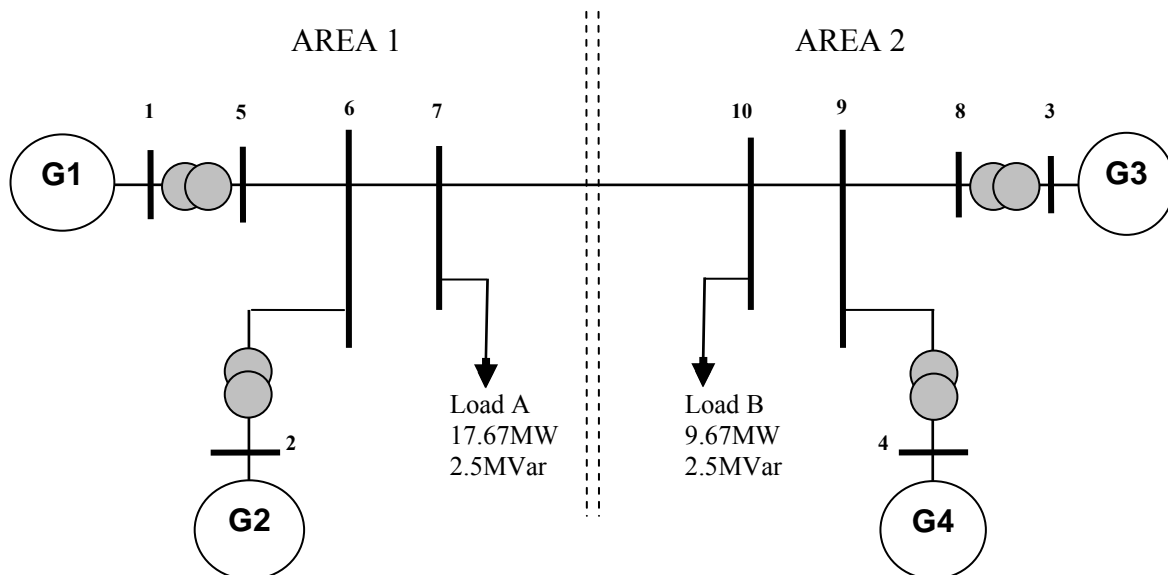


Fig. 7.31: Single line diagram of the two-area system

7.2.1 System Analysis

From the open loop system eigenvalue and participation factor analysis shown in Table 7.9, the system exhibits three electromechanical modes:

- An inter-area mode, with a frequency of 0.5098 Hz, in which the generating units in one area oscillate against those in the other area.
- Local mode, in area 1, with a frequency of 1.1125 Hz. In this mode the machines in Area 1 oscillate against each other.
- Local mode, in area 2, with a frequency of 1.0941 Hz. In this mode the machines in Area 2 oscillate against each other.

The frequencies, damping ratios, and participation factors (PF) for these three electromechanical modes are given in the Table below.

The table shows that the two generating units in each area have close participation factor in the inter-area mode. The same is also true for the two local modes. This is to be expected, since all units are identical, and units in each area are electrically close. The table also shows that the units in Area 1 (the receiving end) have higher participation factor than the units in Area 2 (sending end) to the inter-area mode. It can also be seen that, the inter-area mode has negative damping ratio at this operating condition.

Table 7.9: Two-area system eigenvalues analysis

<i>Eigenvalues</i>	<i>Freq.</i>	<i>Mode</i>	<i>Damping Ratio</i>	<i>Machines Participation Factor</i>			
				G1	G2	G3	G4
-0.660 ± 6.9904i	1.1125	Local	0.094	0.7544	1	0.0015	0.0088
-0.7375 ± 6.8742i	1.0941	Local	0.1067	0.0133	0.0016	0.8438	1
0.0279 ± 3.2030i	0.5098	Inter-Area	-0.0087	1	0.7869	0.3891	0.2432

The first electromechanical mode has a very low damping ratio equal to (0.094) in which Generator no. 1 & 2 have the significant participation factors of that mode. Therefore, PSSs are located at machine number 1 and 2 in addition to machine 4 since it has the significant PF of the inter-area mode.

The TCSC is to be installed at the tie-line while the SVC will be located at the receiving end bus of the tie-line (bus#7) as concluded from the modal analysis result shown in Table 7.10. These locations are satisfied the primary function of TCSC & SVC as will as the practical experience.

Table 7.10: Modal analysis result for two-area system

<i>PQ</i> <i>Buses</i>	<i>Eigenvalues of the reduced Jacobian</i>					
	<i>248.1208</i>	<i>261.48</i>	<i>19.939</i>	<i>32.43</i>	<i>95.17</i>	<i>98.978</i>
B-5	0.046475	0.001237	0.047643	0.041265	0.74773	0.11565
B-6	0.68811	0.021776	0.17868	0.1098	0.0012762	0.00036109
B-7	0.23078	0.011604	0.41921	0.20346	0.10914	0.025813
B-8	0.0019677	0.04161	0.025678	0.073802	0.12715	0.7298
B-9	0.026866	0.67628	0.09756	0.19832	0.00090486	0.000065
B-10	0.0058034	0.24749	0.23123	0.37336	0.013803	0.12832

7.2.2 Individual Design

Based on the linearized multimachine power system model shown in Fig.3.6, PSO has been applied to the optimization problem to search for optimal settings of the proposed stabilizers for individual design.

7.2.2.1 Stabilizer Design

All stabilizers PSSs, TCSC-based & SVC-based are tuned individually by PSO searching for the optimum controllers' parameter settings that maximize the minimum damping ratio of all the system complex eigenvalues. The final settings of the optimized parameters for the proposed stabilizers are given in Table 7.11.

The convergence rate of the objective function for all controllers is shown in Fig. 7.32. It is clear that the PSSs improve greatly the system damping compared to TCSC and SVC. Also it can be seen that the SVC-based stabilizer has a negative damping ratio that will excite the system oscillation which confirm the conclusion given in [74, 75].

Table 7.11: Optimal parameter settings for PSSs, SVC, & TCSC in two-area system

<i>Parameters</i>	<i>PSSs</i>			<i>SVC</i>	<i>TCSC</i>
	<i>PSS1</i>	<i>PSS2</i>	<i>PSS4</i>		
<i>K</i>	73.47	8.9714	17.5189	220.1907	8.4131
<i>T₁</i>	0.058	0.01	0.01	0.6275	0.0795
<i>T₂</i>	0.05	0.05	0.05	0.010	0.5859
<i>T₃</i>	0.0926	0.0444	0.2656	4.980	5.0
<i>T₄</i>	0.05	0.05	0.05	1.0	0.3456

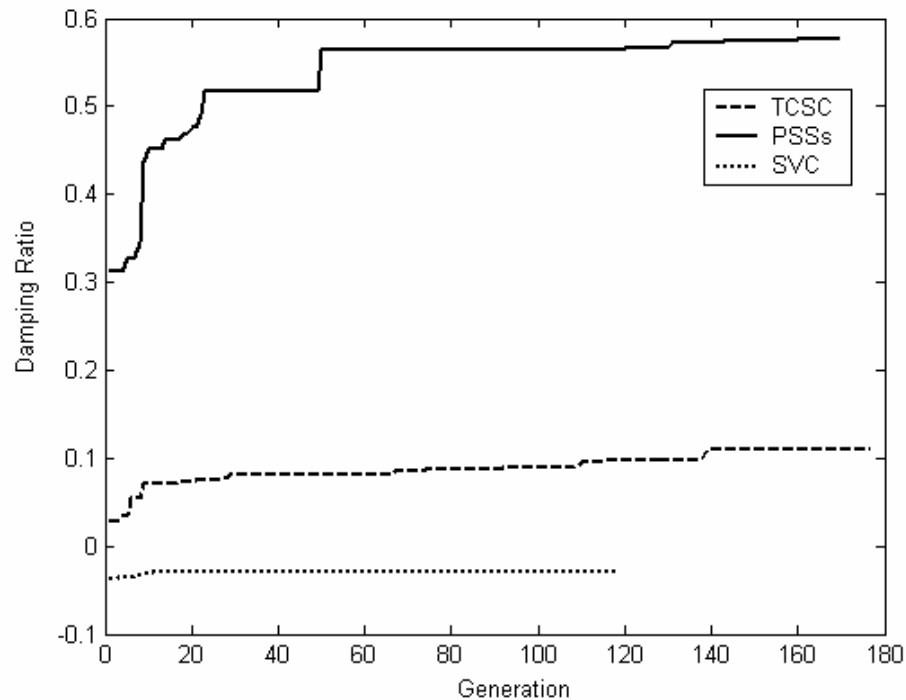


Fig. 7.32: Variation of the objective function of PSS, TCSC, & SVC stabilizers in multimachine two-area power system

7.2.2.2 Eigenvalue Analysis

The system eigenvalues along with damping ratios with the proposed PSSs, SVC-based, and TCSC-based stabilizers when applied individually are given in Table 7.12. The bolded rows of the table represent the EM modes eigenvalue and their damping ratios and frequency.

It is clear that PSS's greatly enhance the system damping while the system damping is slightly improved in case of TCSC-based stabilizer, whereas the SVC has a negative damping effect to the system which is going to be proved by the nonlinear simulation.

Table 7.12: System eigenvalues in case of PSS, SVC & TCSC, two-area system

<i>PSSs</i>	<i>SVC</i>	<i>TCSC</i>
-3.9219±5.7975i	0.2752+9.29463i	-0.7497±6.8431i
0.5603*, 0.9227**	-0.0296*, 1.479**	0.1089*, 1.089**
-3.4337±5.4358i	-0.49126+6.9342i	-0.5099±4.3648i
0.534*, 0.8651**	0.07067*, 1.103**	0.1158*, 0.694**
-1.7682±1.6360i	0.08641+2.9049i	-0.597±5.0238i
0.734*, 0.2604**	-0.02973*, 0.462**	-1.614±4.9672i
-2.6113±3.0188i	-16.75 + 0.69i	-89.0670,-89.4168
-7.7989±11.9581i	-89.05,-89.41,	-79.3902
-12.3718±17.9649i	-79.5,-76.7	-76.6922,-23.9691
-17.3096±0.1076i	-100,-23.42,-188.2	-21.0447,-16.7120
-21.5036±1.8633i		-13.8902,-13.6506
-92.0013,-89.3647	-13.86,-7.18	-7.5208,-6.4332
-81.0185,-76.8115		
-11.8988, -7.4442,	-6.67,-6.12	-5.4079, -4.9082
-6.2647, -4.9271,	-6.17,-1.65	
-0.2024, -0.2122	-0.2	-0.2000

* damping ratio, ** frequency Hz

7.2.2.3 Nonlinear Time domain Simulation

Figs. 7.33-7.37 show the speed deviations, rotor angles, electrical power outputs, machine terminal voltages, and PSS's controllers responses, respectively, for a 6-cycle three-phase fault at bus 10 of the two-area system shown in Fig. 7.31 at the base case while using the proposed PSS's. Moreover, the proposed PSS's stabilizers have been compared with those proposed in reference [105] in Figs. 7.38-7.42. Similarly, Figs. 7.43-7.46 show those simulation results while using the proposed TCSC and Figs. 7.47-7.49 demonstrate the use of SVC. Figs. 7.50-7.53 combined the system response with each proposed stabilizers. It can be readily seen that PSS's and TCSC are the most effective stabilizers in damping the EM modes oscillations. However, the system oscillations are excited by SVC at this loading condition. This is in general consistency with eigenvalue analysis results.

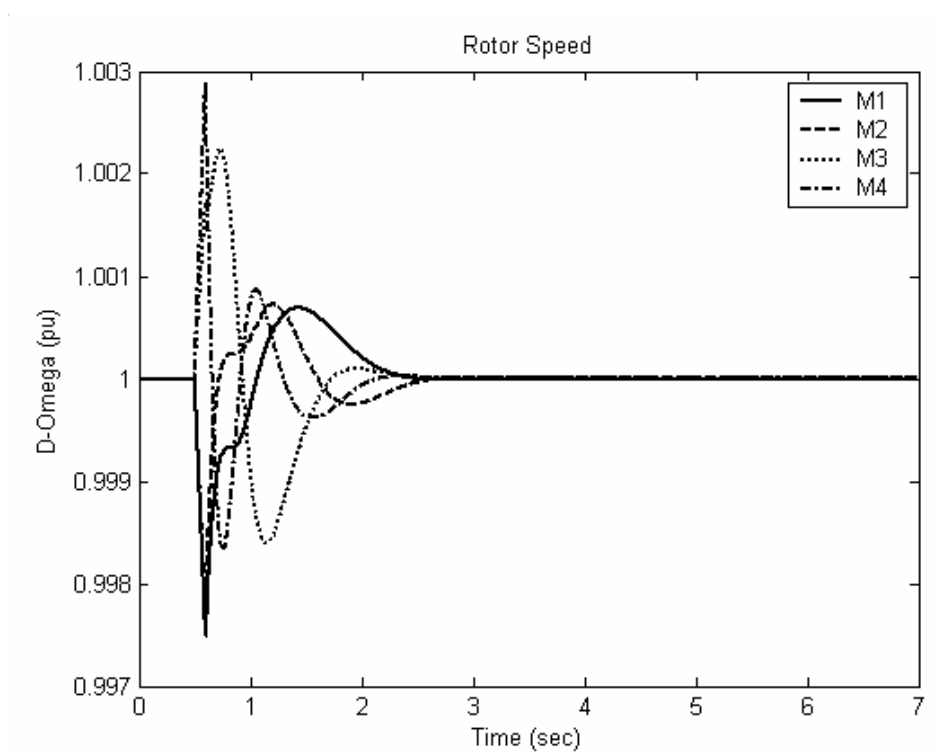


Fig. 7.33: Speed response for 6-cycle fault with PSS's, individual design

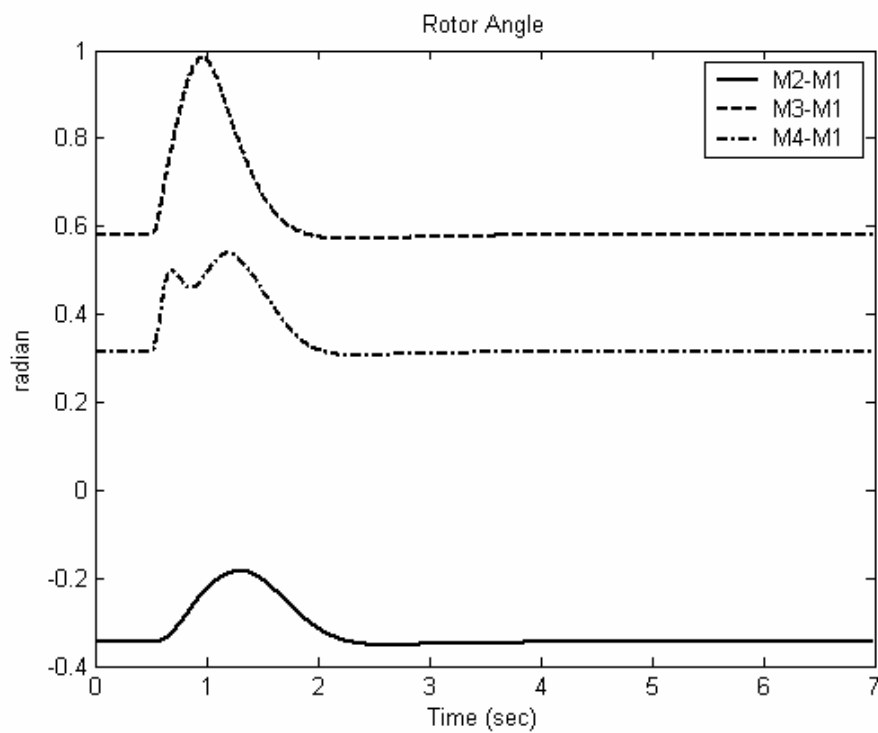


Fig. 7.34: Rotor angle response for 6-cycle fault with PSSs, individual design

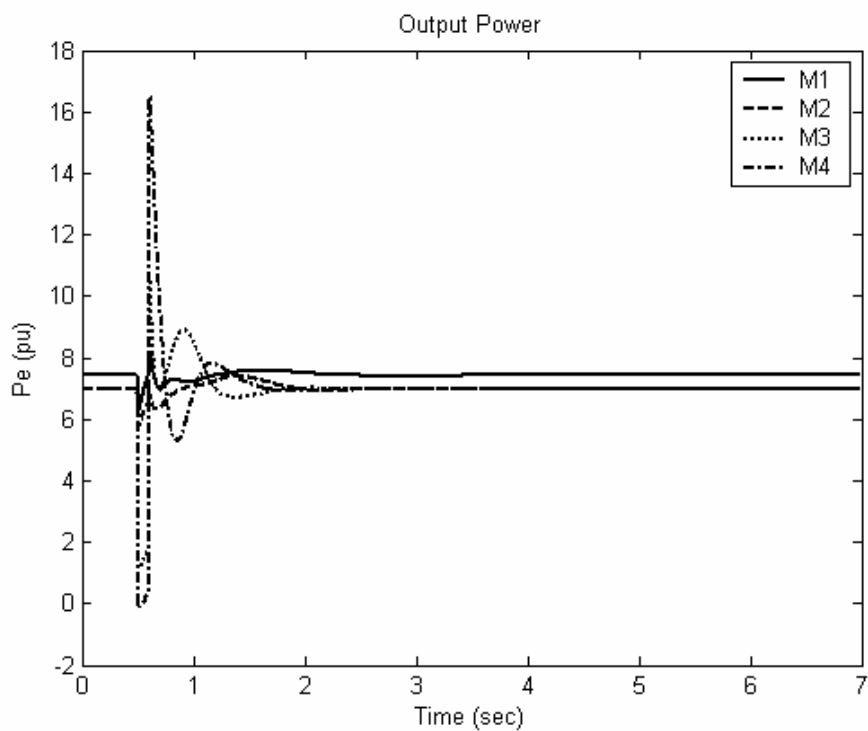


Fig. 7.35: Electrical power response for 6-cycle fault with PSSs, individual design

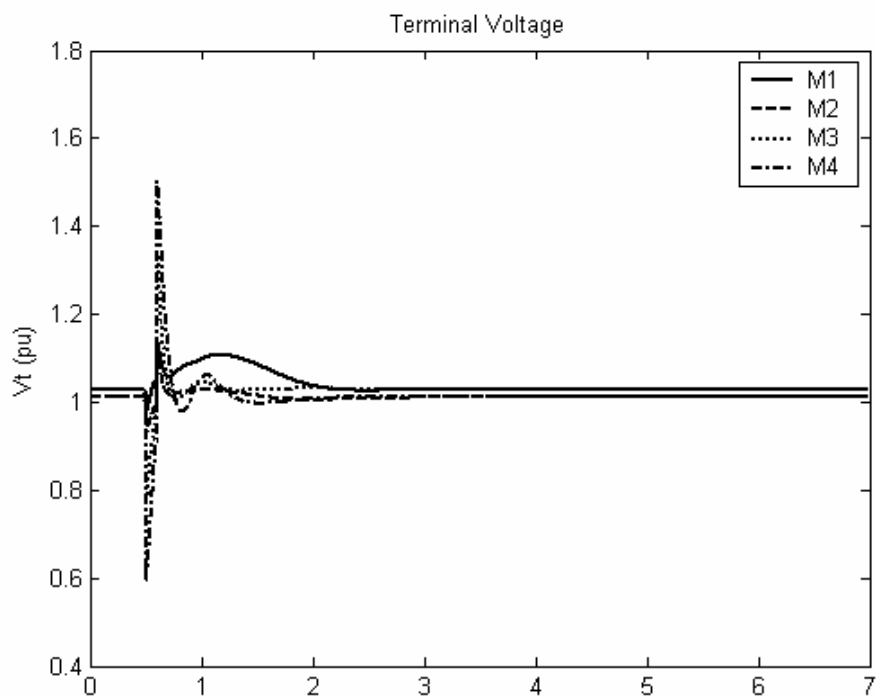


Fig. 7.36: Terminal voltage response for 6-cycle fault with PSSs, individual design

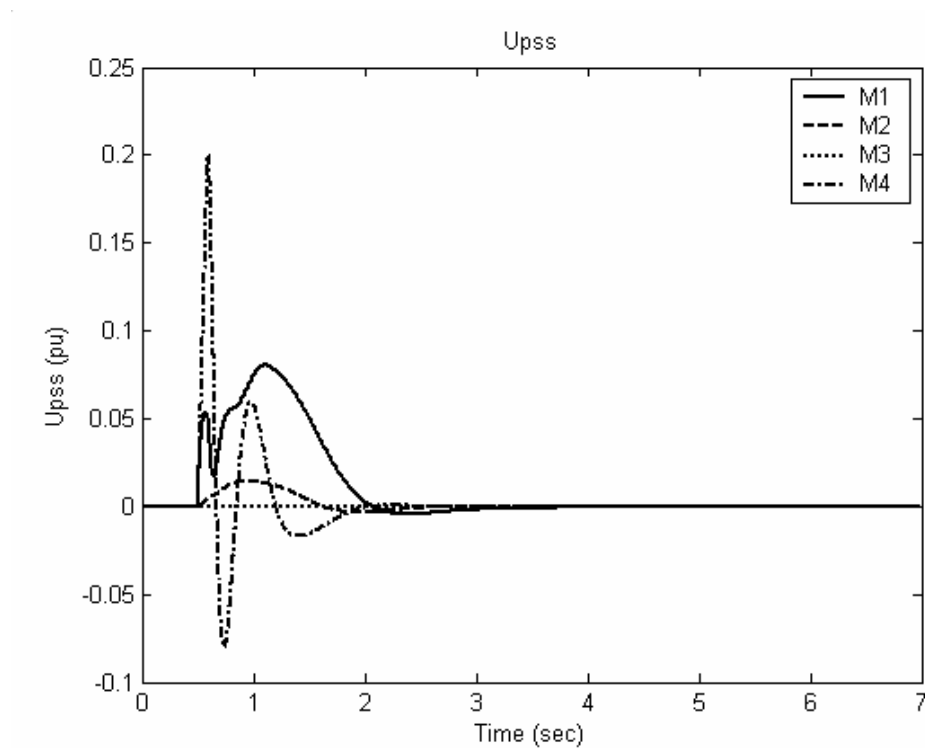


Fig. 7.37: PSSs response for 6-cycle fault, individual design

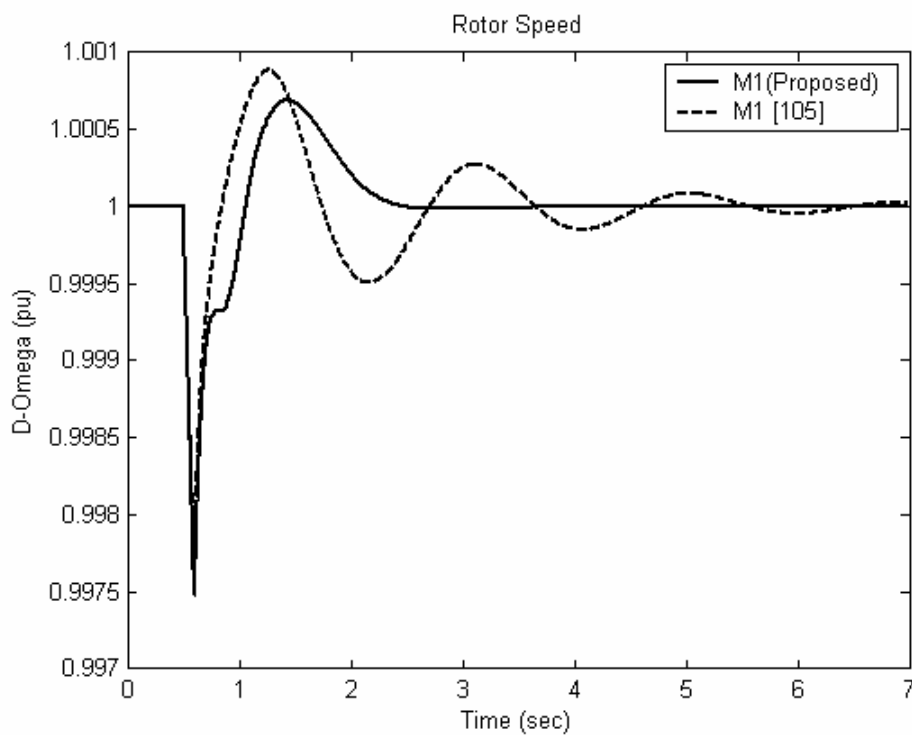


Fig. 7.38: Comparison speed response machine # 1, Kundur [105] and proposed settings

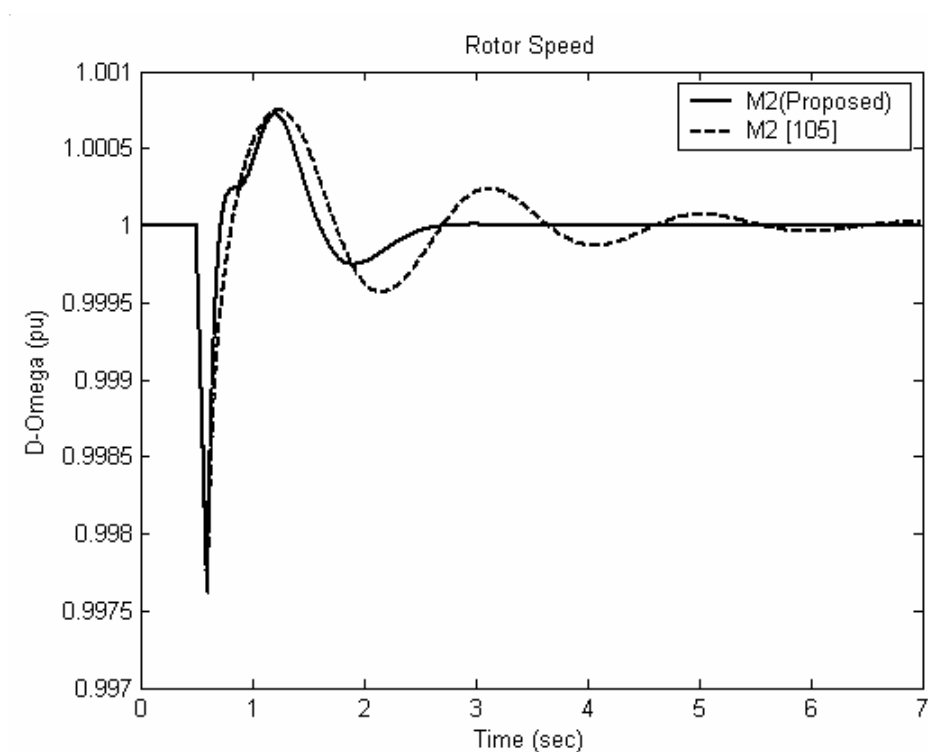


Fig. 7.39: Comparison speed response machine # 2, Kundur [105] and proposed settings

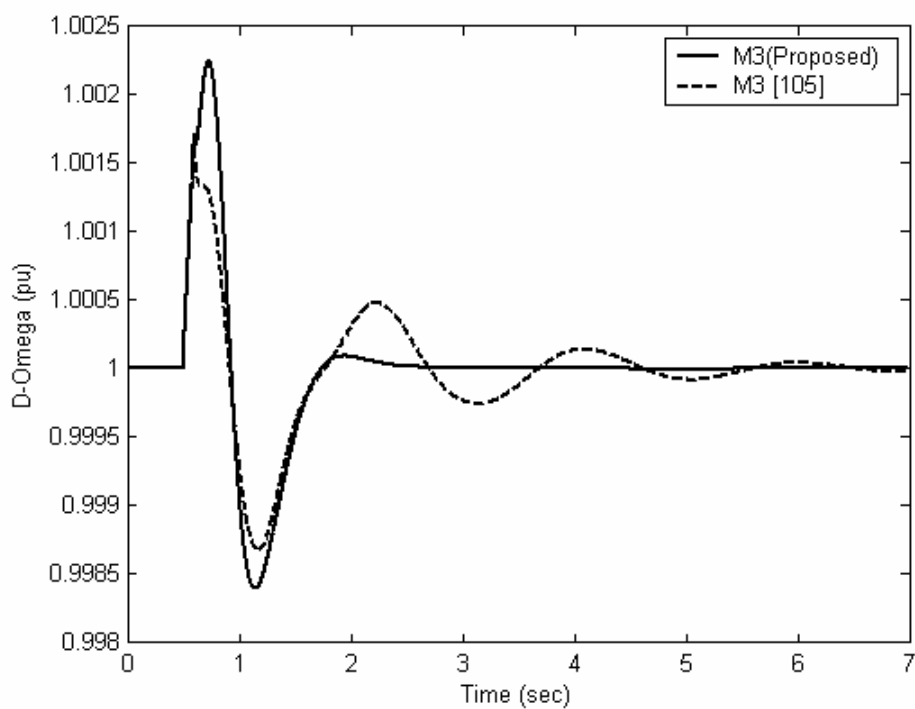


Fig. 7.40: Comparison speed response machine # 3, Kundur [105] and proposed settings

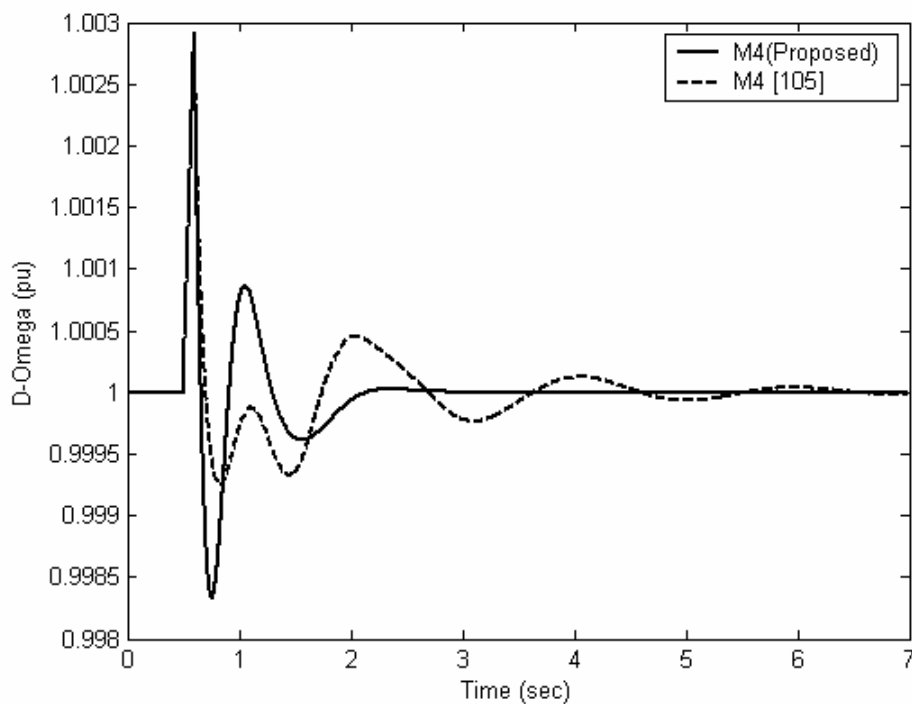


Fig. 7.41: Comparison speed response machine # 4, Kundur [105] and proposed settings

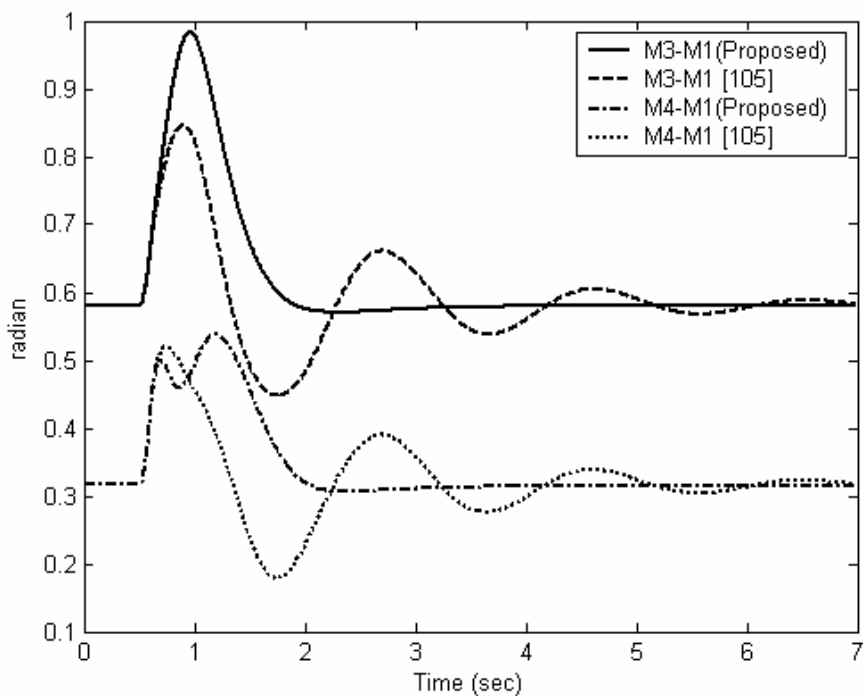


Fig. 7.42: Comparison rotors' angle response, Kundur [105] and proposed settings

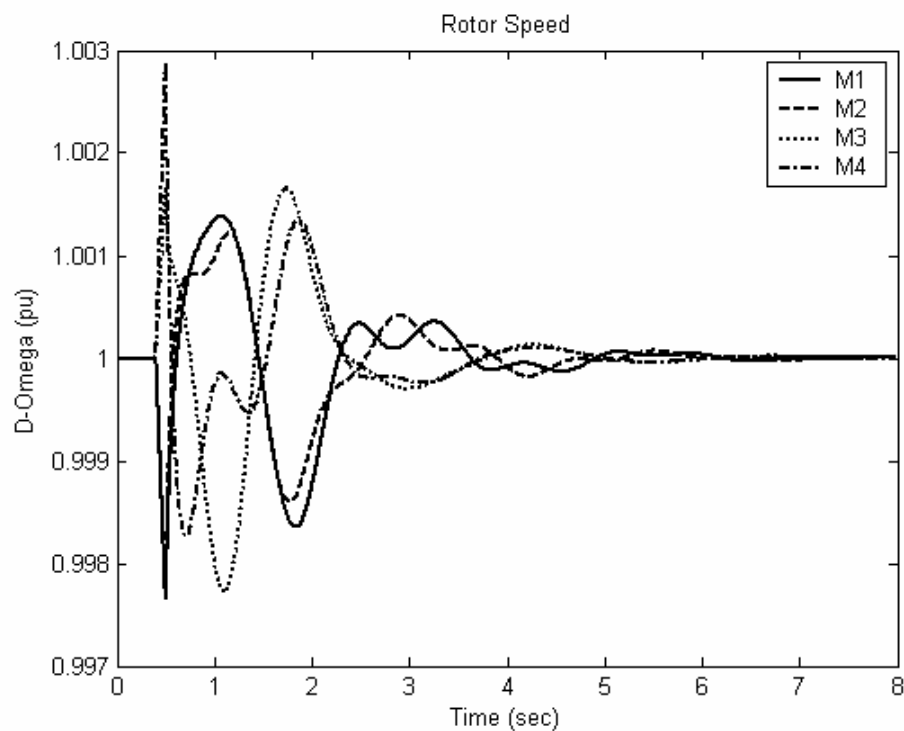


Fig. 7.43: Speed response for 6-cycle fault with TCSC-based stabilizer

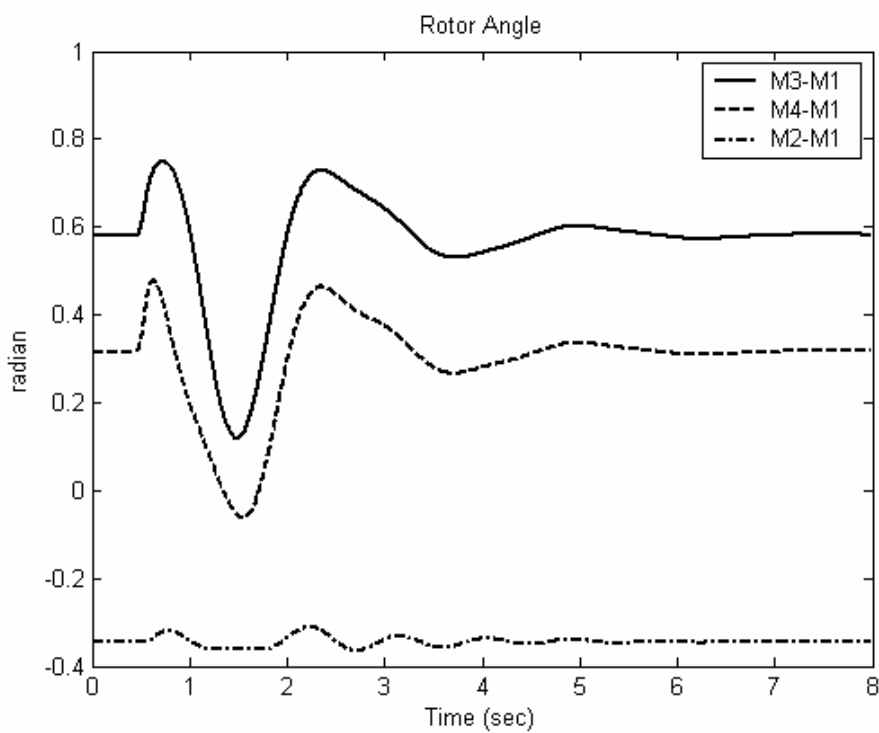


Fig. 7.44: Rotor angle response for 6-cycle fault with TCSC-based stabilizer

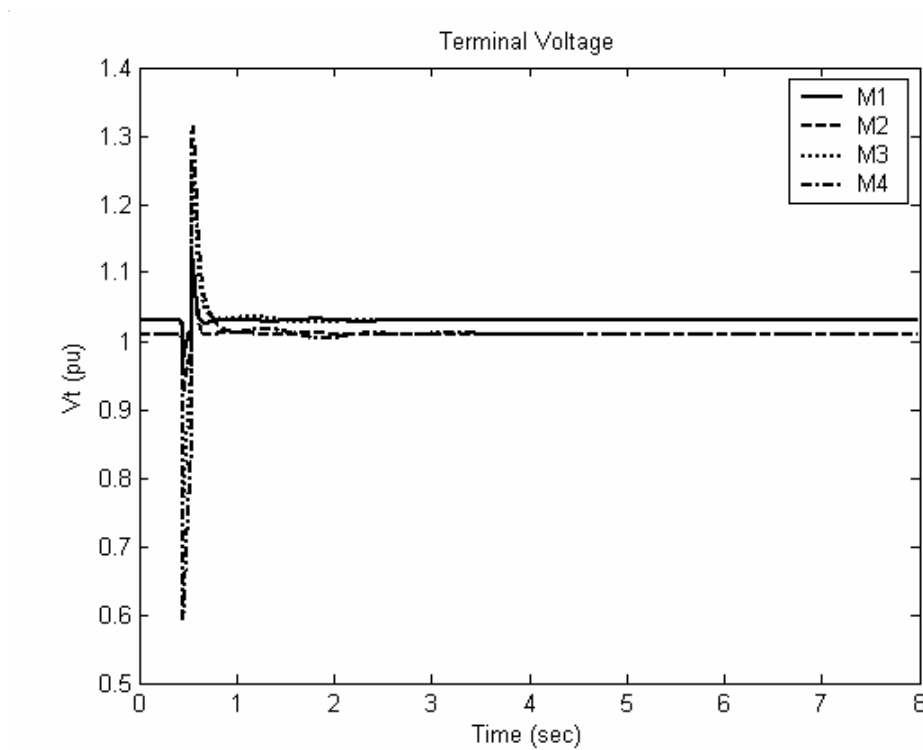


Fig. 7.45: Terminal voltage response for 6-cycle fault with TCSC-based stabilizer

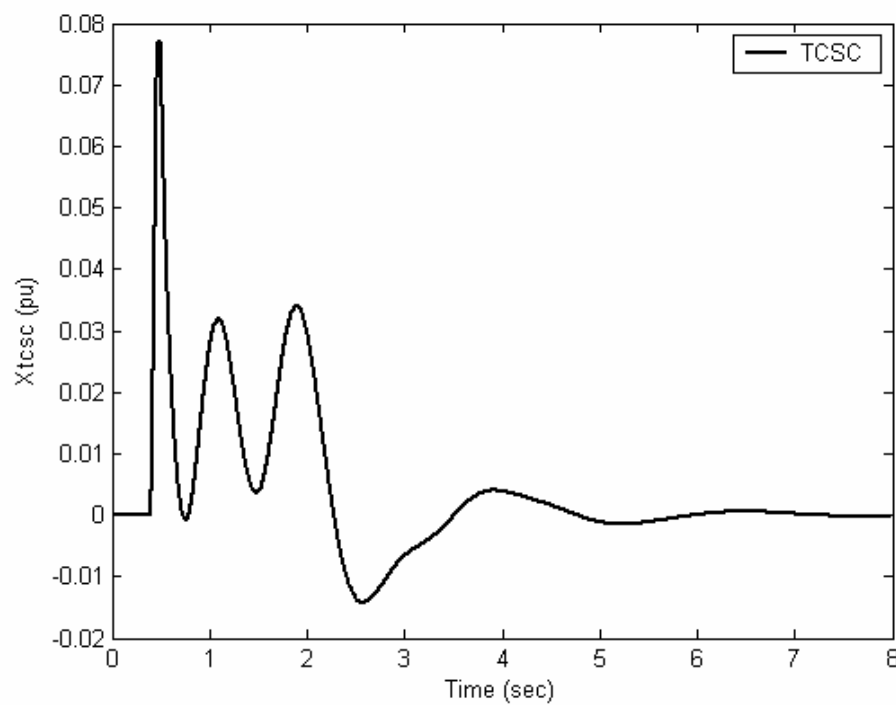


Fig. 7.46: TCSC response for 6-cycle fault with TCSC-based stabilizer

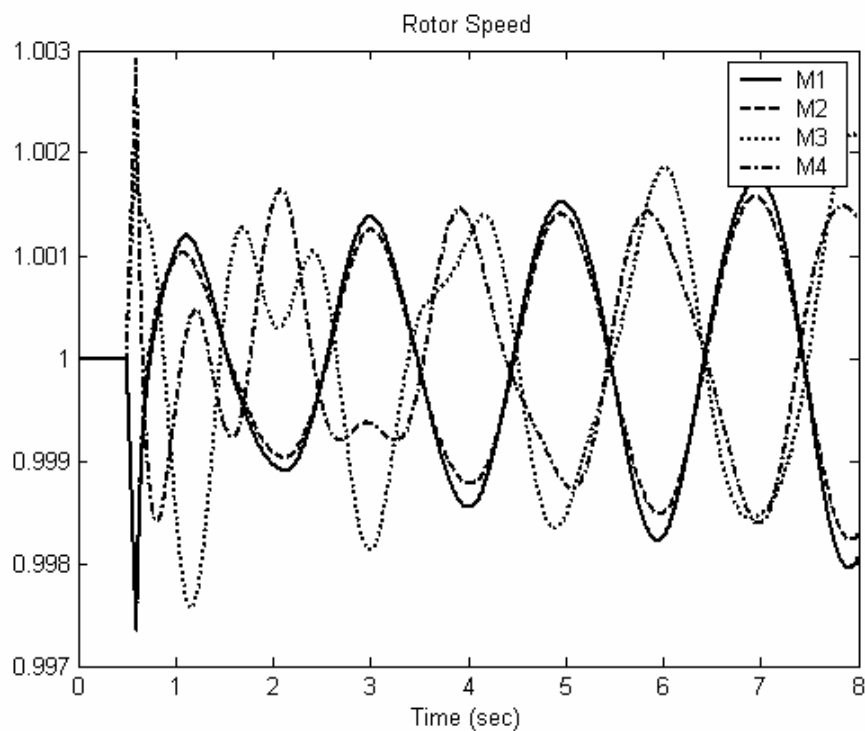


Fig. 7.47: Speed response for 6-cycle fault with SVC-based stabilizer

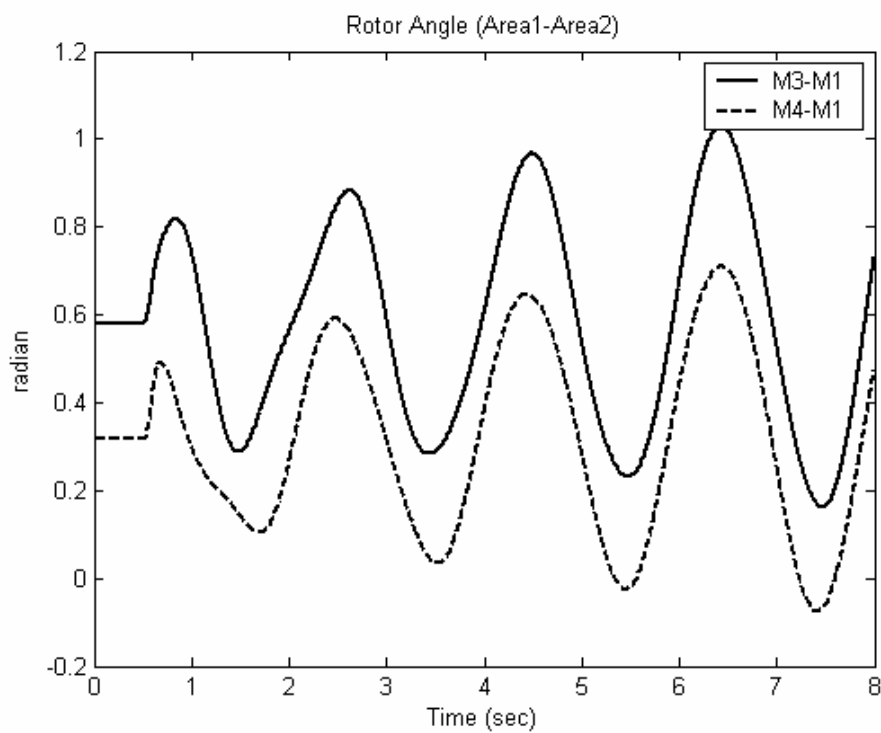


Fig. 7.48: Rotor angle response for 6-cycle fault with SVC-based stabilizer

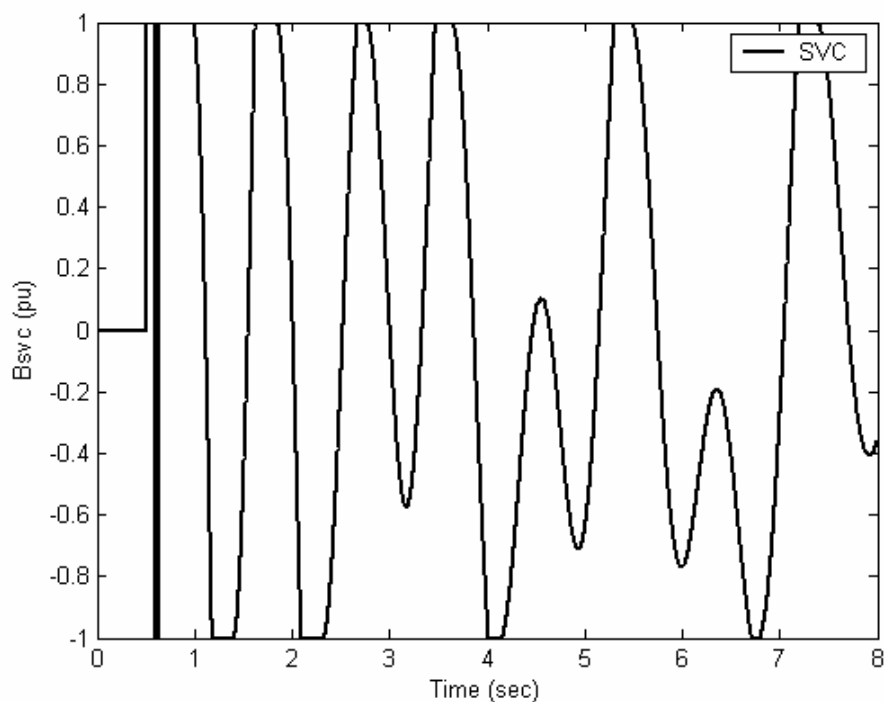


Fig. 7.49: SVC response for 6-cycle fault with SVC-based stabilizer

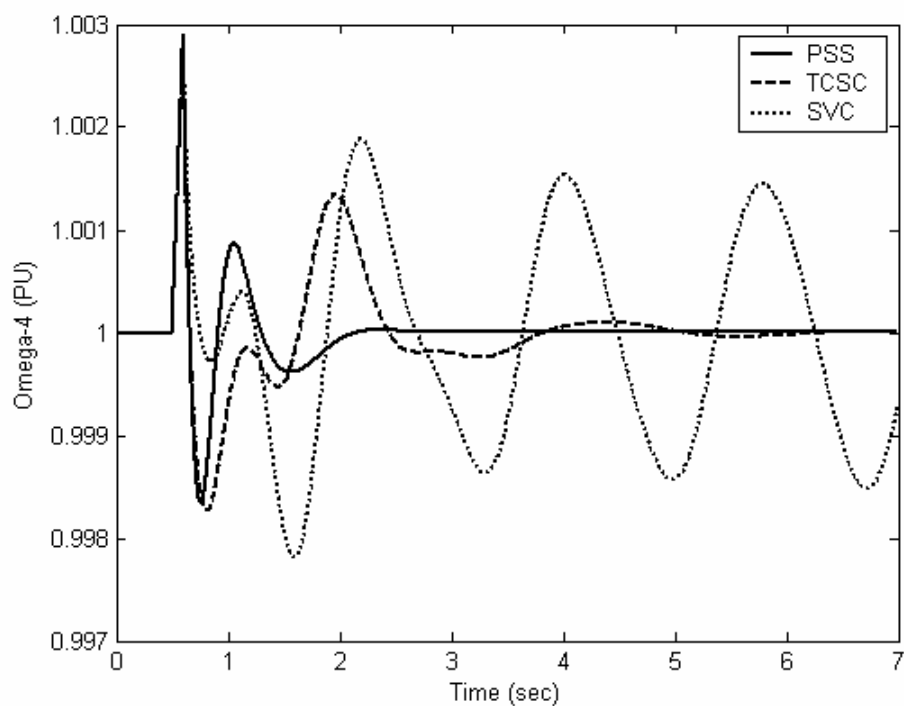


Fig. 7.50: Speed response of machine-4 for 6-cycle fault with PSS, SVC, and TCSC, individual design

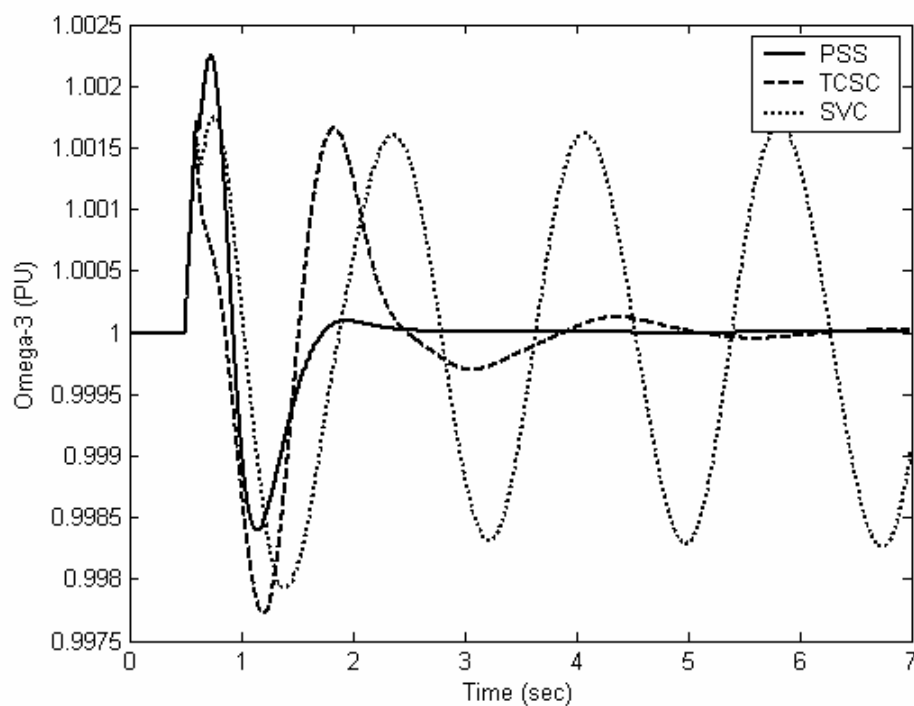


Fig. 7.51: Speed response of machine-3 for 6-cycle fault with PSS, SVC, and TCSC, individual design

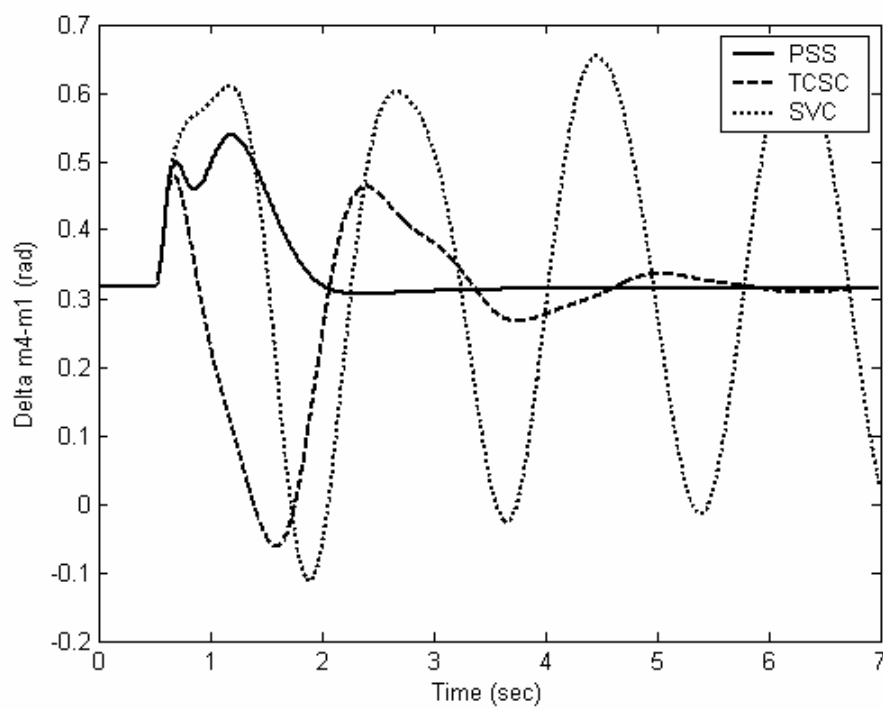


Fig. 7.52: Rotor angle response for 6-cycle fault with PSS, SVC, and TCSC, individual design

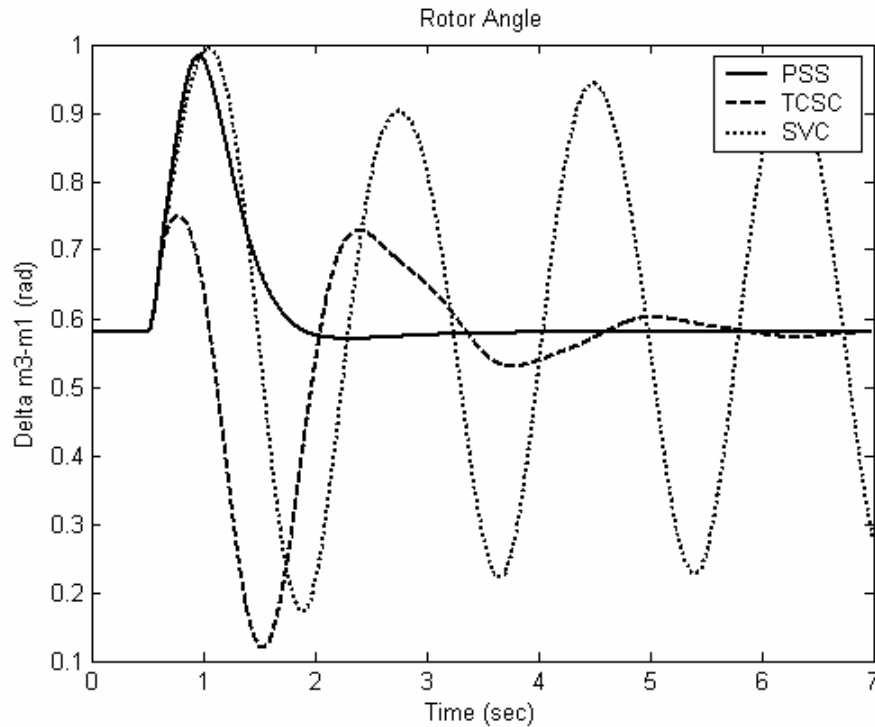


Fig. 7.53: Rotor angle response for 6-cycle fault with PSS, SVC, and TCSC, individual design

7.2.3 Coordinated Design [TCSC & PSS]

All stabilizers PSS's & TCSC are simultaneously tuned by PSO searching for the optimum controllers parameter settings that maximize the minimum damping ratio of all the system complex eigenvalues.

7.2.3.1 Stabilizer Design

The convergence rate of the objective function when PSS's and TCSC-based controllers are designed individually and in a coordinated manner is shown in Fig. 7.54. It is clear that the coordinated design of PSS's and TCSC-based stabilizer improves greatly the

system damping compared to their individual application. The final settings of the optimized parameters for the proposed stabilizers are given in Table 7.13.

Table 7.13: Optimal parameters setting of coordinated PSS's & TCSC design

<i>Parameters</i>	<i>Coordinated Design</i>			
	<i>PSS1</i>	<i>PSS2</i>	<i>PSS4</i>	<i>TCSC</i>
K	100	100	49.2614	1.064
T_1	0.0783	0.0702	0.1354	5.0
T_2	0.01	0.01	0.01	0.021
T_3	-----	-----	-----	0.01
T_4	-----	-----	-----	5.0

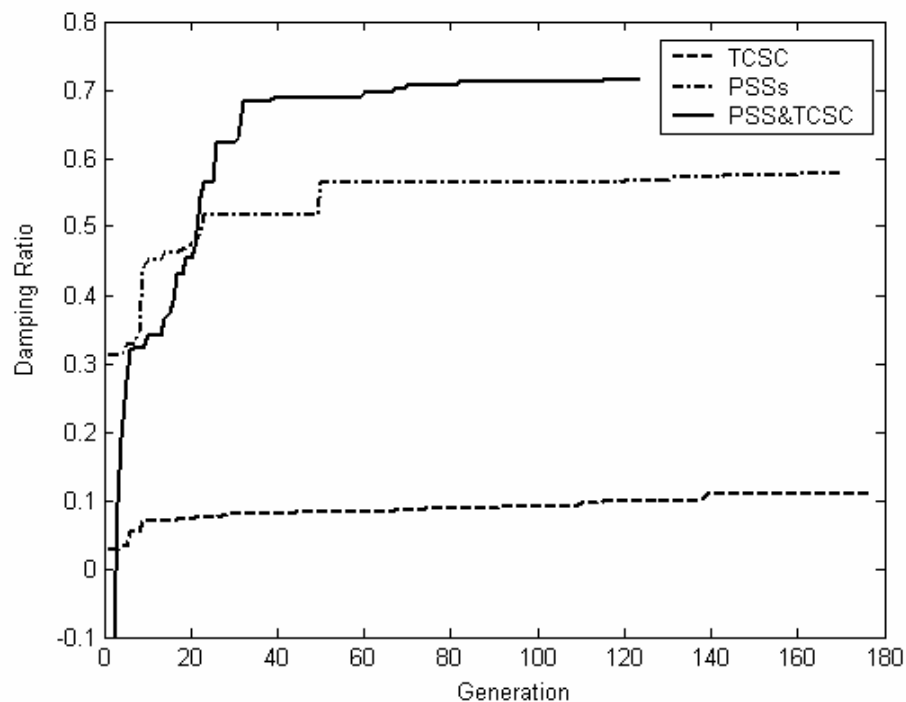


Fig. 7.54: Variation of the objective function of PSS's & TCSC stabilizers in multimachine two-area power system

7.2.3.2 Eigenvalue Analysis

The system eigenvalues with the proposed PSS's and TCSC-based stabilizers when applied individually and by means of coordinated design is given in Table 7.14. The bold rows of this table represent the EM modes eigenvalues and their damping ratios and frequency. It is evident that, using the proposed coordinated stabilizers design, the damping ratio of the EM mode eigenvalue is greatly enhanced. Hence, it can be concluded that this improves the system stability.

Table 7.14: System eigenvalues with coordinated design of PSS & TCSC in two-area system

<i>PSSs</i>	<i>TCSC</i>	<i>TCSC & PSSs</i>
-3.9219±5.7975i	-0.7497±6.8431i	-4.4235±6.07504i
0.5603*, 0.9227**	0.1089*, 1.089**	0.59*, 0.97**
-3.4337±5.4358i	-0.5099±4.3648i	-6.16589±5.0236i
0.534*, 0.8651**	0.1158*, 0.694**	0.783*, 0.8**
-1.7682±1.6360i	-0.597±5.0238i	-2.390±3.2546i
0.734*, 0.2604**		0.59*, 0.526**
-2.6113±3.0188i	-1.614±4.9672i	-1.9658±2.7841i
-7.7989±11.9581i	-89.0670,-89.4168	-6.4785±9.132i
	-79.3902	-13.00±15.812i
-12.3718±17.9649i	-76.6922,-23.9691	
-17.3096±0.1076i	-21.0447,-16.7120	-22.269±4.7965i
-21.5036±1.8633i	-13.8902,-13.6506	
	-7.5208,-6.4332	-100,-100,-0.2,-100
-92.0013,-89.3647		
-81.0185,-76.8115	-5.4079, -4.9082	-128.36,-82.485,-100
-11.8988, -7.4442,	-0.2000	-20.009,-17.72,-15.80
		-12.841,-9.4599
-6.2647, -4.9271,		-6.023,-5.3289,-2.619
-0.2024, -0.2122		-1.216

* damping ratio, ** frequency (Hz)

7.2.3.3 Nonlinear Time domain Simulation

Figs. 7.55-7.60 show the rotor angles, speed deviations, electrical power outputs, and machine terminal voltages responses, as well as PSS2 stabilizing signal and TCSC response, respectively, for a 6-cycle three-phase fault at bus 10 at the end of line 10-7 at the base case while using the proposed PSS's-TCSC coordinated design. These Figs. should be compared with Figs. 7.33-7.37, for individual PSS's design, and 7.43-7.46, for individual TCSC design. Figs. 7.61-7.65 combined the system responses for coordinated and individual desing of TCSC & PSS.

The improvement on the system responses when using the coordinated design is quite evident. This is in agreement with eigenvalue analysis results

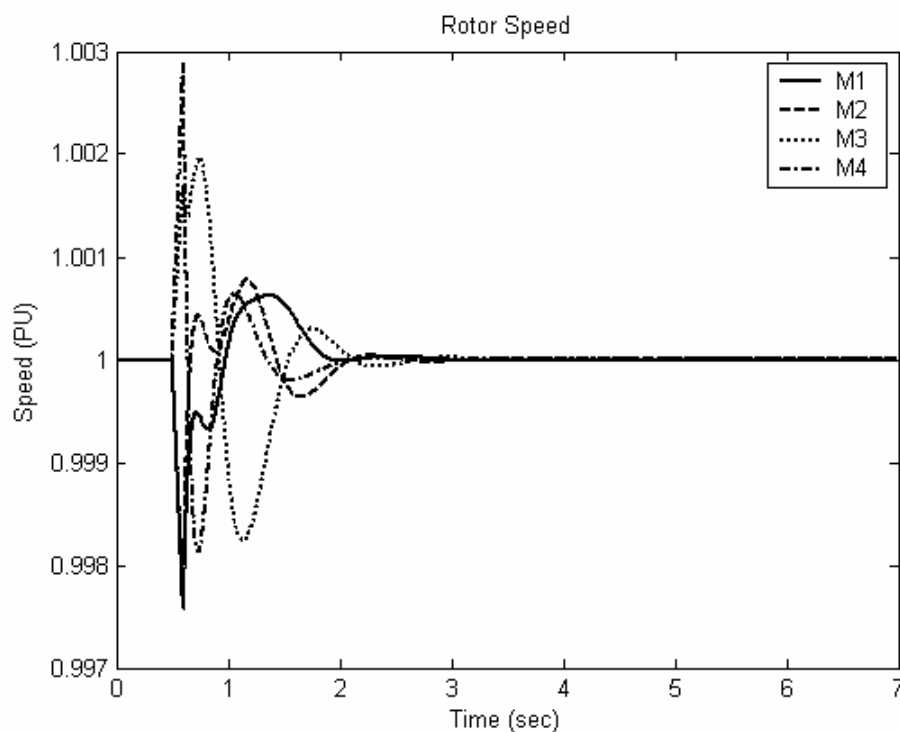


Fig. 7.55: Speed response for 6-cycle fault with PSS's & TCSC, coordinated design in the two-area system

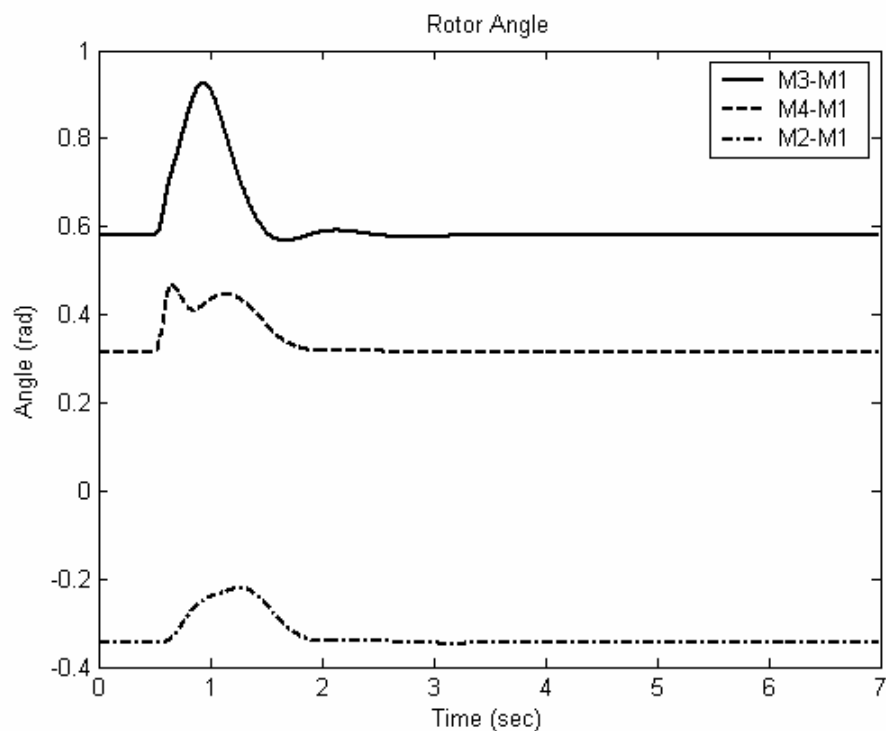


Fig. 7.56: Rotor angle response for 6-cycle fault with PSS's & TCSC, coordinated design in the two-area system

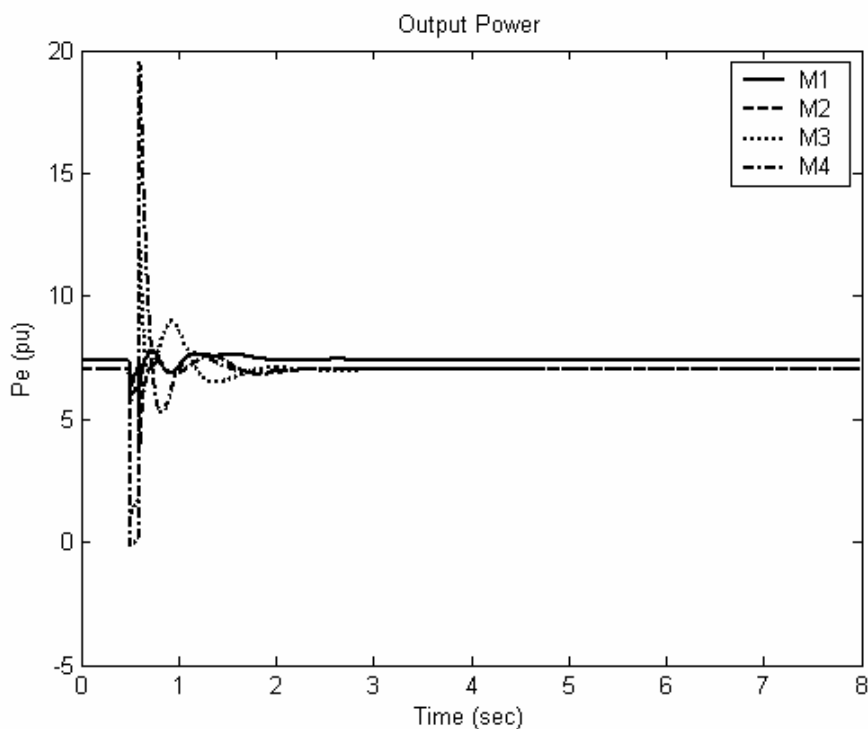


Fig. 7.57: Electrical power response for 6-cycle fault PSS's & TCSC, coordinated design in the two-area system

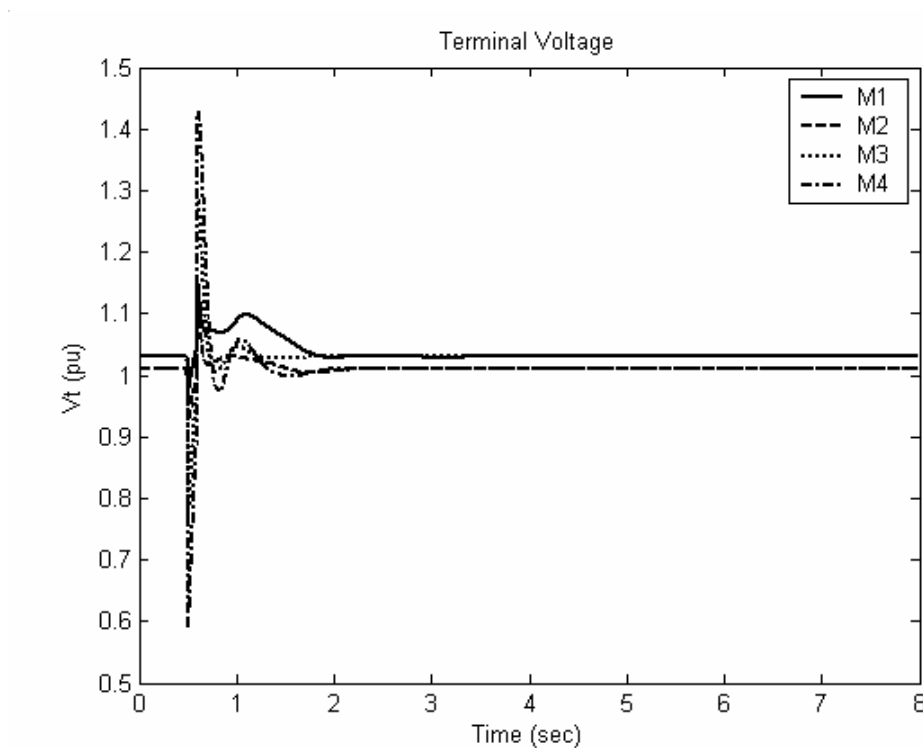


Fig. 7.58: Terminal voltage response for 6-cycle fault with PSS's & TCSC, coordinated design in the two-area system

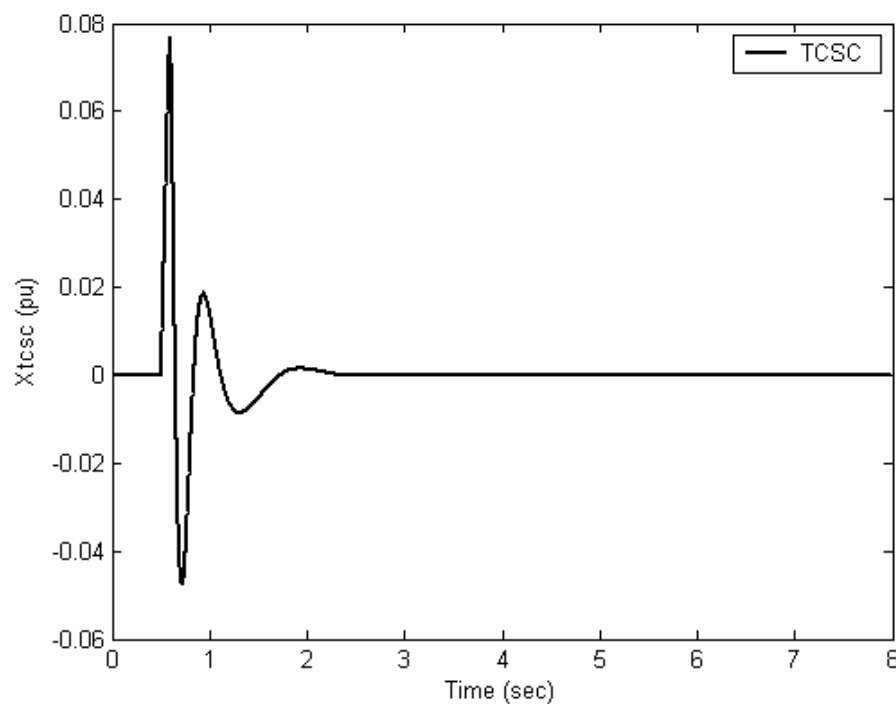


Fig. 7.59: TCSC response for 6-cycle fault, coordinated design with PSS's in the two-area system

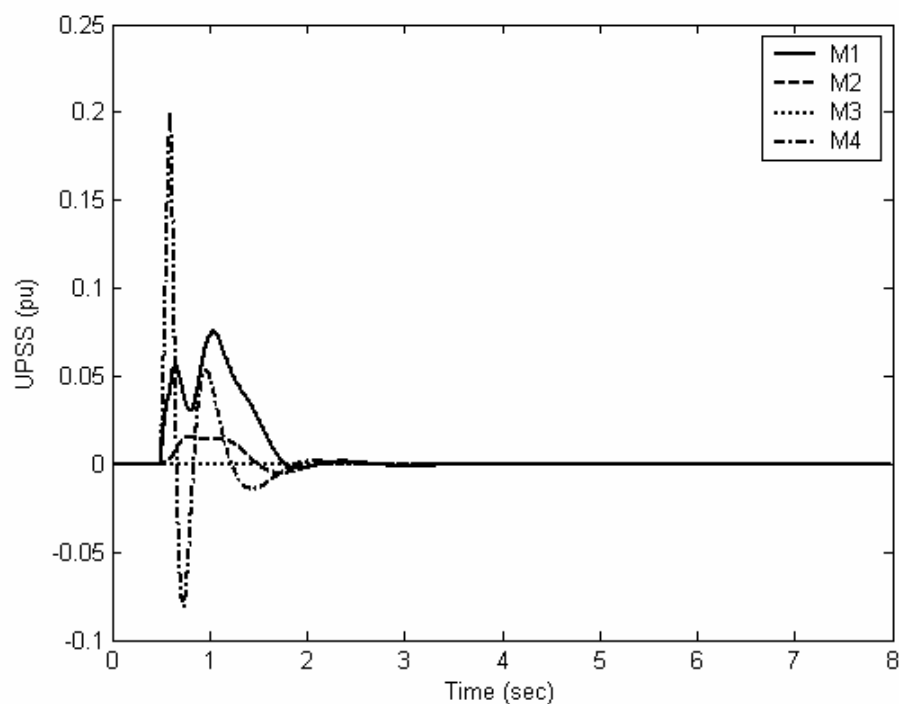


Fig. 7.60: PSS's response for 6-cycle fault, coordinated design with TCSC in the two-area system

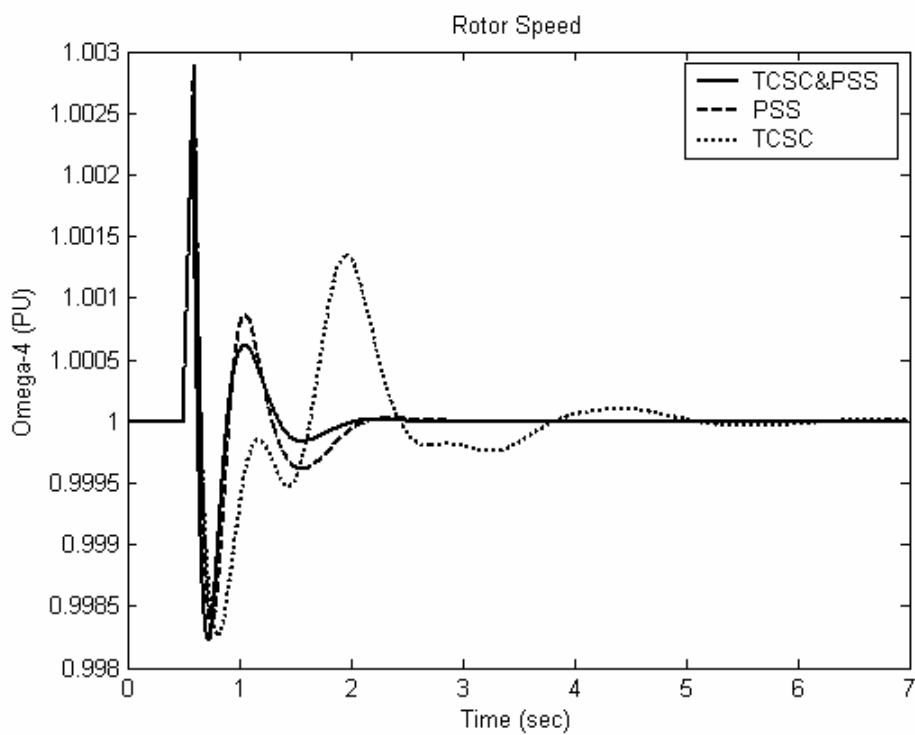


Fig. 7.61: Speed response for 6-cycle fault with PSS's & TCSC, coordinated and individual design in the two-area system

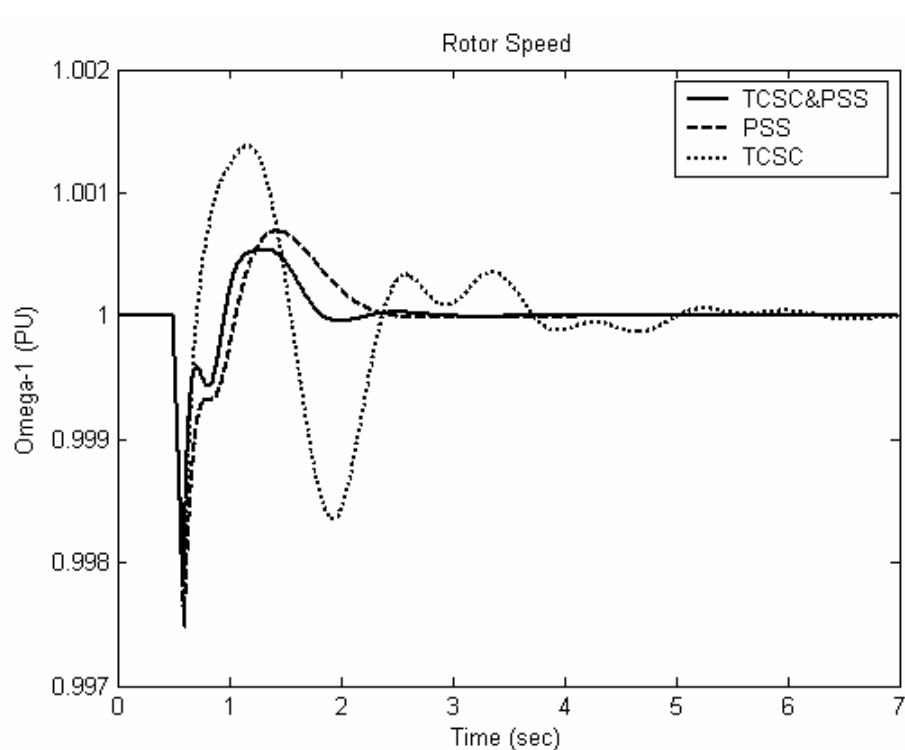


Fig. 7.62: Speed response for 6-cycle fault with PSS's & TCSC, coordinated and individual design in the two-area system

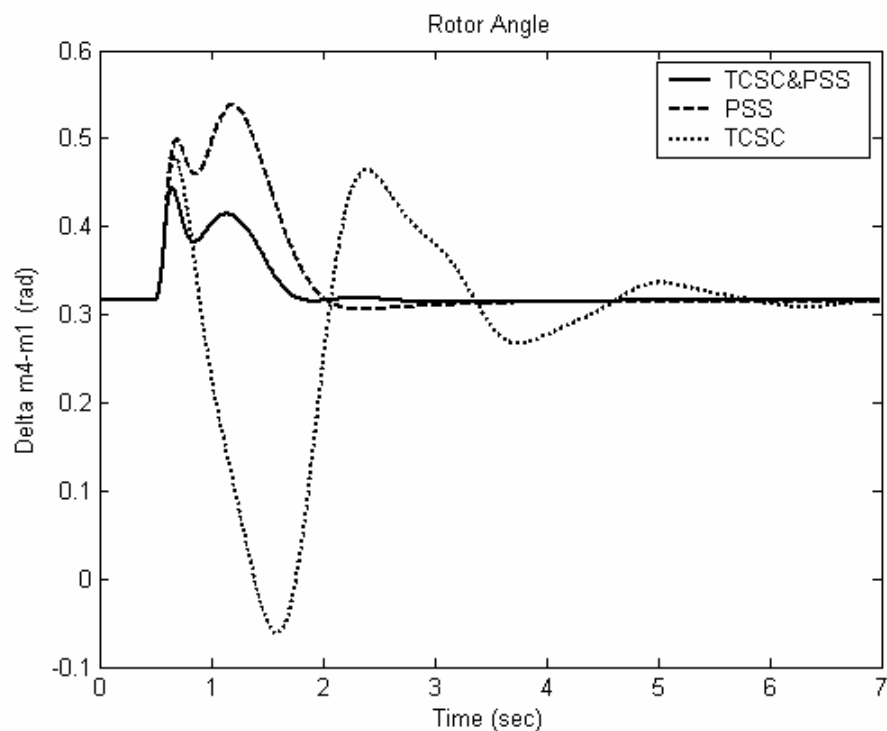


Fig. 7.63: Rotor angle response for 6-cycle fault with PSS's & TCSC, coordinated and individual design in the two-area system

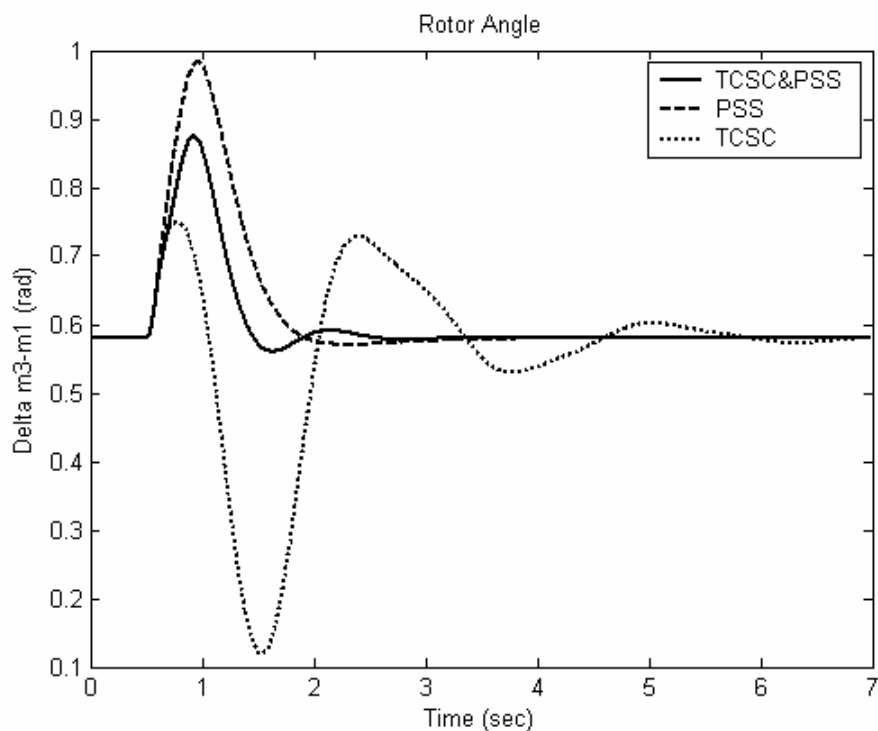


Fig. 7.64: Rotor angle response for 6-cycle fault with PSS's & TCSC, coordinated and individual design in the two-area system

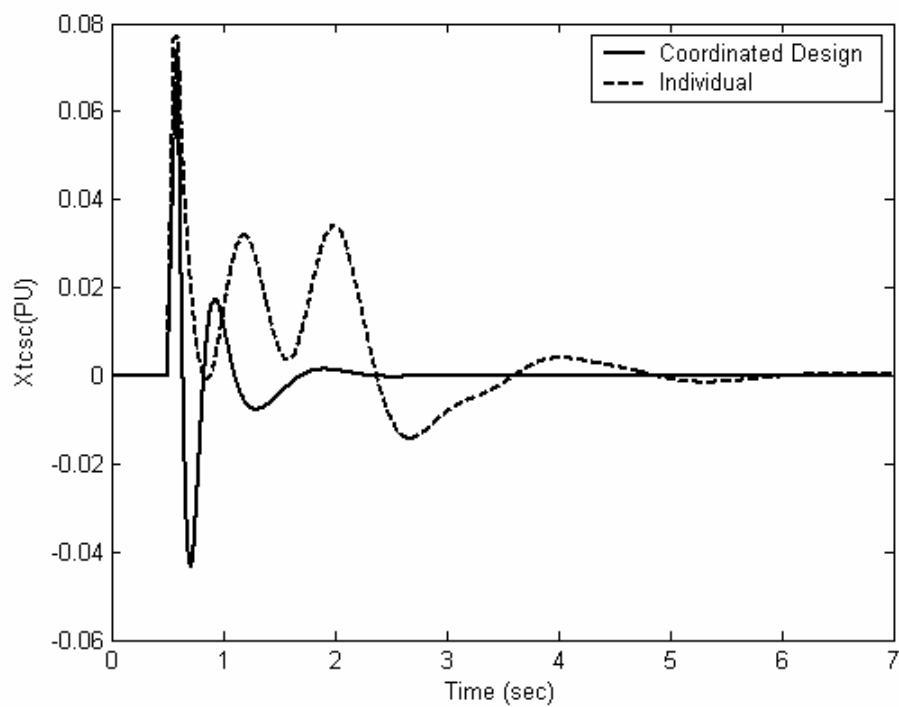


Fig. 7.65: TCSC response for 6-cycle fault, coordinated and individual design in the two-area system

7.2.4 Coordinated Design [SVC & PSS]

All stabilizers PSS's & SVC are simultaneously tuned by PSO searching for the optimum controllers parameter settings that maximize the minimum damping ratio of all the system complex eigenvalues.

7.2.4.1 Stabilizer Design

The convergence rate of the objective function when PSS's and SVC-based controllers are designed individually and in a coordinated manner is shown in Fig. 7.66. It is clear that the coordinated design of PSS's and SVC-based stabilizer improves greatly the system damping compared to their individual application. The final settings of the optimized parameters for the proposed stabilizers are given in Table 7.15.

Table 7.15: Optimal parameters setting of coordinated PSS's & SVC design

<i>Parameters</i>	<i>Coordinated Design</i>			
	<i>PSS1</i>	<i>PSS2</i>	<i>PSS4</i>	<i>SVC</i>
<i>K</i>	26.173	100	51.9935	20.25
<i>T₁</i>	0.025	0.0548	0.1085	0.9441
<i>T₂</i>	0.01	0.01	0.01	0.7922
<i>T₃</i>	-----	-----	-----	5
<i>T₄</i>	-----	-----	-----	0.01

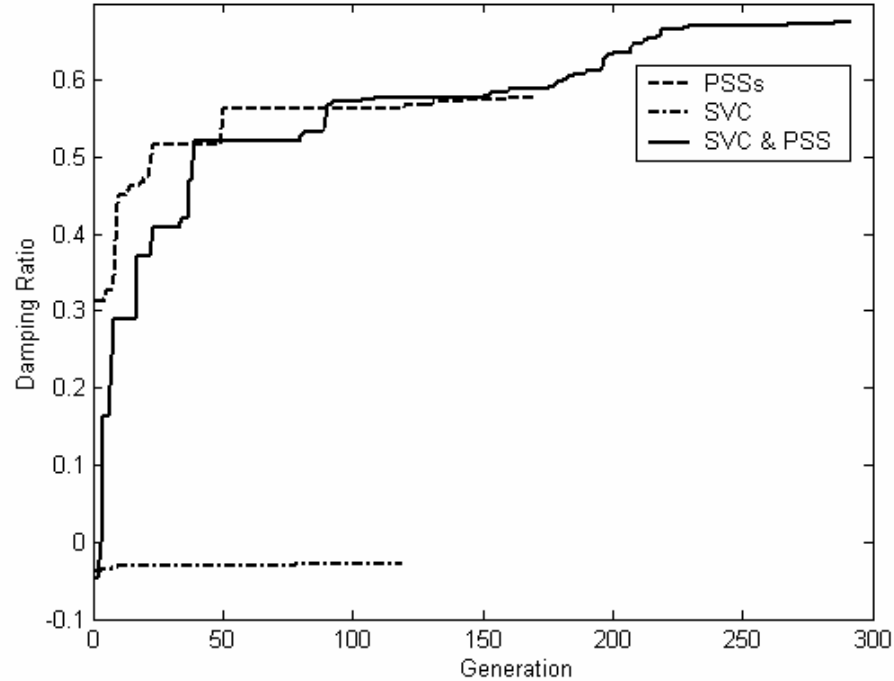


Fig. 7.66: Variation of the objective function of PSS's & SVC-based stabilizers in multimachine two-area power system

7.2.4.2 Eigenvalue Analysis

The system eigenvalues with the proposed PSS's and SVC-based stabilizers when applied individually and by means of coordinated design is given in Table 7.16. The bold rows of this table represent the EM modes eigenvalues and their damping ratios and frequency. It is evident that, using the proposed coordinated stabilizers design, the damping ratio of the EM mode eigenvalue is greatly enhanced. Hence, it can be concluded that this improves the system stability.

Table 7.16: System eigenvalues with coordinated design of PSS & SVC in two-area system

<i>PSSs</i>	<i>SVC</i>	<i>SVC & PSSs</i>
-3.9219±5.7975i	0.2752+9.29463i	-6.8548±6.4321i
0.5603*, 0.9227**	-0.0296*, 1.479**	0.71*, 1.02**
-3.4337±5.4358i	-0.49126+6.9342i	-2.08593±2.222i
0.534*, 0.8651**	0.07067*, 1.103**	0.68*, 0.35**
1.7682±1.6360i	0.08641+2.9049i	-2.836±2.7489i
0.734*, 0.2604**	-0.02973*, 0.462**	-3.854±3.568i
-2.6113±3.0188i	-16.75 + 0.69i	-16.09±0.836i
-7.7989±11.9581i	-89.05,-89.41,	-34.102±22.03i
	-79.5,-76.7	-125.81±0.9685i
-12.3718±17.9649i	-100,-23.42,-188.2	-100,-100,-82.59
-17.3096±0.1076i		
-21.5036±1.8633i	-13.86,-7.18	-84.441, -100, -100
-92.0013,-89.3647	-6.67,-6.12	-21.47,-17.72,-15.80
-81.0185,-76.8115	-6.17,-1.65	-12.841,-9.4599
-11.8988, -7.4442,	-0.2	-6.023,-5.3289,-2.619
-6.2647, -4.9271,		-1.216
-0.2024, -0.2122		

* damping ratio, ** frequency (Hz)

7.2.4.3 Nonlinear Time domain Simulation

Figs. 7.67-7.71 show the rotor angles, speed deviations, and electrical power outputs, as well as PSS2 stabilizing signal and SVC response, respectively, for a 6-cycle three-phase fault at bus 10 at the end of line 10-7 at the base case while using the proposed PSS's-SVC coordinated design. These Figs. should be compared with Figs. 7.32-7.37, for individual PSS's design, and 7.47-7.49, for individual SVC design. The improvement on the system responses when using the coordinated design is quite evident. This is in agreement with eigenvalue analysis results.

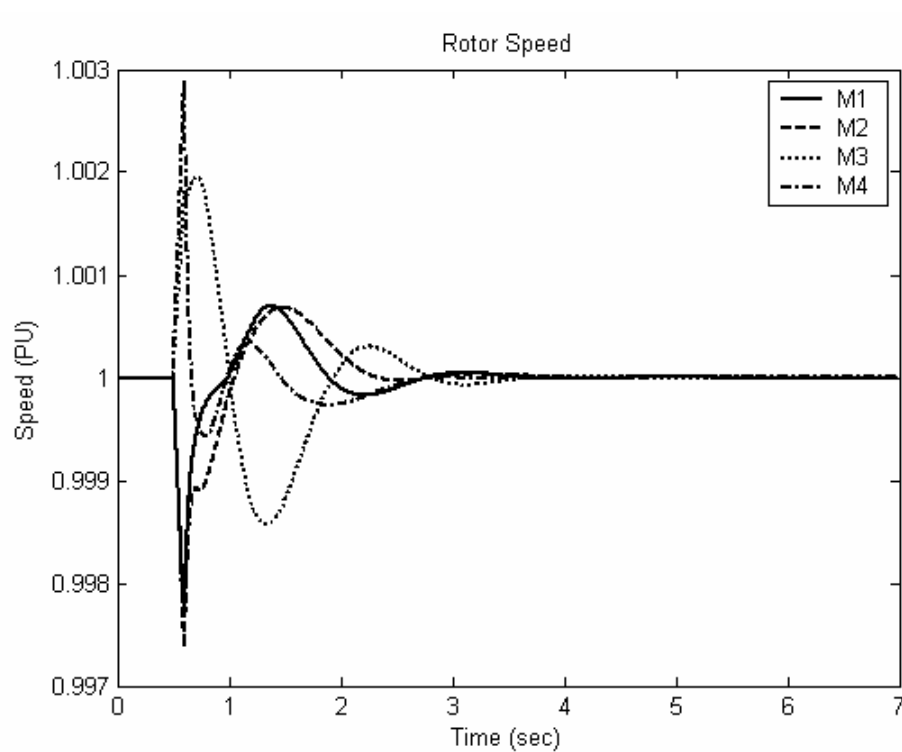


Fig. 7.67: Speed response for 6-cycle fault with PSS's & SVC, coordinated design in the two-area system

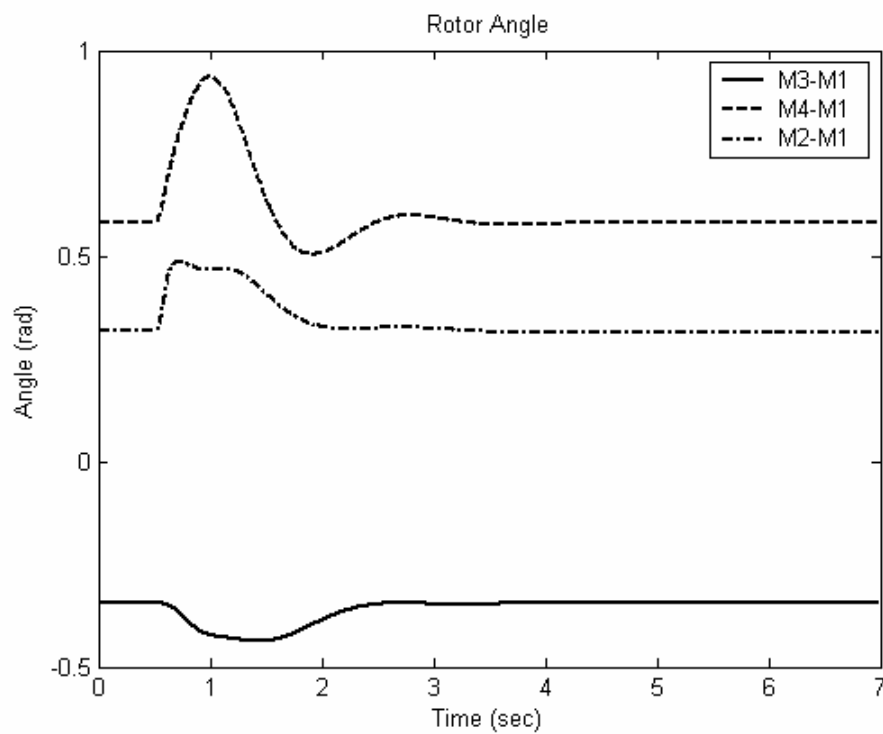


Fig. 7.68: Rotor angle response for 6-cycle fault with PSS's & SVC, coordinated design in the two-area system

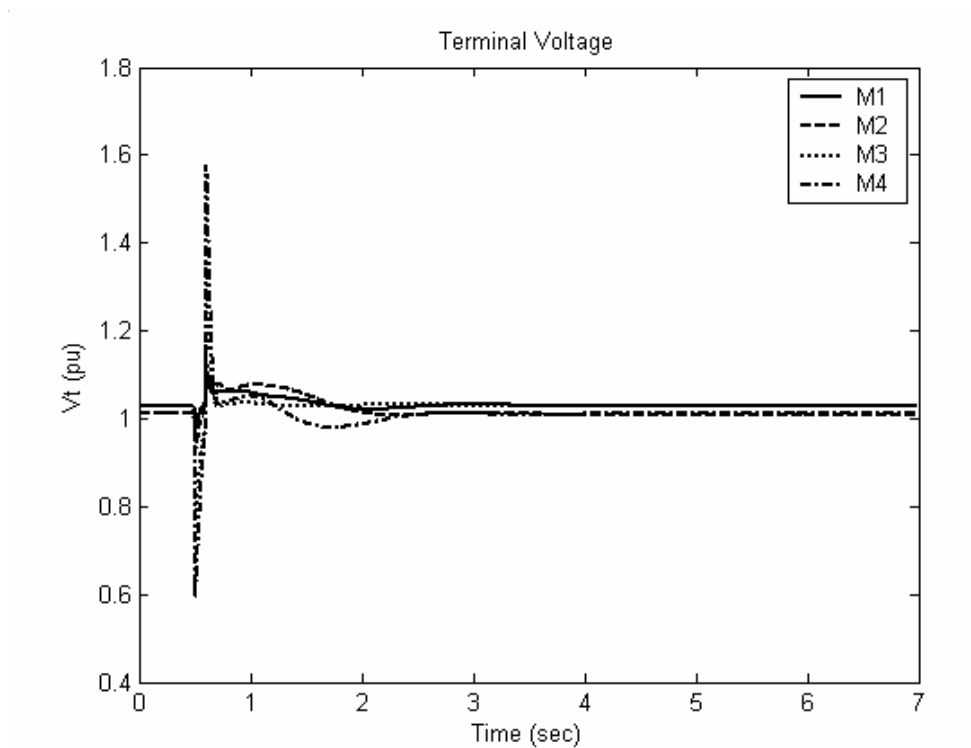


Fig. 7.69: Electrical power response for 6-cycle fault PSS's & SVC, coordinated design in the two-area system

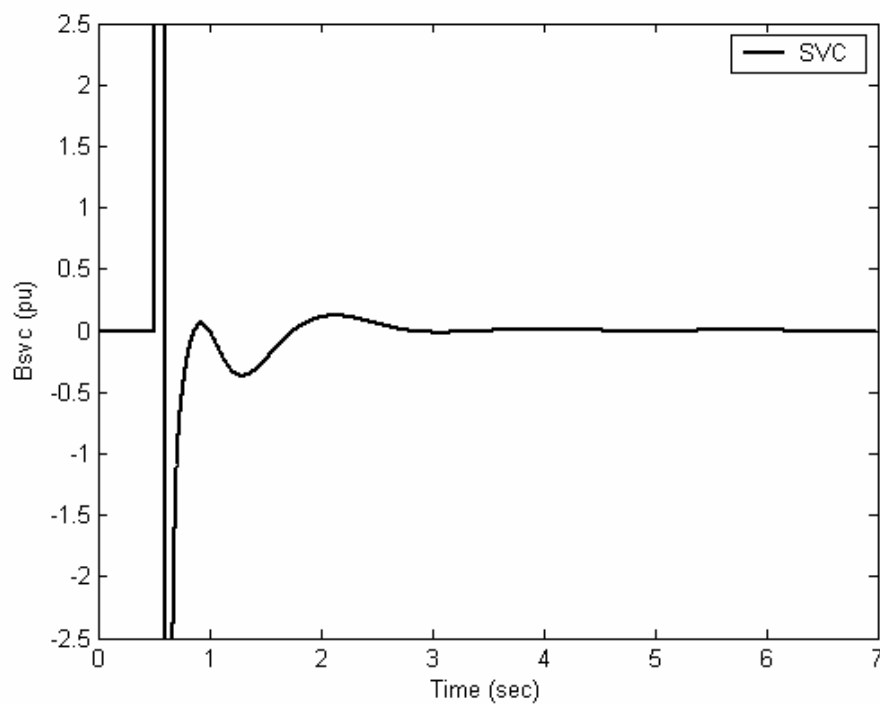


Fig. 7.70: SVC response for 6-cycle fault, coordinated design with PSS's in the two-area system

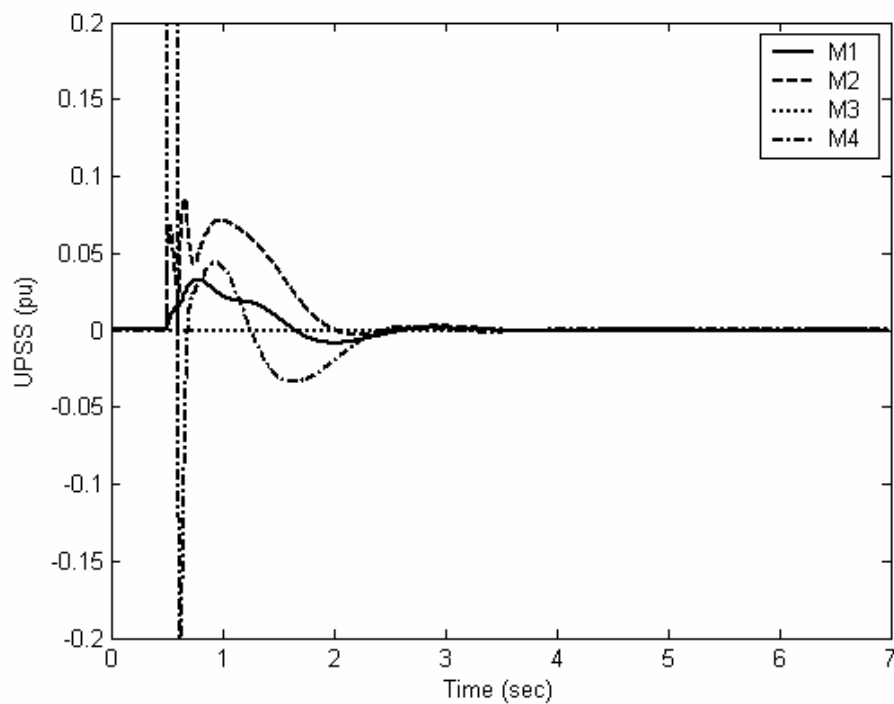


Fig. 7.71: PSS's response for 6-cycle fault, coordinated design with TCSC in the two-area system

CHAPTER 8

CONCLUSION

8.1 Conclusion

In this thesis, the power system stability enhancement via PSS and FACTS-based stabilizers when applied independently and also through coordinated application was discussed and investigated for a SMIB and multimachine power systems. Singular value decomposition has been employed to measure quantitatively the capabilities of the various stabilizers control signals in controlling the system EM mode. For the proposed stabilizer design problem, an eigenvalue-based objective function to maximize the system damping ratio among all complex eigenvalues was developed. The tuning parameters of the proposed stabilizer were optimized using Particle Swarm Optimization (PSO). A supplementary lead-lag controller as an oscillation damping controller is proposed to be a part of FACTS control system in this thesis.

Supplementary damping controllers to the STATCOM AC & DC voltage control loop were proposed to improve STATCOM power oscillation damping. The coordination between STATCOM damping stabilizers and internal PI voltage controllers is taken into consideration in the design stage.

In multimachine power system, the optimal locations of PSS's have been identified using participation factor technique, while the locations of TCSC and SVC have been selected based on their primary objectives such as voltage control and system power transmission capability, and then they utilized by adding the damping controller to their control system.

Individual design and coordinated design of the proposed stabilizers considering a single-operating-point as well as robust multiple-operating-point designs have been discussed. The effectiveness of the proposed control schemes in improving the power system dynamic stability has been verified through eigenvalue analysis, and nonlinear time-domain simulations under different loading conditions and severe fault disturbances.

The proposed tuning approach shows better performance compared with the existing controller parameters in the literatures.

This thesis demonstrates that TCSC, SVC, TCPS, and STATCOM-based controllers, appropriately tuned and located make them a viable alternative to traditional PSS controller or to enhance PSS controller for oscillation control.

8.2 Contribution

The main contributions of this thesis are summarized below:

- Utilizing the STATCOM phase modulation index ψ for power oscillation damping. The additional control circuit has been design and verified by nonlinear time-domain simulation. It has been shown that the ψ -based controller outperform

the STATCOM gain modulation index c -based controller in damping power oscillations.

- Both STATCOM stabilizer signals; c -based and ψ -based controllers, are simultaneously tuned by PSO search for the optimum controllers parameter settings that maximize the minimum damping ratio of all system complex eigenvalues at given loading condition(s).
- PSS has been successfully coordinated with each of STATCOM controller signals to provide composite enhanced performance.
- An eigenvalue based on objective function has been successfully implemented for STATCOM-based stabilizer design in SMIB and for TCSC-based stabilizer in multimachine power system.

8.3 Future Work

There are a number of issues that are still to be addressed in the area of FACTS device and their effect on damping the power system oscillations:

- The thesis approach can be extended to other types of the VSC-based FACTS controllers, such as UPFC, SSSC etc.
- Throughout this thesis the machine speed deviation signal is assumed to be available at the controllers' location. Utilizing the local measurements such as power flow and bus voltage as a controller's input is another area for potential investigation.

- More objective functions, eigenvalue-based or time-domain-based, as well as multi-objective functions need to be considered in the design stage in order to improve the proposed stabilizers performance.
- There is a need for more research in coordinating the control of multiple FACTS devices, not only to avoid undesirable interactions, but also to provide composite enhanced performance.
- Conventional lead-lag controller is proposed in this thesis. However, it will be worth to study the intelligent controllers, such as Fuzzy Logic, Neural Network, and Variable Structure Controller etc.
- Symmetrical transient three phase fault is applied as a disturbance in this study; other types of disturbances such as unsymmetrical faults, switching, permanent faults etc, might be applied to study the system performance.
- The study can be extended by using larger power system that contains a number of FACTS-based stabilizers.
- The effect of dynamic load model on the oscillation damping needs more investigation.

APPENDICES

Appendix A

SMIB system data:

$$\begin{aligned}
 M &= 9.26; & T'_{do} &= 7.76; & D &= 0; & x_d &= 0.973; & x'_d &= 0.3; \\
 x_q &= 0.6; & R &= 0.034; & X &= 0.997; & g &= 0.249; & b &= 0.262; \\
 K_A &= 50; & T_A &= 0.05; & K_s &= 1; & T_s &= 0.05; & v &= 1.05 \text{ pu.} \\
 |u_{pss}| &\leq 0.2 \text{ pu}; & |B_{svc}| &\leq 0.4 \text{ pu}; & |X_{TCSC}| &\leq 0.5 X; & |\Phi_{TCPS}| &\leq 15^\circ \\
 |E_{fd}| &\leq 7.3 \text{ pu}
 \end{aligned}$$

Appendix B

Three-machine power system data:

1. Bus Data

Table 8.1: 3-machine System bus data in per unit value.

Bus no.	Type	Voltage	Angle	Load		Generation	
				P	Q	P	Q
1	1	1.04	0	0	0	0	0
2	2	1.025	0	0	0	1.63	0
3	2	1.025	0	0	0	0.85	0
4	3	1	0	0	0	0	0
5	3	1	0	1.25	0.5	0	0
6	3	1	0	0.9	0.3	0	0
7	3	1	0	0	0	0	0
8	3	1	0	1	0.35	0	0
9	3	1	0	0	0	0	0

2. Line Data

Table 8.2: 3-machine System line data in per unit value.

<i>Line no.</i>	<i>From</i>	<i>To</i>	<i>R</i>	<i>X</i>	<i>B</i>
1	1	4	0	0.0576	0
2	2	7	0	0.0625	0
3	3	9	0	0.0586	0
4	4	5	0.01	0.085	0.088
5	4	6	0.017	0.092	0.079
6	5	7	0.032	0.161	0.153
7	6	9	0.039	0.17	0.179
8	7	8	0.0085	0.072	0.0745

3. Machine Data

Table 8.3: Machines Data, for 3-machine system

<i>Machine</i>	<i>H</i>	<i>X_d</i>	<i>X_d'</i>	<i>X_q</i>	<i>X_q'</i>	<i>T_d'</i>	<i>T_q'</i>	<i>KA</i>	<i>TA</i>	<i>D</i>
1	23.64	0.146	0.0608	0.0969	0.0969	8.96	0.5	100	0.05	2
2	6.4	0.8958	0.1198	0.8645	0.1969	6	0.535	100	0.05	2
3	3.01	1.3125	0.1813	1.2578	0.25	5.89	0.6	100	0.05	2

4. Power Flow Result

Table 8.4: Load flow result of the 3-machine system

<i>Bus no.</i>	<i>Voltage</i>	<i>Angle (degree)</i>	<i>Load</i>		<i>Generation</i>	
			<i>P</i>	<i>Q</i>	<i>P</i>	<i>Q</i>
1	1.04	0.0	0.0	0.0	71.641	27.046
2	1.025	9.28	0.0	0.0	163.0	6.654
3	1.025	4.66	0.0	0.0	85.0	-10.86
4	1.026	-2.217	0.0	0.0	0.0	0.0
5	0.996	-3.989	125	50.0	0.0	0.0
6	1.013	-3.687	90	30.0	0.0	0.0
7	1.026	3.72	0	0	0.0	0.0
8	1.016	0.728	100	35.0	0.0	0.0
9	1.032	1.967	0	0.0	0.0	0.0

Appendix C

Two-area, 4-machine power system data:

1. Bus Data

Table 8.5: 3-machine System bus data in per unit value.

<i>Bus no.</i>	<i>Type</i>	<i>Voltage</i>	<i>Angle</i>	<i>Load</i>		<i>Generation</i>	
				<i>P</i>	<i>Q</i>	<i>P</i>	<i>Q</i>
1	1	1.03	0	0	0	0	0
2	2	1.01	0	0	0	7	0
3	2	1.03	0	0	0	7	0
4	2	1.01	0	0	0	7	0
5	3	1	0	0	0	0	0
6	3	1	0	0	0	0	0
7	3	1	0	17.67	2.5	0	0
8	3	1	0	0	0	0	0
9	3	1	0	0	0	0	0
10	3	1	0	9.67	1	0	0

2. Line Data

Table 8.6: 3-machine System line data in per unit value.

<i>Line no.</i>	<i>From</i>	<i>To</i>	<i>R</i>	<i>X</i>	<i>B</i>
1	1	5	0	0.0167	0
2	2	6	0	0.0167	0
3	3	8	0	0.0167	0
4	4	9	0	0.0167	0
5	5	6	0.0025	0.025	0.021875
6	8	9	0.0025	0.025	0.021875
7	6	7	0.001	0.01	0.00875
8	9	10	0.001	0.01	0.00875

5. Machine Data

Table 8.7: Machines Data, for two-area system

<i>Machine</i>	<i>H</i>	<i>X_d</i>	<i>X_d'</i>	<i>X_q</i>	<i>X_q'</i>	<i>T_d'</i>	<i>T_q'</i>	<i>KA</i>	<i>TA</i>	<i>D</i>
1	55.575	0.2	0.033	0.19	0.016	8	0.4	200	0.01	0
2	55.575	0.2	0.033	0.19	0.016	8	0.4	200	0.01	0
3	58.5	0.2	0.033	0.19	0.016	8	0.4	200	0.01	0
4	58.5	0.2	0.033	0.19	0.016	8	0.4	200	0.01	0

3. Power Flow Result

Table 8.8: Load flow result of the 3-machine system

<i>Bus no.</i>	<i>Voltage</i>	<i>Angle (degree)</i>	<i>Load</i>		<i>Generation</i>	
			<i>P</i>	<i>Q</i>	<i>P</i>	<i>Q</i>
1	1.03	0	0	0	7.2532	2.8008
2	1.01	-10.65	0	0	7	4.4762
3	1.03	27.292	0	0	7	1.7721
4	1.01	17.548	0	0	7	2.155
5	0.99159	-6.8112	0	0	0	0
6	0.94312	-17.7	0	0	0	0
7	0.89954	-27.012	17.67	2.5	0	0
8	1.0077	20.825	0	0	0	0
9	0.98122	10.774	0	0	0	0
10	0.96662	2.4251	9.67	1	0	0

NOMENCLATURE

Abbreviation

SMIB	Single-machine infinite bus
PSS	Power system stabilizer
FACTS	Flexible AC transmission systems
SVC	Static Var compensator
TCSC	Thyristor-controlled series capacitor
TCPS	Thyristor-controlled phase shifter
STATCOM	Shunt Synchronous Static Compensator
STATCON	Static Condenser
ASVC	Advance Static Var Compensator
ASVG	Advance Static Var Generation
SSSC	Series Synchronous Static Compensator
UPFC	Unified power flow controller
GTO	Gate turn off
VSC	Voltage source converter
BESS	Battery Energy Storage System
SMES	Superconducting Magnetic Energy Storage
EM	Electromechanical mode
PSO	Particle swarm optimizer
PF	Participation Factor
Pf	Power factor

SVD	Singular value decomposition
POD	Power Oscillation Damping
pu	Per unit

Symbols

$P_m, P (P_e)$	Mechanical input power and electrical output power of the generator
M, H	Machine inertia coefficient and inertia constant
D	Machine damping coefficient
i_d, i_q	d- and q-axis armature current
v_d, v_q	d- and q-axis terminal voltage
T_{do}'	Open-circuit field time constant
x_d, x_d'	d-axis reactance and d-axis transient reactances
x_q	Generator q-axis reactance
V or v	Generator terminal voltage
E_q', E_{fd}	Generator internal and field voltages
V_{ref}	Reference voltage
v_b	Infinite bus voltage
K_A, T_A	Gain and time constant of the excitation system
u_{PSS}	PSS control signal
K_s, T_s	FACTS gain and time constant
Z, X, R	Transmission line impedance, reactance, and resistance
Y_L	Load impedance

g, b	Load Inductance and susceptance
i_{SVC}, i_L	SVC and load currents
X_{CSC}	TCSC equivalent reactance
B_{SVC}	SVC equivalent susceptance
C	STATCOM AC voltage controller output
ψ	STATCOM DC voltage controller output
δ	Rotor angle
ω	Rotor speed
ω_b	Synchronous speed
Φ, Φ_{TCPS}	Phase shift in the voltage phase angle resulting from the TCPS
α	Thyristor firing angle
ζ	Damping ratio

BIBLIOGRAPHY

- [1] Y. N. Yu, *Electric Power System Dynamics*, Academic Press, 1983.
- [2] P. M. Anderson and A. A. Fouad, *Power System Control and Stability*, IEEE Press, 1994.
- [3] P. W. Sauer and M. A. Pai, *Power system Dynamics and Stability*, Prentice Hall, 1998.
- [4] Rogers G.; *Power System Oscillations*, Kluwer Academic Publishers, 2000
- [5] W. Watson and G. Manchur, "Experience with Supplementary Damping Signals for Generator Static Excitation Systems," *IEEE Trans, PAS*, Vol. 92, pp 199-203, Jan 1973.
- [6] E. V. Larsen, J. S. Gasca, and J. H. Chow, "Concepts for Design of FACTS Controllers to Damp Power Swings," *IEEE Trans. On Power System*, Vol. 10, No. 2, May 1995.
- [7] F. deMello and C. Concordia, "Concepts of Synchronous Machine Stability as Affected by Excitation Control," *IEEE Trans. PAS*, Vol. 88, pp. 316-329, 1969.
- [8] Klein, M.; Rogers, G.J.; Kundur, P., "A fundamental study of inter-area oscillations in power systems," *IEEE Transactions on Power Systems*, Volume: 6 Issue: 3 , Aug. 1991, Page(s): 914 -921
- [9] Klein, M., Rogers G.J., Moorthy S., and Kundur, P., "Analytical investigation of factors influencing power system stabilizers performance", , *IEEE Transactions on Energy Conversion* , Volume: 7 Issue: 3 , Sept. 1992, Page(s): 382 -390
- [10] G. T. Tse and S. K. Tso, "Refinement of Conventional PSS Design in Multimachine System by Modal Analysis," *IEEE Trans. PWRS*, Vol. 8, No. 2, 1993, pp. 598-605.
- [11] Y.Y. Hsu and C.Y. Hsu, "Design of a Proportional-Integral Power System Stabilizer," *IEEE Trans. PWRS*, Vol. 1, No. 2, pp. 46-53, 1986.

- [12] Y.Y. Hsu and K.L. Liou, "Design of Self-Tuning PID Power System Stabilizers for Synchronous Generators," *IEEE Trans. on Energy Conversion*, Vol. 2, No. 3, pp. 343-348, 1987.
- [13] V. Samarasinghe and N. Pahalawaththa, "Damping of Multimodal Oscillations in Power Systems Using Variable Structure Control Techniques," *IEE Proc. Genet. Transm. Distrib.*, Vol. 144, No. 3, Jan. 1997, pp. 323-331.
- [14] Y.Y. Hsu and C.R. Chen, "Tuning of Power System Stabilizers Using an Artificial Neural Network," *IEEE Trans. on Energy Conversion*, Vol. 6, No. 4, pp. 612-619, 1991.
- [15] Abdel-Magid, Y.L., Abido M. A., and Mantawy A. H., "Robust Tuning of Power System Stabilizers in Multimachine Power Systems," *IEEE Transactions on Power Systems*, Volume 15, No. 2, May 2000, pp. 735-740.
- [16] Abdel-Magid Y. L., Bettayeb Maamar, and Dawoud M. M., "Simultaneous stabilization of Power System Genetic Algorithms," *Generation, Transmission and Distribution, IEE Proceedings*, Volume 145, No. 1, 1997, Page(s): 39-44.
- [17] Abdel-Magid Y.L., Abido M.A., Al-Baiyat S., and Mantawy A. H., "Simultaneous Stabilization of Multimachine Power Systems via Genetic Algorithms," *IEEE Transaction on Power Systems*, Volume 14, No. 4, November 1999, pp. 1428-1439.
- [18] Abdel-Magid Y.L., Abido M. A., and Mantawy A. H., "Robust Tuning of Power System Stabilizers in Multimachine Power Systems," *IEEE Transactions on Power Systems* , Volume 15, No. 2, May 2000, pp. 735-740.
- [19] Zhang, Y., Chen G.P., Malik O.P., and Hope G.S., "An artificial neural network based adaptive power system stabilizer," *IEEE Transactions on Energy Conversion* , Volume: 8 Issue: 1 , March 1993, Page(s): 71 -77
- [20] M. A. Abido and Y. L. Abdel-Magid, "Hybridizing rule-based power system stabilizers with genetic algorithms," *IEEE Trans. on PWRS*, Vol.14, May 1999, pp: 600-607
- [21] M. A. Abido and Y. L. Abdel-Magid, "A hybrid neuro-fuzzy power system stabilizer for multimachine power systems," *IEEE Trans. on PWRS*, Vol. 13, No. 4, November 1998, pp. 1323-1230.
- [22] M. A. Abido and Y. L. Abdel-Magid, "A fuzzy basis function network based power system stabilizer for generator excitation control," *Proceedings of the Sixth IEEE International Conference*, Volume: 3 , 1-5 July 1997, Page(s): 1445 -1450

- [23] M. Hassan, O. P. Malik, and G. Hope, "A Fuzzy Logic Based Stabilizer for a Synchronous Machine," *IEEE Trans. On Energy Conversion*, Vol. 3, No. 3, 407, 1991.
- [24] M. Hassan, O. P. Malik, and G. Hope, "Implementation and Laboratory Test Results for a Fuzzy Logic Based Self-Tuned Power System Stabilizer," *IEEE Trans. On Energy Conversion*, Vol. 8, No. 2, 221, 1993.
- [25] M. A. Abido, "Particle Swarm Optimization for Multimachine Power System Stabilizer design," IEEE, Power Engineering Society Summer Meeting, 2001, July 2001, Vol. 3, pp: 1346-1351
- [26] M. A. Abido and Y. L. Abdel-Magid, "Radial basis function network based power system stabilizers for multimachine power systems," *IEEE International Conference on Neural Networks ICNN'97*, Houston, Texas, USA, June 9-12, 1997, pp. 622-626.
- [27] L. Chen, and A. Petroianu, "A new method of tuning power system stabilizers," *Electrical and Computer Engineering, 1996. Canadian Conference on*, Volume: 1, 26-29 May 1996, Page(s): 454 -457
- [28] M. Klein, L. X. Le, G. J. Rogers, S. Farrokhpay, and N. J. Balu, " H_{∞} damping controller design in large power systems," *IEEE Transactions on Power Systems*, Vol. 10 Issue: 1, Feb. 1995, pp: 158 -166
- [29] A. Murdch, H. C. Sanderson, and R. Lawson; Excitation System Performance Specification to Meet Interconnection Requirements,
- [30] F. P. de Mello, P. J. Nolan, T. F. Laskowski, and J. M. Undrill, "Coordinated application of stabilizers in multimachine power systems," *IEEE Transactions PAS*, Vol. 99, No. 3, pp: 892-901, 1980
- [31] Y. Y. Hsu and C. L. Chen, "Identification of optimum location for stabilizer applications using participation factors," *Pt. C, IEE Proceedings*, Volume 134, No. 3, 1987, Page(s): 238-244.
- [32] D. R. Ostojic, "Identification of optimum site for power system stabilizer applications," *Pt. C, IEE Proceedings*, Vol. 135, No. 5, 1988, pp: 416-419.
- [33] N. G. Hingorani, "High Power Electronics and Flexible AC Transmission System," *IEEE Power Engineering Review*, July 1988.

- [34] N. G. Hingorani, "FACTS-Flexible AC Transmission System," *Proceedings of 5th International Conference on AC and DC Power Transmission-IEE Conference Publication 345*, 1991, pp. 1-7.
- [35] N. G. Hingorani, "Flexible AC Transmission," *IEEE Spectrum*, April 1993, pp. 40-45.
- [36] IEEE Power Engineering Society, *FACTS Overview*, IEEE Special Publication 95TP108, 1995.
- [37] IEEE Power Engineering Society, *FACTS Applications*, IEEE Special Publication 96TP116-0, 1996.
- [38] H. F. Wang and F. J. Swift, "A Unified Model for the Analysis of FACTS Devices in Damping Power System Oscillations Part I: Single-machine Infinite-bus Power Systems," *IEEE Trans. PWRD*, Vol. 12, No. 2, 1997, pp. 941-946.
- [39] M. A. Abido and Y. L. Abdel-Magid, "Power System Stability Enhancement via coordinated design of PSS and FACTS-Based stabilizers," *Final Report of a Project Funded by FKUPM*, May 2002
- [40] M. A. Abido and Y. L. Abdel-Magid, "Analysis and Design of Power System Stabilizers and FACTS Based Stabilizers Using Genetic Algorithms," *Proceedings of Power System Computation Conference PSCC-2002*, Session 14 Paper 3, Spain, June 24-28, 2002,
- [41] X. Chen, N. Pahalawaththa, U. Annakkage, and C. Kumble, "Controlled Series Compensation for Improving the Stability of Multimachine Power Systems," *IEE Proc.*, Pt. C, Vol. 142, 1995, pp. 361-366
- [42] J. Chang and J. Chow, "Time Optimal Series Capacitor Control for Damping Inter-Area Modes in Interconnected Power Systems," *IEEE Trans. PWRD*, Vol. 12, No. 1, 1997, pp. 215-221.
- [43] T. Lie, G. Shrestha, and A. Ghosh, "Design and Application Of Fuzzy Logic Control Scheme For Transient Stability Enhancement In Power System", *Electric Power System Research*. 1995, pp, 17-23.
- [44] Y. Wang, Y. Tan, and G. Guo, "Robust nonlinear coordinated excitation and TCSC control for power system", *IEE Proc – Gener. Trns. Distrib.*, vol. 149, no,3, May 2002, pp. 367-372.

- [45] M. A. Abido, "Genetic-based TCSC damping controller design for power system stability enhancement," *Electric Power Engineering, 1999. PowerTech Budapest 99. International Conference on*, 29 Aug.-2 Sept. 1999, Page(s): 165
- [46] M. A. Abido, "Pole placement technique for PSS and TCSC-based stabilizer design using simulated annealing," *Electric Power System Research*, 22, 2000, Page(s) 543-554.
- [47] Y. Wang, R. Mohler, R. Spee, and W. Mittelstadt, "Variable Structure FACTS Controllers for Power System Transient Stability," *IEEE Trans. PWRS*, Vol. 7, 1992, pp. 307-313.
- [48] T. Luor and Y. Hsu, "Design of an Output Feedback Variable Structure Thyristor Controlled Series Compensator for Improving Power System Stability," *Electric Power Systems Research*, 47, 1998, pp. 71-77.
- [49] V. Rajkumar, R. Mohler, "Bilinear generalized predictive control using the thyristor controlled series capacitor," *IEEE Trans. PWRS* 9 (4) (1994) 1987-1993.
- [50] Q. Zhao and J. Jiang, "A TCSC Damping Controller Using Robust Control Theory," *Int. J. of Electrical Power & Energy Systems*, Vol. 20, No. 1, 1998, pp. 25-33.
- [51] X. Zhou and J. Liang, "Nonlinear adaptive control of TCSC to improve the performance of power systems," *IEEE Proc – Gener. Trtans. Distrib.*, vol. 146, no,3, pp. 301-305, 1999.
- [52] R. Baker, G. Guth, W. Egli, and O. Eglin, "Control Algorithm for a Static Phase Shifting Transformer to Enhance Transient and Dynamic Stability of Large Power Systems," *IEEE Trans. PAS*, Vol. 101, No. 9, 1982, pp. 3532-3542.
- [53] A. Edris, "Enhancement of First-Swing Stability Using a High-Speed Phase Shifter," *IEEE Trans. PWRS*, Vol. 6, No. 3, 1991, pp. 1113-1118.
- [54] F. Jiang, S. S. Choi, and G. Shrestha, "Power System Stability Enhancement Using Static Phase Shifter," *IEEE Trans. PWRS*, Vol. 12, No. 1, 1997, pp. 207-214.
- [55] Y. L. Tan and Y. Wang, "Nonlinear Excitation and Phase Shifter Controller for Transient Stability Enhancement of Power Systems Using Adaptive Control Law," *Int. J. Electrical Power & Energy Systems*, Vol. 18, No. 6, 1996, pp. 397-403.

- [56] R. Byerly, D. Poznaniak, and E. Taylor, "Static Reactive Compensation for Power Transmission System," *IEEE Trans. PAS-101*, 1982, pp. 3998-4005
- [57] A. E. Hammad, "Analysis of Power System Stability Enhancement by Static VAR Compensators," *IEEE Trans. PWRS*, Vol. 1, No. 4, 1986, pp. 222-227.
- [58] H. F. Wang and F. J. Swift, "Capability of the Static VAR Compensator in Damping Power System Oscillations," *IEE Proc. Genet. Transm. Distrib.*, Vol. 143, No. 4, 1996, pp. 353-358.
- [59] K. R. Padiyar nad R. K. Varma, "Damping Torque Analysis of Static VAR System Oscillations," *IEEE Trans. PWRS*, Vol. 6, No. 2, 1991, pp. 458-465.
- [60] E. Z. Zhou, "Application of Static VAR Compensators to Increase Power System Damping," *IEEE Trans. PWRS*, Vol. 8, No. 2, 1993, pp. 655-661.
- [61] H. F. Wang, and F. J. Swift, "Capability of the statis VAR compensator in damping power system oscillations," *IEEE Proc – Gener. Trtans. Distrib.*, Vol. 143, No. 4, 1996, pp: 353-358.
- [62] S. Lee and C. C. Liu, "An output feedback static VAR controller for the damping of generator oscillations," *Electric Power System Research*, 29, 1994, Page(s) 9-16.
- [63] Li Wang; Ming-Hsin Tsai, "Design of a H^∞ static VAR controller for the damping of generator oscillations," *Power System Technology, 1998. Proceedings. POWERCON '98. 1998 International Conference on* , Volume: 2, 18-21 Aug. 1998, Page(s): 785 -789 vol.2
- [64] M. Parviani and M. R. Iravani, "Optimal robust control design of static VAR compensators," *IEEE Proc – Gener. Trtans. Distrib*, Volume 145, No. 3, 1998, pp: 301-307.
- [65] S. P. Rao and I Sen, "A QTF-based robust SVC controller for improving the dynamic stability of power systems," *Electric Power System Research*, 46, 1998, pp: 213-219.
- [66] P. K. Dash, N. C. Sahoo, and R. Doraiswami, "A variable structure VAR stabilizer for power system control," *Electric Power System Research*, 26, 1993, Page(s) 127-136.
- [67] P. Pourbeik and M. J. Gibbard, "Damping and Synchronizing Torques Induced on Generators by FACTS Stabilizers in Multimachine Power Sytsems," *IEEE Trans. PWRS*, Vol. 11, No. 4, 1996, pp. 1920-1925.

- [68] A. R. Messina, O. Begovich, and M. Nayebzadeh, "Analytical Investigation of the Use of Static VAR Compensators to Aid Damping of Inter-Area Oscillations," *Electric Power Systems Research*, 51, 1999, pp. 199-210.
- [69] H. F. Wang and F. J. Swift, "A Unified Model for the Analysis of FACTS Devices in Damping Power System Oscillations Part II: multi-machine Infinite-bus Power Systems," *IEEE Trans. PWRD*, Vol. 13, No. 4, 1998, pp. 1355-1362.
- [70] P. Pourbeik, and M. J. Gibbard, "Damping and synchronizing torques induced on generators by FACTS stabilizers in multimachine power systems," *IEEE Transactions on PWRD*, Volume: 11 Issue: 4, Nov. 1996, pp: 1920 -1925
- [71] M. J. Gibbard, D. J. Vowles, P. Pourbeik, "Interactions between, and effectiveness of, power system stabilizers and FACTS device stabilizers in multimachine systems," *IEEE Transactions on PWRD*, Volume: 15 Issue: 2, May 2000, Page(s): 748 -755
- [72] K. Mekki, N. Hadjsid, D. Georges, R. Feuillet, A. Phadke, and F. Wu, "Wide-Area Measurements for Power System Oscillations and FACTS Interactions", *14th PSCC*, Sevilla, 24-28, June 2002.
- [73] M. Noroozian, M. Ghandhari, G. Andersson, J. Gronquist, and I. Hiskens, "A Robust Control Strategy for Shunt and Series Reactive Compensators to Damp Electromechanical Oscillations," *IEEE Trans. On Power Delivery*, Vol. 16, No. 4, October 2001, pp: 812-817.
- [74] M. Noroozian and G. Andersson, "Damping of Inter-Area and Local Modes by use Controllable Components," *IEEE Trans. On Power Delivery*, Vol. 10, No. 4, October 1995, pp: 2007-2012.
- [75] M. Noroozian and G. Andersson, "Damping of Power System Oscillations by use of Controllable Components," *IEEE Trans. On Power Delivery*, Vol. 9, No. 4, October 1994, pp: 2046-2054.
- [76] N. Mithulananthan, C. A. Canizares, L. Reeve, "Tuning, performance and interactions of PSS and FACTS controllers," *IEEE, Power Engineering Society Summer Meeting, 2002*, Vol. 2, 21-25 July 2002, pp: 981 -987
- [77] L. Gyugyi "Dynamic Compensation of AC Transmission Lines by Solid-State Synchronous Voltage Sources," *IEEE Transactions on Power Delivery*, Vol. 9, No. 2, pp.904 – 911, April 1994.
- [78] K. Kalyan Sen, "STATCOM-STATIC synchronous COMPensator: Theory, Modeling, and Applications", *IEEE*, 1998

- [79] S. M. Bamasak and M. A. Abido, "Assessment Study Of Shunt Facts-Based Controllers Effectiveness On Power System Stability Enhancement," *39th UPEC Proceedings*, Vol. 1, pp 65-71, Sept 2004.
- [80] H. F. Wang, "Phillips-heffron model of power systems installed with statcom and applications," *IEE Proc.-Geer, Trans. Distr.*, Vol. 146 No.5, Sept. 1999
- [81] H. F. Wang, "Interaction and multivariable design of STATCOM AC and DC voltage control," *Int, Electric Power System Research* 25 387-394, 2003.
- [82] H. F. Wang and F.Li, "multivariable sampled regulators for the coordinated control of STATCOM AC and DC voltage," *IEE proc-Gener. Transm. Distrib*, Vol147, No 2, March, 2000
- [83] A.H.M.A. Rahim, S.A.Al-Baiyat and H. M. Maghrabi, "Robust damping controller design for a static compensator," *IEE proc-Gener. Transm. Distrib*, Vol 149 No 4, 2002
- [84] A.H.M.A. Rahim, S.A.Al-Baiyat, and F.M. Kandlawala. "A robust STATCOM controller for power system dynamic performance enhancement," *2001 IEEE power engineering Society Summer Meeting*, Vancouver, Canada, July 2001.
- [85] A.H.M.A. Rahim and F.M. Kandlawala. "A robust design of a power system STATCOM controller using loop-shaping Technique," *Saudi engineering society conference*, June 2002.
- [86] M.F. Kandlawala and A.H.M.A. Rahim. "Power system dynamic performance with statcom controller," *8th Annual IEEE technical exchange meeting*, April 2001.
- [87] Sun Qu and Chen chen, "Low Frequency Oscillations Damping by STATCOM with a Fuzzy Supplementary Controller," *IEEE*, 2002.
- [88] Stella Morris, P.K. Dash, K.P. Basu, "A fuzzy variable structure controller for STATCOM.", *Int, Electric Power System Research* 65 23-34, 2003.
- [89] Yuang Lee and San Yung, "STATCOM controller design for power system stabilization with sub-optimal control strip pole assignment," *Int, J Electrical Power and Energy Systems* 24 771-779, 2002.
- [90] M. Sekoguchi, H. Konishi, M. Goto, and A. Yokoyama, "Nonlinear Optimal Control Applied to STATCOM for Power System Stabilization", *IEEE*, 2002.

- [91] K. R. Padiyar, V. S. Parakash, "Tuning and performance evaluation of damping controller for a STATCOM", *Int, J Electrical Power and Energy Systems* 25 155-166, 2003
- [92] S. Abazari and J. Mahdavi, "Transient Stability Improvement by Using Advanced Static Var Compensator," *IEEE Bolongna Power Tech Conference*, June 2003.
- [93] Claudio A. Canizares, Massimo Pozzi, Sandro Corsi, and Edvina Uzunovic, "STATCOM modeling for voltage and angle stability studies," *Int, J Electrical Power and Energy Systems* 25 431-441, 2003.
- [94] Pablo Carcia and Aurelio D, "Control System for a PWM-based STATCOM," *IEEE Trans, on Power Delivery*, Vol.15, No.4, Oct. 2000.
- [95] Y. Ni and L.Snyder, "STATCOM Power Frequency Model with VSC Charging Dynamics and its Application in the Power System Stability Analysis", *4th APSCOM*, Nov. 1997, pp 119-124.
- [96] D. Menniti, A. Burgio, A. Pinnarelli, and N. Sorrentino, "Synchronizing Fuzzy Power System Stabilizer and Fuzzy FACTS Device,"
- [97] N. Mithulanathan, C. Canizares, J. Rooeve, and G. Rogers, "Comparison of PSS, SVC, and STATCOM for Damping Power System Oscillations," *IEEE Trans. On Power Systems*, Vol. 18, No. 2, May 2003.
- [98] C. Qian, M. L. Crow, "A Cascaded Converter-Based StatCom with Energy Storage," *2002 IEEE Power Engineering Society Winter*, No. 03-3488-0054,2002.
- [99] S. Schoenung and C. Burns, "Utility Energy Storage Application Studies," *IEEE Trans. On Energy Conversion*, Vol. 11, No. 3, Sept. 1996.
- [100] Z. Yang, et. Al, "The steady-state Characteristics of StatCom with energy storage," *Proc. NAPS, San Luis Obispo, California*, October, 1999
- [101] K. Kobayashi, M. Goto, K. Wu, Y. Yokomizu and T. Matsumura, "Power System Stability Improvement by Energy Storage Type STATCOM," *IEEE Power Society Meeting*, paper 0-7803-7967-5, 2003.
- [102] D. A. Pastos and N. A. Vovos, "Influence of real power modulation provided by the shunt compensator on damping power swings," *Proceedings of IEEE Intl. Conference on Electronics, circuits and system*, 2:884-877, 1996

- [103] A Arsoy, Y Liu, S Chen, Z Yang, L Crow, and P Ribeiro, "Dynamic Performance of a Static Synchronous Compensator with Energy Storage", *IEEE Power Society Winter Meeting*, paper 0-7803-6674-3, 2001.
- [104] S. M. Bamasak and M. A Abido, "Damping Improvement of Power System Oscillation Using STATCOM." *2nd GCC-IEEE conf.*, Vol. 1, pp 65-71, Nov 2004.
- [105] P. Kundur, *Power System Stability and Control*. McGraw, New York, 1994.
- [106] M. J. Gibbard, D. J. Vowles, P. Pourbeik, "Interactions between, and effectiveness of, power system stabilizers and FACTS device stabilizers in multimachine systems," *IEEE Transactions on PWRs*, Vol.: 15 Issue: 2 , May 2000, pp: 748 - 755
- [107] A. R. Mahran, B. W. Hogg, M. L. El-Sayed, "Co-ordinated control of synchronous generator excitation and static VAR compensator," *IEEE Transactions on Energy Conversion* , Volume: 7 Issue: 4 , Dec. 1992, pp: 615 - 622
- [108] A. H. M. Rahim and S. G. Nassimi, "Synchronous generator damping enhancement through coordinated control of exciter and SVC," *Generation Transmission and Distribution, IEE Proceedings*, Vol. 143, No. 2, 1996, pp: 211-218.
- [109] T. Hiyama, M. Mishiro, H. Kihara, and T. Ortmeyer, "Coordinated Fuzzy Logic Control for Series Capacitor Modules and PSS to Enhance Stability of Power System," *IEEE Trans. PWRD*, Vol. 10, No. 2, 1995, pp. 1098-1104.
- [110] Y. L. Abdel-Magid and M. A. Abido, "Robust coordinated design of excitation and TCSC-based stabilizers using genetic algorithm," *Electric Power System Research*, 69, 2004, pp: 129-141.
- [111] P. Pourbeik, M. J. Gibbard, "Simultaneous coordination of power system stabilizers and FACTS device stabilizers in a multimachine power system for enhancing dynamic performance," *IEEE Transactions on PWRs*, Vol.: 13 Issue: 2 , May 1998, pp: 473 -479
- [112] W. Fang and H. W. Ngan, "Enhancing small signal power system stability by coordinating unified power flow controller with power system stabilizer," *Electric Power System Research*, 65, 2003, pp: 91-99.

- [113] J. M. Ramirez, R. J. Davalos, V. A. Valenzuela, "Coordination of FACTS-based stabilizers for damping oscillations," *IEEE Power Engineering Review*, Volume: 20 Issue: 12, Dec. 2000, pp: 46 -49
- [114] Li Wang and Zon-Yan Tsai. Stabilization of generator oscillations using a PID statcom damping controllers and PID power system stabilizers. *IEEE Engineering society, winter meeting, 1999*, pp:616-621
- [115] L. Cong, and Y. Wang "Coordinated control of generator excitation and STATCOM for rotor angle stability and voltage regulation enhancement of power system," *IEE proc. Gener. Transm. Distrib.* Vol 149, No. 6, 2002, pp:256-266
- [116] A. Canizares, S. Corsi, and M. Pozzi, "Modeling and Implementation of TCR and VSI Based FACTS Controllers," *Technical report, AT-Unita Controllo e Regolazione No. 99/595, ENEL Ricerca, Area Trasmissione e Dispacciamento*, December 1999.
- [117] J. C. Passelergue, N. Hadjsaid, and Y. Basanger, "Low frequency oscillations damping by FACTS and power system stabilizers". *Proceedings of 32nd universities power engineering conference*, 1:9-12, 1997.
- [118] J. Kennedy, "The Particles Swarm: Social Adaptation of Knowledge," *Proceedings of the 1997 IEEE international Conference on Evolutionary Computation ICE'97, Indianapolis, Indiana, USA 1997*, pp. 303-308

Vita

- Saleh Mohammad Omar Bamasak
- Born in Jeddah, Saudi Arabia on June 17, 1977.
- Received Bachelor of Science (B.S.) degree in Electrical Engineering from King Fahd University of Petroleum & Minerals (KFUPM), Dhahran, Saudi Arabia in 2001.
- Joined Saudi Electricity Company in Jan 2002.
- E-mail: h2smb@se.com.sa

LIST OF PUBLICATIONS

- [1] S. M. Bamasak and M. A Abido, "Assessment Study Of Shunt Facts-Based Controllers Effectiveness On Power System Stability Enhancement" 39th UPEC Proceedings, Vol. 1, pp 65-71, Sept 2004.
- [2] S. M. Bamasak and M. A Abido, "Damping Improvement of Power System Oscillation Using STATCOM." 2nd GCC-IEEE conf., Vol. 1, pp 65-71, Nov 2004.
- [3] S. M. Bamasak and M. A Abido, "Effectiveness Of Series Compensation On Power System Stability Enhancement." GCC-Cigre conf., Vol. 1, pp 65-71, Nov 2004.
- [4] S. M. Bamasak and M. A Abido, "Robust Coordinated Design of PSS & STATCOM Controllers for Damping Power System Oscillation" **Accepted for presentation in 15th PSCC, Liege, Belgium, 22-26 August 2005.**
- [5] S. M. Bamasak and M. A Abido, "Power System Transient Stability Enhancement via Coordinated Design of SVC and PSS in Multi-Machine System" **Accepted for presentation in GCC-Cigre 2005, Qatar, 27-29 November 2005.**